Respirasome-Mediated Activation of T Lymphocytes

Von der Fakultät für Lebenswissenschaften

der Technischen Universität Carolo-Wilhelmina zu Braunschweig

zur Erlangung des Grades

eines Doktors der Naturwissenschaften

(Dr. rer. nat.)

genehmigte

D i s s e r t a t i o n

von Daniel Jon Meston

aus South Shields

1. Referent:	Professor Dr. Lothar Jänsch
2. Referent:	Professor Dr. Ralf Mendel
eingereicht am:	24.04.2020
mündliche Prüfung (Disputation) am:	13.07.2020

Vorveröffentlichungen der Dissertation

Teilergebnisse aus dieser Arbeit wurden mit Genehmigung der Fakultät für Lebenswissenschaften, vertreten durch den Mentor der Arbeit,
in folgenden Beiträgen vorab veröffentlicht:

Posterbeiträge

47th annual meeting of the German society for immunology 11.-16.09.2017 Erlangen, Germany

Poster: Respirasome Dynamics and Turnover in Activated T Lymphocytes

11th German Meeting on Immune Regulation 19.-21.06.2017 Berlin, Germany

Poster: Respirasome Dynamics and Turnover in Activated T Lymphocytes

1st Gordon Research Conference on Mitochondria in Health and Disease: Mitochondrial Dynamics and Signaling 17.-22.03.2019 Ventura, USA

Poster: ROS-sensitivity of respirasome in activated human T cells (Poster)

Contents

Table of Figures

Table of Tables

1.0 Introduction

1.1 T cell immunity

T lymphocytes (T cells) originate as hematopoietic stem cells from the bone marrow which travel to the thymus. Following which, they differentiate into double negative (DN) T cells, named due to the lack of a cluster of differentiation (CD) protein such as the CD4 or CD8 receptor. DN T cells possess an invariant α chain as well as a variable β chain T cell receptor (TCR), theβ chain being generated from variable recombination of the V(D)J gene fragments [1]. Following the generation of a functional TCR which retains a structurally competent variable β chain, the T cells can progress through the beta selection stage.

Rearrangement of the progenitor invariant α chain again through recombination of the V (D) J gene fragments in combination with upregulation of CD4 and CD8 receptors yield double positive (DP) T cells. These cells must be capable of binding the self-major histocompatibility complex (MHC) proteins, which are present on the surface of cortical thymic epithelial cells (cTECs), with a certain affinity. Cells that lack a functional TCR at this time point cannot bind the MHC and undergo apoptosis by neglect [2] while DP T cells which bind too strongly to self-MHC proteins will yield an apoptotic response to prevent autoimmune-related damage (negative selection). Conversely, DP T cells which are capable of conjugating with the self-MHC proteins with medium affinity will continue to survive (positive selection). T cells which can adequately conjugate MHC receptors subsequently migrate to the medulla where they can develop fully into either CD4+ or CD8+ single positive (SP) T cells [3].

Following generation of SP naïve T cells (T_N), these then circulate between the lymphoid organs where they seek out the correct antigen presenting cell (APC) displaying the MHC coupled to a pathogenic antigen (Ag). Successful conjugation of the MHC:Ag complex on the APC with the TCR of the T cell and additional costimulatory receptors, e.g. CD28, yields activation. Following activation, T cells undergo differentiation (depending on subset) and clonal expansion and begin to circulate into the tissues to execute their effector function [4].

This effector function requires a shift in the metabolic activity of the mitochondria (discussed later) away from oxidative phosphorylation (OXPHOS) and fatty acid beta-oxidation (FAO) to glycolysis to support the large energetic demand [5].

1.1.1 T cell subsets

T cells exist as a number of different subsets specialized to perform discrete functions. For the purposes of this thesis I will focus on the major $CD4^+$ and $CD8^+$ subsets. On conjugation of the TCR both subsets recognize a differing MHC molecule, with $CD4^+$ T cells associating the MHC class II and $CD8^+$ conjugating with cells expressing MHC class I molecules [6]. These alternate MHC molecules trigger the differentiation of $CD4^+$ and $CD8^+$ T cells into their diverging effector functions (Figure. 1). $CD4^+$ T cells, termed T helper (T_H) cells act by releasing immune-modulatory cytokines (Figure. 1A). Cytokines are a highly diverse group of biomolecules which have a range of effects on other cells including the $CD4^+$ and $CD8^+$ T cell populations. The primary activating molecules are IL2, IL12 and IFNγ [7,8], which upregulate the activation marker CD69 and inhibitory marker CTLA-4 [9] on $CD8^+$ T cells and even other $CD4^+$ populations.

They also stimulate APCs to activate $CD8^+$ T cells. Complementarily, the $CD8^+$ cytotoxic T (T_C) cells mediate a direct lysis of infected cells through the release of cytotoxic proteins (Figure. 1B) such as perforin which induces pore formation in cells and granzymes which trigger apoptosis [10]. Subset-specific metabolism has also been shown to play a role in deciding T cell fate and effector function with $CD4^+$ T cells utilizing OXPHOS more than the $CD8^+$ subset [11]. $CD4^+$ T cells also exhibit greater glycolytic activity which was found to coincide with higher activation and induced mitochondrial reactive oxygen species [5,12].

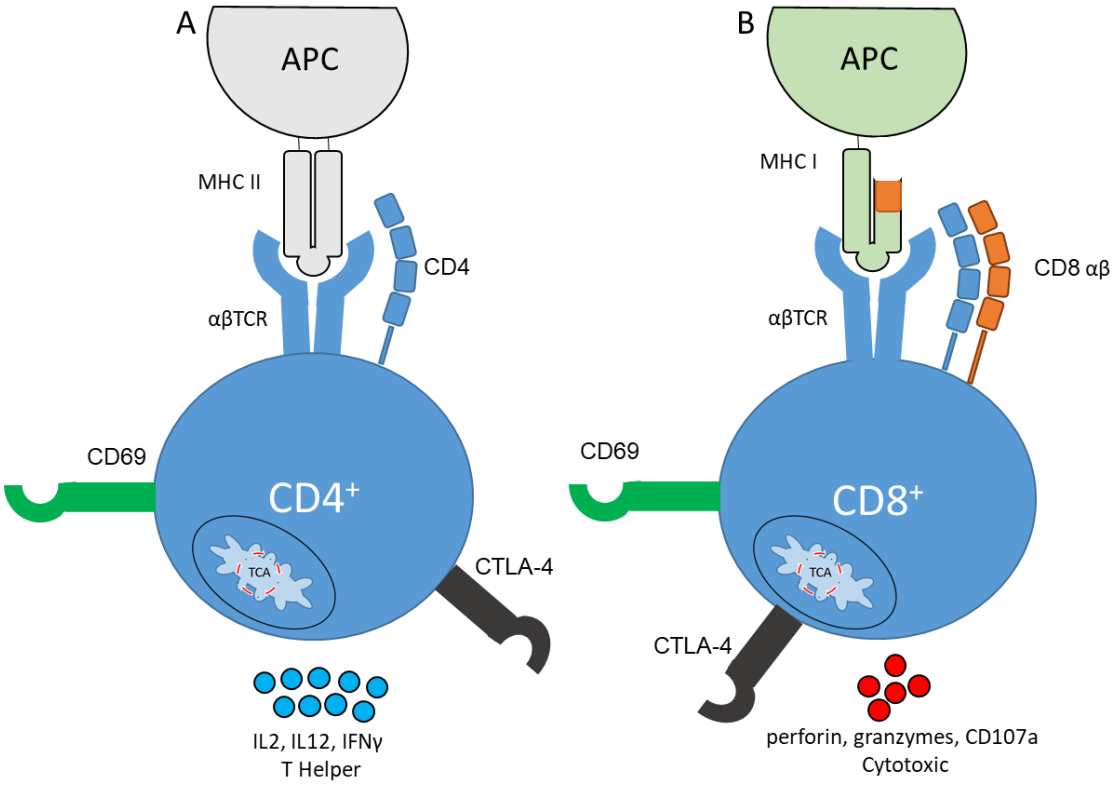

Figure 1: Comparative view of $CD4^+$ and $CD8^+$ T cell subsets and effector function.

A) $CD4^+$ T cells conjugate with class II MHC:Ag complexes present on APCs and differentiate into T_H cells which release stimulatory cytokines (IL2, 12 and IFNγ). B) In contrast, $CD8^+$ T cells associate with the class I MHC:Ag complex displayed on APCs and differentiate to T_C cells which produce cytotoxic molecules, such as perforin and granzymes that mediate the apoptosis of infected cells. Both differentiations involve a metabolic shift in the mitochondria to support the bioenergetics demand.

1.2 T cell activation

Naïve T cells (T_N) cells are energetically quiescent and do not perform notable immune function as presently known. However, they do require IL-7 as well as self-MHC signaling to remain responsive [13].

T_N cells display CD26L (L-selectin) as well as CD197 (Chemokine (C-C motif) Receptor (CCR-7)) [14]. These surface markers induce localization of T_N cells to secondary lymphoid organs such as the lymph nodes wherein they can encounter

APCs displaying MHC:Ag complexes. Induction of the TCR and costimulatory receptors propagates signals into an extensive signaling network, commencing with the initial phosphorylation of Immunoreceptor tyrosine-based Activator Motifs (ITAMs) on TCR ζ chains by Lymphocyte-specific protein tyrosine kinase (LCK) which activates the ITAMS [15] (Figure. 2 Step 1).

Additionally, LCK can phosphorylate Zeta-chain Associated Protein Kinase of 70 kDa (ZAP-70) which binds to phosphorylated ITAMs through SH2 domains. This leads to activation of the protein kinase function of ZAP-70 by phosphorylation of Tyr319 and subsequent trans-autophosphorylation of Tyr493 [16] which then serves to propagate the proximal signaling cascade. Activated ZAP-70 phosphorylates the Linker for Activation of T cells (LAT) at 9 discrete positions which begins the organization of the LAT signalosome. In parallel, ZAP-70 phosphorylates SLP76 at Tyr112, 128, and 145 [17] (Figure. 2 Step 2). LAT recruits PLCɣ1 (phospholipase Cɣ1) which hydrolyzes phosphatidylinositol 4, 5-bisphosphate (PIP3) to generate the second messengers inositol 3, 4, 5-triphosphate (IP3) and diacylglycerol (DAG) (Figure. 2 Step 3).

At this point the signaling splits into two distinct cascades (Figure. 2 Step 4). IP3 leads to the release of intracellular calcium as well as the influx of calcium *via* CRAC channels, which generates a calcium rich environment. Ca^{2+} binds to the calcium-modulated protein (calmodulin) which leads to phosphorylation of calcineurin [18]. This ultimately initiates the nuclear localization of the Nuclear factor of activated T-cells, cytoplasmic 1 (NFATc1) transcription factor by dephosphorylating NFATc1 and revealing nuclear localization sequences [19], leading finally to IL-2 upregulation and clonal expansion of the activated T cell [20]. Additionally, calcium-dependent signaling has been implicated in T cell adhesion following activation, as both calmodulin [18] and calcineurin [21] are shown to impact on T cell adhesion through ICAM upregulation, which is necessary for APC conjugation and further signaling.

In parallel, DAG recruits both Protein kinase C–theta (PKC-ɵ) and RasGRP to the cell membrane through their C1 DAG binding domains [22]. PKC-ɵ is an isoform of a family of proteins which, when activated, undergo a conformational change to perform their function [23] including the activation of nuclear factor-KB (NF-κB) signaling. RasGRP is a nucleotide exchange factor protein which exchanges GDP for GTP, leading to

RAS activation which induces signal transduction through the Ras–ERK–AP-1 pathway, ultimately activating AP-1 signaling [22] .

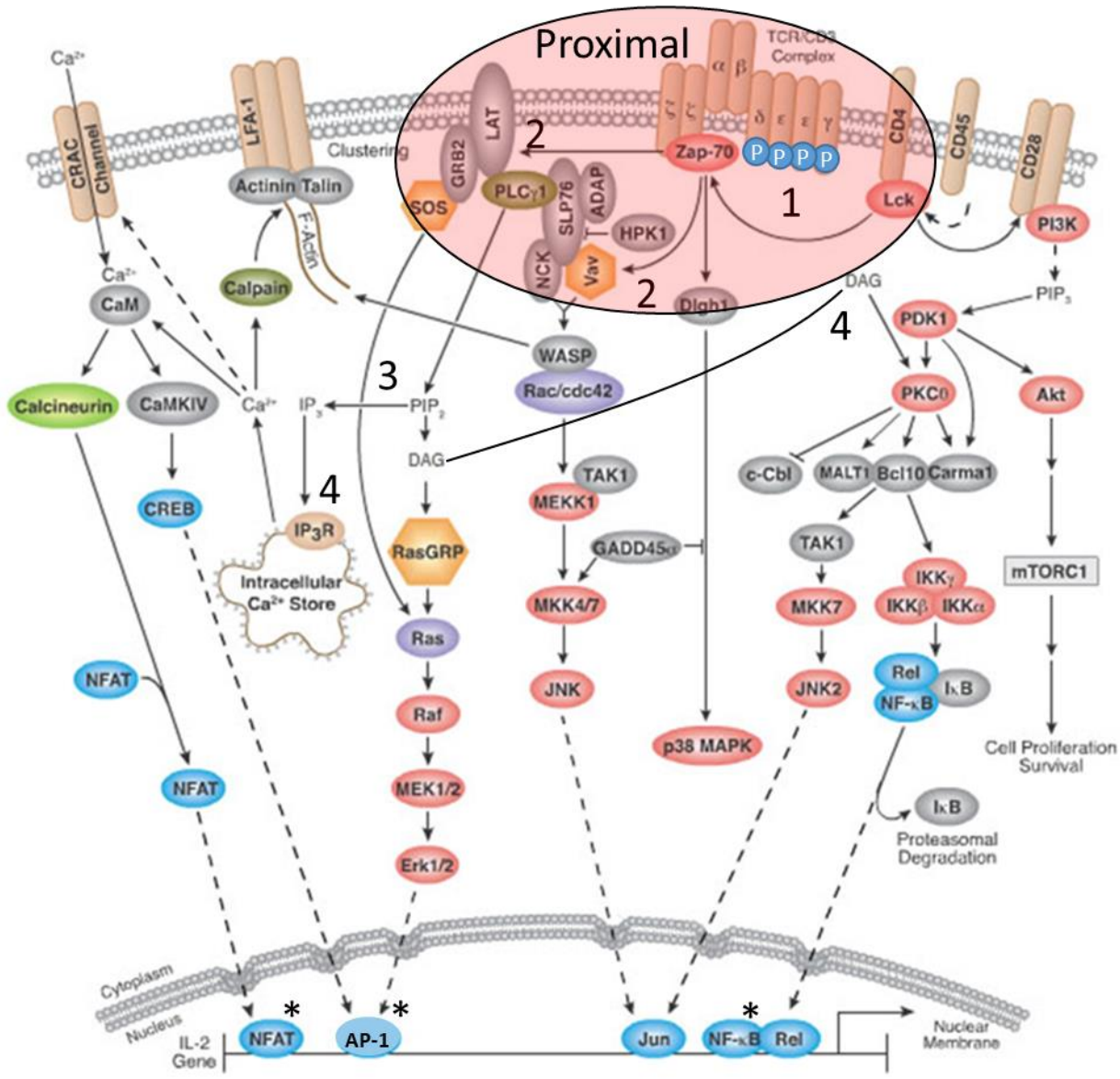

Figure 2: Conventional T cell activation signaling pathway.

1) LCK phosphorylates both ITAMS (in blue) and ZAP-70 to initiate proximal signaling. 2) ZAP-70 phosphorylates LAT and SLP76. 3) LAP recruits PLCγ1 which cleaves PIP_3 to IP_3 and DAG. 4) IP3 triggers calcium signaling leading to NFATc1 signaling, while DAG activates RAS-ERK-AP-1 signaling as well as NF-κB signaling (labelled with *).

1.2.1 Metabolic reprogramming in T cell activation

T_N cells exist in an energetically quiescent state until encountering an activating APC upon which T cells undergo a marked differentiation and clonal expansion (Chapter. 1.3) after 24h. To support this outcome requires in addition a metabolic shift mediated by the transcription factor Myc proto-oncogene protein (Myc) [24]. T_N cells shift away from FAO and pyruvate oxidation through the Tricarboxylic acid cycle (TCA) to glycolytic, glutaminolytic, and pentose-phosphate pathways (PPP) [25] (Figure. 3). Indeed, it has been found that similar to cancerous cells, activated T cells will forgo

conventional full oxidative metabolism of pyruvate *via* the TCA cycle in favor of the aerobic fermentation of pyruvate to lactate, termed aerobic glycolysis [26,27].

The primary reason for the preference of aerobic glycolysis is the increased generation of biosynthetic substrates necessary for cellular growth. This biogenesis requires the PPP [28] which catabolizes approximately 85% of the carbon in glucose biomolecules for producing nucleotides and amino acids [29]. The rate-limiting step in PPP is the accumulation of NADH. Aerobic glycolysis serves a facile pathway to oxidize NADH back to NAD+ which fuels the PPP.

Paradoxically, glutamine is upregulated by mitogen-activated protein kinase 1 (MAPK-1) [30] and is catabolized to α-ketoglutarate (α-KG) to feed into the TCA cycle which also provides reduced substrates for OXPHOS as well as adenosine triphosphate (ATP) [31]. However, it has been found that in the first 24h of cell growth mitochondrial metabolism remains indispensable [32].

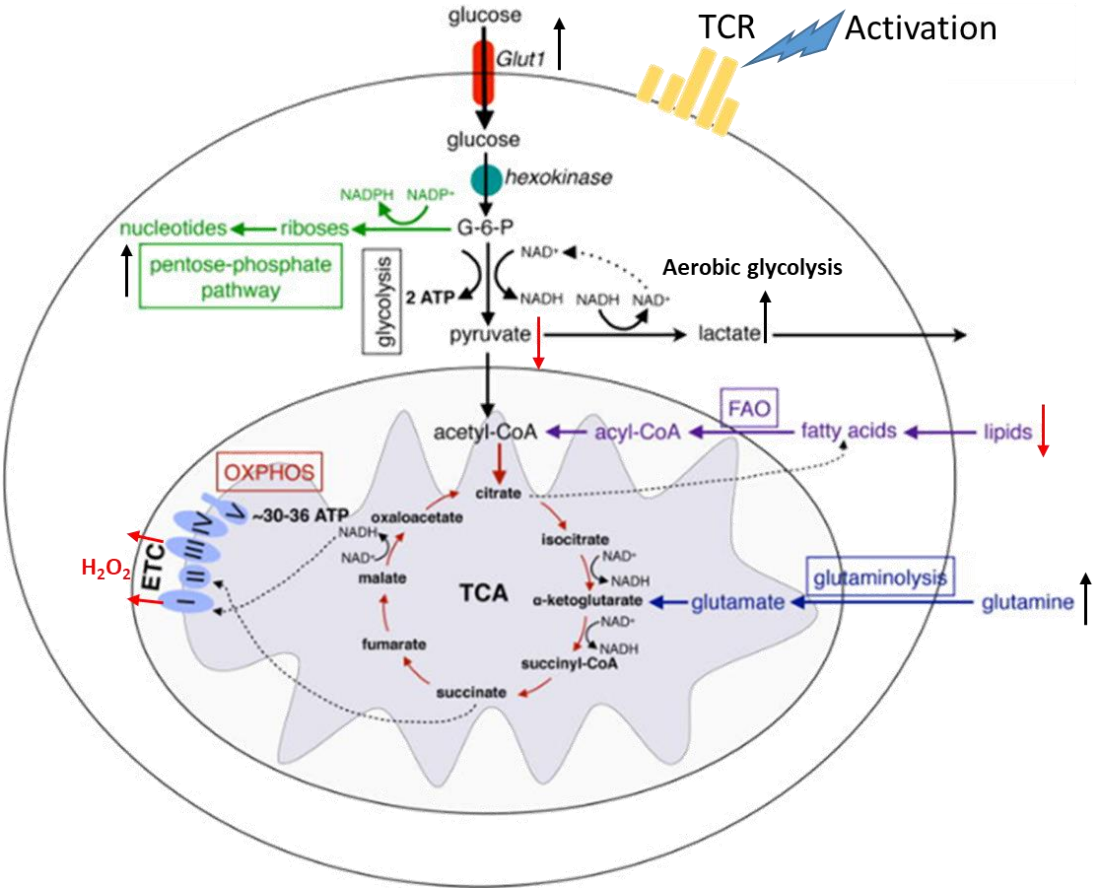

Figure 3: The metabolic shift in T cell activation.

TCR engagement by APCs trigger a metabolic shift which upregulates the PPP, glutaminolysis and glycolysis while downregulating pyruvate catabolism and FAO. Adapted from [33], H_2O_2 production is also increased following increased metabolic demand.

With this in mind, it has been demonstrated that mitochondrial metabolism is upregulated in T cell activation through Estrogen-related receptor-α (ERR-α) [34]. In fact, the inhibition of ERR-α was confirmed to downregulate T cell growth as well as function following both activation in knockout mice as well as treatment with small

molecules [32]. It is obvious that the mitochondria and oxidative phosphorylation still play a critical role in the metabolic shift even if not as the primary generator of ATP or biomolecules. Since it has been suggested that the production of reactive oxygen species (ROS), namely hydrogen peroxide (H_2O_2) by the electron transport chain (ETC) is implicated as a mitochondrial signaling cascade in T cell activation, this will be expanded on later (Chapter 1.5.1).

1.3 Mitochondrial function and mitochondrial reactive oxygen species in T cell activation

The mitochondria is the primary ATP-producing organelle It utilizes reduced substrates (NADH and $FADH_2$) to catalyze the export of these protons into the mitochondrial intermembrane space while shuttling the excess electrons along to the terminal acceptor molecule $\frac{1}{2}O_2$ to produce H_2O [35].

The machinery that accomplishes this is known as the mitochondrial electron transport chain (ETC), which is a system composed of 4 discrete protein complexes (Figure. 4). NADH: ubiquinone oxidoreductase (Complex CI) oxidizes NADH molecules from both the TCA cycle and the PPP, yielding NAD^+ and an electron. While the proton is pumped into the mitochondrial matrix the electron is stabilized by reducing the aromatic system in the flavin mononucleotide (FMN). It is then transported through 4 iron sulfur containing proteins (2Fe-2S), leading to protons being pumped into the intermembrane space (IMS) and ending with the reduction of coenzyme Q (Q) [36].

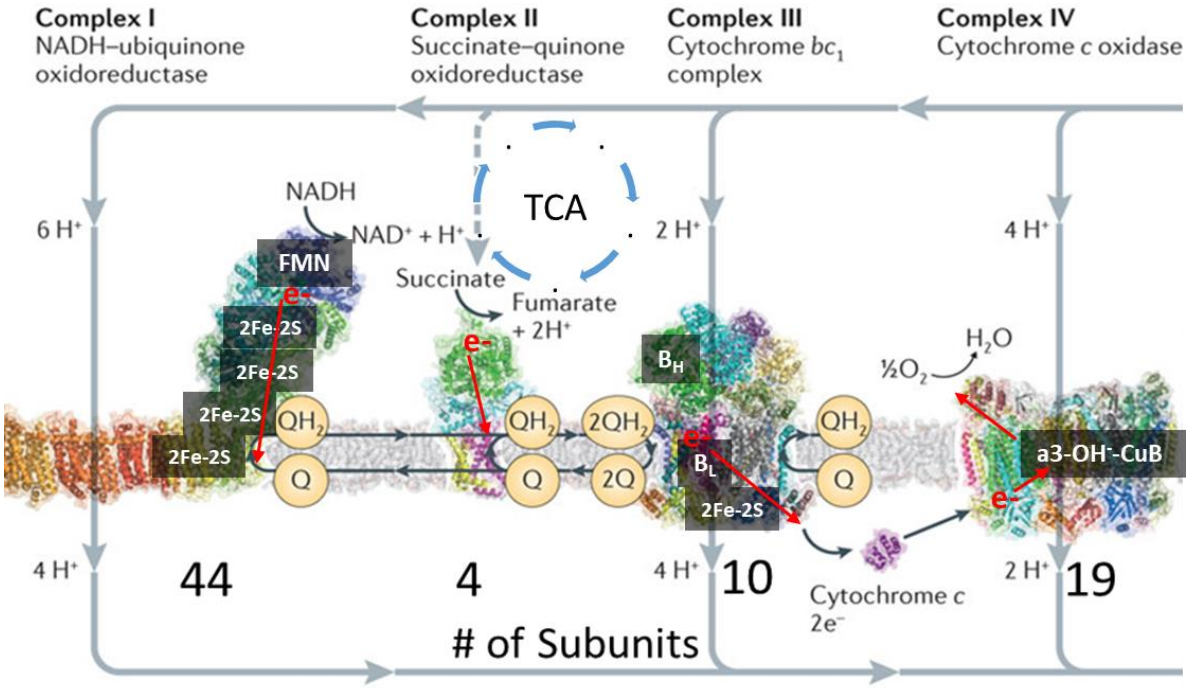

Figure 4: Structure of the mitochondrial electron transport chain (ETC).

The ETC is composed of CI (44 subunits), II (4 subunits), III (10 subunits) and IV (19 subunits). Electrons are transferred from CI and CII through CIII into CIV. Movement of electrons is highlighted in red. Adapted from [36].

Succinate-Quinone oxidoreductase (Complex CII) does very much the same thing with $FADH_2$ from the TCA cycle. It is situated in the inner mitochondrial membrane and links the TCA cycle with the ETC, where FADH is reduced to $FADH_2$ and then CII catalyzes

the oxidation of $FADH_2$ and subsequent reduction of Q to QH_2 [37]. Both of these complexes feed into the Cytochrome BC_1 (Complex CIII) which catalyzes the oxidation and regeneration of Q and the subsequent reduction of Cytochrome C (CytoC) to transfer electrons to the terminal acceptor. CIII utilizes a Q cycle in which 2 molecules of QH_2 bind to Cytochrome B units (B_L and B_H). B_L and a neighboring iron-containing protein remove the 2 electrons from $COQH_2$ and transfers 1 to B_H while the 2Fe-2S protein transfers the other to cytochrome C_1 which transfers the electron to CytoC. B_H transfers its electron to $CoQH_2$. This is only a half oxidation, so the cycle must go once again to regenerate the protein active sites [38].

The final protein is Cytochrome C oxidase (CIV) that catalysis the reduction of oxygen to water. CIV binds reduced CytoC and transfers the electron to cytochrome a_3 and Cu_B which form the active site of the enzyme. This coordinates a hydroxyl radical that is reduced and lost as H_2O. The enzyme is then regenerated by the reduction of a neighboring tyrosine and the hydroxyl radical is reformed on the binding of a second molecule of CytoC [39].

Recent advances in structural analysis have elucidated that the ETC does not exist as a stationary sequence of protein complexes as was conventionally thought. Instead, the electron transport chain is collated into a supercomplex [40] consisting of a single unit of CI, a dimer of CIII and one unit of CIV. This supercomplex is known as the respirasome ($CICIII_2CIV$) (Figure. 5).

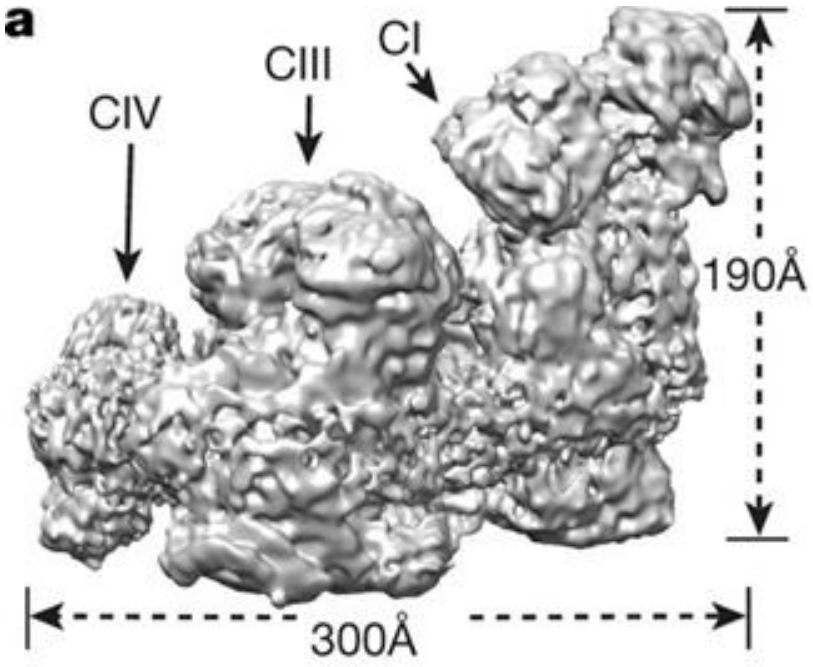

Figure 5: Structure of the major mitochondrial respirasome supercomplex.

The major mitochondrial respirasome is composed of a monomer of CI, a dimer of CIII and a monomer of CIV. Adapted from [40].

It has been hypothesized that the respirasome performs a number of different functions, including the compartmentalization of Q and CytoC to allow for more efficient electron transfer [41] and a subsequent reduction of H_2O_2 emanating from CI [42]Cooperatively, respirasome formation allows for greater stabilization of CI

assembly [43]. The respirasome dynamically associates and dissociates depending on the metabolic need to the cell [44]. This has implied that the respirasome has multiple formations as well as heterogeneous protein turnover [44,45].

1.3.1 Mitochondrial-derived reactive oxygen species

It is understood that while the respirasome is a highly efficient system, it is not infallible, as there is a certain percentage (1-2% of metabolic output) of electrons which are known to leak out [46]. Additionally, it is known that ETC output is coupled to the ratio of reduced substrates, to be exact, the ratio of $NADH/NAD^+$. This itself is dependent on cellular activity and metabolic demand as such that an increase in this ratio leads to an increase in electron leakage [47–51].

These free electrons are highly reactive and immediately come into contact with molecular oxygen [52] by virtue or aerobic oxidative phosphorylation, forming the superoxide ($O_2^{\cdot -}$) anionic radical. To prevent severe radical-induced oxidation of surrounding biomolecules, the mitochondrial matrix possesses a range of antioxidant proteins. The full complement of which includes the Superoxide dismutase [Cu-Zn] (SOD1) [53–55] which catalyzes the conversion of superoxide to hydrogen peroxide (H_2O_2). Additional protection is provided by peroxiredoxins (PRDX) 5 and 3 (PRDX3/5) [56], glutathione peroxidase 1 (GPX1) and glutathione (GSH), which all serve to react with H_2O_2 as well as reducing oxidized proteins. Moreover, the mitochondria also contain catalase [57,58] which converts H_2O_2 to water (Figure. 6). H_2O_2 is far less reactive due to its filled valence orbital and is much longer lived than the superoxide radical. As such, it is known as the primary form of mitochondrial ROS (mtROS) and will be referred to as such in this work.

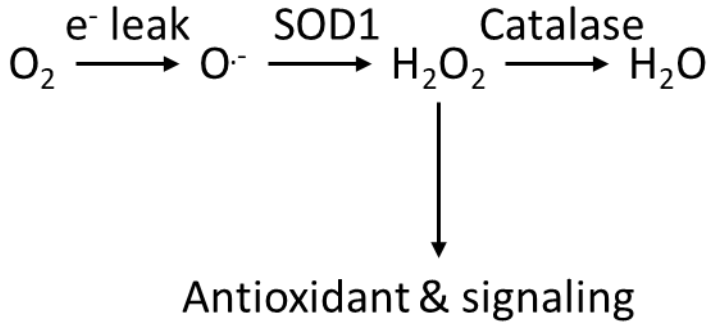

Figure 6: Conventional antioxidant pathway in mitochondria.

Electron leakage from the mitochondria converts molecular oxygen to the superoxide radical. SOD1 converts superoxide to hydrogen peroxide (H_2O_2), a number of antioxidant molecules react with hydrogen peroxide to prevent oxidative damage and catalase converts H_2O_2 to water. H_2O_2 is also utilized as a signaling molecule suggesting physiological effects.

The exact topology of electron leakage is under large debate but the consensus is that both CI [51,59,60] and CIII [61–64] have sites of electron leakage. Literature does seem to hint, however, that the leakage sites are most likely the interfaces between the respirasome component and the electron transfer protein that shuttles between either CI and CIII or CIII and CIV, namely, Q [65] or CytoC [66]. There are other sources of superoxide, for example the Dihydrolipoyl dehydrogenase (DLD) protein [67]. However, the impact they have on the gross mtROS produced is unknown.

1.3.2 T cells and oxidative stress

As previously mentioned, cells can produce ROS from metabolic processes. However, circulating T cells routinely encounter ROS. Phagocytic cells for example release ROS *via* their respiratory burst which has been shown to lead to hyper-responsiveness [68] in T cell activation with impaired calcium release, suggesting a PKC-ɵ like activation mechanism.

Cancerous cells also release significant amounts of ROS due to unregulated metabolic processes. This ROS has also been implicated in the immune evasion of cancer cells by dysregulating T cell metabolism from hypoxic and low glucose microenvironments which leads to reduced effector function and cell lifetime [69–71]. High oxidative stress from the ROS produced from cancer cell metabolism can yield downregulation of T cell activation through disruption of NF-κB signaling [72] as well as downregulation of calcium mobilization, thus reducing the effectiveness of calcineurin and NFATc1 transcription [73]. Taken together, it seems that cancer cells are capable of inducing immune cell dysfunction to improve immune response evasion.

1.4 ROS as secondary signals

Signaling molecules require a number of properties to be effective in their role [74]: They should be able to travel to any part of the cell, they should induce reversible modifications, and finally, they should have dedicated regulatory mechanisms in place. H_2O_2 possesses the correct polarity to diffuse through cellular membranes and enter the cytoplasm and is therefore ubiquitous. H_2O_2 is also under tight regulatory control *via* a diverse number of antioxidant enzymes (Chapter. 1.3.1). H_2O_2 can be dynamically produced as a cellular response to stimulus, accumulate in cell compartments as well as be degraded quickly to prevent oxidative damage (k_a/K_m =6-61 x $10^7 M^{-1}sec^{-1}$ for catalase/H_2O_2 reaction [75]). As such, H_2O_2 represents an ideal signaling molecule.

H_2O_2 reacts with cysteine residues which are resident in their anionic thiolate state (S-). This is determined by the pKa of the residue [76] and the pH of the aqueous media, which under physiological conditions can be assumed to be approximately 7. To generate a cysteine thiolate, the pKa of the thiol functional group must be below that of the pH of the aqueous media, with a pKa of 6 yielding a 90% thiolate population. **It should be noted that the vast majority of protein cysteine residues are in there protonated thiol form at physiological pH (pKa of thiol 8.3).**

The pKa of a thiol can be reduced by stabilizing the conjugate thiolate anion. This can be influenced by the presence of positively charged residues [77], distinct functional motifs such as α-helices [78,79] as well as intermolecular stabilization through hydrogen bonding [80]. This ensures that cysteine residues are selectively modified. An example are tyrosine phosphatases which possess a thiolate anion in the active site of the enzyme [81] as well as antioxidant proteins such as thioredoxins (TXN) and peroxiredoxins (PRDX) [79,82]. All of these proteins utilize catalytic thiolates for their activities.

Additional forms of thiolate reactivity can be seen with zinc-binding proteins, in fact the zinc binding motif has recently been implicated as a ROS-mediated method of oxidative stress response through Protein/nucleic acid deglycase DJ-1 (PARK7 –

HPS33 in bacteria) [83,84], wherein the zinc is excluded from the motif following high H_2O_2 concentrations and the coordinating thiolate forms protective disulfide bonds with other proteins to protect from oxidative damage.

It has been shown that mtROS is fine-tuned by the ratio of oxidative species over antioxidant molecules, thus subtle changes in the degree of oxidation for reactive thiolates can yield biological effects [85,86]. NFATc1 has also been shown to be fine-tuned by ROS where a low physiological level upregulated NFATc1 activity while too high levels inhibit NFATc1 [87]. Physiologically, excess H_2O_2 tends to be throttled by the action of the previously mentioned antioxidant molecules [63].

The progression of modification tends to follow a set order (Figure. 7). When H_2O_2 encounters a susceptible cysteine thiolate ($R\text{-}S^-$) a sulfenylation will occur from nucleophilic attack of the peroxide bond (O-O) in hydrogen peroxide by the formal negative charge on the thiolate, resulting in a sulfenic acid (R-SOH) [88]. Sulfenic acids are highly reactive and are known to be short lived [89]. At physiological levels of mtROS the sulfenic acid will oxidize further to a reversible disulfide bond (Figure. 7A) which is the main form of transient oxidative modification utilized for signaling [90].

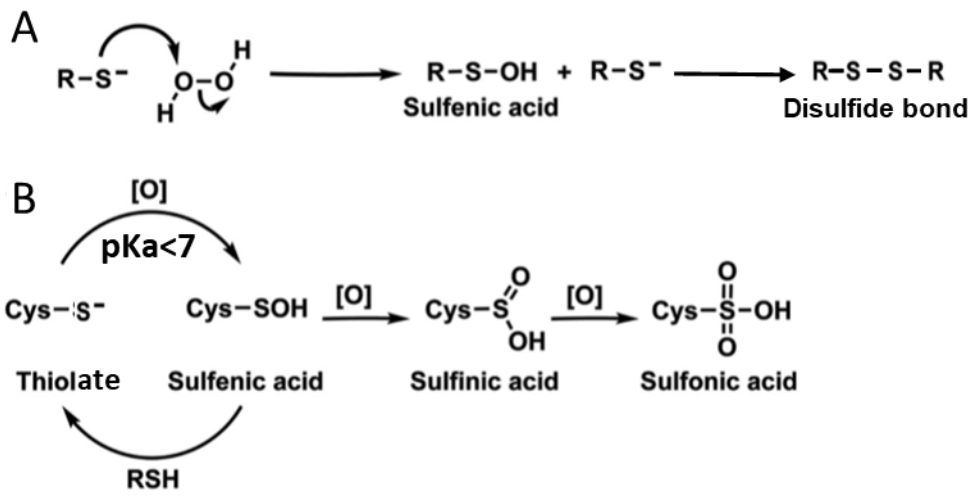

Figure 7: Chemical mechanisms of H_2O_2 signaling and oxidative stress.

A) The mechanism of thiolate nucleophilic attack of hydrogen peroxide and formation of a disulfide bond. B) Progression of thiol oxidation from thiol to sulfenic acid (reversible) through to sulfinic and sulfonic acids (irreversible). Adapted from [88]

Disulfide bonds mediate both intermolecular and intramolecular structural reconfiguration. Indeed it is known that disulfide bonds can induce transient protein complexation [91] for example CD3 subunits at the TCR can complex [92] through transient disulfide bond formation. Additionally the mitochondria utilize transient intermolecular disulfides to mediate import through the Mitochondrial Intermembrane space Assembly machinery (MIA) importer [93]. Structural reorganization of protein monomers can also be mediated by disulfide bonds, termed redox switches, such as the antioxidant proteins Hydrogen peroxide-inducible genes activator (OxyR) as well as TXNs [94].Irreversible oxidation constitutes oxidative stress and depends on the concentration of mtROS surrounding the protein thiolates. Under high ROS conditions (Figure. 8B) there is a continuation from sulfenic acid to sulfinic ($R\text{-}SO_2H$) and then

sulfonic (R-SO_3H) acids which are irreversible modifications and lead to protein degradation [95].

1.4.1 ROS and T cell activation

As mentioned previously, physiological T cell activation is propagated *via* conjugation of the T cell receptor and co-stimulatory receptors (Chapter. 1.2). It is known that, upon T cell activation, within 5 minutes [96] there is an increase in global oxidation of susceptible cysteine thiolates [97,98] and TCR receptor machinery is found to become oxidized, including ZAP-70 [99,100], Lck [101] and SHP-1 [102]. Additionally, since it is known that during T cell activation exogenous thiols [103] are imported into T cells from the APC, it is thought that ROS is necessary for formation and function of the immunological synapse [98] as well as T cell effector function [104].

Intracellularly, it was found that when the mtROS signal originating from complex III of the respirasome was downregulated, accomplished *via* deletion of the Rieske iron-sulfur-containing protein (2Fe-2S), then NFATc1 was unable to localize to the nucleus [61,105]. This was a major indicator of the ROS dependency of IL-2 upregulation and T cell clonal expansion. This observation was confirmed by an orthogonal study which determined the GSH dependence of T cell activation in which mtROS was again necessary for NFATc1 activity [106]. This suggested that in addition to the exposure of NFATc1 nuclear localization factors *via* the kinase activity of calcineurin, NFATc1 also requires additional ROS signaling (Figure. 8) to be able to localize, potentially through the action of structural disulfides.

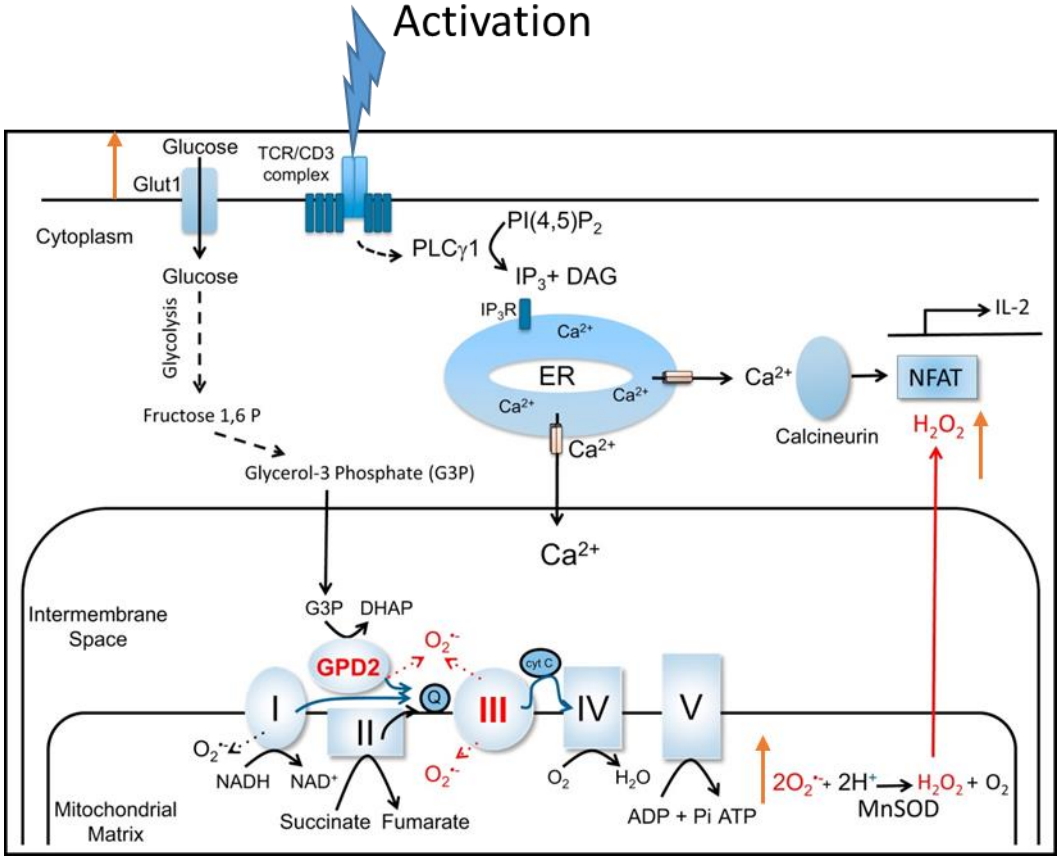

Figure 8: Overview of the mtROS dependency of T cell activation.

Additionally, NF-κB as well as AP-1 activation occurs, primarily through PKC-ɵ, which has been found to be modified by ROS through its zinc finger motifs [107]. Furthermore, evidence has suggested that hydrogen peroxide can inhibit tyrosine kinase phosphatases leading to increased phosphorylation and activation of Lck [108] in addition to direct oxidation.

As mentioned previously (Chapter. 1.2.1), T cells are unique in that they have a well-established metabolic shift phenotype which is prompted by T cell activation and involves a complex signaling pathway which upregulates glucose as well as macromolecule uptake and biogenesis. It has been seen in $CD4^+$ T cells that this metabolic shift phenotype is at least in part ROS-mediated. It was shown [106,109] that the Myc transcription factor which is responsible for mediating the majority of the metabolic shift in T cell activation was downregulated at the transcription level when the mtROS signal, in particular H_2O_2, was diminished by incubation with a membrane soluble antioxidant. Additionally, the transcription rates of its downstream protein gene sequences such as GLUT1, Hexokinase 2 (HK2), Pyruvate Kinase M2 (PKM2) and Lactose dehydrogenase A (LDHA) were downregulated as well.

It is becoming increasingly obvious that the metabolic shift in T cell activation is at least partly modulated by ROS, most likely as a fine-tuning mechanism in concert with phosphorylation and other post translational modifications (PTMs).

1.5 Proteomic analysis of Immune cells

Proteomics is the study of the changes in the protein complement of a system. Proteomics has become almost synonymous with liquid chromatography interfaced to mass spectrometry (LC-MS) [110]. The primary reason is the global degree of protein coverage one can obtain with LC-MS, unlike more classical methods such as western blotting which requires the use of specific antibodies raised against epitopes on proteins of interest [111].

LC-MS relies on the generation of peptides [110] from protein digests generated from the action of protease enzymes such as trypsin which cleaves proteins after every lysine and arginine and thus guarantees a uniform charge on the peptides. LC-MS allows for the unbiased identification and quantification of thousands of proteins through the sequencing of the amino acid sequence.

Peptides are separated based on their hydrophobicity, that is to say shorter charged peptides will elute quicker than longer or less charged peptides allowing for more identifications with MS due to less ion suppression [112], which is the masking of lower abundant peptides by more copious ions.

Following separation, peptides in the eluent are converted to gaseous ions. The most common method employed in global proteomics is electrospray ionization (ESI) in which aqueous peptides are sprayed as a fine mist from the tip of a needle under a strong current. ESI leads to evaporation of the solvent as well as ionization of the peptides [113]. The gaseous ions are then directed towards a detector in such a way that the mass and charge ratio (M/Z) can be determined (MS1).

Subsequently, ions can be fragmented into their amino acids which can be sequenced based on the characteristic masses, which are the so called b, y ions (MS2), allowing for the identification of ions quantified in the MS1 [114]. Furthermore, MS2 allows for the identification of amino acid modifications by adding the mass of the modification to that of the amino acid.

1.5.1 Proteomic analysis of cysteine PTMs

As mentioned previously (Chapter. 1.6) the major form of mtROS signaling is in the oxidation of cysteine to sulfenic acids and then transient disulfide bonds. LC-MS has been employed thoroughly in the analysis of disulfide bond formation in the generation of inter-protein bonding [115–117] including T cell signaling [100], as well as intra-protein characterization, although this is primarily done in the analysis of monoclonal antibodies (mAb's) [118,119].

More recently, proteomics has been used to characterize the global change in cysteine redox state. Studies have utilized thiol-specific isobaric tags in knockout clones to quantify and characterize the mechanistic impact of antioxidant depletion, such as GSNOR [120], or the targeted analysis of microglial cell lines [121] . However, the analysis of the global change in cysteine residue oxidation states in primary human T cells following activation-induced mtROS formation are currently undescribed.

1.5.2 Metabolic labeling technologies

A particularly versatile technique in the repertoire of LC-MS proteomics is the use of metabolic labeling technologies, pioneered with the introduction of heavy oxygen [122] into the proteome allowing for discrimination of two biological conditions. Following this came the development of Stable Isotope Labeling by Amino Acids in Cell Culture (SILAC) [123] that utilized isotopically labeled lysine and arginine amino acids, which provided a means to label all tryptic peptides and mix two samples together for quantitative LC-MS.

More recently was the development of bio-orthogonal non-canonical amino acid-tagging (BONCAT). This method involves incorporating non-canonical amino acids (NCAAs), such as a structural homolog of L-methionine into the cell [124]. In particular, the small molecule L-Azidohomoalanine (AHA), which competes with endogenous methionine for incorporation into newly synthesized proteins and contains an azide functional group. The azide can participate in a Cu^{1+} catalyzed cycloaddition reaction with an immobilized alkyne moiety (Figure. 9A) which allows for the enrichment of newly synthesized proteins (Figure. 9B).

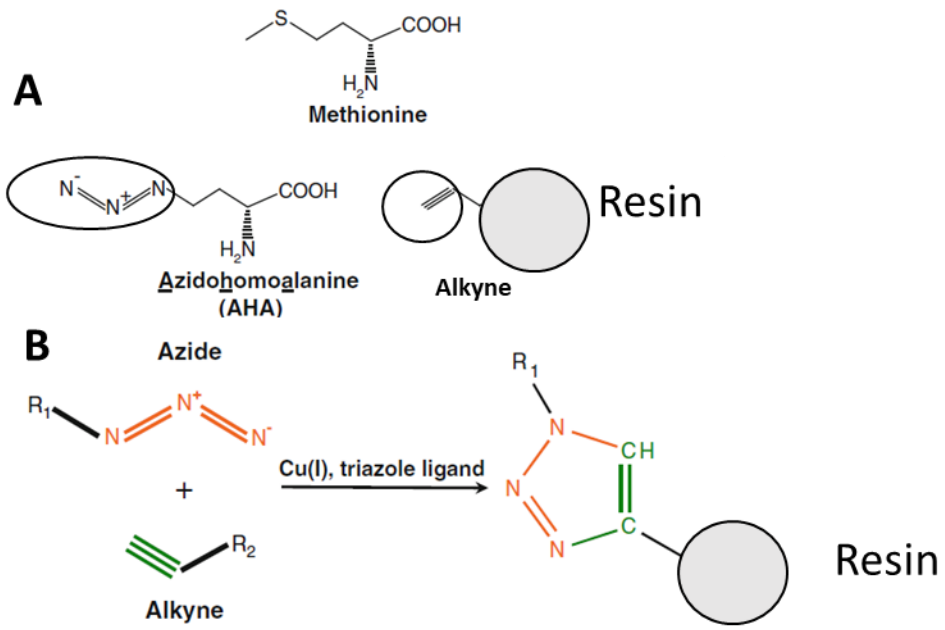

Figure 9: Mechanism of click enrichment of newly synthesized AHA labeled proteins.

A) Azidohomoalanine (AHA) is a homolog of methionine and reacts with alkynes. B) Azides and alkynes participate in a Cu^{1+} catalyzed cycloaddition reaction which allows for enrichment of AHA containing proteins

This technique allows for the quantification of the response to perturbation in a global proteome analysis. BONCAT has seen extensive use recently because of its specificity and reproducibility [125–127] in measuring protein synthesis kinetics under differing conditions.

2.0 Dissertation Aims

It is obvious that T cell activation is a highly complex metabolic activity which involves mobilization of numerous protein complexes and organelles. Additionally, sweeping changes in cell metabolism and transcription/translation processes are needed to achieve cell growth and clonal expansion. Finally, the effector function of T cells relies on a diverse complement of different PTMs.

H_2O_2 has becoming increasingly relevant in T cell activation. However, the majority of work done in this field has set out to probe the correlation between T cell activation phenotypes and ROS levels in the cell. This has classically relied on biochemical probing and the use of antioxidants or genetic manipulations (knock outs etc.). The disadvantage of these techniques is that they require an initial candidate to modulate or quantify.

As such, the major goals of this work will be to initially characterize the suitability of T cells as a model system to distinguish the ROS-mediated T cell activation from other confounding mechanisms such as calcium signaling. Following this, the global network of susceptible cysteine residues during T cell activation will be determined to elucidate the signaling pathways that mtROS modulates. As such, for the first time, I will utilize a global thiol switching technique (iodoTMT) to characterize the site-specific changes in cysteine residue oxidation following T cell activation.

Finally, I will determine which downstream processes this regulates by looking on which systems undergo significant protein turnover following activation in the presence and absence of the oxidative signal. In doing so I aim to correlate changes in cysteine redox state with subsequent change in protein level as well as analyze what types of cysteine oxidations are observed as irreversible oxidations that will inevitably lead to protein degradation.

The advantage of global proteomics is its ability to provide an unbiased global view on the overall impacts of T cell activation. Additionally, the use of biochemical tags allows for mechanistic data to be generated which has historically been lacking in the field. An example is NFATc1, which wile being well understood as ROS-sensitive has no current reactive site known.

This work should help elucidate areas of particular sensitivity to ROS when considering T cell activation in regard to susceptible thiolate residues, and thus will allow to determine whether any discrete protein networks are impacted. The ROS sensitivity of the respirasome is of particular interest, considering it is the major site of ROS release in T cells. Therefore, respirasome plasticity and turnover during T cell activation will be especially investigated.

3.0 Methodology

3.1 Equipment and Software

3.1.1 Equipment

Nano LC-MS

UltiMate 3000 RSLCnano, Thermo Fisher Scientific (Dionex)

Orbitrap Fusion™ Tribrid™, Thermo Fisher Scientific

LTQ Orbitrap Velos Pro™ Fourier Transform, Thermo Fisher Scientific

ÄKTA purifier UPC10, GE Healthcare

Bioruptor® Plus sonicator, Diagenode

GC-MS

Finnigan GCQ, Thermo Fisher Scientific

Flow cytometry

BD Accuri C6 Flow Cytometer, Accuri Cytometers Inc.

BD LSR II SORP Cytometer, BD Biosciences

Fluorescent Microscopy

Inverted microscope Ti Eclipse, Nikon

Cell Culture

Innova CO-170 CO_2 incubator, New Brunswick Scientific

CKX41 Inverted Microscope, Olympus Life Science

RC10101 SpeedVac, Sorvall

Sorvall discovery M120 SE Centrifuge, Sorvall

Eppendorf ThermoMixer C, Eppendorf

3.1.2 Software

LC-MS Proteomics

Chromeleon 6.8, Dionex

Xcalibur software suite 3.0.63, Thermo Scientific

Rawmeat 2.1.1007, Vast Scientific

ProteomeDiscoverer 2.2, Thermo Scientific

Mascot Server 2.4.2, Matrix Science

Flow Cytometry

BD Accuri CFlow Sampler 1.0.264.21, Accuri Cytometers Inc.

BD Accuri CFlow Analysis Plus 1.0.264.21, Accuri Cytometers Inc.

FACSDiva 6.1, BD Biosciences

FlowJo 10.0.7, TreeStar Inc.

Fluorescent Microscopy

NIS-Elements AR 4.30.20, Nikon

Data Analysis

Inkscape 0.92.4

Microsoft Excel 2010, Microsoft

Perseus 1.6.2.3

RStudio 1.1.456.0, RStudio Inc

3.2 Reagents

3.2.1 Suppliers

If not indicated otherwise, all used chemicals were obtained from the following companies: JT Baker (Phillipsburg, NJ, USA), Life Technologies/Invitrogen/Gibco (Carlsbad, CA, USA), Sigma Aldrich/Fluka (St. Louis, MO, USA), Carl Roth GmbH (Karlsruhe, Germany), BD Biosciences (Franklin Lakes, NJ, USA), Miltenyi (Bergisch Gladbach, Germany) and GE healthcare (Chicago, IL, USA). All buffers and solutions were prepared with MilliQ water, obtained from a MembraPure Astacus purification system (Membrapure GmbH, Bodenheim, Germany). All media and buffers used for cell culture were sterilized by filtering through Steritop Filter Units (Merck Millipore, Burlington, MA, USA)

3.2.2 Cell cultures

PBMCs were isolated from the peripheral blood of healthy human donors. Buffy coats were kindly provided by the Deutsches Rotes Kreuz (NSTOB Springe). Jurkat E6.1 from acute T cell leukemia were purchased from Manassas, VA, USA) ATCC TIB-152™.

3.2.3 Cell culture media

Table 1: Cell culture media with components

Media	Components
Primary cell and Jurkat Growth Media	RPMI1640 + 10% fetal bovine serum (FBS) + 2mM L-Glutamine
Primary cell starvation media	RPMI1640 – (L-methionine) + 10% dialysed FBS

Primary cell Azidohomoalanine (AHA) media	RPMI1640 – (L-methionine) + 10% dialysed FBS + 2mM AHA

3.2.4 Solutions and buffers

Table 2: Buffers and solutions with components

Buffer and solutions	
10x Phosphate buffered saline (PBS)	1.37M NaCl, 27mM KCl, 100mM Na_2HPO_4, 20mM KH2PO4 (pH 7.4)
1xPBS:	100ml 10xPBS Up to 1L with 18.2MΩ water
Peripheral blood mononuclear cell (PBMC) isolation buffer	4% FBS in 1xPBS
Denaturing Alkylation Buffer (DAB)	6M urea, .5% SDS w/v, 10mM Ethylenediaminetetraacetic acid (EDTA), 200mM tris-HCl (pH 8.5) +2µl/ml Benzonase
Dissolution buffer	0.5M TEAB pH 8.0
Reducing agent 1	50mM Tris(2-carboxyethyl)phosphine (TCEP)
Reducing agent 2	50mM Dithiothreitol (DTT)+B18B19AA15:B18
Alkylating agent 1	200mM methyl methanethiosulfonate (MMTS)
Alkylating agent 2	200mM Iodoacetamide (IAA)
Urea lysis buffer	8 M urea, 200 mM Tris pH 8, 4% CHAPS, 1 M NaCl
Digestion buffer	100 mM Tris, pH 8/2 mM CaCl2/10% acetonitrile (ACN)
Urea wash buffer	8 M urea/100 mM Tris, pH 8
SPE cartridge wetting/washing buffer	3% ACN in 0.2% trifluoroacetic acid (TFA)
SPE cartridge elution buffer	60% ACN in 0.2% TFA
bRP buffer A	1% ACN in 10 mM Ammonium hydroxide
bRP buffer B	90% ACN in 10 mM Ammonium hydroxide
Nano LC-MS buffer A	0.1% formic acid (FA)
Nano LC-MS buffer B	80% ACN in 0.1% FA
Fluorescence-activated cell sorting (FACS) Buffer	2%FBS + 2mMEDTA in 1xPBS

phorbol 12-myristate 13-acetate (PMA) stock solution	10µg/ml in ethanol (etOH) diluted
2',7'-dichlorodihydrofluorescein diacetate (H2DCFDA) stock solution	5mM H2DCFDA in anhydrous dimethylsulfoxide DMSO
Fluo-4FF stock solution	5mM Fluo-4FF in anhydrous DMSO
Mitotracker red stock solution	1mM MitoTracker Red CMXRos in anhydrous DMSO

3.2.5. Antibodies

Table 3: Antibodies used for flow cytometry experiments

Antigen	Clone	Conjugate	Manufacturer	Catalogue number	Dilution
CD3	OKT-3	BV605	BioLegend	317322	1:50
CD4	OKT-4	PerCP	Miltenyi Biotec	130113228	1:50
CD8	RPA-T8	PE	BD Bioscience	555367	1:50
CD69	REA824	APC	Miltenyi Biotec	130112614	1:50

3.3 Cell Biology

3.3.1 Cell culture

Jurkat E6.1 cells were maintained in Primary cell and Jurkat growth media. Freshly isolated human PBMCs were cultured in Primary cell and Jurkat growth media. All cell types were cultured in culture flasks (Nunc) at a temperature of 37°C with 5% per volume CO2, at a maximal density of 1×10^7 cells per mL (PBMCs) and 1×10^6 cells per mL (Jurkat E6.1).

3.3.2 Quantifying rate of respiration by GC-MS

To measure the increase in cellular respiration Jurkat E6.1 T cells were suspended in Primary cell and Jurkat Growth Media at a cell density of $1x10^7$ cells/ml and placed in airtight open-top screw caps (Thermo Scientific), cells were incubated for 1h in the presence of or absence of 10ng/ml PMA at 37^{o}C. Following incubation vials were placed in the autosampler of a … GC-MS and sampled in the headspace area above the liquid surface. Molecular oxygen consumption and CO_2 production were measured and quantified as the AUC of the peak belonging to the M/Z of O_2 and CO_2.

3.3.3 PBMC isolation and cell sorting

Buffy coats from healthy human donors were kindly provided by the Deutsches Rotes Kreuz (NSTOB, Springe). All donors were tested negatively for HIV, HBV and HCV. Peripheral blood obtained from one buffy coat was equally distributed to 50 mL falcon tubes and diluted with 7.5 mL isolation buffer. Isolated buffy coats were layered over

14 mL of Ficoll separating solution. The tubes were centrifuged at 2000 rpm for 25 minutes (deceleration - 1) at room temperature (RT). Following centrifugation, the PBMC layer was extracted and the cells were spun down at 1600 RPM for 10 minutes (deceleration – 8) at RT and suspended with 50 mL isolation buffer, the washing was repeated twice. The cell suspension was filtered to remove aggregates and debris (Cell Strainer 40 µm, Falcon). Subsequently, PBMCs were spun down at 1600 RPM for 10 minutes at RT, suspended in RPMI medium at a concentration of 1×10^7 cells per mL and processed within one day after isolation

3.3.4 Fluorescence activated cell sorting of primary human $CD4^+$ T cells
For cell sorting, PBMCs were spun down at 300xg for 10 minutes at RT and washed in FACS buffer. Following which, PBMCs were suspended to a cell density of $2x10^8$ per ml and stained with $CD3^+$ (BV605) and $CD4^+$ (PerCP) antibodies at a dilution of 1:50 cells were incubated at 4°C for 15 minutes. Following which, cells were washed in FACS buffer twice 300xg for 10 minutes at 4°C and suspended in FACS buffer. $CD3^+CD4^+$ T cells were gated on and were then sorted with the kind help of Dr. Lothar Gröbe (HZI, Braunschweig)

3.3.5 Immunofluorescence analysis of $CD4^+$ T cell ROS production
Sorted cells were spun down at 300×g for 10 minutes and cultured overnight in RPMI complete medium. Cells were first incubated with mitotracker red (1:10000 dilution) and 5µM H_2DCFDA (1in1000 dilution) for 30 minutes in the dark to label the mitochondria as well as load cells with H_2DCFDA. Following incubation, cells were washed with PBS before being adhered to poly-L-lysine for 10 minutes. Cells were activated with 10ng/ml PMA (1 in 1000 dilution) in media added dropwise and images were taken after discrete time periods. Microscopy was performed on an inverted TI eclipse microscope by Nikon (Minato City, Tokyo, Japan) using a conventional Intensilight epi-fluorescence Illuminator by Nikon analysis was performed using NIS-Elements AR software by Nikon.

3.3.6 Flow cytometric analysis of T cell activation and oxidation
To measure ROS and activation PBMCs or isolated $CD4^+$ T cells were suspended in Primary cell and Jurkat Growth Media at a cell density of $1x10^7$ (PBMCs) or $1x10^6$ ($CD4^+$ T cells), respectively, containing 5µM H_2DCFDA in anhydrous DMSO, and were incubated for 1h with 10ng/ml PMA at 37°C. After activation, cells were suspended (600xg, 10 minutes, 4°C) in 100µl FACS and incubated with CD69 (APC) only in the case of isolated cells or, in the case of PBMCs, CD69 (APC), CD3 (BV605), CD8 (PE) and CD4 (PerCP) for 15 minutes at 4°C in the dark. Cells were washed in FACS before being suspended (600xg, 10 minutes, 4°C) in 100µl FACS for flow cytometry.

Analysis of PBMC and isolated $CD4^+$ T cell activation and ROS production was carried out on a BD Accuri C6 Flow Cytometer (Ann Arbor, MI, USA). The flow cytometer operating software was Accuri CFlow Sampler, the compensation matrix was generated with BD Accuri CFlow Analysis Plus. BD CFlow Analysis Plus was also used to analyses data. Additionally, data was acquired on a BD LSR II SORP cytometer (Franklin Lakes, NJ, USA), operated by FACSDiva software. Data analysis was then carried out by FlowJo.

3.4 Thiol-selective (IodoTMT) labelling of T cell proteins

To characterize cysteine oxidation FACS sorted $CD4^+$ T cells were spun down (300xg, 10 minutes, RT) and suspended in 1ml Primary cell and Jurkat Growth Media and plated in a 24 well plate at a cell density of $1x10^7$ cells per ml. Cells were either activated with 10ng/ml PMA or left unstimulated for 1 hour at 37ºC. Cells were washed twice in ice cold PBS (300xg, 10 minutes, 4ºC) before being transferred to 1.5ml Lo-Bind Eppendorf cups and lysed in ice cold DAB buffer containing one distinct Thermo Fisher iodoTMT labels per condition (active vs unstimulated) for example 128 for the unstimulated sample and 129 for the active sample for 10 minutes with sonication.

Lysates were then incubated at 37ºC with shaking in the dark for 2 hours with shaking in an Eppendorf ThermoMixer allowing all free cysteine residues (R-SH) to be alkylated by the first iodoTMT label. Following initial labelling, the reaction was quenched with the addition of 400µl of ice cold acetone and incubated overnight at -20ºC to precipitate protein and remove excess iodoTMT salt.

Protein was pelleted for 30 minutes at 13,000g, -4ºC and washed once with ice cold acetone carefully to not disturb the cell pellet, excess acetone was allowed to evaporate at RT with open Eppendorf cups being loosely covered with aluminum foil. Following evaporation, the protein pellet was solubilized with DAB buffer containing 5mM TCEP for 10 minutes at 37ºC to reduce any cysteine residues, which had undergone transient disulfide bond formation (R-S-S-R') back to an unoxidised thiol or free cysteine (R-SH).

Following reduction an iodoTMT label with a different reporter mass for each condition (active vs unstimulated) was added for example 130 for unstimulated and 131 for active conditions, lysates were incubated again at 37ºC for 2h in the dark with shaking on an Eppendorf ThermoMixer.

The reaction was quenched a second time with the addition of 400µl of ice cold acetone and incubated for 4 hours at -20ºC, to remove excess iodoTMT salt. Protein was pelleted for 30 minutes at 13,000g -4ºC and washed once with ice cold acetone, excess acetone was allowed to evaporate at RT with open Eppendorf cups being loosely covered with aluminum foil. Following evaporation, the protein pellet was dissolved in 100µl Dissolution buffer and active and unstimulated conditions were mixed and trypsin was added to a ratio of 1:20 of trypsin: protein, samples were incubated o/n at 37ºC with shaking on an Eppendorf ThermoMixer.

3.4.1 ZipTip clean-up of peptide samples

Following protein digestion a 5% volume of the peptide solution was cleaned up with a reverse phase (C18) ZipTip from Eppendorf. The Peptide sample was acidified with the addition of 1µl 1M hydrochloric acid (HCl). ZipTip pipette tips were first wet with 10 µl of SPE cartridge wetting/elution buffer with 10 uptake and dispensing strokes of the pipette before being equilibrated with 10 µl SPE cartridge washing buffer with 10 uptake and dispensing strokes of the pipette. Peptide samples were loaded onto the ZipTip with 20 slow uptake and dispensing strokes of the pipette.

Peptides were washed with 10 µl SPE cartridge washing buffer with 10 slow uptake and dispensing strokes of the pipette, peptides were eluted into a new Eppendorf with

10 µl SPE cartridge wetting/elution buffer with 10 fast uptake and dispensing strokes of the pipette.

Peptide samples were dried in a SpeedVac and suspended in 10 µl Nano LC-MS buffer A before being injected onto an UltiMate 3000 RSLCnano coupled to an Orbitrap Velos Pro MS to determine digest efficiency as well as peptide amount.

3.4.2 Solid phase extraction (SPE) of peptide samples

Following confirmation of a complete digest the peptide samples are dried and suspended in 200 µl SPE cartridge washing buffer. Hydrophilic lipophilic balance (HLB) 1CC (10mg) SPE columns from Waters corporation (Milford, MA, USA) were first wet with 200 µl SPE cartridge wetting/elution buffer followed by equilibration with 200 µl SPE cartridge washing buffer.

Suspended peptides were then loaded onto the cartridge and allowed to flow through the cartridge. Following loading, the samples were washed with 200 µl SPE cartridge washing buffer, peptides are then eluted with 100 µl SPE cartridge wetting/elution buffer into a 1.5ml Eppendorf, and samples were dried in a SpeedVac.

3.4.3 bRP fractionation of iodoTMT labelled samples

Peptide samples were suspended in 300µl of bRP buffer A and loaded manually into a 500µl injection loop. Samples were separated on an ÄKTA purifier UPC10 consisting of a INV907 column switcher, a M925 UV flow cell coupled to a Frac-950 fraction collector under high pH reverse phase conditions. Fractionation was performed on a Zorbax 300 extend 25cm x 9.4mm I.D, 5 µm, 300Å semi preparative column (Agilent Technologies, CA).

The Zorbax 300 column was maintained at 30^{o}C and a flow rate of 1ml/min was used. Peptides were separated using a binary solvent system consisting of bRP buffer A and bRP buffer B. They were eluted with a gradient of 5-28% B in 50 minutes, 26-70% B in 4 maintained at 70% B for 5 minutes and finally re-equilibrated to 5% B in 4 minutes. 100 1ml fractions were collected into 2ml Eppendorf cups every minute.

Fractions were dried in a SpeedVac until a small volume remained, following which samples were concatenated to 13 samples by mixing every 12th fraction together. Samples were again dried down and suspended in 10 µl Nano LC-MS buffer A before being injected onto an UltiMate 3000 RSLCnano coupled to an Orbitrap Fusion MS for analysis.

3.4.4 nLC separation of iodoTMT peptides

Peptides were separated on an UltiMate 3000 RSLCnano system consisting of a NCF3500PS pump module, a WPS3000 Autosampler and a TCC-3000S column compartment under reversed phase conditions, interfaced via Electrospray ionization (ESI) to an Orbitrap fusion tribrid MS. Peptides were washed under non-eluting conditions on a Thermo Fisher Acclaim PepMap 2cm x 100 µm I.D. 5µm, 100 Å guard column (Waltham, MA, USA) for 6 minutes, column was maintained at 60^{o}C with a 1ml/min flow rate of NanoLC buffer A before eluting on to the analytical flow path by increase to 6ml/min flow rate.

Analytical separation was performed using an Acclaim PepMap RSLC 50 cm x 75µm I.D. 2µm, 100 Å column (Thermo Scientific, MA). Column was maintained at 60^{o}C and a flow rate of 200nl/min was used. Peptides were separated using a binary solvent system consisting of Nano LC-MS buffer A and Nano LC-MS buffer B. They were eluted with a gradient of 3.7–31.3% B in 120 min, 31.3–62.5% in 45 min, 62.5–90% B in 8 min, maintained at 90%B for 5 minutes and finally re-equilibrated to 3.7% B in 18 min.

3.4.5 MS analysis of iodoTMT peptides

Eluting peptides were interfaced via a fused silica Picotip 5 cm x 10 µm ID emitter (NewObjective) for ESI (spray voltage, 2 kV; heated capillary, 300 °C) using a nano-electrospray source (Thermo Scientific). MS spectra were acquired in the positive ion mode on the orbitrap with an m/z range of 375–1,700 with R of 120,000 at m/z 200. AGC target was 4×10^5 with an injection time of 50 ms. The top 50 most intense precursors were selected for higher-energy collisional dissociation (HCD) again on the orbitrap for high resolution MS2 spectra of iodoTMT reporter tags with a collisional energy of 32% MS2 parameters were as follows: charges= 2-4^{+}, R= 15,000 at m/z 200; AGC, 5×10^4 with an injection time of 60 ms.

3.4.6 Identification of iodoTMT labelled peptides

For peptide identification Mascot [128] integrated into proteome discoverer (v2.2 Thermo Fisher Scientific, Ma) was used to search peak lists against the H. sapiens proteome (UniprotKB canonical set) iodoTMT sixplex reporter tags (126.127725, 127.124760, 128.134433, 129.1311468, 130.141141, 131.138176) were chosen as quantification method. IodoTMT modification (329.226595) was set with cysteine residue specificity, and up to 5 modified amino acids per peptide were allowed.

Trypsin/P was set as the enzyme with a specific digest method with up to 1 missed cleavage site allowed. Mass tolerance was set at 7ppm for precursor identification and 50mmu for fragment masses, variable modifications were set as oxidation of methionine and acetylation of N terminal peptides. PSM selection criteria was set at a FDR of 0.01 for only high confidence matches with a minimum peptide length of 6 amino acids, the decoy database was deployed in concatenated mode. **Note**: The data was reevaluated following submission of this thesis and can be seen at https://doi.org/10.1101/2020.06.15.152116

3.5 Protein Turnover utilizing non-canonical amino acids

PBMCs were isolated from healthy donors and suspended at a cell density of $1x10^7$ per ml in Primary cell and Jurkat Growth Media. The cells were counted and the sample cells are split into 4 conditions at $1x10^8$ cells per ml, with and without 10ng/ml PMA as well as with and without 1mg/ml catalase. Samples were incubated in a 24 well plate for 30 minutes at 37^{o}C, after which a sample of cells intended for flow cytometry ($1x10^6$ per condition) were isolated and plated in a 96 well plate and incubated with 5µM H_2DCFDA (1 in 1000 dilution) and incubated for a further 30 minutes.

Following 1h incubation, PBMCs were spun down (300xg, 10 minutes, 4^{o}C) and suspended in 50µl FACS buffer containing CD3 (BV605), CD4 (PerCP) and CD69 (PE) all with a 1 in 50 dilution and incubated in the dark at 4^{o}C for 15 minutes.

Cells were washed once in FACS buffer (300xg, 10 minutes, 4ºC) and suspended in 100µl FACS buffer before being loaded onto an LSR-II SORP cytometer to determine activation state, ROS production and catalase quenching.

3.5.1 Isolation of Activated $CD4^+$ T cells

Following successful ROS generation and catalase quenching, $1X10^8$ PBMCs per condition were taken for negative selection using the Miltenyi CD4+ T Cell Isolation Kit, PBMCs were spun down (300xg, 10 minutes, 4ºC) and suspended in 400 µl FACS buffer. To each condition 100 µl of CD4+ T Cell Biotin-Antibody Cocktail was added and cells were incubated in the dark at 4ºC for 5 minutes. Following binding of the antibodies, 300 µl of FACS buffer were added to each condition followed by 200 µl of CD4+ T Cell MicroBead Cocktail.

Cells were incubated in the dark at 4ºC for 10 minutes, during which an LS magnetic separation column from Miltenyi (Bergisch Gladbach, Germany) was equilibrated with the addition of 3ml FACS buffer per column, the columns were secured to a QuadroMACS™ Separator. Cell suspensions were loaded onto the columns and allowed to flow through, columns were then washed with 3ml of FACS buffer, and both fractions were kept as the untouched $CD4^+$ T cells. Cells were suspended in Primary cell and Jurkat Growth Media and rested overnight at 37ºC.

3.5.2 Metabolic Labelling of $CD4^+$ T cells with AHA and Cu catalyzed click purification

Isolated $CD4^+$ T cells were spun down (300xg, 10 minutes, RT) and suspended at a cell density of $1x10^6$ in Primary cell starvation media. Cells were starved for 1h at 37ºC before being spun down (300xg, 10 minutes, RT) and suspended in Primary cell AHA medium and left overnight to pulse in the non-canonical amino acid.

Following incorporation cells were washed twice in ice cold PBS (300xg, 10minutes, 4ºC) and suspended in 425µL Urea Lysis Buffer and vortexed and incubated on ice for 10 minutes and then lysed in a Bioruptor (4 cycles 30 seconds high energy). Lysates were mixed with 100 µL of alkyne-immobilized resin and incubated on a shaker overnight.

Resin was centrifuged (100xg, 1min, RT) and suspended in 1ml MQ water and centrifuged again before being suspended in 500 µL of SDS wash buffer (from kit) containing 10mM DTT, DTT functioned to reduce cysteine disulfide bridges, the alkyne resin was incubated at 70ºC for 15 minutes and then cooled to RT in an Eppendorf ThermoMixer.

The alkyne resin was centrifuged (100xg, 1 min, RT) before being suspended in 500 µL 40mM Iodoacetamide for 30 minutes in the dark at RT to alkylate free thiol groups (R-SH).

Resin was then transferred to a gravity flow cartridge and washed 5 times with SDS wash buffer (From kit) and 8 times with both Urea wash buffer and then 20% ACN. Resin was transferred to a 1.5ml Eppendorf and suspended in 250 µL digestion buffer 0.5 µg trypsin was added and the resin was incubated overnight at 37ºC.

The supernatant was transferred to a new Eppendorf cup and evaporated in a SpeedVac until 50 µL remaining, following which 1ml of ACN was added to the

Eppendorf followed by 20 µL of carboxylate magnetic beads following the Single-pot, solid-phase-enhanced sample preparation (SP3) [129] and incubated overnight to bind the peptides.

Following incubation the supernatant was decanted and the beads were washed twice with ACN before being eluted with 20 µL DMSO and 20 µL MQ water, peptides were evaporated to dryness and suspended in 20 µL Nano LC-MS buffer A, peptides were ultracentrifuged at 50k RCF for 20 minutes before being injected onto an UltiMate 3000 RSLCnano system.

3.5.3 nLC separation of newly synthesized proteins

Peptides were separated on an UltiMate 3000 RSLCnano system consisting of a NCF3500PS pump module, a WPS3000 Autosampler and a TCC-3000S column compartment under reversed phase conditions, interfaced via Electrospray ionization (ESI) to an Orbitrap fusion tribrid MS. Peptides were washed under non eluting conditions on a Thermo Fisher Acclaim PepMap 2cm x 100 µm I.D. 5µm, 100 Å guard column (Waltham, MA, USA) for 6 minutes, column was maintained at 60^{o}C with a 1ml/min flow rate of NanoLC buffer A before eluting on to the analytical flow path by increase to 6ml/min flow rate.

Analytical separation was performed using an Acclaim PepMap RSLC 50 cm x 75µm I.D. 2µm, 100 Å column (Thermo Scientific, MA). Column was maintained at 60^{o}C and a flow rate of 200nl/min was used. Peptides were separated using a binary solvent system consisting of Nano LC-MS buffer A and Nano LC-MS buffer B. They were eluted with a gradient of 3.7–31.3% B in 120 min, 31.3–62.5% in 45 min, 62.5–90% B in 8 min, maintained at 90%B for 5 minutes and finally re-equilibrated to 3.7% B in 18 min.

3.5.4 MS analysis of newly synthesized peptides

Eluting peptides were interfaced via a fused silica Picotip 5 cm x 10 µm ID emitter (NewObjective) for ESI (spray voltage, 2 kV; heated capillary, 300 °C) using a nano-electrospray source (Thermo Scientific). MS spectra were acquired in the positive ion mode on the orbitrap with an m/z range of 375–1,700 with R of 120,000 at m/z 200. AGC target was 4×10^5 with an injection time of 50 ms. The top 50 most intense precursors were selected for higher-energy collisional dissociation (HCD) on the linear ion trap for high scan speed MS2 spectra of with a collisional energy of 32%, MS2 parameters were as follows: charges= 2-4^{+}, R= 15,000 at m/z 200; AGC, 5×10^4 with an injection time of 60 ms.

3.5.5 Identification of newly synthesized peptides

For peptide identification Mascot [128] integrated into proteome discoverer (v2.2 Thermo Fisher Scientific, Ma) was used to search peak lists against the H. sapiens proteome (UniprotKB canonical set). Trypsin/P was set as the enzyme with a specific digest method with up to 1 missed cleavage site allowed. Mass tolerance was set at 7ppm for precursor identification and 50mmu for fragment masses, variable modifications were set as oxidation of methionine and acetylation of N terminal peptides. PSM selection criteria was set at a FDR of 0.01 for only high confidence matches with a minimum peptide length of 6 amino acids, the decoy database was deployed in concatenated mode.

3.6 Statistical analysis

Sample size, replicates and statistical tests were performed in accordance with literature with similar methodology. For statistical analysis a two-sided, paired T-test was performed, a P value of 0.05 was taken as the statistical significance minimum, where; * is <0.05, ** is <0.01 and *** is <0.001. All statistical analysis was performed using R studio[130]; additionally R studio was used for all data visualization (R scripts in Supplement).

4.0 Results

4.1 Introducing a T cell model to study mtROS as an inducible signaling molecule

The metabolic switch of T cells is required for both their development and their effector function. Mitochondria essentially contribute to metabolic reprogramming which includes mtROS. mtROS levels can increase in activated T cells and there is growing evidence of mtROS acting as a signaling molecule at a network which is principally undefined. The definition of the mtROS signaling network can be achieved by proteomics. However, this required a cell model that allows for reproducible induction of mtROS signal. Instead of TCR/antigen-specific stimulations, which would confound the largely PKC-Θ mediated mtROS induction, I decided to perform primarily a Phorbol-12-myristate-13 acetate (PMA) induced activation.

Phorbol-12-myristate-13 acetate (PMA) functions as a mimetic of DAG which as mentioned previously (Chapter. 1.2) is an activator of PKC- θ, which propagates the subsequent activation of NF-κB as well as AP-1 signaling. PMA has been utilized previously to study ROS generation in a number of cell types [52,131,132]. Additionally, it was shown that PMA alone triggers metabolic reprogramming in primary T cells as well as mitochondrial derived ROS [51,133]

4.1.1 Constitutive generation of oxidative species in Jurkat T cells

Initially it was thought that the E6.1 Jurkat cell line could prove a suitable model system for the characterization of mtROS' impact on the proteome. Jurkat cells have been used in the past to characterize phosphorylation signaling in T cell activation [134]. Additionally, cell lines allow for the facile generation of knockouts as well as the ease of obtaining large quantities of cells [135].

It was theorized that, as Jurkat cells are a T cell line, they should undergo the well documented metabolic shift and generate an increase in mitochondrial electron leakage when stimulated. To validate this hypothesis, Jurkat cells were sealed within an airtight glass gas chromatography (GC) vial to prevent leakage of up taken O_2 or produced CO_2. Cells were stimulated with 10ng/ml PMA for 1h to induce the metabolic shift and oxidative signal. Following which, the gas phase above the cell suspension was sampled and the molecular oxygen and CO_2 were quantified. GC revealed that 10ng/ml PMA yielded an increase in the production of molecular CO_2 from an ion intensity of 15.2 to 18 (Figure. 10A), signifying an increase in cellular respiration.

In parallel, cells were activated with either 10ng/ml PMA or 100ng/ml ionomycin, alone or in combination for 1 hour to confirm PMA can generate mtROS signal alone. Following which, cells were loaded with 5µM H_2DCFDA which is oxidized by ROS to yield a fluorescent signal and allows quantification of ROS signal. Flow cytometry was used to analyze the change in fluorescence following Jurkat T cell activation (Figure. 10B). However, flow cytometry indicated that Jurkat cells possessed a high basal level of ROS with an average mean fluorescence intensity (MFI) of 2600. Consequently, when stimulated there was no significant difference in H_2DCFDA signal between stimulated and unstimulated cells.

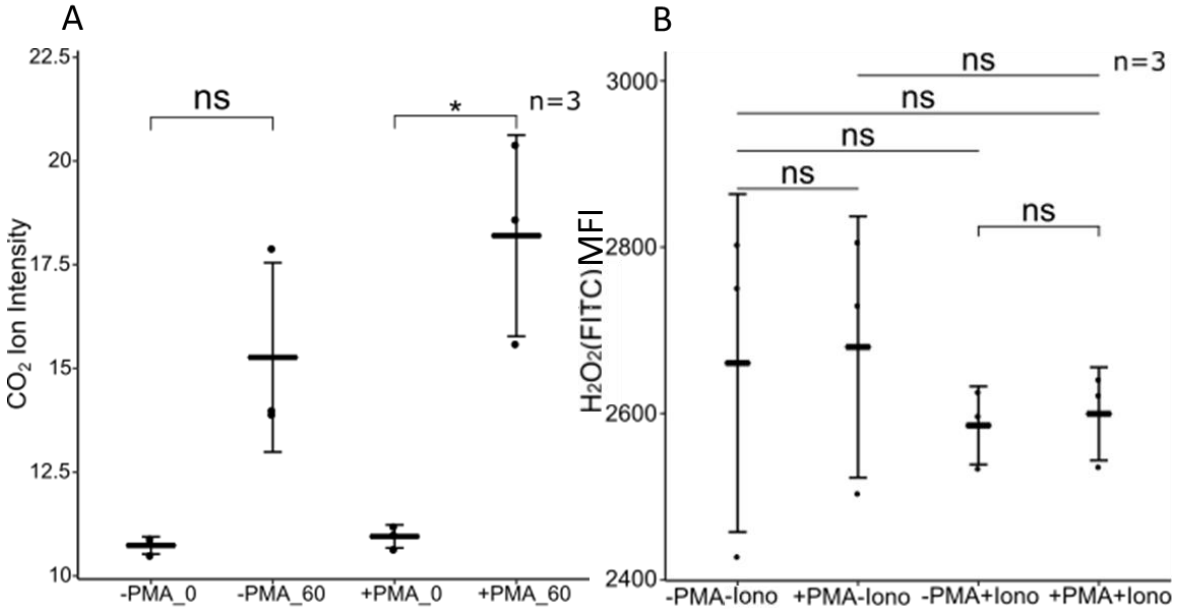

Figure 10: Jurkat stimulation with PMA triggers an increase in cellular respiration without induction of oxidative signal.

A) Stimulation of Jurkat cells with 10ng/ml PMA yields an increase in CO_2 production, as seen by an increase in the CO_2 ion intensity by GC-MS B) No Significant difference in mtROS generation between stimulated and unstimulated Jurkat cells as seen by H_2DCFDA fluorescence in flow cytometry. Statistical significance was determined with a two-sided, paired T-test, and a P value of 0.05 was taken as significant and indicated by asterisks (* < 0.05).

In conclusion, it is apparent that while Jurkat cells can undergo the expected increase in cellular activity following stimulation, the background ROS generated by virtue of the cancerous nature of the cell line rendered this model system inappropriate for our purposes of probing the redox proteome of activated T cells. Furthermore, PMA was used independent of ionomycin in all further experiments as literature suggests the PKC- θ dependent pathway is the main producer of the T cell ROS phenotype and would allow for less confounding variables in the data analysis. For the same reason CD3/CD28 activation was also not used.

4.1.2 Oxidative species are inducible in primary $CD4^+$ T cells without calcium signaling

As the Jurkat T cell model system was found not suitable it was decided to forego the less physiological system and take advantage of the primary cell system which are known to not produce excessive ROS[136] in their quiescent stage. However may be induced with activation stimulus to produce ROS.

To confirm this, blood donations from 3 heathy donors were acquired and the PBMC fraction was purified. From this purification, $CD4^+$ T cells were isolated by positive selection with flow cytometry-based cell sorting to look on a discrete subset. Sorting utilized anti-CD3 (BV605) and anti-CD4 (PerCP) antibodies for gating and isolation of the $CD3^+CD4^+$ subsets (termed $CD4^+$). Cells were loaded for 30 minutes with 5µM H_2DCFDA, to measure ROS signal and 5µM 7-AAD to determine cell viability. $CD4^+$ cells were then stimulated with 10ng/ml PMA for 1 hour to generate a metabolic shift as well as the ROS signal. Following stimulation, cells were labelled with CD69 (APC) to quantify T cell activation. CD69 surface expression and ROS production were analyzed with flow cytometry.

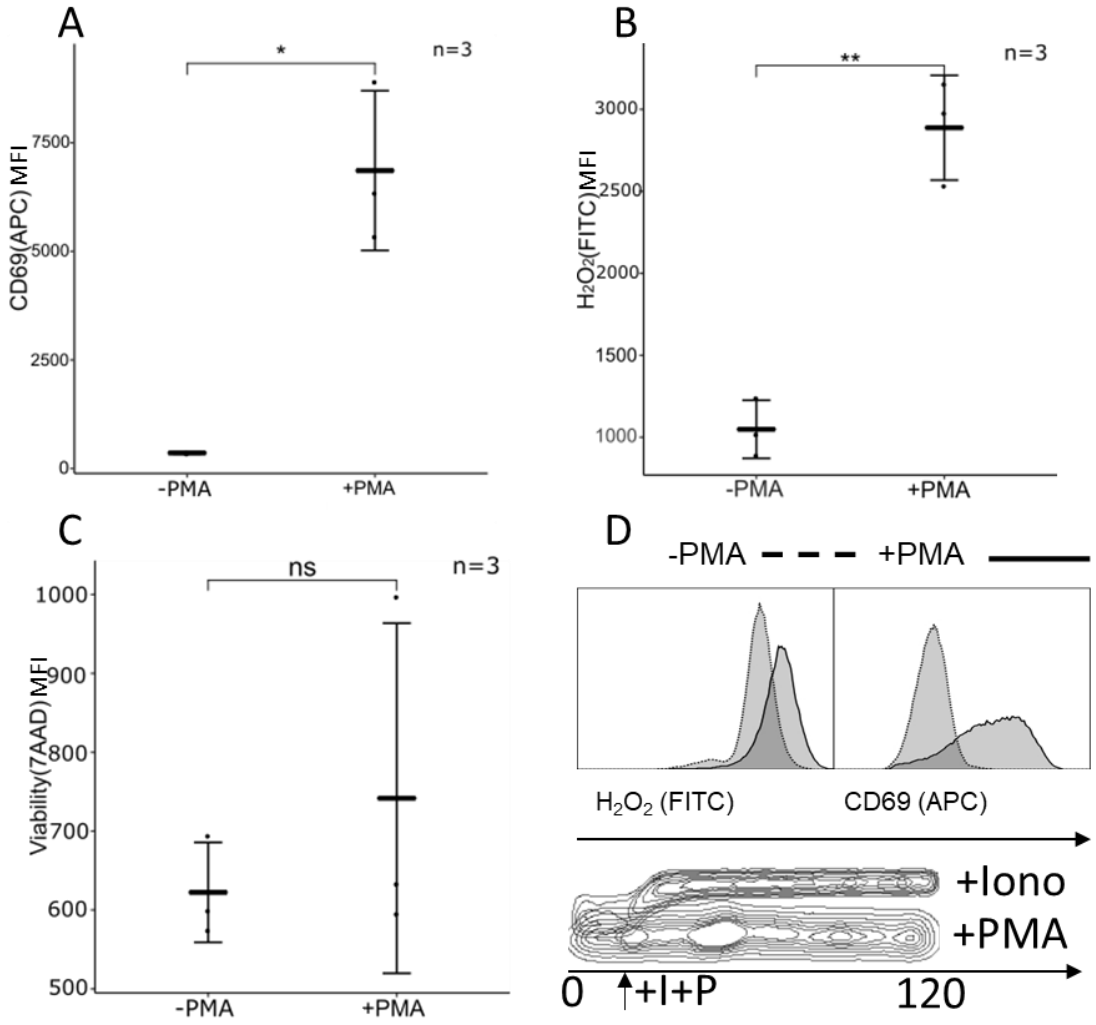

Figure 11: PMA stimulation triggers an activation phenotype with mtROS signaling without inducing calcium signaling in viable CD4⁺ T cells.

A) T cell activation is induced by PMA as seen by CD69 surface expression, B) ROS production is also induced in primary human T cells as seen by H_2DCFDA fluorescence, C) cell viability as seen by 7AAD fluorescence viability remains unchanged and D) Representative flow cytometry data showing the difference in CD69 signal and H_2O_2 signal in active vs unstimulated T cells as well as the difference in calcium uptake as seen with Fluo-4FF staining. Statistical significance was determined with a two-sided, paired T-test, and a P value of 0.05 was taken as significant and indicated by asterisks (* < 0.05, ** < 0.01).

Flow cytometry demonstrated that 1h stimulation with 10ng/ml PMA alone, significantly upregulated the CD69 signal from an average of 350 MFI units to 6500 MFI units (Figure. 11A). CD69 is an early activation marker of T cell activation and its upregulation confirmed engagement of the NF-κB and AP1 transcription pathways [137].

Additionally, there was a significant ROS generation shown via fluorescence of H_2DCFDA, from an average of 1000 MFI units to 3000 MFI units (Figure. 11B). 7AAD fluorescence signifies lysis of the nuclear envelope which is indicative of cell apoptosis[138]. It was observed that 10ng/ml PMA alone does not yield cell apoptosis which could be seen by the lack of a significant increase of 7AAD fluorescence with stimulated and unstimulated conditions having a similar average MFI of 610 and 720

MFI. Data suggests the oxidative signal generated is within the physiological levels of cell signaling (Figure. 11C).

For calcium staining experiments, cells were loaded with Fluo-4FF for 30 minutes to quantify intracellular free calcium and then stimulated with either 10ng/ml PMA or as a positive control, 100ng/ml Ionomycin. $CD4^+$ cells were analyzed continuously over 2 minutes for Fluo-4FF signal with flow cytometry to look on the early induction of calcium signaling.

To confirm PMA does not yield any off-target calcium signaling and that only PKC-ɵ dependent pathways were engaged, I employed Fluo-4FF which is a cell permeable calcium stain. I could determine that 10ng/ml PMA does not yield any significant increase in intracellular calcium levels when compared to ionomycin a known calcium channel ionophore. Indeed, the PMA dependent Fluo-4FF signal did not change from an average MFI of 4500 while Ionomycin MFI increased to 15300 MFI units (Figure. 11D).

To summarize, 10ng/ml PMA is capable of eliciting a T cell activation coupled with an increase in ROS signal in isolated $CD4^+$ T cells without affecting cell viability or calcium signaling, suggesting that primary human T cells can serve as a physiological model system for redox proteomics.

4.1.3 Detection of mitochondrial derived H_2O_2 in PMA stimulated T cells

Having determined that $CD3^+CD4^+$ primary human T cells exhibit ROS production when stimulated with PMA, it was necessary to elucidate the type of ROS species generated. This determination was required as H_2DCFDA oxidation is not specific to any oxidizing agent. Additionally, the localization of the signal was required to confirm whether it was mtROS.

To confirm the production of H_2O_2, I took advantage from the substrate selectivity of catalase. Catalase specifically converts H_2O_2 to water and would allow for the quantification of the contribution of H_2O_2 to the total oxidative signal generated with PMA stimulation.

PBMCs from 3 healthy donors were isolated, loaded with 5µM H_2DCFDA as previously performed. Cells were then incubated in the presence or absence of 10ng/ml PMA and/or 1mg/ml catalase for 1 hour to determine the differential impact of catalase on ROS signal. Following, the catalase-sensitive ROS production of T cells were determined by using flow cytometry gating on $CD3^+$ T cells (BV605: CD3) to look on the total $CD3^+$ T cell ROS generation.

Indeed, it was noted that when co-incubating PBMCs with PMA and catalase there was a marked reduction in H_2O_2, as observed in the $CD3^+$ gated T cells (Figure. 12A). PMA activated cells possessed an average MFI of 2900 MFI units in the cell population stimulated with PMA but without catalase versus 1300 when additionally incubated with catalase. Data suggested that the vast majority of physiologically relevant ROS produced by the T cell is H_2O_2.

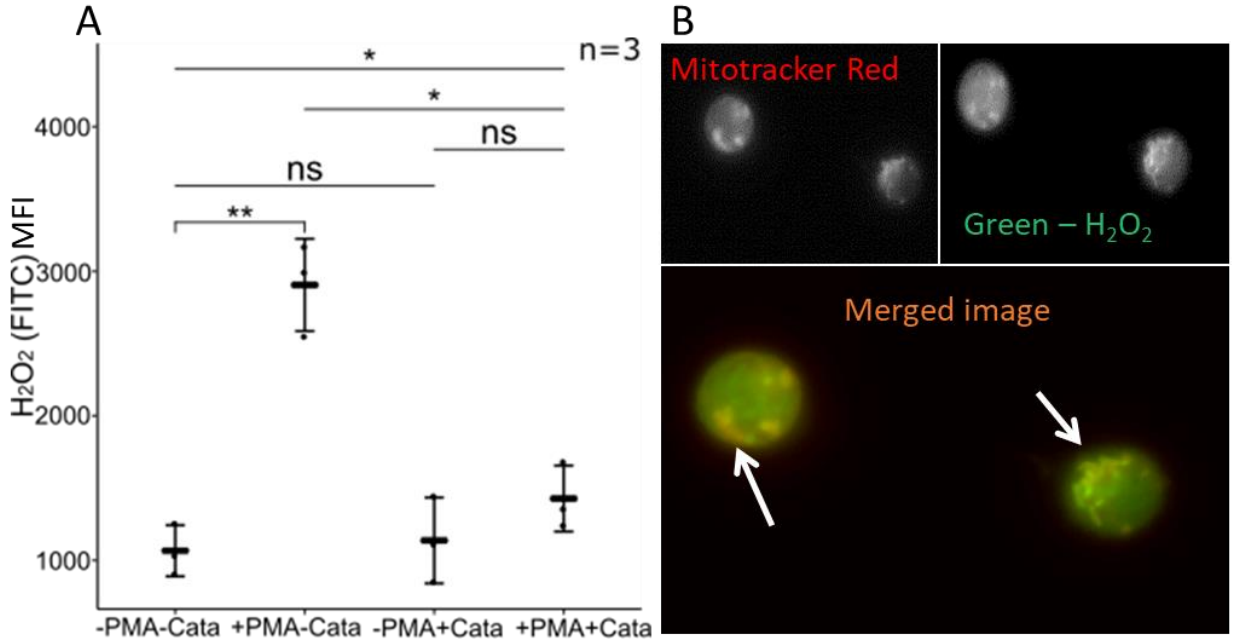

Figure 12: Hydrogen peroxide is the major source of mtROS following PMA stimulation

A) Catalase incubation with PMA reduces the H_2O_2 signal of $CD3^+$ T cells inside the PBMC fraction. B) Mitochondria (red) co-localize with highest concentrations of H_2O_2 (green), arrows indicate overlapping signal. Statistical significance was determined with a two-sided, paired T-test, and a P value of 0.05 was taken as significant and indicated by asterisks (* < 0.05, ** < 0.01).

Next, I aimed to determine that the H_2O_2 signal observed in flow cytometry derived from the mitochondrial compartment. To this end, $CD4^+$ T cells were positively isolated from PBMCs as above (Chapter 4.1.1) and loaded with 5µM H_2DCFDA and 100nM mitotracker red to visualize the H_2O_2 signal as well as the mitochondria respectively. Cells were then stimulated with 10ng/ml PMA and were then visualized by fluorescent microscopy over time to track the production of H_2O_2 from the mitochondria. H_2DCFDA signals were found to constitute discrete points in the cell which overlapped with fluorescence resulting from mitotracker red, suggesting a mitochondrial origin of the H_2O_2 (Figure. 12B).

Taken together, PMA induced activation of T cells leads to a marked increase in ROS which is emanating from the mitochondria and therefore, is most likely due to electron leakage converting molecular oxygen to superoxide which is then dismutased to hydrogen peroxide.

4.1.4 mtROS induction discriminate $CD4^+$ T helper from $CD8^+$ cytotoxic T cells

Having confirmed primary $CD3^+$ T cells in PBMCs as a model system to induce and study mitochondrial derived H_2O_2 I asked the question whether or not functional distinct major T cell subsets have a differential respond.

$CD4^+$ T helper cells work to elicit immune responses from peripheral cell populations such as the cytotoxic $CD8^+$ T cells, it has been shown that T cell populations have differing mtROS responses depending on their function [139,140], as such I wanted to confirm this is the case in our system.

To accomplish this, PBMCs from 3 healthy donors were isolated from blood samples and loaded with H_2DCFDA before being incubated with 10ng/ml PMA for 1 hour as performed in the previous chapter. Cells were labelled with anti-CD3 (BV605), anti-CD4 (PerCP) and anti-CD8 (PE) to allow gating on both the $CD3^+CD4^+$ and $CD3^+CD8^+$ T cell populations in the PBMCs when analyzed with flow cytometry (Supplementary Figure. 1).

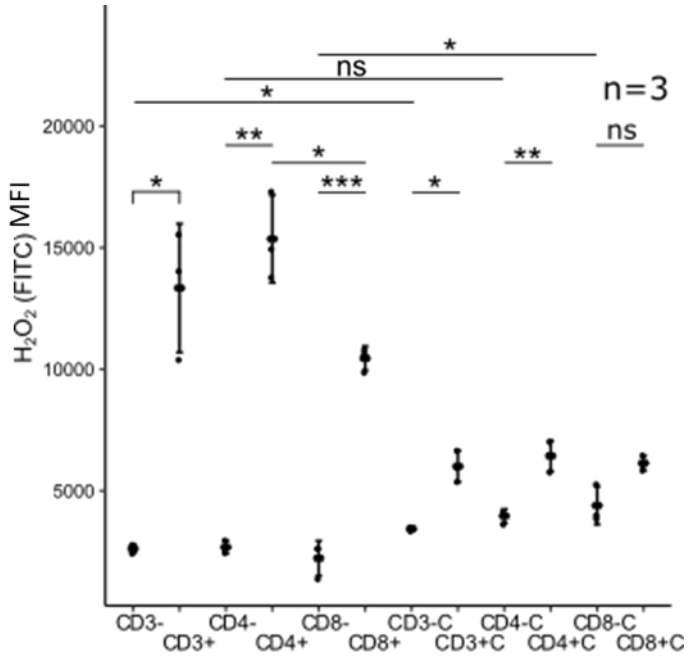

Figure 13: $CD4^+$ T cells produce more mtROS on stimulation with PMA than $CD8^+$T cells within the PBMC fraction.

$CD4^+$ T cells in PBMCs generate a higher mtROS signal than $CD8^+$ T cell within the PBMC fraction following PMA stimulation. Additionally, catalase reduces the mtROS signal in all PMA stimulated T cell subsets while increasing the mtROS signal in the unstimulated T cell subsets. Where - means -PMA -Catalase, + means +PMA -Catalase, -C means -PMA +Catalase, +C means +PMA +Catalase. Statistical significance was determined with a two-sided, paired T-test, and a P value of 0.05 was taken as significant and indicated by asterisks (* < 0.05, ** < 0.01, ***<0.001).

Indeed, there are significant differences between $CD4^+$ T cells and $CD8^+$ T cells. Data indicated that the $CD4^+$ T cell subset produces more mitochondrial derived H_2O_2 than the $CD8^+$ subset (Figure. 13), from an average MFI of 2600 to 15000 MFI for the $CD4^+$ population in comparison to an average MFI of 2200 to 10500 MFI for the $CD8^+$ population. Additionally, catalase was found to reduce the ROS signal in all three cell populations. However, in the $CD3^+$ and $CD3^+CD8^+$ T cells population's catalase did not quench the signal to baseline suggesting that other oxidative species are present (as Chapter 3.1.3) and that H_2O_2 may constitute a greater proportion of the total ROS produced in $CD4^+$ T cells than other subsets.

This data suggested that differential T cell effector functions may require differing levels of ROS and that $CD4^+$ T cells utilize mtROS for its phenotype more than $CD3^+$ T cell ROS and provide the best model to study mtROS dependent mechanisms by proteomics.

4.1.5 PBMCs support reduction of mtROS in $CD4^+$ T cells by catalase

The previous 2 chapters characterized the effect of catalase quenching on mtROS production. However, this was surprising as catalase was not expected to be able to enter T cells. Although, literature has suggested that ROS is capable of inducing endocytosis of catalase in multiple cell types to catalyze the degradation of H_2O_2 [141,142].

To determine if catalase was directly acting on $CD4^+$ T cells, PBMCs from 3 healthy donors were isolated from blood. Following which, half of the PBMC fraction were reserved and the other half taken and the $CD4^+$ T cells were negatively isolated to generate $CD4^+$ T cells without peripheral cell populations. It was hypothesized that the peripheral cell populations may mediate an indirect catalase induced antioxidant effect on $CD4^+$ T cells in the PMBC fraction. Both PBMCs and isolated $CD4^+$ T cells were loaded with 5µM H_2DCFDA and incubated in the presence or absence of 10ng/ml PMA and/or 1mg/ml catalase as previously described. Relative H_2O_2 levels in $CD4^+$ T cells were subsequently analyzed using flow cytometry

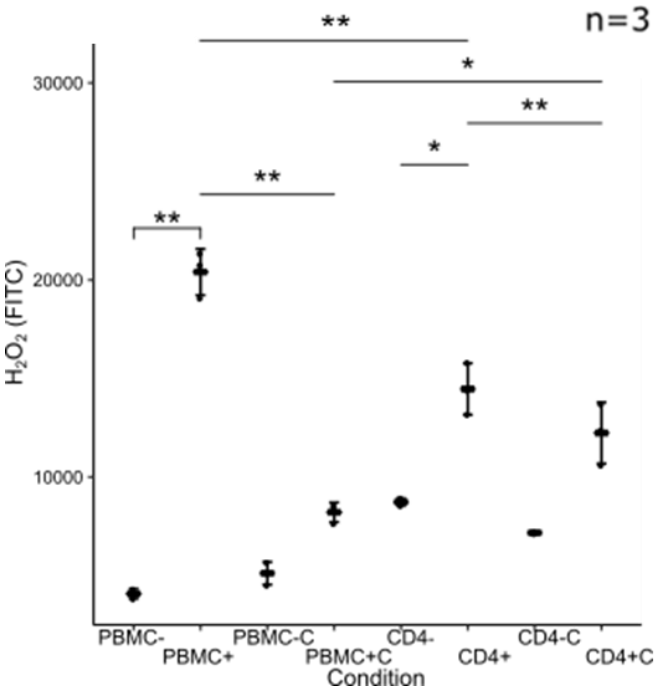

Figure 14: PBMCs support catalase mediated quenching of mtROS in $CD4^+$ T cells

Catalase incubation quenched the mtROS signal more effectively in $CD4^+$ T cells in the PBMC fraction than in the negatively isolated $CD4^+$ T cells. Where PBMC means $CD4^+$ T cells gated on in the PBMC fraction, CD4 means negatively isolated CD4 T cells, - means -PMA, + means +PMA, -C means -PMA +Catalase, +C means +PMA + Catalase. Statistical significance was determined with a two-sided, paired T-test, and a P value of 0.05 was taken as significant and indicated by asterisks (* < 0.05, ** < 0.01).

Strikingly, it was seen that isolated $CD4^+$ T cells have a higher baseline ROS level than $CD4^+$ cells gated in PBMCs (Figure. 14; 8500 vs 4100 MFI) indicating the importance of peripheral cell populations in controlling mtROS signaling in T cells. Additionally, I could observe a higher induction in mtROS signal in $CD4^+$ T cells inside the PBMC

fraction when compared to isolated $CD4^+$ T cells (from MFI 4100 to 21000 versus 8500 MFI units to 14500 MFI units). However, this could be due to ROS produced from other cell types diffusing into the T cells [143].

Finally, catalase was found to have an attenuated quenching of mtROS in isolated $CD4^+$ T cells than $CD4^+$ T cells in the PBMC fraction with isolated cells having a fold reduction of 1.2 for the isolated cells and 2.5 for $CD4^+$ cells in PBMCs. Taken together, this data suggests that catalase is capable of mediating an mtROS reduction in $CD4^+$ T cells by other cell types and may induce an antioxidant effect directly on $CD4^+$ T cells but the mechanism is unknown.

4.2 Identification of mtROS modified proteins in activated CD4⁺ primary human T cells

Having determined the suitability of (i) PMA activation, (ii) CD4⁺ T cells as a major "professional" mtROS producing subset in which (iii) mtROS can be reproducibly induced. I sought, to establish a workflow to characterize cysteine oxidation that occurs when exposed to this mtROS signal generated by stimulated CD4⁺ T cells.

As previously mentioned (Figure. 7), the primary target of mtROS are thiolate anions, the formal charge on this moiety is capable of nucleophilic attack of the peroxide bond of H_2O_2 generating a sulfenic acid as well as a hydroxide anion. Further oxidation is then possible to a disulfide bond which constitutes the major form of mtROS signaling [144].

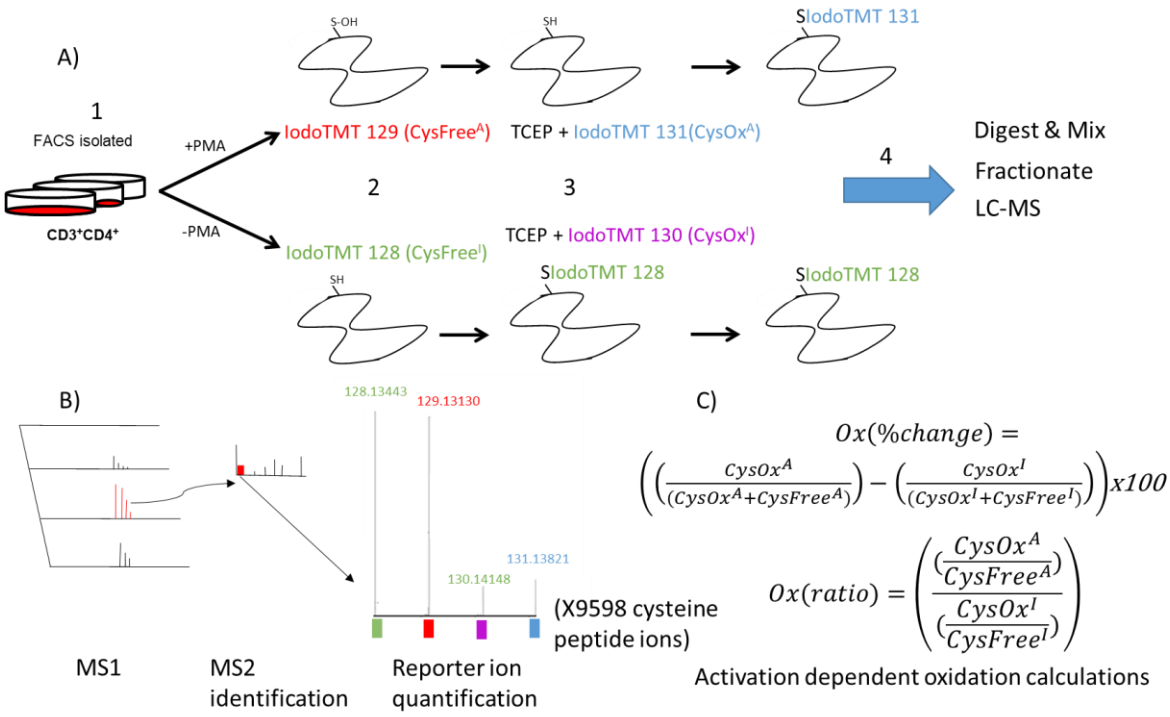

Figure 15: Multiplexed thiol-specific quantitative proteome workflow allows for the quantification of residue specific cysteine oxidations generated from MS² spectra.

A) Following FACS cell sorting CD4⁺ T cells are differentially stimulated with PMA for 1h. Following which, cells are lysed and free cysteine residues are labelled with thiol specific iodoTMT label 128 and 129 for the unstimulated and stimulated conditions, named $CysFree^I$ and $CysFree^A$ respectively. Reversibly oxidized cysteine residues are reduced with TCEP and labelled with IodoTMT tags with differing reporter masses, 130 and 131 for unstimulated and stimulated conditions, named $CysOx^I$ and $CysOx^A$ respectively. Subsequent, offline 2D-LC separation allows for deeper global proteome coverage before LC-MS with Orbitrap detection. B) MS1 peptide mass fingerprints are taken for subsequent activation experiments utilizing Higher-energy C-trap dissociation (HCD) fragmentation to generate high quality MS2 spectra that can be identified utilizing automated software to identify and quantify 9598 cysteine containing peptides utilizing the reporter tags which are identified in the MS². C) Quantification of identified peptides was performed either utilizing the total % change in oxidation of each residue between stimulated minus unstimulated conditions or on the fold change in oxidation between stimulated over unstimulated conditions.

Cysteine specific oxidations were determined utilizing a multiplexed thiol switching method (Figure. 15A). In which, CD4⁺ T cells were isolated from PBMCs *via* flow

cytometry based cell sorting (Figure. 15A, Step 1) as in previous chapters (Chapter. 4.1.2).

Isolated $CD4^+$ T cells were incubated for 1 hour in the presence or absence of 10ng/ml PMA to generate the mtROS signal. Following PMA stimulation, cells were washed and chemically lysed in the presence of different isobaric alkylating agents (Figure. 15A, Step 2). The alkylating agents are IodoTMT tags which contained 2 discrete reporter tags of differing masses which specifically modify unoxidised "free" thiol groups. The masses are indicative of the reporter mass that will be analyzed in the MS^2 spectra. **In this study I utilized masses of 128 and 129 for the free thiol groups in the unstimulated and stimulated cells, and termed them $CysFree^I$ and $CysFree^A$ respectively.**

Following complete "protection" of unreacted free thiols by the applied iodoTMT tags, the samples were then reduced with tris(2-carboxyethyl)phosphine (TCEP) to convert reversibly oxidized thiol groups back to free thiols (Figure 15A, Step 3). **Samples were again incubated with cysteine specific isobaric tags of 2 different MS^2 reporters to label the previously reversibly oxidized cysteine residues. The masses were 130 and 131 for unstimulated and stimulated conditions, termed $CysOx^I$ and $CysOx^A$ respectively.** This IodoTMT approach allowed for the differential labelling of both free and oxidized thiols under both stimulated and unstimulated conditions.

Following tryptic digestion and mixing of the labelled samples, high pH reverse phase chromatography (Figure. 15A, step 4 and Figure. 16) was utilized to improve proteome coverage. Considering cysteine residues only make up a small amount of the total amino acid composition of the human proteome, fractionation allows for more cysteine containing residues to be identified and quantified. In total, 144 fractions were collected and combined into 13 samples per donor which were then analyzed by peptide sequencing (LC-MS). 13 samples were chosen to yield relatively low complexity samples while not leading to excessive analysis time per donor to prevent appreciable peptide degradation in unanalyzed samples.

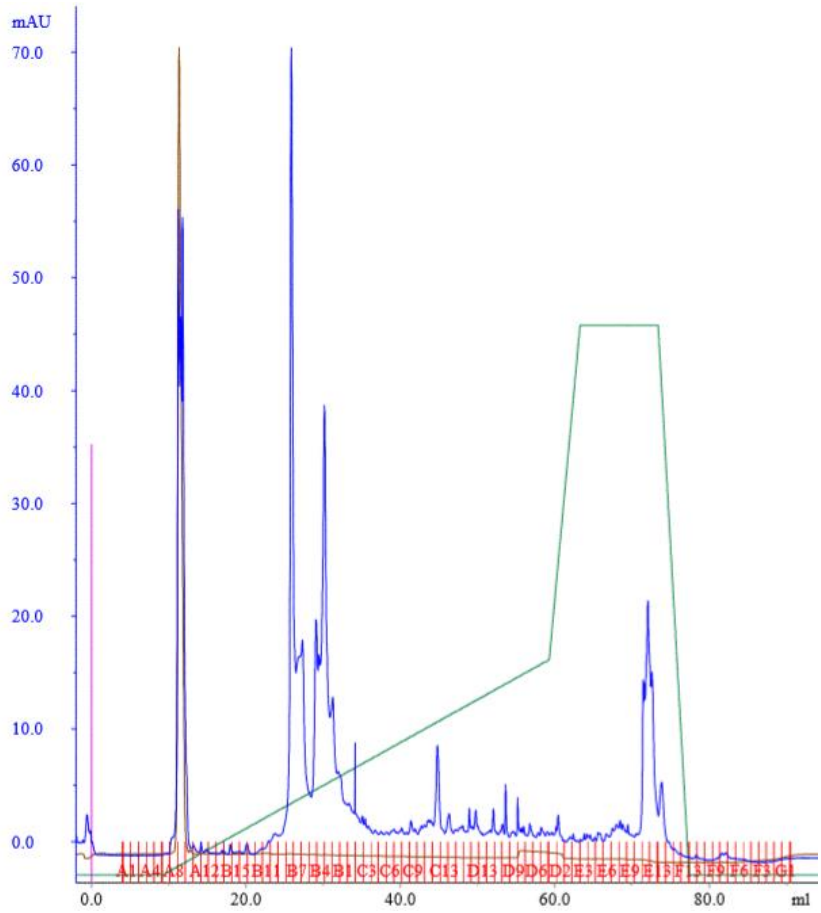

Figure 16: Off-line fractionation of combined thiol-labeled proteomes from stimulated & unstimulated T cells from one representative donor.

Chromatogram shows the peptide elution profile from high pH reverse phase. Fractions were collected every minute from a linear gradient of 5-28% solvent B (90% ACN + 10mM ammonium hydroxide) over 50 minutes and then 28-70% over 5 minutes. Samples were concatenated before analytical separation as 13 fractions followed by peptide sequencing.

Utilizing this multiplexed thiol switching method and analysis with an Orbitrap fusion tribrid MS. It was possible to robustly compare the degree of oxidation following activation of isolated $CD4^+$ primary human T cells. From this, I identified 9598 cysteine containing peptides in total (Supplementary table. 1). Of these peptides 2311 were found to be robustly identified and quantified in all 3 biological donors (Supplementary Figure. 2).

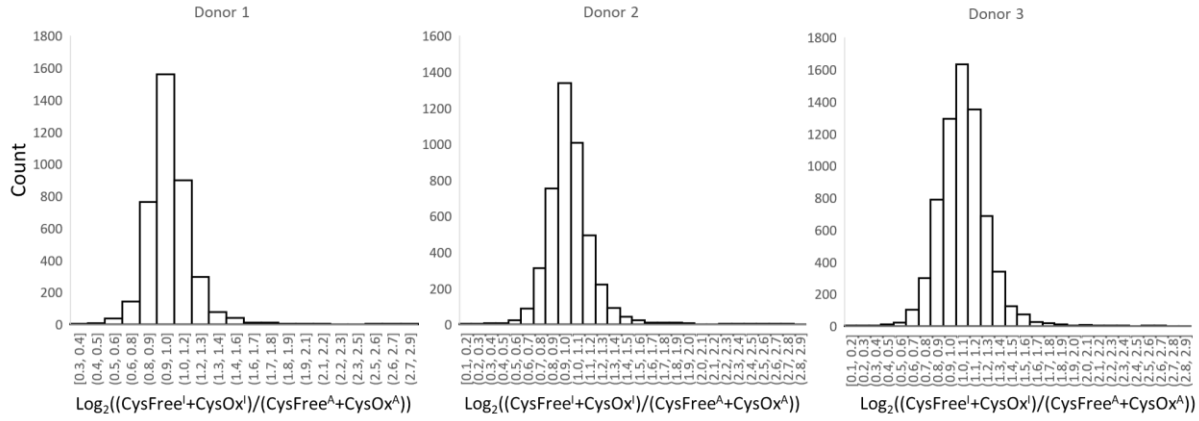

Figure 17: Distribution of total ion intensity from unstimulated cells vs stimulated cells

Combining cell lysates from unstimulated and stimulated conditions did not introduce a systematic bias into the quantitation of the reporter tags, it can be observed that in all donors there is a distribution of condition specific reporters (-PMA: CysFreeI + CysOxI/ +PMA: CysFreeA + CysOxA) around 1. Therefore, neither cell population is more abundant than the other.

As mentioned, IodoTMT is a multiplexing method which allowed for the removal of analytical variance by separating and analyzing both conditions together. However, to ensure that there was no systematic bias in the generation of regulatory information, the total reporter tag intensity of the unstimulated ($CysFree^{I}$+$CysOx^{I}$) and the stimulated (CysFreeA+CysOxA) conditions were compared. The equation (($CysFree^{I}$+$CysOx^{I}$)/($CysFree^{A}$+$CysOx^{A}$)) was utilized for comparison and it was apparent that the represented a distribution around 1 (Figure. 17), confirming an equal amount of protein from both stimulated and unstimulated conditions.

What was particularly striking was the degree of variation between donors (Supplementary Figure. 2). It was observed that only 30% of the cysteine containing peptides found in all donors were conserved. Due to the limited number of quantifiable peptides in all 3 donors it was determined to allow peptides which were found instead in 2 of 3 donors. Which permitted the quantification of 4784 cysteine containing peptides which is an increase to 50% of the total cysteine containing peptide pool from all 3 donors (9598 peptides). The reporter tags from the MS^2 spectra (Figure. 15B) of these peptides were used to determine the % change in oxidation of each cysteine as well as the fold change in oxidation (Figure. 15C).

I decided to utilize both equations here as both equations provided a complementary view of the redox proteome of $CD4^+$ T cells. While the % change in oxidation (Figure. C top equation) allowed for the identification of proteins which undergo the greatest shift in the oxidations of the total cellular pool of a specific cysteine residue. Cooperatively, the fold change equation (Figure. 15C lower equation) characterized cysteine residues which demonstrated the highest regulation factors. While only a small portion of the total pool of a particular residue may have responded to the oxidative signal, the responsive pool may have constituted a discrete cellular localization/compartment to mediate a function. Having said that, Candidates of particular interest were highlighted in both analyses and may represented the main targets of mtROS in stimulated T cells.

4.2.1 Compartment-specific oxidation of the mitochondrial respirasome

It is well known that the vast majority of cysteine residues exist in the reduced state due to the reducing environment in the cytoplasm[145] perpetuated by the abundant antioxidant species present. It was expected that this would be mirrored in our labelling method in which the "free" cysteine residues (S-H/S^-) should show a greater intensity in the "free" cysteine reporter tags ($CysFree^I$ and $CysFree^A$) than the oxidized cysteine reporter tags ($CysOx^I$ and $CysOx^A$).

To determine this, the log_2 distribution of the label intensities of all cysteine containing peptides were quantified for each donor and was analyzed. It was noted that the CysFree labels are of significantly higher intensity than the CysOx labels suggesting the majority of cysteine residues were labelled before reduction and therefore largely reduced. (Figure. 18).

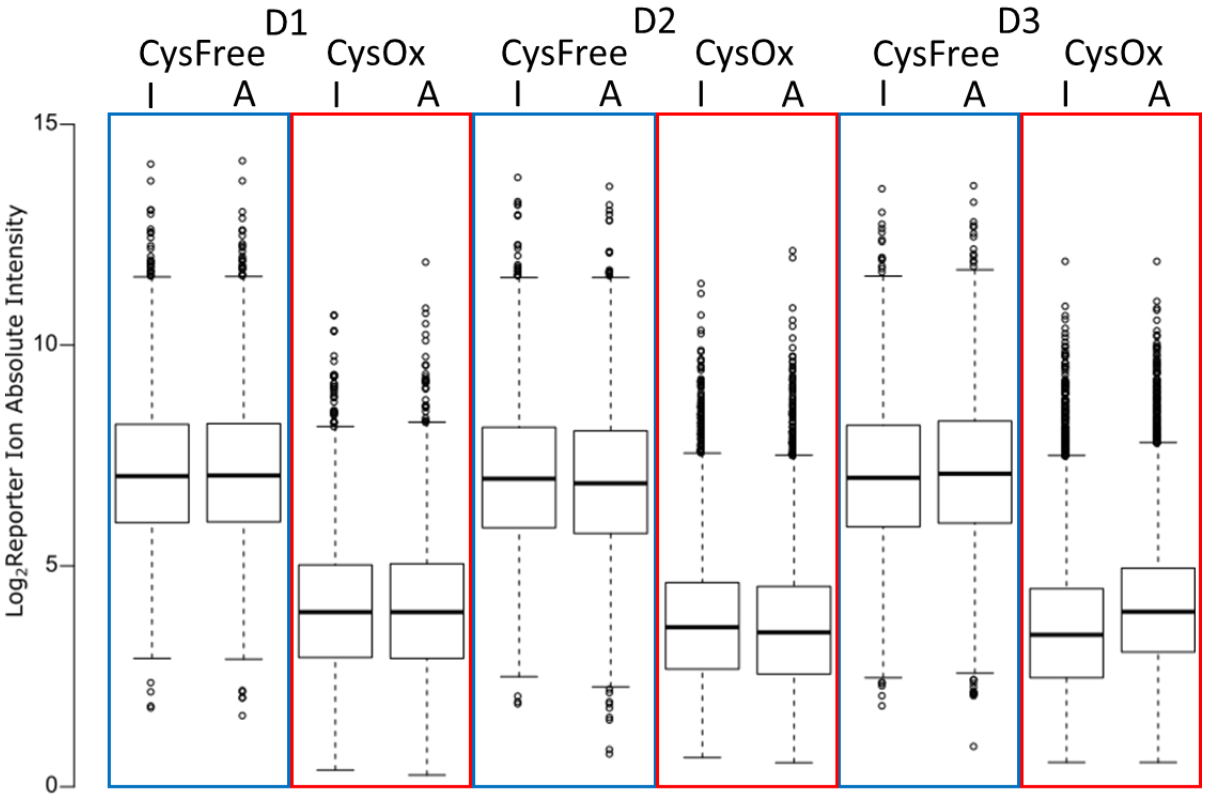

Figure 18: Absolute intensities of each label used to quantify the oxidation state of all cysteine containing peptides show no shift following PMA stimulation

All donors show significantly higher intensities for the free cysteine (CysFree) labels ($CysFree^I$ and $CysFree^A$) in blue than the oxidized (CysOx) labels ($CysOx^I$ and $CysOx^A$) in red. Additionally, there is no major decrease in intensity between the $CysFree^I$ and $CysFree^A$ or increase in signal intensity between $CysOx^I$ and $CysOx^A$.

This data confirmed no global shift in the oxidation of the stimulated condition in relation to the unstimulated condition as there is no major decrease in the intensities between $CysFree^I$ and $CysFree^A$ following stimulation, suggesting an increase in oxidation. Additionally, there is no major increase in the intensities of the CysOX reporters between unstimulated and stimulated conditions. This lack of a global shift was expected as only a small number of cysteine residues are capable of being

deprotonated under physiological conditions as has been observed in other global redox studies [146,147].

As the respirasome is the primary source of mtROS following T cell stimulation (Chapter. 1.3), I decided to inspect the redox state of the differing complexes. When looking on the respirasome, the data from the stimulated and unstimulated conditions characterized the redox state of 252 mitochondrial proteins (Supplementary Table. 2) which is roughly 21% of the mitochondrial compartment [148]. In this compartment I was capable of characterizing the redox state of 40% of the human respirasome (Figure. 19), obtaining redox data for subunits of all 3 components of the respiratory active super complex (CI, $CIII_{dimer}$, CIV). MS characterized cysteine-containing peptides from 14 subunits of CI (32%), 4 subunits of CIII (40%) and 6 subunits of CIV (32%). In general, more matrix associated proteins were identified than those imbedded in the inner membrane. This is most likely due to difficulty in extracting transmembrane proteins during sample preparation.

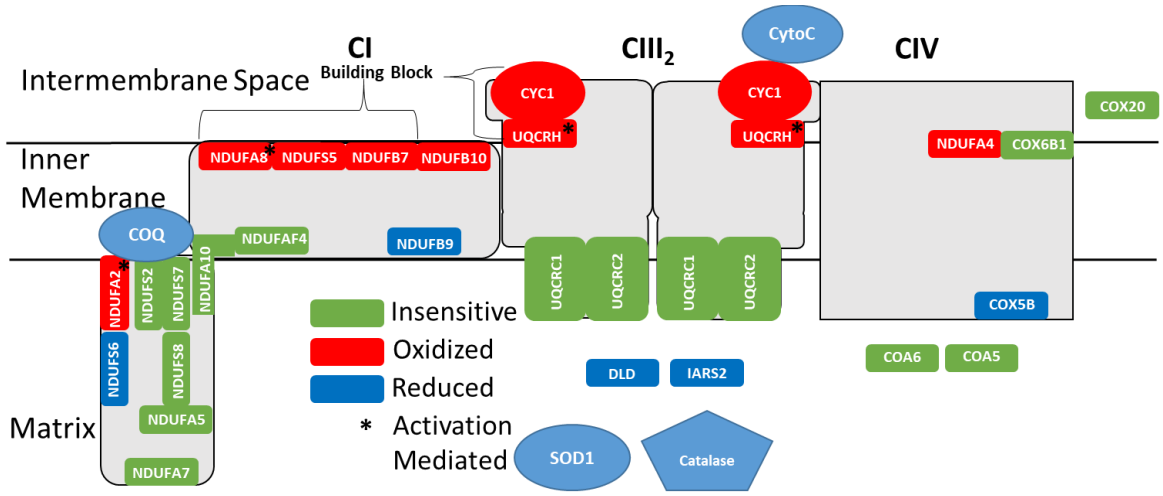

Figure 19: The respirasome exhibits multiple redox states, with the intermembrane facing proteins being largely oxidized and the matrix side being largely reducing.

The respirasome is composed of 4 protein complexes a monomer of CI and IV as well as a dimer of CIII complexes, the intermembrane space facing arm of CI was found to contain only oxidized subunits, this was mirrored in CIII. Conversely when looking on the matrix side of the respirasome the subunits are mainly reduced or displayed no significant oxidation. The matrix is far more reducing than the intermembrane space due to the presence of a number of antioxidant molecules. * represents significantly differential oxidation of subunits following PMA stimulation.

It was observed that subunits show three differential redox states. I have defined oxidized cysteine residues (in red) as showing a greater than 1% increase in residue oxidation, reduced (in blue) cysteine residues existed below -1% oxidation and redox insensitive (in green) which are between -1% and +1%. Interestingly, this differential redox state seemed to be compartmentalized and higher oxidation state seemed to correlate with the proximity of the affected subunit to the intermembrane space.

Indeed CI components NADH dehydrogenase [ubiquinone] 1 alpha subcomplex subunit 8 (NDUFA8), NADH dehydrogenase [ubiquinone] iron-sulfur protein 5 (NDUFS5), NADH dehydrogenase [ubiquinone] 1 beta subcomplex subunit 7 (NDUFB7) and NADH dehydrogenase [ubiquinone] 1 beta subcomplex subunit 10 (NDUFB10) (9.1%, 3.4%, 5% and 8.9% respectively). As well as CIII subunits

ubiquinol-cytochrome c reductase hinge protein (UQCRH) and Cytochrome c1, heme protein (CYC1) (8% and 2% respectively) exhibited a % increase in oxidation of the cysteine residues in subunits close to the intermembrane space. Conversely, subunits closer to the matrix side remained largely insensitive or reducing, most likely due to the abundance of antioxidant proteins.

It was also apparent that CI and CIII seemed to be more oxidized than CIV. As mentioned previously (Chapter. 1.3.1) electron leakage is known to emanate from complexes CI and CIII. Both CI and CIII show oxidation in expected sites of electron leakage, namely CYC1 which encodes the heme containing cytochrome CI protein and is the site of electron transfer from cytochrome C1 to cytochrome C and therefore can be expected to leak electrons [149,150]. While NADH dehydrogenase [ubiquinone] 1 alpha subcomplex subunit 2 (NDUFA2) is a member of the electron transfer modules of CI [151].

Paradoxically, as the transmembrane arm of CI was found largely oxidizing it was surprising to observe NADH dehydrogenase [ubiquinone] 1 beta subcomplex subunit 9 (NDUB9) as mostly reduced. NDUB9 may be reduced due to its role as the major binding site of CIII [40]. The interface may be kept reducing so that NDUFB9 can be available to bind through its thiol group. Additionally, it is know that the components that are share similar oxidation states in both CI as well as CIII are also components of the same “building blocks” and are inserted at the same time into the respective complexes before additional insertion into the respirasome. Indeed, NDUFA8, NDUFS5 and NDUFB7, not only have been implicated as a building block [152] but are also imported through the Mitochondrial Intermembrane space Assembly (MIA) disulfide mediated import pathway[152]. Furthermore, UQCRH as well as CYC1 are known interaction partners [153].

In summary, the observed respirasome oxidations concur with previous literature that the intermembrane space is largely oxidizing while the mitochondrial matrix maintains a reducing condition. Furthermore, I have provided cysteine residue specific data that may infer which cysteine residues contribute to this differential oxidation state. As well as demonstrated that respirasome building blocks exhibit a similar oxidation state.

4.2.2 Only a discrete set of proteins undergo shifts in cysteine oxidation

To better understand the susceptibility of a cysteine residue to oxidation on T cell stimulation, I analyzed the % oxidation shift in T cells (Figure. 15C top equation, & Supplementary Table. 3). $CysOx^{I}$ and $CysOx^{A}$ were divided by the total label intensity of each stimulation condition ($CysOx^{I}$ + $CysFree^{I}$ or $CysOX^{A}$ + $CysFree^{A}$) and a percentage of the proportion of a cysteine which is oxidized vs the total population of that cysteine was generated and plotted as histograms for both stimulation conditions (Figure. 20).

Looking on the overall redox state of unstimulated $CD4^{+}$ T cells (Figure. 20A) it was found that a significant proportion of the cysteine residues resided in the cytoplasm, which, when taken with previous data (Figure. 18), suggests that the cytoplasm is a reducing environment in $CD4^{+}$ T cells[145]. It is known that for the majority of proteins the cysteine residues exist as either significantly oxidized or significantly reduced [154] with only a few exceptions residing at 50% oxidized. On observation of the data, I

found this was also the case in CD4^{+} T cells as the histograms take on a valley shape with a large number of proteins at the extremes (<30% oxidized and >70% oxidized).

Of the highly oxidized population (90-100%) of proteins the major functional motif was a large number of structural disulfide bonds which are necessary for the function of the protein. Indeed, proteins such as Albumin (ALB) and Integrin beta-2 (ITGB2) both contain a large number of constitutive structural disulfide bonds and remained highly oxidized regardless of stimulation.

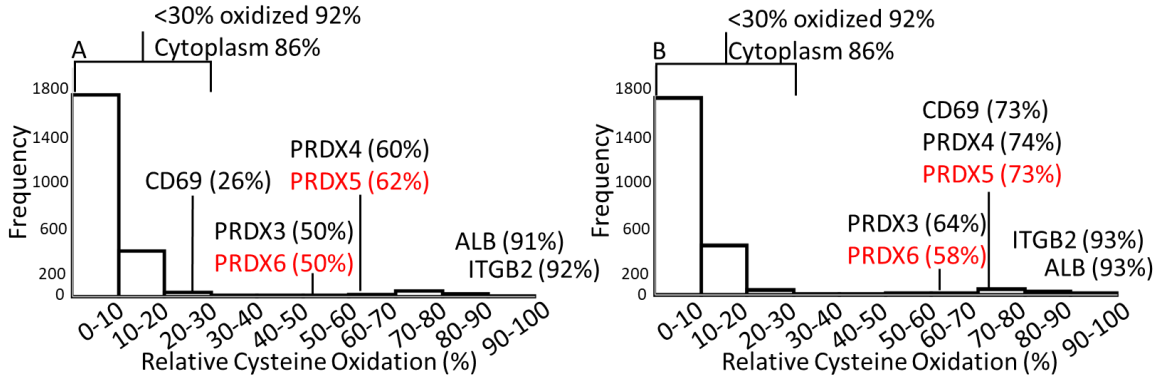

Figure 20: Global view of % cysteine residue oxidation between stimulated and unstimulated conditions.

A) Distribution of % oxidation in the unstimulated proteome (($CysOx^{I}$/ $CysOx^{I}$+$CysFree^{I}$)*100), 92% of cysteine residues exist in their reduced state additionally the 86% of reduced proteins are localized to the cytoplasm, a candidate found differentially oxidized in activation peroxiredoxin 5 (PRDX5) has an average cysteine oxidation of 62% at Cys204 (in red). B) Distribution of % oxidation in the active population (($CysOx^{A}$/$CysOx^{A}$+$CysFree^{A}$)*100, 92% of cysteine residues exist in their reduced state additionally 86% of reduced proteins are localized to the cytoplasm, PRDX5 has an average cysteine oxidation of 73% at Cys204. Taken together this suggest that there is no major shift in oxidation following T cell activation. However, a few highlighted examples (PRDX3, 4 and CD69) show a significant shift in oxidation suggesting there is an increase in oxidation that can be compensated by antioxidant mechanisms.

As previously mentioned (Figure. 18), there was a moderate degree of change when comparing the % shift in oxidation between the unstimulated and stimulated conditions (Figure. 15C top equation). However. In the unstimulated cell population, I identified a group of proteins, which utilize redox active disulfide bonds for their activity, and function as a proof of concept. Namely, the peroxiredoxin class of proteins [56] which have a specific motif which lowers the pKa of their catalytic cysteine residue. Four of these proteins (PRDX3/4/5/6) were identified in this thesis as being increasingly oxidized on incubation with PMA (Figure. 20, A & B). These proteins were found to increase by an average of 15% in their cysteine residue oxidation following T cell activation (Figure. 20B). PRDX5 and 6 in particular are interesting as their change in oxidation is statistically significant and they are known oxidative stress response proteins [155]. The cysteine residues that were oxidized in both proteins are the redox active sulfenic acids responsible for the activity of the enzyme (Cys204 in the case of PRDX5 and cys47 in the case of PRDX6) [56,156].

Strikingly, the two cysteine residues which underwent the greatest same shift in oxidation (26% to 73% when comparing unstimulated to active conditions) were in fact part of the extracellular domain of cluster of differentiation 69 (CD69). CD69 is the early activation marker used to quantify the degree of T cell activation utilizing PMA. This shift in oxidation was not necessarily surprising as CD69 localizes to the cell

surface on T cell activation where it encounters molecular oxygen in the atmosphere and is no longer reduced by antioxidant molecules (Mentioned in detail in outlook).

4.2.3 Global redox proteomics characterizes the mtROS dependent signaling network Following classification of the global cysteine redox state in the $CD4^+$ T cell populations. The subsequent aim was to identify susceptible cysteine thiolates which following the generation of an mtROS signal from the respirasome are robustly oxidized.

To this end, the degree of oxidation between the stimulated and unstimulated conditions for each cysteine thiol was determined utilizing the ratio of ratios equation termed Ox(ratio) (Figure. 15C, lower equation). With the intent of identifying the most regulated cysteine residues. With this approach it was possible to identify 76 significantly differentially oxidized cysteine residues between stimulated and unstimulated conditions (Supplementary Table. 4) when allowing for candidates to be correlated in 2 of 3 donors (Figure. 21).

The range of P values of candidates ranged from $-\log_{10}$ of 1.3 ($P< 0.05$) up to a $-\log_{10}$ of 4.5 ($P< 0.000032$), while the differences ranged from $\log_2$ -1.14 to 1.67 (Figure. 15C, lower equation). However, the majority of candidates lie between -1 and 1 $\log_2$ difference, potentially due to a low amount of sustained oxidation being generated through fine tuning of the mtROS signal.

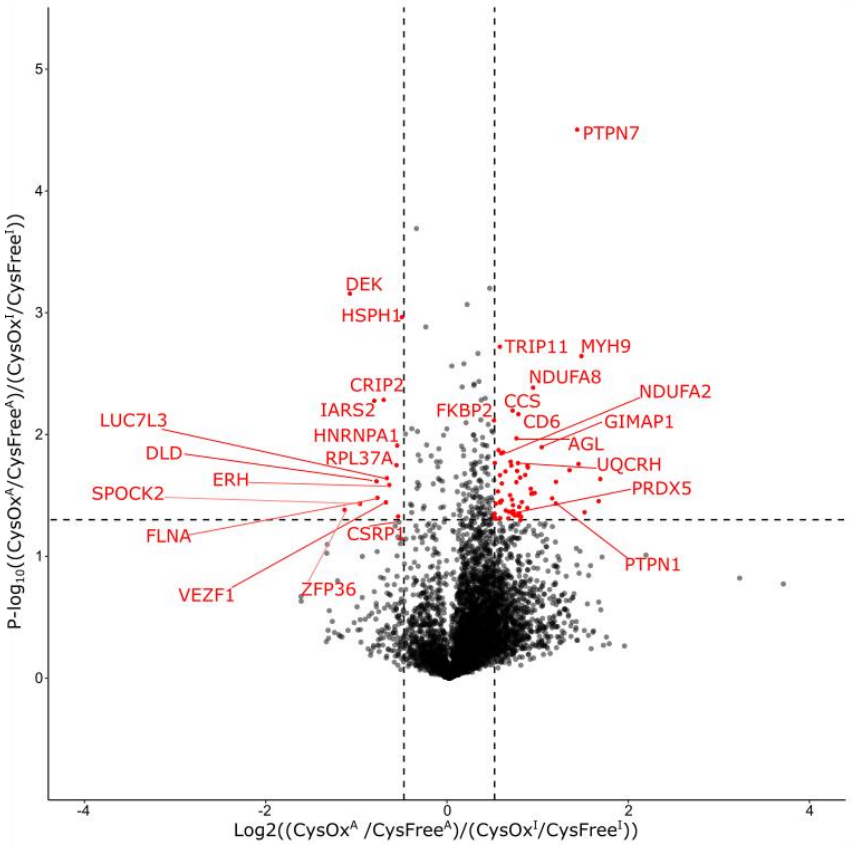

Figure 21: Volcano plot of proteins with regulated (fold-change) reduced (left) and oxidized (right) cysteine residues in PMA-activated CD4 T cells.

Thiol switching allows for the identification of 76 conserved proteins which are either differentially oxidised (62) or differentially reduced (14) in activated CD4+ T cells versus inactive CD4+ T cells isolated from human PBMCs (highlighted in red), when incubated with 10ng/ml PMA for 1 hour. X axis shows the $\log_2$ fold change of the ratio between the stimulated ratio over the unstimulated oxidation ratio for each cysteine residue. Y axis shows the $-\text{Log}_{10}$ P value of the ratio between the stimulated ratio over the unstimulated oxidation ratio for each cysteine residue. Statistical significance was determined with a two-sided, paired T-test, and a P value of –log10 1.3 ($P < 0.05$) was taken as significant.

When comparing the degree of oxidation vs reduction following PMA stimulation, there is a shift towards oxidation as can be observed in the degree of shift of the cysteine residues to the positive sided of the volcano plot, regardless of significance. Moreover, this is mirrored in the number of significantly modified proteins, of which 62 were found increasingly oxidized while only 14 residues were determined to be differentially reduced following stimulation.

When looking on the major molecular functions of the significantly regulated proteins (Figure. 22) it was found that cytoskeleton dynamics (Table. 4) were found regulated by oxidation.

Table 4: Proteins containing differentially oxidized cysteine residues involved in cytoskeleton dynamics.

Sequence	Gene name	Fold Change ($\text{Log}_{(2)}$)	% Change in oxidation	Localization
LVLACEDVR	TRIP11	0.57	5%	Cytoskeleton
KAGCAVTSLLASELTK	DIAPH1	0.87	7%	Cytoskeleton
CSQFCTTGMDGGMSIWDVK	ARPC1B	1.14	2%	Cytoskeleton
LCCGLSMFEVILTR	CYFIP1	1.66	7%	Cytoskeleton
LTTPTYGDLNHLVSATMSGVTTCLR	TUBB4B	1.44	4%	Cytoskeleton
LQLQEQLQAETELCAEAEELR	MYH9	1.47	4%	Cytoskeleton
CSYQPTMEGVHTVHVTFAGVPIPR	FLNA	0.55	15%	Cytoskeleton
GIPMVLIGCK	RHOF	0.76	6%	Cytoskeleton
RAQDVDATNPNYEIMCMIR	KIF2A	0.63	1%	Cytoskeleton
SQSYIPTSGCR	PLEKHA2	1.68	11%	Cytoskeleton
NLCSDDTPMVR	PPP2R1A	1.19	3%	Cytoskeleton
SEAHLTELLEEICDR	CNPY2	0.95	7%	Cytoskeleton
ALLALCGGED	ANXA6	0.52	1%	Cytoskeleton
LGTTASVCQLLK	EML2	0.69	7%	Cytoskeleton
NCSETQYESK	YWHAG	0.58	3%	Cytoskeleton

Additionally, mitochondrial immune functions and antioxidant systems were enriched in the oxidized population. Such as PRDX5 which was mentioned previously (Chapter. 4.2.2), in addition Copper Chaperone for Superoxide dismutase (CCS), BAG family

molecular chaperone regulator 2 (BAG2) and Thiosulfate:glutathione sulfurtransferase (TSTD1) (Supplementary Table. 4).

Conversely, the major function in the reduced candidates (Figure. 23) was zinc binding proteins and RNA binding. Interestingly, the susceptibility of zinc binding proteins has been found in a similar proteomics study [157].

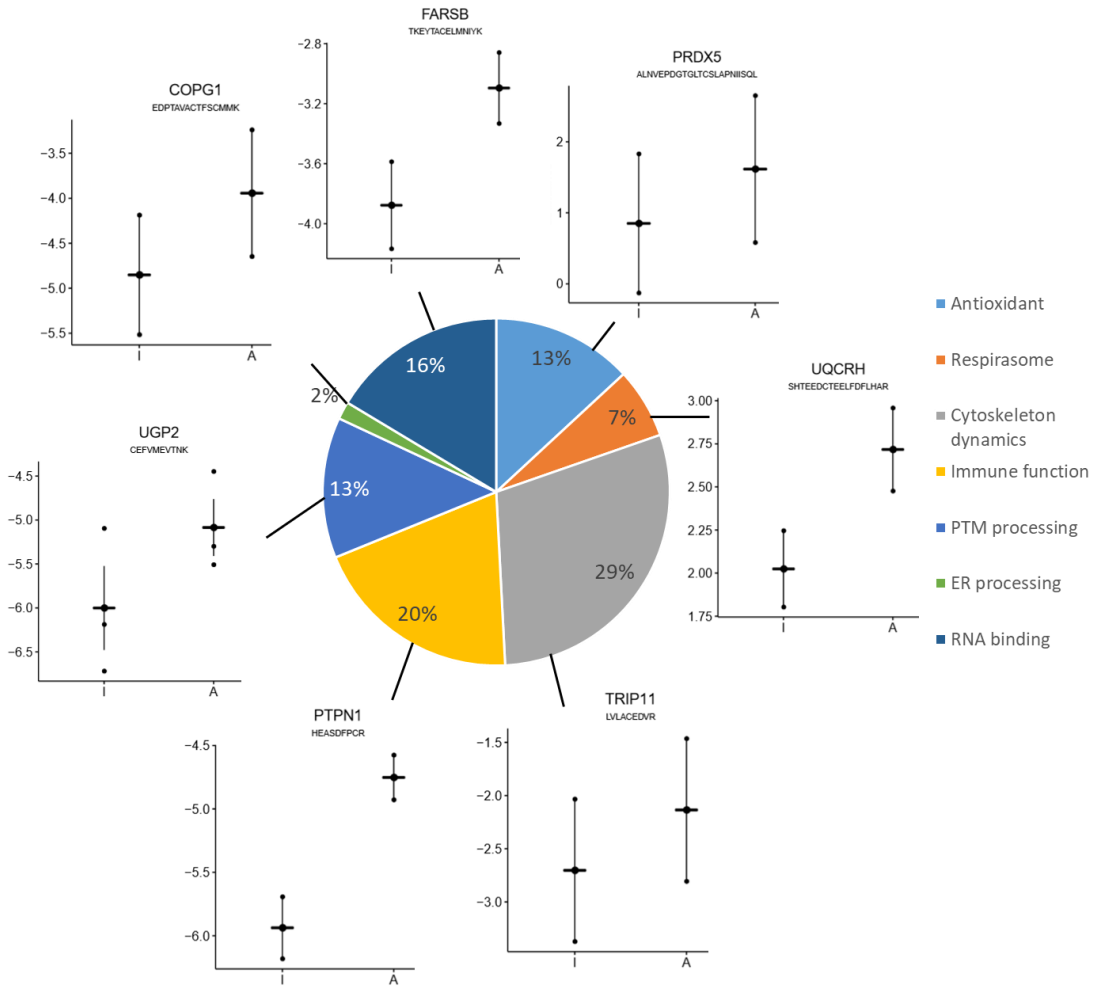

Figure 22: Enriched cellular processes in the groups of differentially regulated oxidized components in activated T cells following PMA stimulation.

Of the oxidized candidate pool (62) a large proportion were cytoskeleton dynamics and mitochondrial immune function, with representative data points.

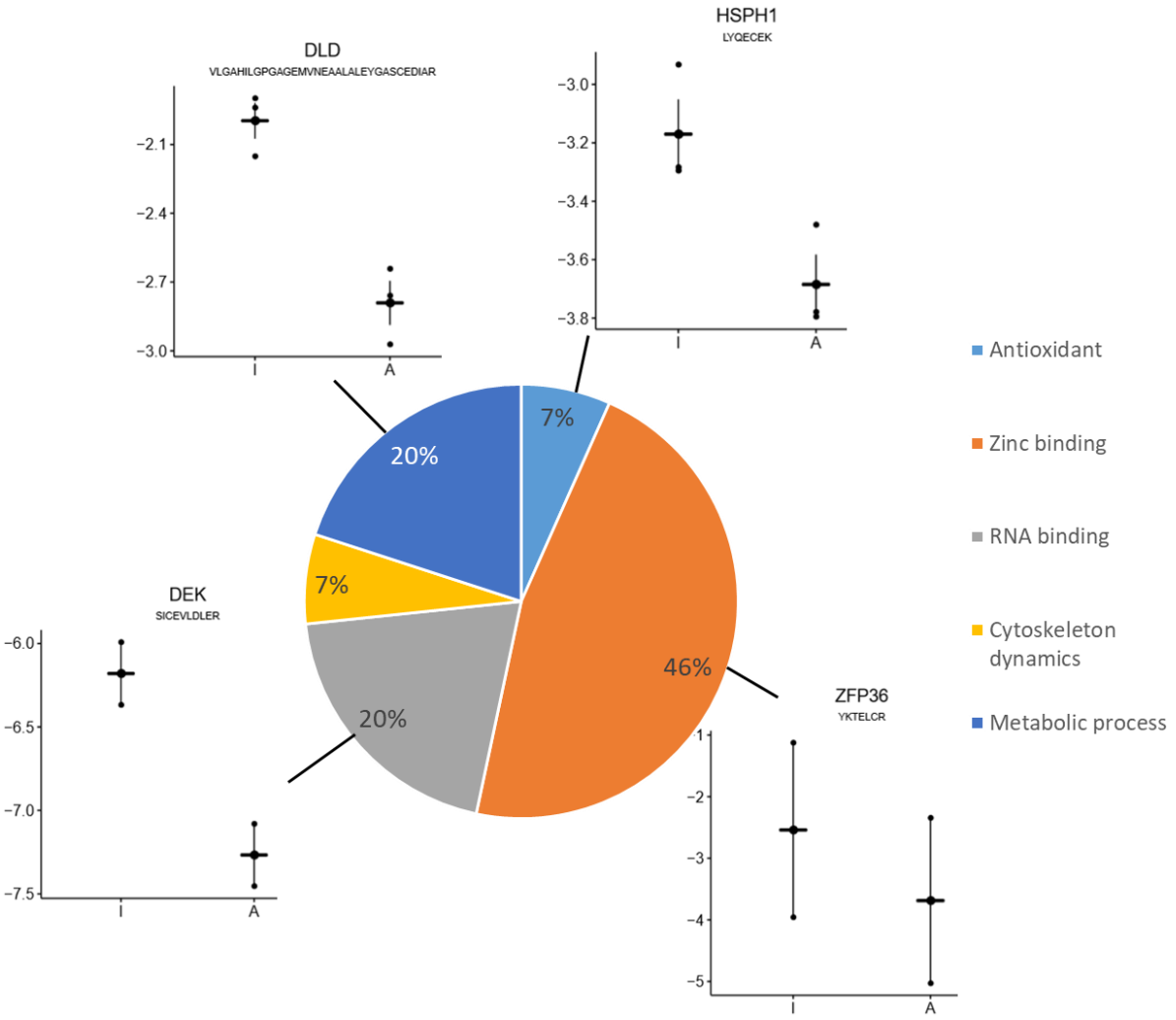

Figure 23: Enriched cellular processes in the groups of differentially regulated reduced components in activated T cells following PMA stimulation.

In the reduced candidate pool (14) the large majority of reduced cysteine residues were members of zinc binding motifs (45%) as well as some RNA binding and metabolic processes, with representative data points.

Strikingly, when focusing on the top 10 highly significantly regulated oxidized peptides/proteins (Table. 5), the majority of candidates were found to be cytoskeleton or cytoskeleton-associated proteins. Of these, binding partners of the Actin-related protein 2/3 complex (ARP2/3), such as Actin-related protein 2/3 complex subunit 1B (ARPC1B), and wave regulatory complex (WRC).

Additionally, a component of the CI Complex NDUFA8 as well as other components of the respirasome NDUFA2 and UQCRH showed to be highly oxidized upon T cell activation. The latter is not surprising, since the respirasome has been described to be particularly sensitive to oxidation in other cell systems as well [157,158].

Table 5: Top 10 most statistically significant (fold-change) differentially oxidized candidates from redox proteome data following PMA stimulation.

Identified sequence and modified cysteine residues are highlighted along with associated gene names, Log2 fold change, and % change in oxidation, function and localization of cysteine residue candidates. The major functions are cytoskeleton dynamics as well as mitochondrial electron transport while the major localizations are the cytoplasm and cytoskeleton

Sequence	Gene name	Fold change ($Log_{(2)}$)	% Change in oxidation	Function	Localization
SLGAVEPICSVNTPR	PTPN7	1.42	10	Immune response	Cytoplasm
LVLACEDVR	TRIP11	0.57	5	Cytoskeleton dynamics	Golgi
LQLQEQLQAETELCAEAEELR	MYH9	1.47	1	Cytoskeleton dynamics	Cytoskeleton
AAAHHYGAQCDKPNK	NDUFA8	0.93	8	Oxidative phosphorylation	Mitochondrial inner membrane
QICSCDGLTIWEER	CCS	0.71	4	Antioxidant	Cytoplasm
LCEVVEHACR	CD6	0.77	5	Immune response	Cell membrane
GWDQGLLGMCEGEKR	FKBP2	0.50	7	Immune response	Cell membrane
SHTEEDCTEELFDFLHAR	UQCRH	0.70	7	Oxidative phosphorylation	Mitochondrial inner membrane
CHVEVVDTPDIFSSQVSK	GIMAP1	1.03	10	Cytoskeleton dynamics	Endoplasmic Reticulum
RAPSVANVGSHCDLSLK	FLNA	1.55	15	Cytoskeleton dynamics	Cytoskeleton

In addition to the mitochondria, I identified the endoplasmic reticulum (ER), an organelle attached to the mitochondria [159], as ROS sensitive. GTPase IMAP family member 1 (GIMAP1), GIMAP1 is an ER protein known to mediate an oxidative stress response[160] in the ER. Furthermore, ERO1A is a protein known to induce disulfide bond formation in the ER and therefore utilizes disulfide bonds which may implicate ERO1A in ER stress.

Conversely, when focusing on the top 10 highly significantly regulated reduced peptides/proteins (Table 6), it was obvious that the vast majority were zinc-binding proteins (60%), and more specifically, zinc finger proteins. For example mRNA decay

activator protein ZFP36 (ZFP36) and 60S ribosomal protein L37-A (RPL37A). Additionally, since many of candidates are associated to the nucleus (40%), the nucleus seemed particularly resistant to oxidation as described before [128]. Interestingly, the only mitochondrial proteins identified Isoleucine--tRNA ligase (IARS2) and DLD are annotated as mitochondrial matrix localized, which is a highly reducing compartment [129].

Table 6: Top 10 most statistically significant (fold-change) differentially reduced candidates from redox proteome data following PMA stimulation.

Identified sequence and modified cysteine residues are highlighted along with associated gene names, Log2 fold change, % change in oxidation function and localization. The major function is zinc binding while the major localizations are the nucleus and mitochondrial matrix.

Sequence	Gene name	Fold change ($Log_{(2)}$)	% Change in oxidation	Function	Localization
SICEVLDLER	DEK	-1.09	-1	RNA binding	Nucleus
LYQECEK	HSPH1	-0.51	-3	Antioxidant	Cytoplasm
CDKTVYFAEK	CRIP2	-0.71	-4	Zinc binding	Cell membrane
RPYWCISR	IARS2	-0.82	-3	Zinc binding	Mitochondrial matrix
EKPPCLAELER	SPOCK 2	-0.57	-9	Metabolic process	Extracellular
YTCSFCGK	RPL37A	-0.57	-5	Zinc binding	Cytoplasm
SDLGPCEK	LUC7L3	-0.68	-1	Zinc binding	Nucleus
VLGAHILGPGA GEMVNEAALAL EYGASCEDIAR	DLD	-0.79	-7	Metabolic process	Mitochondrial matrix
NHACEMCGK	VEZF1	-0.69	-4	Zinc binding	Nucleus
YKTELCR	ZFP36	-1.15	-9	Zinc binding	Nucleus

When looking on the largest changes in absolute protein oxidation (Figure. 24) as described previously (Figure. 15C top equation), a cutoff of 5% change in absolute oxidation was chosen as it is conventional in similar studies [147,157]. From these criteria 17 candidates were found significantly oxidized or reduced following

stimulation (Supplementary Table. 5), of which 15 were oxidized and 2 were reduced mirroring the bias to oxidation in previous analysis. The range of P values of candidates ranged from $-\log_{10}$ of 1.3 ($P < 0.05$) up to a $-\log_{10}$ of 2.54 ($P < 0.0029$), while the changes in oxidation ranged from -7% to +15%.

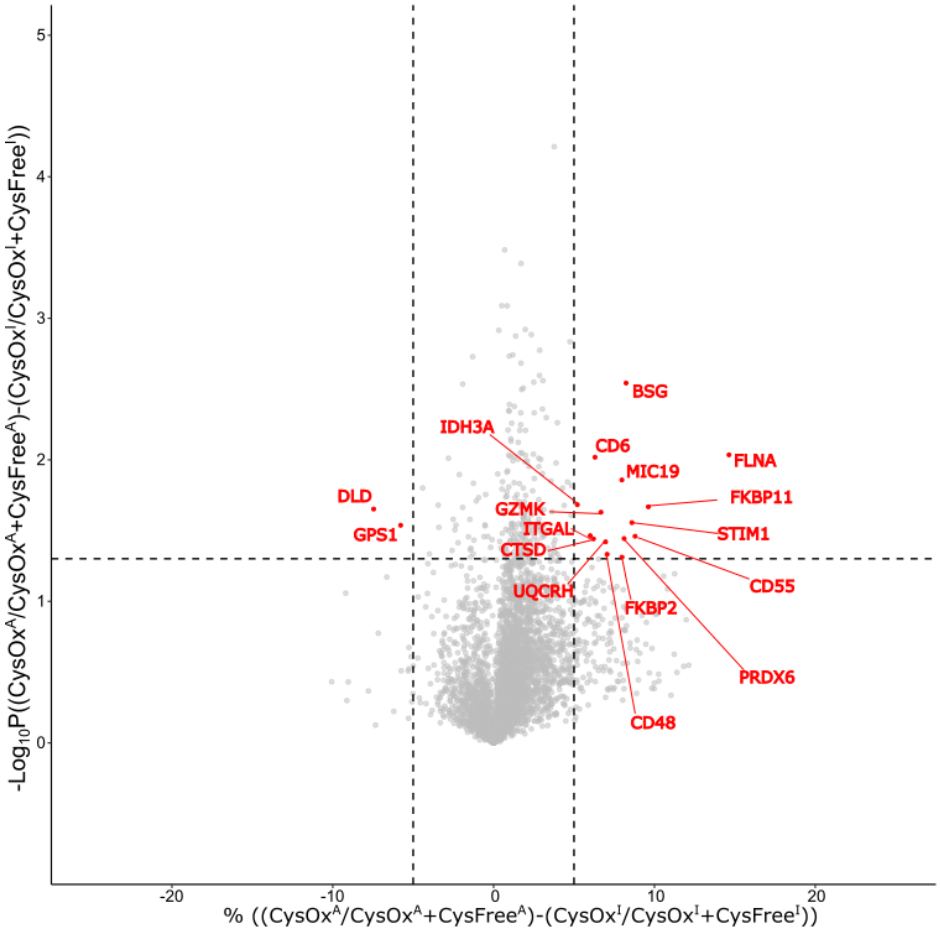

Figure 24: Volcano plot of proteins with % change in oxidation of reduced (left) and oxidized (right) cysteine residues in CD4⁺ T cells following incubation of PBMCs with PMA

Thiol switching allows for the identification of 17 conserved proteins which are either differentially oxidized (15) or differentially reduced (2) in stimulated CD4+ T cells versus unstimulated CD4+ T cells isolated from human PBMCs (highlighted in red), when incubated with 10ng/ml PMA for 1 hour. X axis shows the % change in oxidation between the stimulated minus the unstimulated condition for each cysteine residue. Y axis shows the $-\text{Log}_{10}$ P value of the ratio between the % change in oxidation between the stimulated minus the unstimulated condition for each cysteine residue. Statistical significance was determined with a two-sided, paired T-test, and a P value of –log10 1.3 ($P < 0.05$) was taken as significant.

When comparing both quantitative methods, that is to say fold change (Figure. 15C lower equation) against % change in oxidation (Figure. 15C top equation) it was obvious that as both methods identified differential candidates in most cases, they provide orthogonal data. (Table. 7).

Table 7: Top 10 most statistically significant %changes in cysteine oxidation from redox proteome data following stimulation with PMA

Identified sequence and modified cysteine residues are highlighted along with associated gene names, Log_2 fold change, % change in oxidation function and localization. The major function is surface marker expression while the major localizations are the plasma membrane and mitochondria.

Sequence	Gene name	Fold Change ($Log_{(2)}$)	% Change in oxidation	Function	Localization
SSEHINEGETAMLVCK	BSG	0.72	8.29	Surface marker	Plasma membrane
RAPSVANVGSHCDLSLK	FLNA	1.50	15	Cytoskeleton dynamics	Cytoskeleton
VTCAENR	CD6	0.98	6.36	Immune function	Plasma membrane
YESHPVCADLQAK	MIC19	0.88	8.03	Mitochondrial morphology	Mitochondria
TFDLYANVRPCVSIEGYK	IDH3A	0.52	5.26	α-ketoglutarate metabolism	Mitochondria
QVIPGLEQSLLDMCVGEKR	FKBP11	0.57	9.67	Protein folding	Cytoskeleton
VLGAHILGPGAGEMVNEAALALEYGASCEDIAR	DLD	-0.79	-7.41	Metabolic process	Mitochondrial matrix
DSCKGDSGGPLICK	GZMK	0.92	6.73	Immune function	Plasma membrane
ATGTSSGANSEESTAAEFCR	STIM1	0.72	8.65	Immune function	Plasma membrane
CAAGLAELAAR	GPS1	-0.81	-5.73	GTPase Inhibitor	Cytoplasm

The most significant candidates when looking on the change in % oxidation (Table. 7) followed a similar tendency to CD69 mentioned previously (Chapter 6.1), which was however not found significant, (Figure. 20). Basigin (BSG), CD6, Granzyme K (GZMK) and (Stromal interaction molecule 1) STIM1 all localize to the plasma membrane on T cell activation [161–164]. Data therefore suggests that % change in oxidation highlights proteins which undergo a major shift in oxidation but potentially not more moderate regulations, which are identified by the fold change (Figure. 21). Interestingly, when looking on candidates significant in both analyses (Figures. 21 and 24) I identified UQCRH (+8%), FLNA (+15%) and DLD (-7%) suggesting these cysteine modifications are regulated and robustly oxidized.

I decided to take advantage of these complementary evaluation methods to generate a more robust data set in which both regulated cysteine residues (fold change) and cysteine residues which undergo a large shift in oxidation are evaluated. Additionally, I have included for all major candidates found in the fold change experiments the average % change in oxidation, to give better context on mechanism of the candidates identified by fold change

To summarize, I established a multiplexed thiol switching technology to characterize the shift in cysteine oxidations following T cell stimulation with PMA. Cytoskeleton dynamics seem to be particularly susceptible to oxidation as well as known sites of electron leakage from the mitochondrial intermembrane space, while certain mitochondrial matrix associated proteins exhibited a shift to reduced cysteine residues such as DLD while antioxidant proteins in the mitochondria (PRDX5 and CCS) exhibit oxidation. In parallel, Zinc finger containing proteins as well as nuclear associated proteins show a susceptibility to reduction and may mediate a method of mtROS signaling to mediate transcription/translation.

Additionally, when looking on the proteins with the highest degree of shift in cysteine oxidation I enriched for surface markers which, in a similar manner to CD69 undergo extreme oxidation from the extracellular space. This data highlights in particular the mitochondria as an organelle with a diverse and controlled redox environment and the nucleus as a highly reducing compartment.

4.2.4 Exogenous Hydrogen Peroxide induces an oxidative stress response in the $CD4^+$ T cells redox proteome

Having examined the physiological response to PMA mediated T cell stimulation it was thought that by exposing the $CD4^+$ T cells to an excess of exogenous H_2O_2 it may be possible to identify the cysteine residues with the highest resistance to oxidation. This approach was thought to help determine proteins involved in antioxidant systems as well as confirm previous data which hinted at the ROS susceptibility of the mitochondria and apparent resistance of the nucleus (Figure. 21).

To accomplish this, PBMCs from 3 healthy donors were isolated and loaded with 5µM H_2DCFDA and 5µM 7AAD to quantify ROS signal and cell viability. Following which, cells were incubated with exogenous H_2O_2 from 0µM up to 1mM in the presence or absence of 10ng/ml PMA to determine the maximum oxidative stress that could be analyzed. Cells were then analyzed by flow cytometry (Figure. 25).

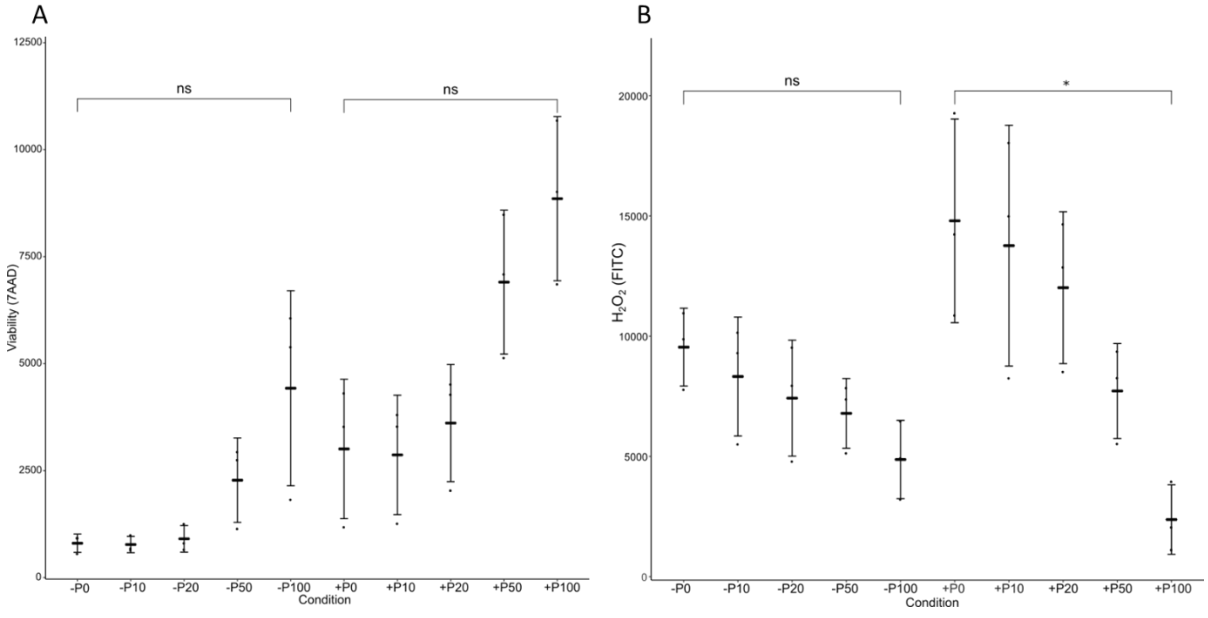

Figure 25: Increasing concentrations of exogenous hydrogen peroxide yield no significant loss of viability while reducing H_2O_2 signal in unstimulated and PMA stimulated cells.

A) Cell viability is no statistically significantly changed as shown by 7AAD staining of nuclear DNA in either stimulated or unstimulated CD4+ T cells. B) Increasing concentrations of exogenous H_2O_2 lead to a decreasing ROS signal as shown by H_2DCFDA fluorescence. Where –P is the absence of 10ng/ml PMA, +P is the presence of 10ng/ml PMA and the numbers signify the µM concentration of exogenous H_2O_2.

In regards to the cell viability there was no significant change in either the unstimulated or PMA activated cells between 0 and 100µM H_2O_2 (after 100µm cells began to lyse excessively – not shown) as shown with 7AAD staining (Figure. 25A). On the contrary, with respect to the ROS production (Figure. 25B) I noticed an interesting trend independent of activation state. In which, increasing concentrations of exogenous H_2O_2 resulted in a decrease in the intracellular ROS signal. As such, there was a significant reduction in H_2O_2 signal at 100 µM from an average of 15000 MFI units to 2500 MFI units. I hypothesized that this decrease in ROS signal was due to a hitherto unknown antioxidant compensatory system which was reducing the increasing amounts of ROS.

With this in mind I performed redox proteomics from 3 healthy donors as done previously (Figure. 15A), in the presence or absence of 10ng/ml PMA. Additionally, cells were incubated with 100µM of H_2O_2, which was chosen as it yielded a major change in intracellular ROS signal without significant loss of cell viability.

The workflow resulted in the generation of 3720 cysteine containing peptides from all donors, of which 787 were found robustly quantified in 2 out of 3 donors and were used for data analysis (Supplementary Table. 6).

I observed only a moderate number of 10 modified candidates (Supplementary Table. 7). However, I assumed that potentially I are seeing only the most ”protected” cysteine residues, as the above conditions could quite easily lead to the generation of irreversible sulfinic and sulfonic acids (Figure. 7) which would not be labelled by our methodology and therefore not generate a ratio.

When comparing the degree of oxidation vs reduction following PMA stimulation with the equation $((CysOx^A/CysFree^A)/(CysOx^I/CysFree^I))$, there was again a shift towards oxidation. However, it can be seen (Figure. 26) that there are far more oxidized residues (80%) than reduced. The range of P values of all candidates ranged from $-\log_{10}$ of 1.3 ($P< 0.05$) up to a $-\log_{10}$ of 2.4 ($P<0.0039$) while the differences ranged from $\log_2$ -1.81 to 1.77.

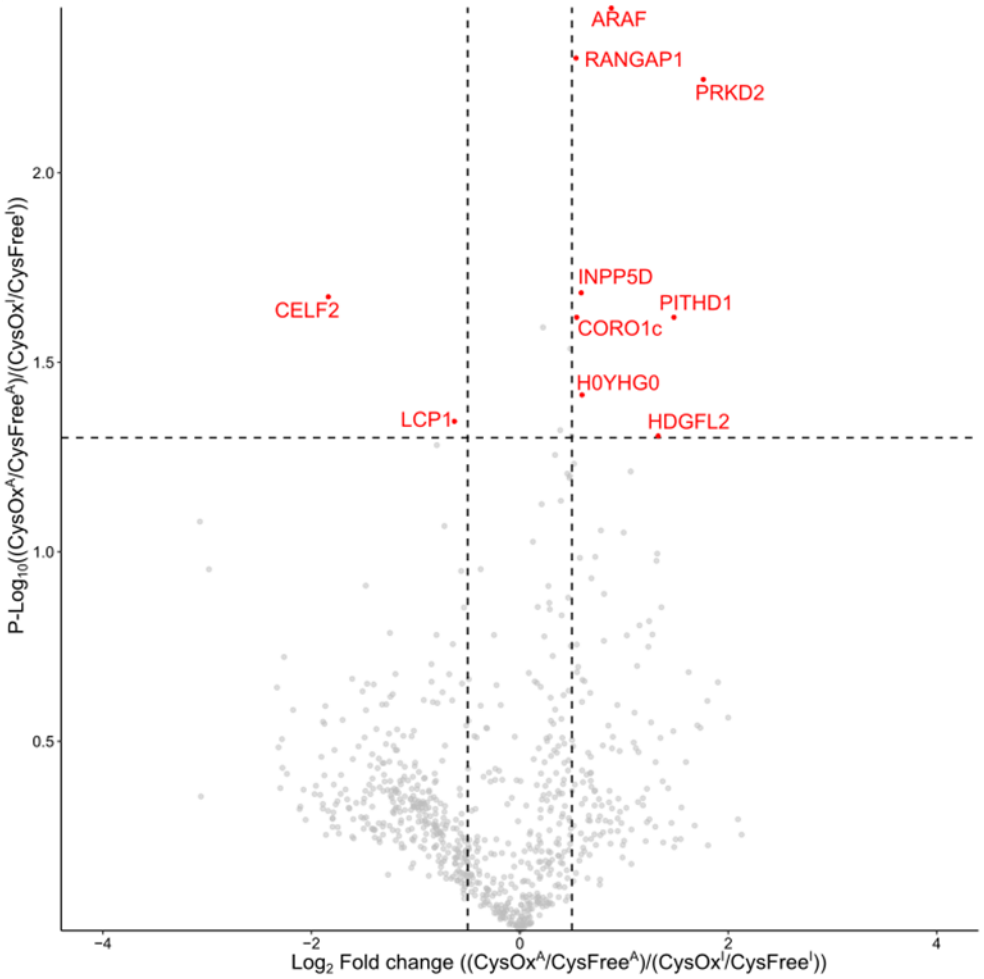

Figure 26: Volcano plot of proteins with regulated (fold-changed) reduced (left) and oxidized (right) cysteine residues in CD4⁺ T cells following incubation of PBMCs with 100µM H_2O_2

Thiol switching allows for the identification of 10 conserved proteins which are either differentially oxidized or differentially reduced in activated CD4+ T cells versus unstimulated CD4+ T cells isolated from human PBMCs (highlighted in red), when incubated with 10ng/ml PMA for 1 hour, both conditions were additionally incubated with 100µM H_2O_2. X axis shows the log2 fold change of the ratio between ($CysOx^A/CysFree^A$) over ($CysOx^I/CysFree^I$) for each cysteine residue while the Y axis shows the $-\log_{10}$ of the P value. Statistical significance was determined with a two-sided, paired T-test, and a P value of $-\log_{10}$ 1.3 ($P< 0.05$) was taken as significant.

The majority of these proteins were found to be involved in NF-κB signaling and oxidative stress response proteins (60%) as well as actin cytoskeleton dynamics (20%) (Table. 8). Data theorized that under these extreme conditions the T cells mediate protection of the most important anti-oxidative pathways which would suggest why they are reversibly oxidized which is a known protection mechanism [84,115]. However, it was observed that the exogenous H_2O_2 induced a larger shift in oxidation than under physiological conditions [154], this could suggest that H_2O_2 induces actin stiffening [132,165,166] *via* actin cytoskeleton disulfide bond formation.

Table 8: Top 10 most statistically significant candidates from redox proteome data in the presence of 100μM H2O2

Identified sequence and modified cysteine residues are highlighted along with associated gene names, Log_2 fold change, % change in oxidation function and localization. The major functions are antioxidant signaling and actin cytoskeleton dynamics.

Sequence	Gene Name	Fold Change ($_{Log(2)}$)	% Change in oxidation	Function	Localization
CAAEREEPPEQR	PITHD1	1.49	20.71	Antioxidant/NF-KB	Cytoplasm/ nucleus
CDLISIPK	CORO1C	0.55	9.33	Cytoskeleton dynamics	Cytoskeleton
CGSSEDLHDSVR	HDGFL2	1.34	20.24	Cell survival	Nucleus
GCAFVTFSTR	CELF2	-1.83	-16.90	Antioxidant/NF-KB	Nucleus
LAELKQECLAR	H0YHG0	0.61	9.82	Unknown	Nucleus
LGTSESLPCTAEELSR	PRKD2	1.77	26.60	Antioxidant/NF-KB	Nucleus
MVMTVFACLMGK	LCP1	-0.62	-14.33	Cytoskeleton dynamics	Cytoskeleton
QVEVINFGDCLVR	RANGAP1	0.55	7.84	Antioxidant/NF-KB	Nucleus
SFTCSSSAEGR	INPP5D	0.60	10.18	Antioxidant/NF-KB	Cytoplasm
TQADELPACLLSAAR	ARAF	0.89	14.52	Antioxidant/NF-KB	Cytoplasm/ mitochondria

When looking on the % shift in oxidation $((CysOx^A/(CysOx^A+CysFree^A))-(CysOx^I/(CysOx^I+CysFree^I)))$, it was apparent that more candidates were identified, suggesting there is a greater shift in total oxidation of discrete cysteine residues than a large number of regulations (Figure. 27).

Indeed 22 cysteine residues from the original 787 cysteine residues exhibited significant shifts in % oxidation following PMA stimulation (Supplementary Table. 8) in the presence of 100μM H_2O_2. Of which, 12 were differentially oxidized and 10 were differentially reduced (Supplementary Table. 9). A cutoff of 5% change in absolute oxidation was selected again as significant. The range of P values of candidates ranged from $-log_{10}$ of 1.3 ($P< 0.05$) up to a $-log_{10}$ of 2.85 ($P< 0.0014$), while the changes in oxidation ranged from -16% to +20%.

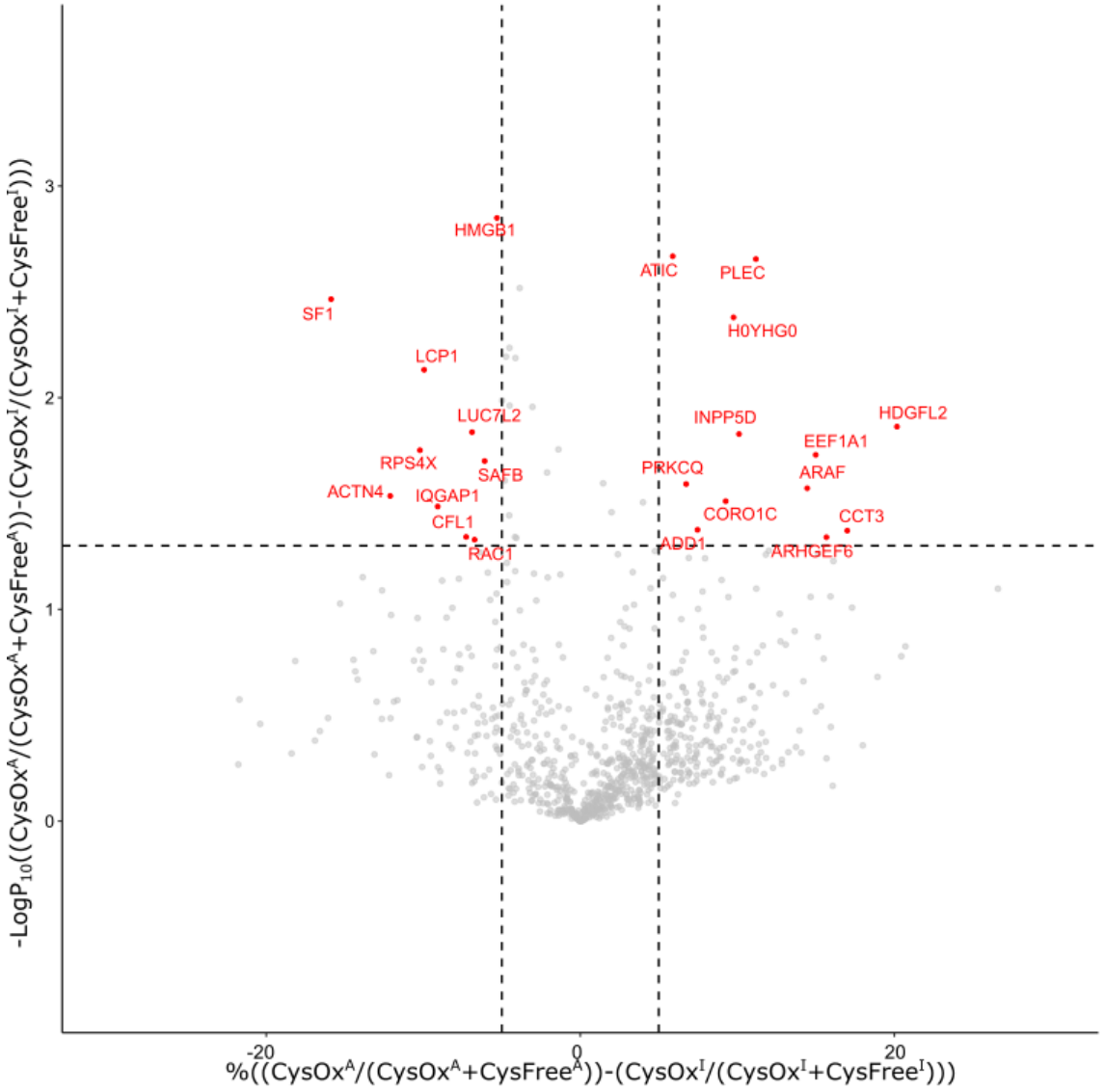

Figure 27: Volcano plot of proteins with % change in oxidation of reduced (left) and oxidized (right) cysteine residues in CD4+ T cells following incubation of PBMCs with 100µM H2O2

Thiol switching allows for the identification of 22 conserved proteins which are either differentially oxidized (12) or differentially reduced (10) in stimulated CD4+ T cells versus unstimulated CD4+ T cells isolated from human PBMCs (highlighted in red), when incubated with 10ng/ml PMA for 1 hour, *both conditions were additionally incubated with 100µM H_2O_2* . X axis shows the % change in oxidation between the stimulated minus the unstimulated condition for each cysteine residue. Y axis shows the $-Log_{10}$ P value of the ratio between the % change in oxidation between the stimulated minus the unstimulated condition for each cysteine residue. Statistical significance was determined with a two-sided, paired T-test, and a P value of –log10 1.3 ($P< 0.05$) was taken as significant.

When looking on the most significantly regulated major shifts in oxidation (Table. 9) it was possible to observe that similarly to the log_2 regulations above, cytoskeleton dynamics were a major target of exogenous ROS. Interestingly however, the most regulated candidate was High mobility group protein B1 (HMGB1). Which is a redox active protein localized to the plasma membrane In the presence of exogenous H_2O_2 [167]. Additionally, Plectin (PLEC) is known to form disulfide bonds between actin and induce stiffness in oxidative stress [168].

When looking on the reduced candidates, a particularly interesting candidate was Ras-related C3 botulinum toxin substrate 1 (RAC1) which is an activator of the WRC and has been found to be a target of physiological mtROS signaling in previous data (Chapter. 4.2.3). RAC1 and was protected under oxidative stress, suggesting as with Plastin-1 (LCP1) $CD4^+$ T cells attempt to protect cell motility in oxidative stress.

Table 9: Top 10 most statistically significant %changes in cysteine oxidation from redox proteome data in the presence of 100µM H2O2

Identified sequence and modified cysteine residues are highlighted along with associated gene names, Log_2 fold change, % change in oxidation function and localization

Sequence	Gene Name	Fold Change (Log_2)	% Change in oxidation	Function	Localization
MSSYAFFVQTCR	HMGB1	-1.28	-5.10	Extracellular H_2O_2 signal	Plasma membrane
MSSFGDFVALSDVCDVPTAK	ATIC	0.39	5.95	Metabolic function	Cytoplasm
AFCGFEDPR	PLEC	0.78	11.25	Cytoskeleton dynamics	Cytoskeleton
CGGAGHIASDCK	SF1	-0.92	-15.81	Zinc ion binding	Nucleus
LAELKQECLAR	H0YHG0	0.61	9.82	Unknown	Nucleus
MVMTVFACLMGK	LCP1	-0.85	-9.88	Cytoskeleton dynamics	Cytoskeleton
CGSSEDLHDSVR	HDGFL2	1.34	20.24	Cell survival	Nucleus
MDLGECLK	LUC7L2	-1.38	-6.83	RNA binding	Nucleus
SFTCSSSAEGR	INPP5D	0.60	10.18	Antioxidant/NF-KB	Cytoplasm
FDTGNLCMVTGGANLGR	RPS4X	-0.59	-10.15	RNA binding	Cytoplasm

To conclude, oxidative stress mediates the induction of oxidations which induce NF-κB signaling to reduce oxidative stress. Additionally, under stress conditions actin stiffening is induced, potentially as a mechanism to avoid oxidative stress [132].

4.3 Protein translation characterizes mtROS mediated immune response in $CD4^+$ T cells

Redox proteomics was capable of elucidating PMA induced changes in the oxidation state of discrete groups of proteins. Confirming the theory that PMA stimulation induces mtROS signaling in $CD4^+$ T cells.

In particular, the nucleus was found to be resistant to oxidative stress and that zinc binding proteins, such as zinc fingers which are nucleus associated were differentially

reduced suggesting an impact on transcription/translation (Chapter. 4.2.3). The corollary of this observation was whether this mtROS signaling invoked a subsequent change in $CD4^+$ T cell protein synthesis. As such, the primary aim of the following work was to elucidate mtROS dependent protein turnover.

To accomplish this it was necessary to employ a method to remove the oxidative signal while keeping the PMA mediated $CD4^+$ T cell activation intact. With this aim in mind, I made use of exogenous catalase to reduce the mtROS signal invoked by PMA. It was observed that catalase is capable of reducing the oxidative signal of $CD4^+$ T cells within the PBMC fraction (Figure. 13). However, this ROS reduction via catalase was found to be only moderately effective in isolated T cells while it was far more effective in PBMCs. Suggesting that catalase utilized an indirect intercellular signaling pathway and a direct antioxidant effect on $CD4^+$ T cells to mediate an mtROS quenching effect (Figure. 14).

As such, it was decided to utilize the interactions between PBMCs and catalase to generate a model system in which it was possible to measure the ROS dependent transcription & translation as well as the anti-oxidative signaling generated by catalase dependent pathways.

Protein synthesis was measured utilizing the non-canonical amino acid (NCAA), non-canonical methionine (NCM) derivative L-Azidohomoalanine (AHA) that allowed for enrichment of newly synthesized proteins (Chapter. 1.5.2). It is know that AHA incorporation occurs via the replacement of methionine residues. AHA was taken up by cells from the media and incorporated into newly translated proteins without damaging the protein structure or function [124].

To analyze the protein turnover dependent on mtROS (Figure. 28A) PBMCs were first isolated from the blood of 3 healthy donors and incubated for 1h in the presence or absence of PMA and/or catalase (Figure. 28A step 1). This time point was utilized to trigger or quench the early mtROS response characterized in the previous chapters (Chapter. 4.1.2-4.1.5). Following activation, the $CD3^+CD4^+$ T cells were negatively isolated and depleted of endogenous methionine (Figure. 28A Step 2) for 1h which improves the incorporation of AHA due to the preferential affinity of methionine with the associated tRNA. Cells were incubated for 16h with AHA to allow labelling of newly synthesized proteins, generated in part by mtROS signaling (Figure. 28A Step 3).

Following lysis cells were covalently “clicked” to alkyne beads(Figure. 28A Step 4) and stringently washed, the aggressive washing allows for higher specificity than is possible with conventional affinity purification (Figure. 28A Step 5) an example is 8M urea used on clicked samples (Chapter. 3.5.2) compared to 1M in conventional affinity workflows [169]. Peptides were then dried in a speedvac before being analyzed by nano-LC coupled to an Orbitrap fusion tribrid MS (Figure. 28A Step 6).

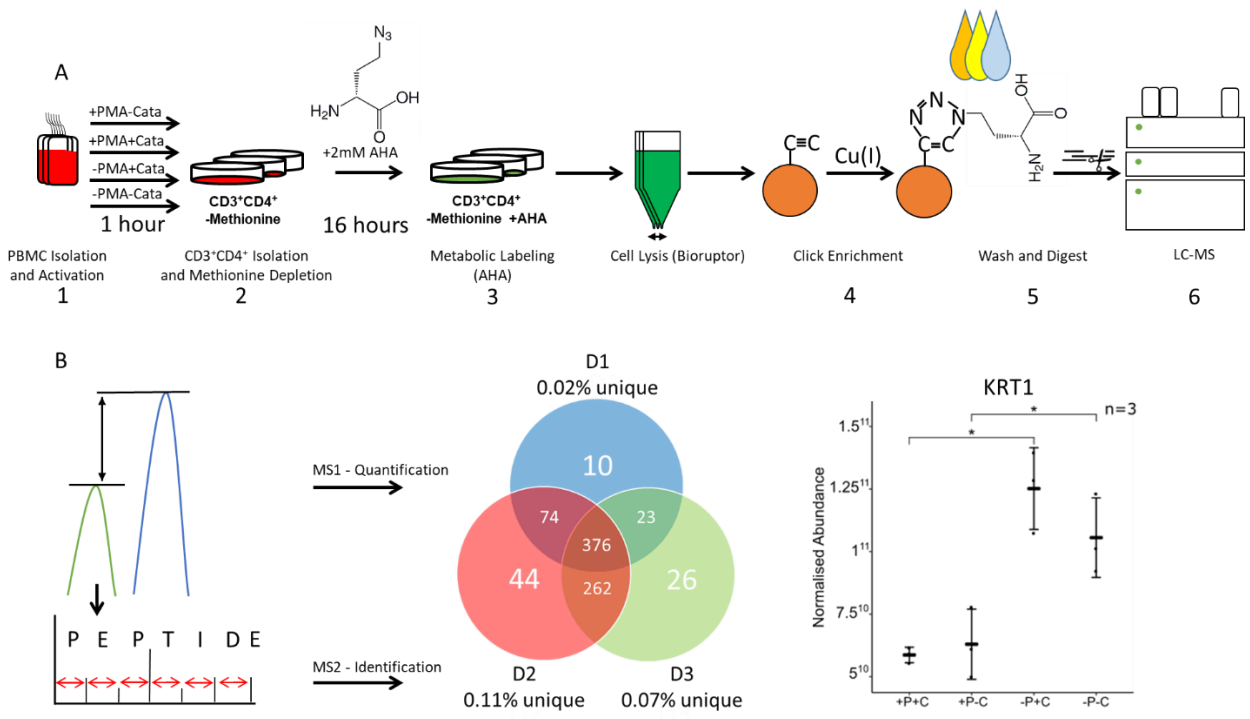

Figure 28: NCAA workflow allows for identification and quantification of newly synthesized proteins following PMA and catalase stimulation. MS¹ spectra were used for quantification while MS² spectra were used for identification.

A) 16 hour metabolic labeling with AHA allows for the incorporation of an azide moiety into newly synthesized proteins from 12 independent CD4+ T cell samples, which can be covalently bonded to a resin via a copper catalyzed cycloaddition with an immobilized alkyne. Allowing for the enrichment of newly synthesized proteins following stimulation in the presence or absence of 1mg/ml catalase and/or 10ng/ml PMA. Covalent enrichment allows for the use of aggressive washing increasing specificity, proteins are eluted from alkyne beads via enzymatic digestion by trypsin before being analyzed by nanoLC coupled to an Orbitrap fusion MS. B) Peptide ions are quantified via the ion intensity of the MS1 chromatogram, in parallel peptides are identified via HCD fragmentation experiments which generate amino acid sequences. Allowing the quantification of 590 newly synthesized proteins from all 3 biological donors. An example includes the fold increase in keratin presence in the unstimulated cells.

Utilizing this label free click enrichment experiment in cooperation with MS^1 quantification and MS^2 identification (Figure. 28B left), I was able to obtain a total of 815 Identified and quantified proteins (Supplementary Table. 10) from 12 independent proteomics experiments. Of these 815 proteins I identified 376 proteins (Figure. 28B center) from all 12 conditions from three donors (Supplementary Table. 11). I observed that when comparing the unstimulated to PMA stimulated conditions, the data show a major bias towards induced protein expression in the presence of PMA (Figures. 29 & 32).

This was expected as the unstimulated negative controls, which were largely quiescent would only produce a limited number of proteins [170]. Consequently, during the washing step (Figure 28. Step 5) the highly abundant impurities would constitute a greater proportion of the protein nonspecifically adhered to the beads. Indeed, in the control samples Keratin protein accounted for an average of 75% of the protein amount while in activated samples it accounted for an average of 25% (exemplified for Keratin 1 (KRT1) Figure. 28B right).

Therefore, Interpretation of data from the 4 aforementioned separate conditions (+PMA +Catalase, -PMA +Catalase, +PMA –Catalase & -PMA –Catalase) allowed me to define (i) the total immune response (+PMA –Catalase/-PMA –Catalase) derived from this early stimulation time point (Chapter. 4.3.1). (ii) The signaling capacity of catalase in $CD4^+$ primary T cells (-PMA -Catalase/-PMA +Catalase) explored, independent of PMA in Chapter. 4.3.2. And in cooperation with PMA in Chapter. 4.3.3 respectively (-PMA +Catalase/+PMA +Catalase). (iii) And finally, the mtROS dependent proteome which will constitute the differential significant candidates which are not present in the catalase specific T cell activation (+PMA +Catalase/-PMA +Catalase. Chapter 4.3.4).

4.3.1 PMA stimulation complements knowledge of known protein synthetic pathways in T cell stimulation

As mentioned previously, (Chapter. 4.3) the primary aim of this study was to identify how mtROS signaling mediates downstream transcription/translation, to ascertain how the mtROS signal impacts T cell activation and downstream immune function. In this line I utilized NCAAs to determine the protein turnover in the earliest stages of T cell activation and metabolic shift in $CD4^+$ T cells.

To this end, $CD4^+$ T cells were stimulated in the presence of 10ng/ml PMA and in the absence of 1mg/ml catalase. Cells were then isolated from the PBMC fraction purified from the blood of 3 healthy donors. Following data analysis, the abundances of the newly synthesized proteins produced following PMA stimulation were compared to the conditions without stimulation in the absence of catalase (+PMA-Catalase/-PMA-Catalase) and a fold change was generated.

With this approach it was possible to identify 60 proteins (Supplementary table. 12) that were newly synthesized in PMA stimulation without catalase from the 376 proteins mentioned previously (Figure. 29). The range of P values of candidates ranged from $-\log_{10}$ of 1.3 ($P< 0.05$) up to a $-\log_{10}$ of 3.5 ($P< 0.00032$), while the differences ranged from $\log_2$ 1.14 to 6.71.

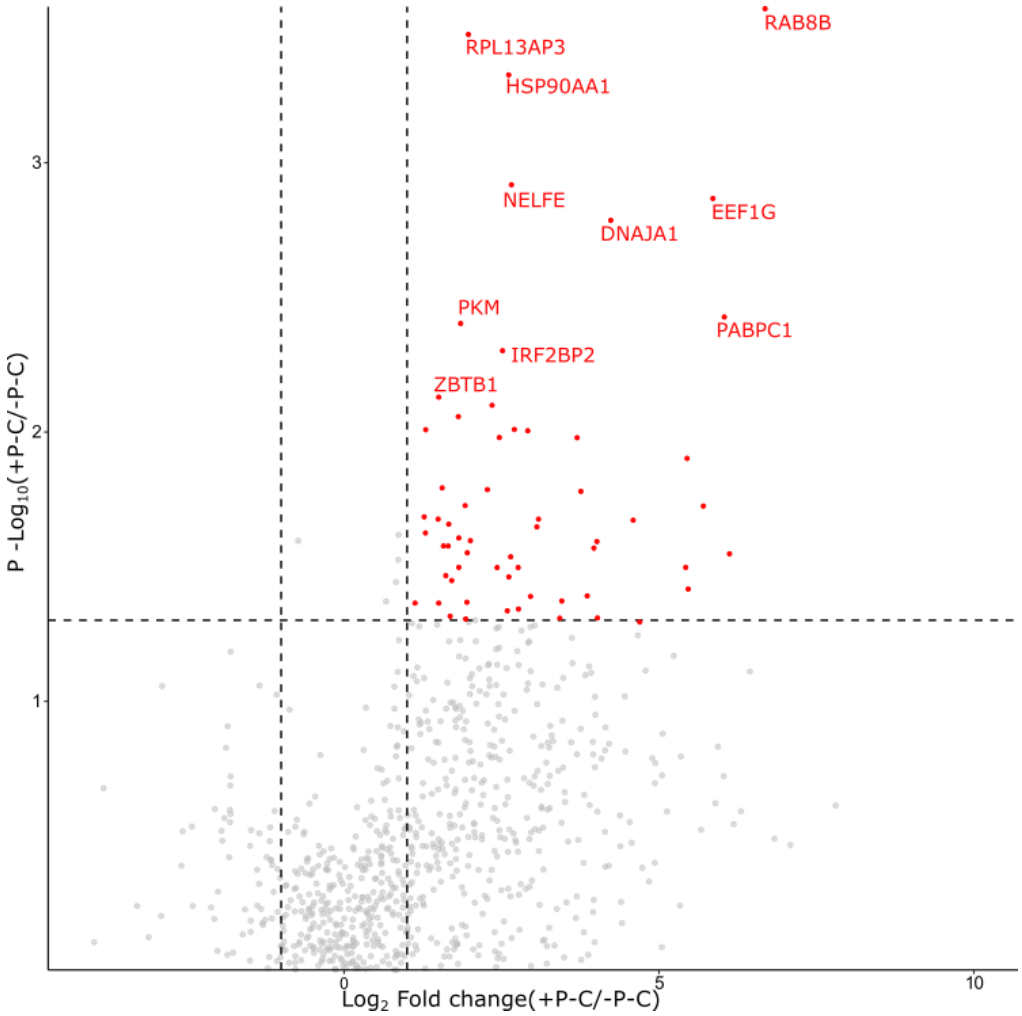

Figure 29: Volcano plot of newly synthesized proteins induced (fold-change) following PMA stimulation in the absence of catalase

AHA labelling of $CD4^+$ T cells allows for the identification of 60 significantly regulated newly synthesized proteins in the presence or absence of 10ng/ml PMA and in the absence of 1mg/ml catalase (highlighted in red). Cells were incubated with 10ng/ml PMA for 1 hour. X axis shows the $\log_2$ fold change of the ratio between the stimulated cells over the unstimulated. Where +P is +PMA and –C is –catalase. Y axis shows the $-\log_{10}$ of the P value. Statistical significance was determined with a two-sided, paired T-test, and a P value of $-\log_{10}$ 1.3 ($P < 0.05$) was taken as significant.

As a proof of concept it was necessary to compare this data set with published data. Indeed, Dieterich and colleagues looked on the protein translation in primary human T cells stimulated with PMA and ionomycin [171]. It was found that 50% of the generated data overlapped with previous data (Table. 10). This suggests that my data set could complement the established knowledge base.

Table 10: Overlapping proteins found in my study of the PMA stimulated immune response without catalase which follow the same transcription profile as [182].

Gene name	P value ($-Log_{10}$)	Fold Change ($Log_{(2)}$)
HSP90AA1	3.33	2.63
DNAJA1	2.79	4.25
PABPC1	2.43	6.06
PKM	2.41	1.87
YBX1	2.06	1.83
HSP90AB1	2.02	2.72
FUS	2.02	1.32
FUBP1	1.99	2.49
NFKB2	1.99	3.72
CD44	1.79	3.78
HNRNPU	1.69	1.29
PRRC2C	1.67	1.68
HSPA5	1.66	3.08
DDX3X	1.60	2.03
DDX3X	1.60	2.03
SNRPB	1.60	4.03
TUBB4B	1.58	1.67
EIF4A1	1.50	1.84
HNRNPH1	1.50	5.45
EIF4A3	1.50	2.78
VIM	1.46	1.73
EEF1D	1.42	5.48
CHMP4A	1.40	2.98
HNRNPA1	1.37	1.15
HSPA9	1.35	2.79
HSPA9	1.35	2.79
CSTF2T	1.32	1.70

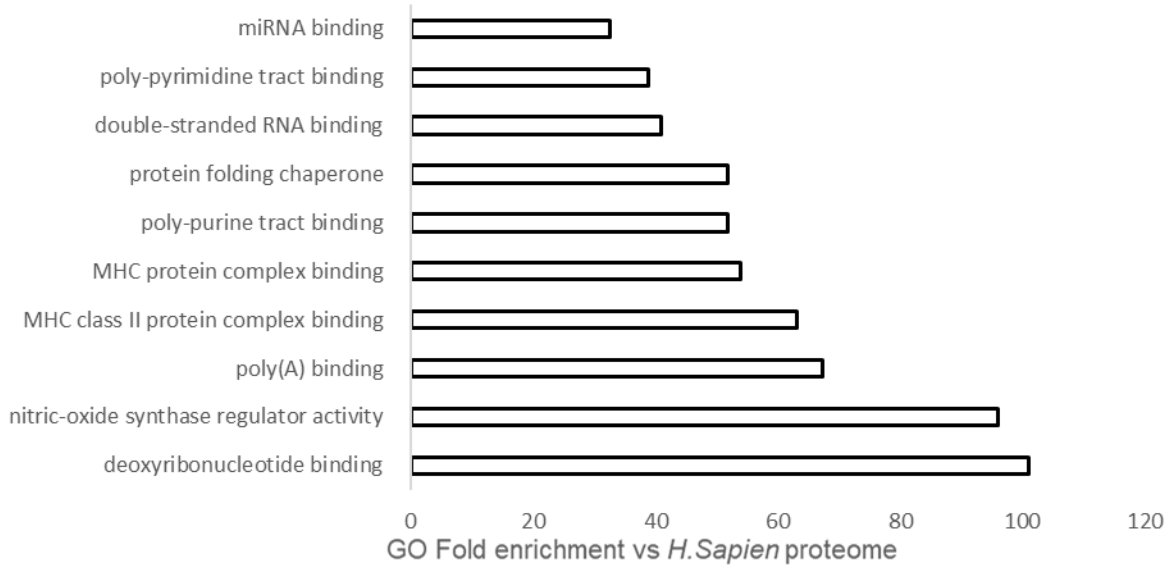

Figure 30: Enriched molecular function of newly synthesized proteins following PMA stimulation without catalase

Statistically significant enriched molecular functions from protein turnover. Enriched functions were determined by comparison of candidates to *homo sapien* gene ontology database. Enriched functions include DNA binding. Statistical significance was determined with a two-sided, paired T-test, and a P value of 0.05 was taken as significant.

When looking on the enriched functions, which were found by comparing candidates against the gene ontology database (Figure. 30) [172]. It was found that both DNA binding was upregulated. In particular a group of elongation factors which partly overlapped with literature data (Table. 10) were found (Table. 11)

Table 11: DNA binding candidates which are transcribed in the PMA stimulated immune response without catalase

Gene names	P ($-\log_{(10)}$)	Average Fold Change ($\text{Log}_{(2)}$)
EEF1G	2.87	5.88
EEF1D	1.42	5.48
EIF4A1	1.50	1.84
EIF4A3	1.50	2.78
HNRNPU	1.69	1.29
HNRNPA1	1.37	1.15

These factors are known to be associated with NF-κB signaling and will be expanded on in future chapters (Chapter. 5.6.1).

Interestingly, the following components were found transcribed following stimulation with PMA. Family with sequence similarity 49 member B (FAM49B) was transcribed with PMA stimulation. FAM49B plays a role in downregulating cytoskeleton dynamics [173] and is known to be redox sensitive [174]. Additionally, both Heat shock protein HSP 90-alpha and beta (HSP90AA1, HSP90AB1) are known to induce T cell activity and survival [175,176] via Major histocompatibility complex (MHC) interactions mediated by the cytoskeleton [177].

Table 12: Top 10 most significant newly synthesized proteins following PMA stimulation without catalase

Gene names, Log2 fold change values, function and localization are highlighted. The major enriched functions are transcription translation machinery including NFATc1 signaling components as well as metabolic shift regulators.

Gene Name	Fold Change ($_{Log(2)}$)	Function	Localization
RAB8B	6.71	GTPase activity	Plasma membrane
RPL13A	2.00	Oxidative stress response	Cytoplasm
HSP90A	2.63	Immune function	Plasma membrane
NELFE	2.68	Transcription/Translation	Nucleus
EEF1G	5.88	Transcription/Translation	Nucleus
DNAJA1	4.25	NFATc1 binding	Cytoskeleton
PABPC1	6.06	Oxidative stress response	Cytoplasm
PKM	1.87	Metabolic shift	Cytoplasm
IRF2BP2	2.54	NFATc1 binding	Nucleus
ZBTB1	1.52	Transcription/Translation	Nucleus

The candidates with the highest P values (Table. 12) partly mirrored the overall trend in the dataset, that is to say, the most significantly regulated functions also enriched for transcription/translation machinery (30%) as was hinted to previously in this chapter (Table. 11). Additionally, two of the most significant candidates Pyruvate kinase (PKM) and Insulin Receptor Substrate 2 (IRS2) are known mediators of the metabolic shift in T cell activation and clonal expansion [178,179]. Interestingly PKM is known to destabilize ZFP36 (Chapter. 4.2.3) which may explain why it was reduced under PMA stimulation [180].

Additionally, Interferon regulatory factor 2-binding protein 2 (IRF2BP2), which is known to downregulate Nuclear factor of activated T-cells, cytoplasmic 1 (NFATc1) [181] was found in my study as transcriptionally upregulated while found downregulated by the Dieterich lab (explained in greater detail in Chapter. 4.3.4 and Chapter. 5.6.5), potentially indicating the cooperation of calcium signaling and mtROS signaling.

Taken together, it is apparent that PMA stimulation triggers turnover of known T cell activation machinery, potentially novel is the enrichment of DNA binding components and proteins associated with actin dynamics and NF-κB activity which function to improve T cell activation and signaling. As well as metabolic reprogramming

machinery which displayed potentially synergistic results with the previous redox proteome study.

4.3.2 Catalase upregulates endocytosis in primary $CD4^+$ T cells while downregulating respiration.

Following elucidation of the immune response, it was necessary to determine the impact of catalase on protein turnover independent of PMA stimulation (Chapter. 4.1.5). The goal of this was to determine the signaling mechanisms invoked by catalase without the extensive confounding PMA signaling which was observed in the previous chapter.

To this end, I compared the differential expression of proteins (Chapter 4.3) in the absence of 10ng/ml PMA but in the presence of 1mg/ml catalase (-P-C/-P+C). From this, 15 significantly regulated proteins (Figure. 31 & Supplementary Table. 13) were identified from the original 376 proteins. The majority of proteins (13) were downregulated at the level of transcription and 2 were upregulated, which suggests that catalase is acting to inhibit protein translation and inhibiting biological processes. The range of P values of candidates ranged from $-\log_{10}$ of 1.3 ($P< 0.05$) up to a $-\log_{10}$ of 2.17 ($P< 0.0068$), while the differences ranged from $\log_2$ -2.25 to 2.81.

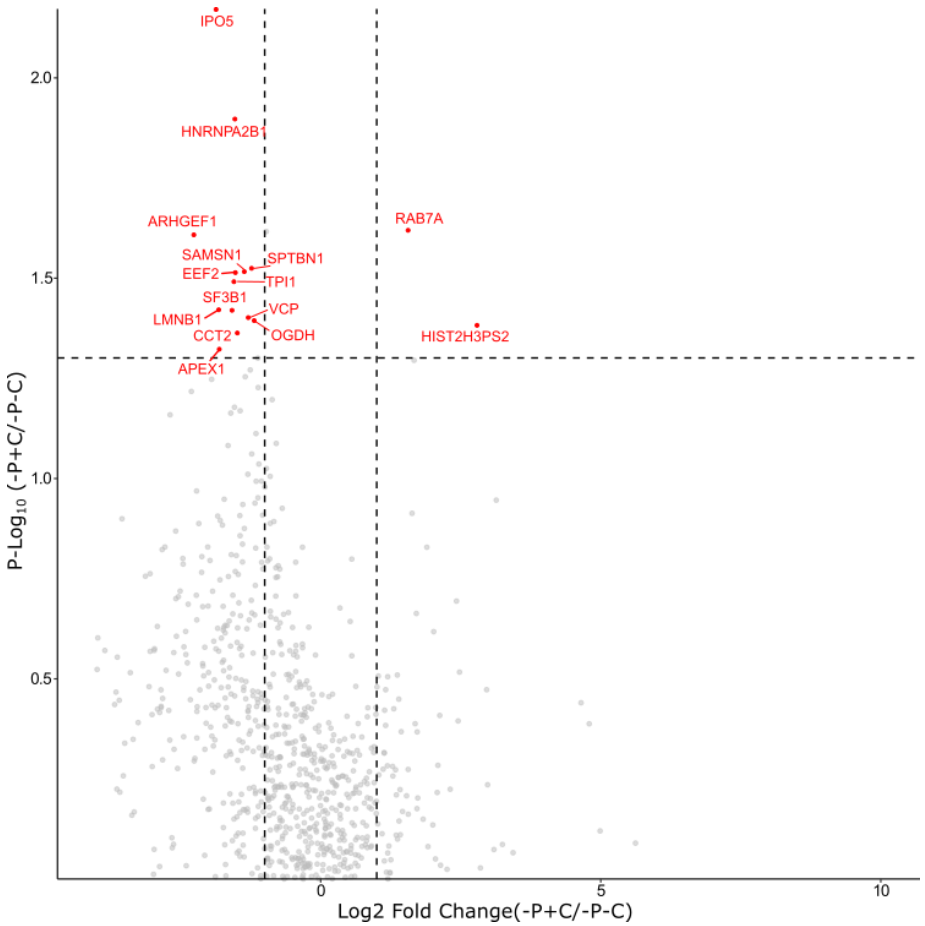

Figure 31: Volcano plot of both newly transcribed and downregulated proteins induced (fold-change) following catalase stimulation in the absence of PMA

AHA labelling of $CD4^+$ T cells allows for the identification of 15 significantly transcriptionally regulated proteins of which 13 are transcriptionally downregulated and 2 are upregulated in unstimulated CD4+ T cells isolated from human PBMCs in the presence or absence of catalase (highlighted in red). X axis shows the log2 fold change of the ratio between the catalase stimulated cells over the unstimulated, Y axis shows the $-\log_{10}$ of the P value. Statistical significance was determined with a two-sided, paired T-test was performed, and a P value of $-\log_{10}$ 1.3 ($P < 0.05$) was taken as significant.

When looking on any significantly enriched biological processes in the transcriptionally downregulated protein candidates it was found that cellular respiration was the most downregulated (Table. 13), potentially suggesting that catalase works to downregulate mtROS by potentially reducing the production of NADH and downregulating oxidative phosphorylation (OXPHOS) which was mentioned in the introduction as the known source of mtROS (Chapter. 1.5.1).

Strikingly, it was found that of the 2 proteins which were upregulated, Ras-related protein Rab-7a (RAB7A) is known to be a component of cellular endocytosis pathways. RAB7A upregulation signified that the direct impact of catalase on $CD4^+$ T cells may have been via an endocytic pathway (Chapter. 4.1.5. Figure. 14).

Table 13: Top 10 most significant newly synthesized proteins following catalase stimulation without PMA

Gene names, Log2 fold change values, function and localization are highlighted. The major enriched transcriptionally upregulated functions include Endocytosis, while enriched downregulated processes include cellular metabolism.

Gene Names	Fold Change ($Log_{(2)}$)	Function	Localization
IPO5	-1.85	Nuclear import	Nucleus
HNRNPA2B1	-1.52	RNA Binding	Extracellular
RAB7A	1.57	Protein transport	Lysosome
ARHGEF1	-2.25	Cell adhesion	Cytoplasm
SPTBN1	-1.22	Cell mobility	Cytoskeleton
SAMSN1	-1.35	Cell mobility	Cytoplasm
EEF2	-1.51	GTPase binding	Nucleus
TPI1	-1.53	Cellular metabolism	Cytoplasm
VCP	-1.28	Cellular metabolism	Endoplasmic reticulum
OGDH	-1.17	Cellular metabolism	Mitochondrial Matrix

Taken together, our data suggests that catalase incubation works by 2 independent mechanisms, a direct endocytosis into the T cell for enzymatic functions. As well as intercellular signaling which potentially works to reduce the NADH/NAD^+ ratio to reduce electron leakage and subsequent ROS through Tricarboxylic acid cycle (TCA) *via* 2-oxoglutarate dehydrogenase (OGDH), pentose-phosphate pathways (PPP) through downregulation of Triosephosphate isomerase (TPI1) and oxidative phosphorylation through downregulation of Transitional endoplasmic reticulum ATPase VCP (OXPHOS).

4.3.3 Extracellular catalase signaling induces cytoskeleton dynamics

Having evaluated the sole impact of catalase on unstimulated $CD4^+$ T cells, it was necessary to demonstrate the coordinated signaling of PMA stimulation with catalase. To evaluate the catalase dependent intercellular signaling which was hypothesized from previous data (Chapter 4.1.5).

To determine this, I compared the PMA mediated immune response in the presence of catalase and analyzed the differential protein translation with the equation (+PMA +Catalase/-PMA +Catalase). From the aforementioned 376 regulated proteins, 120 significantly regulated newly synthesized proteins were identified under these conditions (Supplementary Table. 14 & Figure. 32). Moreover, the catalase dependent activation included 2 downregulated proteins. These 2 proteins were keratins which served as a proof of concept of the low amount of clicked protein in the unstimulated cells (Figure. 26B right). The range of P values of candidates ranged from $-\log_{10}$ of 1.3 ($P < 0.05$) up to a $-\log_{10}$ of 4.16 ($P < 0.000069$), while the differences ranged from $\log_2$ -1.12 to 7.03.

Figure 32: Volcano plot of both newly transcribed and downregulated proteins induced (fold-change) following PMA stimulation in the presence of catalase

AHA labelling of CD4+ T cells allows for the identification of 120 significantly regulated newly synthesized proteins of which 118 are transcriptionally induced and 2 are downregulated following PMA stimulation in the presence of catalase (highlighted in red). Cells were incubated in the presence or absence of 10ng/ml PMA and in the presence of 1mg/ml catalase for 1 hour. X axis shows the log2 fold change of the ratio between the stimulated cells over the unstimulated, both in the presence of catalase, Y axis shows the $-\log_{10}$ of the P value. Statistical significance was determined with a two-sided, paired T-test, and a P value of $-\log_{10}$ 1.3 ($P < 0.05$) was taken as significant.

Catalase augmentation of PMA mediated immune response was found, to enrich in a similar manner to PMA alone (Figure. 30), DNA binding (Figure. 33), which were found by comparing candidates against the gene ontology database [172]. This suggests that these functions are critical to T cell activation and therefore are always activated regardless of mtROS signaling following PMA stimulation in $CD4^+$ T cells.

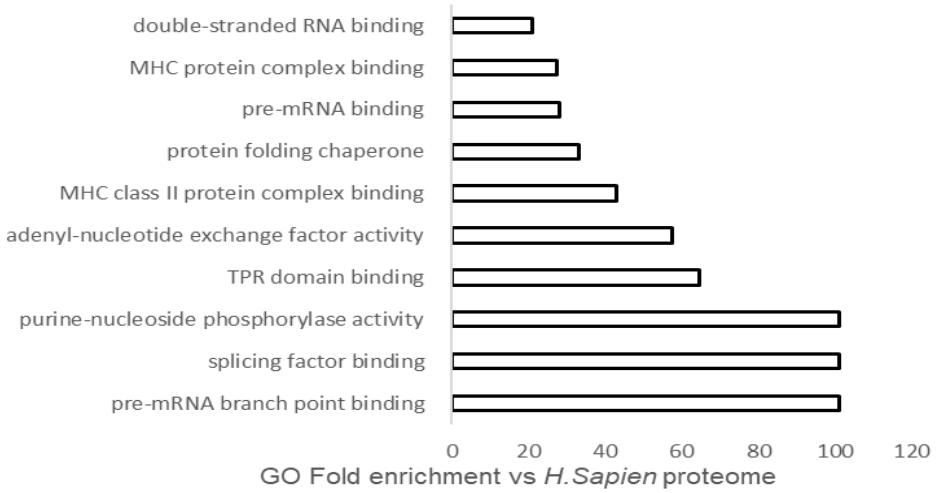

Figure 33: Enriched molecular function of newly synthesized proteins following PMA stimulation with catalase

Statistically significant enriched molecular functions from protein turnover induced by PMA and catalase. Enriched functions were determined by comparison of candidates to *homo sapien* gene ontology database. Enriched functions include DNA synthesis. Statistical significance was determined with a two-sided, paired T-test, and a P value of 0.05 was taken as significant.

However, when focusing on only the top 10 most significantly upregulated components, I observed an enrichment (50%) of cytoskeleton associated proteins (Table. 14) in addition Ezrin (EZR) was found transcribed but not in the top 10 list. The transcription of actin dynamic proteins was particularly interesting as it is known that extracellular ROS leads to actin stiffening while low ROS conditions induce actin cytoskeleton dynamics [132,166], this correlated with the redox proteomic study performed in the presence of 100µM H_2O_2 (Chapter. 4.2.4), which suggested H_2O_2 induces actin stiffness.

Table 14: Top 10 most significant newly synthesized proteins following PMA stimulation with catalase

Gene names, Log2 fold change values, function and localization are highlighted. The major enriched functions are cytoskeleton dynamics.

Gene Names	Fold Change ($Log_{(2)}$)	Function	Localization
TUBA1C	2.89	Cytoskeleton dynamics	Microtubules
HSPA8	3.42	Protein Folding	Nucleus
LCP1	3.22	Cytoskeleton dynamics	Cytoskeleton
ACTB	2.36	Cytoskeleton dynamics	Cytoskeleton
CCT4	2.57	Protein Folding	Cytoplasm
SF3B1	2.64	mRNA binding	Nucleus
CFL1	2.14	Cytoskeleton dynamics	Cytoskeleton
SAMSN1	2.79	Cytoskeleton dynamics	Cell Membrane
HLA-A	2.61	T cell activation	Cell Membrane
SF1	1.67	Transcription regulation	Nucleus

In summary, PMA mediated stimulation in the presence of catalase was found to upregulate cytoskeleton dynamics and therefore improved actin cytoskeleton motility. Which seems to correlate with redox proteome data, suggesting that catalase theoretically acts to mediate immune cell evasion from exogenous H_2O_2.

4.3.4 Characterizing the mtROS specific protein turnover

The initial aim of this set of experiments (outlined in Chapter. 4.3) was to characterize the protein translation induced by a physiological mtROS signal following PMA stimulation. As such, having determined the immune response as well as the catalase mediated immune response I sought to determine the protein turnover that is unique to the PMA stimulated condition and not significant in the catalase dependent transcriptional regulation. In this line, I compared the significant candidates which are present in the PMA mediated immune response in the absence of catalase (+PMA -Catalase/-PMA -Catalase) against the PMA mediated candidates in the presence of catalase (+PMA +Catalase/ -PMA +Catalase) (Figure. 34).

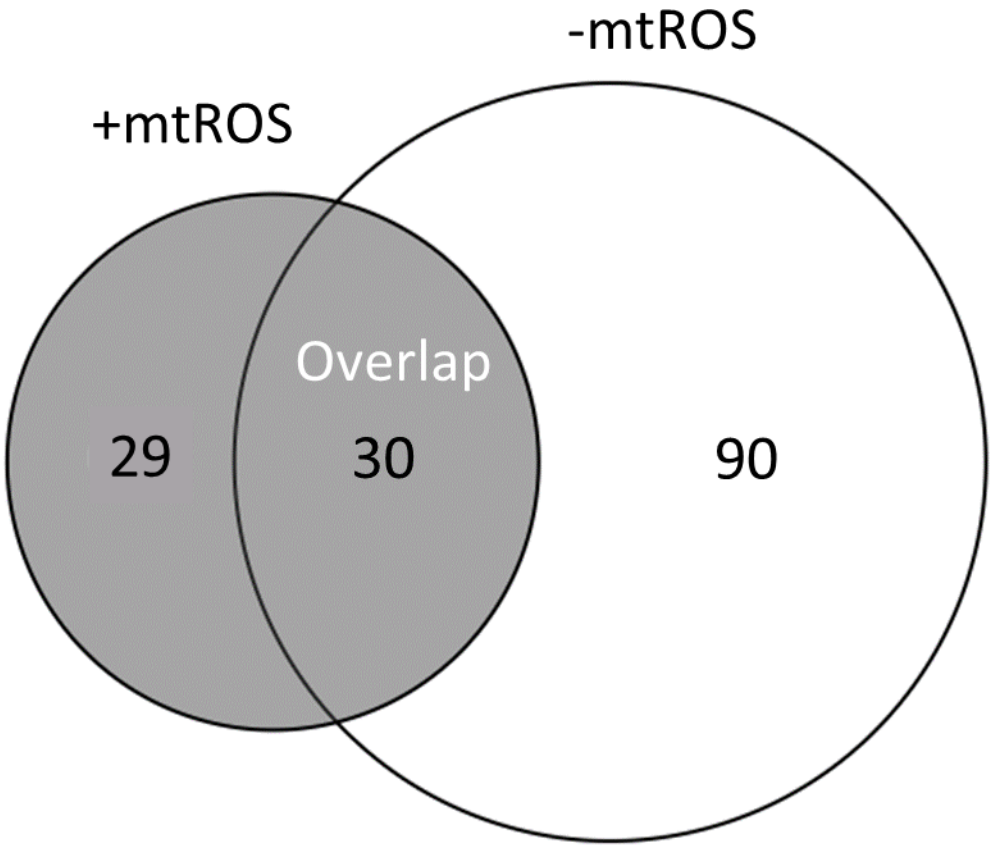

Figure 34: Comparative analysis of the significantly transcriptionally regulated candidates present in the PMA stimulated condition in the absence or presence of catalase.

T cell activation in the presence of 10ng/ml PMA without catalase produced 29 significant candidates. Conversely, activation in the presence of 10ng/ml PMA with catalase yielded 90 significant candidate proteins which were upregulated 30 candidates were found significantly upregulated in both conditions.

In total I identified 29 candidates from the original 376 proteins that were uniquely upregulated in the presence of mtROS (without catalase), while 90 were catalase dependent and 30 proteins were shared between both stimulation conditions. Catalase inducing a larger number of proteins (90) was not surprising considering that previous data (Chapter. 4.1.5) suggested that catalase is working *via* a hitherto unknown signaling pathway through an ancillary cell population.

Of the 29 significant candidates which are unique to the mtROS high condition in the absence of catalase it was apparent that the major molecular function upregulated was still DNA binding (Figure. 35) when comparing to the catalase dependent PMA stimulation (Figure. 33). This suggests that once again transcriptional regulation constitutes the most critical aspect of PMA induced T cell stimulation.

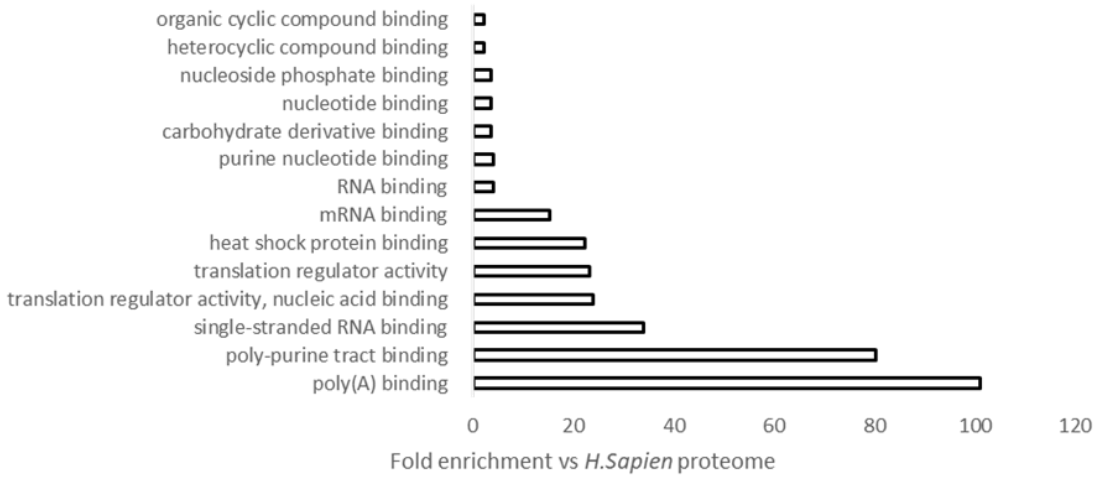

Figure 35: Enriched molecular function of newly synthesized proteins following PMA stimulation that are not significant with catalase incubation

Statistically significant enriched molecular functions from protein turnover induced by PMA and catalase. Enriched functions include DNA synthesis and MHC conjugation. Statistical significance was determined with a two-sided, paired T-test, and a P value of 0.05 was taken as significant.

Additionally, when observing the string network generated by these candidates (Figure. 36) I could see a major network of proteins were present in regards to DNA binding. In particular a number of the DNA binding I found in the original PMA mediated immune response (Table. 11) additionally, it was apparent that IRS2 and FAM49B were additionally mtROS dependent. FAM49B was previously mentioned as redox sensitive so this was not surprising (Chapter. 4.3.1) these proteins are labelled with a * in Figure. 36.

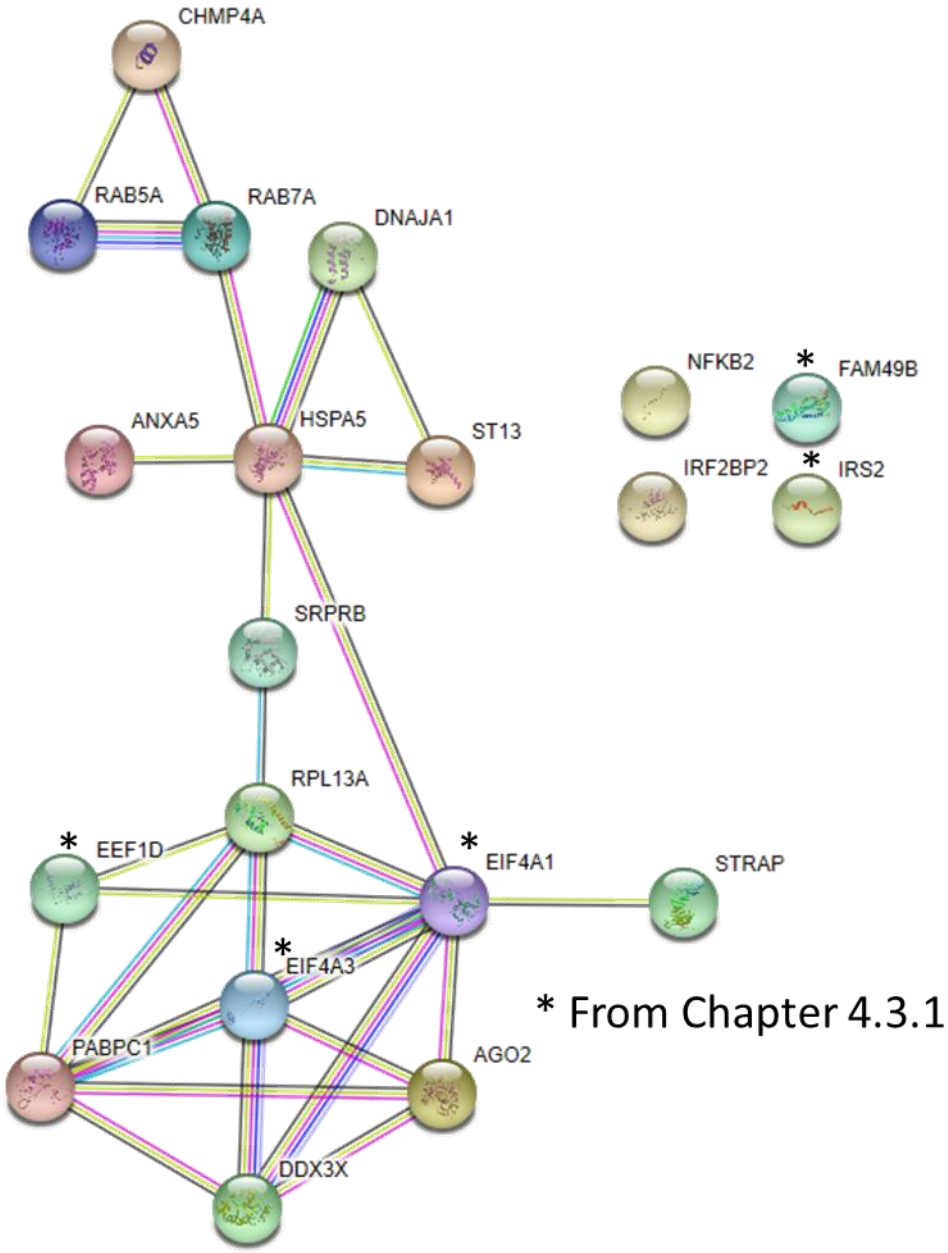

Figure 36: String network [182] of the mtROS dependent newly synthesized proteins

It could be observed that DNA binding proteins form an interacting network between themselves (left). Additionally, proteins marked with a * are in the top 10 significantly regulated proteins.

When considering the top 10 most significant candidates however, (Table. 15) it was clear that the redox high activation without catalase yielded upregulation of proteins involved in antioxidant systems. Namely, Ribosomal protein 13A (RPL13A), Polyadenylate-binding protein 1 (PABPC1) and Signal recognition particle receptor subunit beta (SRPRB). Furthermore, with respect to previous redox proteomics results (Chapter 5.2.3), I identified Endoplasmic reticulum chaperone BiP (HSPA5) as transcribed, this protein is known to downregulate ERO1A and may be an oxidative stress response in the ER.

Strikingly, I confirmed IRF2BP2 as significantly transcriptionally induced under mtROS dependent conditions which was briefly mentioned previously (Chapter. 4.3.1) as mtROS dependent. IRF2BP2 is known to regulate NFATc1 activity at its c terminus [181,183]. IRF2BP2 is uniquely active on NFATc1 and not other members of the NFAT family of transcription factors, suggesting a specific mediation of T cell activation [184]. NFATc1 is known to regulate clonal expansion in T cell activation [20] (Chapter. 1.2 and Chapter. 1.4.1). In parallel, I have found DnaJ homolog subfamily A member 1 (DNAJA1) which additionally binds NFATc1 in T cells [185]. I also identified NFKB2 which is a member of the NF-κB signaling cascade and suggests a level of ROS mediation in NF-κB signaling which has been observed previously when exposing T cells to exogenous ROS[186].

Table 15: Top 10 most significant newly synthesized proteins unique to the mtROS dependent conditions excluding catalase dependent proteins

Gene names, Log2 fold change values, function and localization are highlighted. The major enriched functions are antioxidant response and transcriptional regulation including NFATc1 / NF-κB signaling pathways.

Gene Names	Fold Change ($Log_{(2)}$)	Function	Localization
RPL13A	2.00	Oxidative stress response	Cytoplasm
NELFE	2.68	Transcription/Translation	Nucleus
DNAJA1	4.25	NFATc1 binding	Cytoskeleton
PABPC1	6.06	Oxidative stress response	Cytoplasm
IRF2BP2	2.54	NFATc1 binding	Nucleus
ZBTB1	1.52	Transcription/Translation	Nucleus
SRPRB	2.37	Oxidative stress response	Cell Membrane
NFKB2	3.7	NF-KB signaling	Nucleus
AFTPH	1.58	Intercellular transport	Cytoplasm
IRS2	3.11	Metabolic shift	Cytoplasm

To summarize, mtROS signaling induces protein synthesis primarily in the form of antioxidant function as well as immune function signaling, through NF-κB signaling [187] and NFATc1, which has been shown to be modulated in mtROS specific T cell activation, which is well accepted but currently has no mechanistic data to support the observations [61]. My data was found to concur with literature which implies mtROS is critical in T cell activation [51,61,106].

5.0 Discussion

mtROS, initially classified as a side-product of respiration is now synonymous with T cell activation [51,61,105,106,109,188]. However, mechanistic knowledge is fragmentary due, in part, to immunology research historically relying on more classical cell biology techniques, which can only observe the phenotype of cells on perturbation of mtROS production. Classical biology also has difficulty interrogating systems critical for cellular viability, in this case respiration, as the loss of function tends to have a diverse impact on the cell.

Global LC-MS proteomics is in a prime position to characterize changes in redox state, as proteomics uniquely directly monitors PTMs at the level of discrete amino acid residues, which is the primary method that mtROS mediates signaling in T cells. Additionally, through the use of biochemical probes it is possible to quantify changes in the abundance of these PTMs, generating regulatory information. Cooperatively, proteomics is also capable of dynamically monitoring the change in protein content of T cells following T cell activation. Subsequently, I have employed orthogonal global analyses to characterize the early mtROS response in T cell activation.

In concert, redox proteomics identified a number of regulatory mechanisms that T cells invoke in their role as “professional” ROS producing cells that utilize mtROS for signaling and must therefore fine-tune mtROS to maintain a physiological signaling environment. Below I will outline how T cells mediate fine-tuning of mtROS in the mitochondria and interconnected endoplasmic reticulum (ER). Following, I will highlight the actin cytoskeleton as a primary target of ROS and redox regulation in general in $CD4^+$ T cell activation. Conversely, I will underscore the particular ROS resistance of the nuclear compartment and how this otherwise reducing environment utilizes mtROS to perform discrete signaling events mediated through zinc binding proteins.

5.1 Primary human CD4+ T cells are professional mtROS producing cells

Cell lines constitute important model systems to characterize biological signaling pathways and phenotypes with the hope of the observations translating to the primary system. Genetic tools including CRISPR-Cas9 are available to mediate genetic manipulation in cell lines allowing for superior selectivity when probing a specific pathway via generation of single protein or amino acid residue knockout clones [189]. However, when analyzing the mtROS induction in the Jurkat E6.1 T cell line it was apparent that this cancerous cell line constitutively produced mtROS without notable regulation. Consequently, it was observed that when incubated with PMA there was no significant induction of mtROS (Figure. 10). Only in genetically manipulated Jurkat clones mtROS induction was measurable. It was found in a limited number of publications, that Jurkat clones overexpressing antioxidant proteins such as, B-cell lymphoma 2 (Bcl-2) [190] or Superoxide dismutase [Cu-Zn] (SOD1) [191,192] could generate a moderate mtROS signal on T cell activation.

Jurkat cells have been used to investigate the changes in redox state, but only with H_2O_2 incubation[99,193]. As such, we have shown that wild type (WT) Jurkat cells were incapable of generating an inducible mtROS signal when incubated with PMA and were therefore unsuitable for mtROS based proteomics studies.

It was therefore decided to utilize primary human T cells instead as they do not constitutively produce an excess of ROS. Additionally, it is well accepted that T cells generate mtROS during activation which mediates T cell clonal expansion and effector function [194,195]. However, when considering the mtROS signal propagated by PMA stimulation of $CD4^+$ T helper cells in comparison to $CD8^+$ cytotoxic T cells, I discerned that indeed $CD4^+$ T cells induce a greater mtROS response than $CD8^+$ cells (Figure. 13), which has been shown with orthogonal stimulation previously [11]. Therefore, I could utilize a single functionally distinct T cell subset, which had the additional benefit of reducing variation as indeed $CD4^+$ and $CD8^+$ T cells induce the expression of differing levels of proteins. To conclude, $CD4^+$ T cells constituted a more appropriate model of mtROS induction for further downstream proteomic characterization.

5.2 Proteome strategies to characterize major mtROS-dependent cysteine modifications

Redox proteomics is the study of the change in the oxidation states of proteins. The most commonly utilized readout for a change in redox state is the change in the oxidation state of cysteine residues. Cysteine constitute the major target of H_2O_2 as the anionic thiolate can mediate nucleophilic attack of the peroxide bond (Chapter. 1.4). Although this reaction is also possible by methionine, it is orders of magnitude less energetically favorable and therefore remains a minor interaction [196].

There are a number of methods to probe the change in oxidation state of cysteine (Figure. 37). However, broadly speaking there are two alkylating methods employed both of which involve nucleophilic attack of either a disulfide bond in the case of (DNTB, 5, 5′-dithiobis(2-nitrobenzoic acid)) and MMTS by the cysteine thiolate. Conversely, attack of an organoiodine bond in the case of Iodoacetamide (IAA), iodoTMT and the isotope coded affinity tag (ICAT) by the thiolate additionally leads to cysteine alkylation in a similar manner as H_2O_2 (Figure. 7).

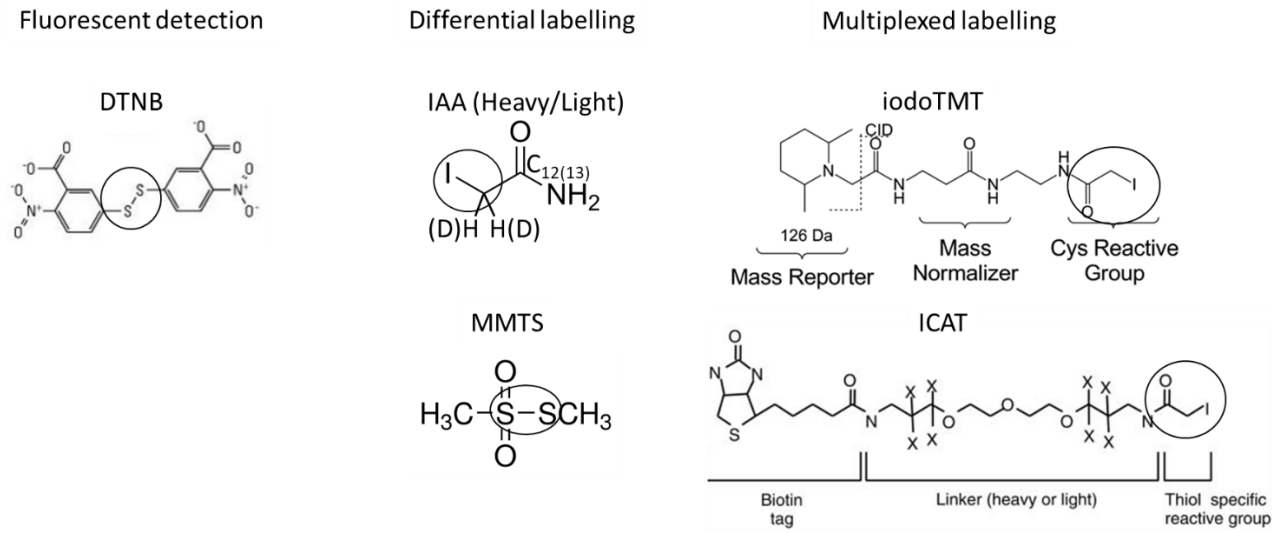

Figure 37: Most commonly utilized thiol reactive probes

DTNB and MMTS utilize a thiol reactive disulfide bond while IAA, iodoTMT and ICAT tags utilize an organoiodine bond. Adapted from [197–199]

Historically, DNTB was utilized to allow for quantification of cysteine oxidation through covalent bonding of the fluorescent DTNB tag to cysteine containing proteins. However, this method fell out of favor due to the prevalence LC-MS analysis and the superior alkylation reaction kinetics of IAC and MMTS [200].

IAC and MMTS are both small fast reacting alkylating agents routinely used with LC-MS. These alkylating agents yield differential cysteine masses and are therefore used to distinguish free cysteine residues from oxidized cysteine residues in global analysis [201]. However, this technique cannot be used to mix multiple samples together (multiplexing) as the peptides will elute with different retentions and cannot be co-analyzed. In comparison, IAA alone is capable of being multiplexed through the use of isotopically labelled variants [202,203]. However, isotopic thiol switching with IAA is limited to two conditions. The biggest improvements in redox proteomics came in the form of IodoTMT and ICAT. ICAT allows for the multiplexing of three conditions as well as the ability to enrich labelled cysteine residues through biotin affinity enrichment [204]. ICAT was the gold standard until the need for more conditions arose. Spurring iodoTMT tags, which constitute the newest technology to quantify differential cysteine oxidation states, iodoTMT allows for the multiplexing of six conditions.

IodoTMT is also supposedly capable of enriching the tag through a proprietary resin specific to the tag [121]. However, in our hands and the hands of others it has proven ineffective. As such, we utilized offline 2D-LC fractionation to improve coverage of the cysteine containing peptides in the total proteome.

Considering the multiplexing advantages of iodoTMT for characterizing the oxidation states in both stimulated and unstimulated $CD4^+$ T cells, I chose to utilize iodoTMT tags (Figure. 15). Subsequently, employment of this method produced 2 discrete groups of proteins which were either oxidized following activation, in that the reporter tags which had labelled the reversibly oxidized cysteine residues (131 & 130 termed $CysOx^A$ & $CysOx^I$ for the stimulated and unstimulated conditions respectively) were greater than the tags which labelled free cysteine residues (129 & 128, termed $CysFree^A$ & $CysFree^I$ for the stimulated and unstimulated conditions respectively).

Generally, there were no situations in which a cysteine residue transitioned from 100% reduced to 100% oxidized following T cell activation, this is in line with other proteomics studies that suggest that before T cell activation there is a certain basal level of H_2O_2 [120,121,146,147,202].

5.2.1 Respirasome electron transfer can be optimized by mtROS propagated reorganization through Complex III and Complex I reverse electron transfer

CI and CIII have both been implicated as sites of electron leakage [60–62,64], so it was particularly interesting that I have observed significant stimulation induced oxidations in both of them.

NADH dehydrogenase [ubiquinone] 1 alpha subcomplex subunit 2 (NDUFA2) and NADH dehydrogenase [ubiquinone] 1 alpha subcomplex subunit 8 (NDUFA8) were found to be significantly oxidised (+2% and +9% at Cys58 and Cys36 respectively) following PMA stimulation. NDUFA2 is a component of the CI electron transfer arm while NDUFA8 is a part of the intermembrane arm [205]. Additionally, NDUFA8's

Cys36 has additionally been shown to be redox sensitive [206]. Both components are in close proximity to the Coenzyme Q (Q) binding site which has been implicated in leaking electrons [207], particularily, in the case of reverse electron transfer (RET). RET is known to occur during T cell activation and is indicative in CI being saturated with NADH [208]. Consequently, electrons accumulate in the respirasome at CytoC and Q and travel back through the ETC and leak out of CI [209] at NDUFA2 and NDUFA8. This has been suggested as a ROS producing phenotype on T cell activation [210], but I have shown the potential mechanism.

I observed strong oxidation of the structural disulfide of the ubiquinol-cytochrome c reductase hinge protein (UQCRH – known as QCR6 in bacteria) [211–213]. UQCRH has been shown to mediate a stronger interaction between Cytochrome C (CytoC) and cytochrome c1 (CYC1) through the unique sequence of 8 glutamate residues near its C-terminus [211,213–215]. UQCRH utilizes electrostatic interactions in the proximity to the catalytic heme of cytochrome c1 to mediate its enhanced interaction with CytoC. I have identified Cys53 as oxidized following PMA stimulation (+8%) and therefore as a potential activation mediated disulfide bond. C53 was shown in bovine heart mitochondria to be constitutively oxidized to structural disulfides with C67. This disulfide mediates a favorable position of the glutamic acid rich sequence near to CytoC for efficient electron transfer (Figure. 38). Efficient electron transport will reduce RET and therefore, I suggest that in unstimulated T cells this structural disulfide is not as present and is likely a method of the respirasome to fine-tune and increase its own respiration. Indeed, modulation of CIII structure to alter respirasome function has been shown by a number of different groups [216–218].

This is exemplified by the reduced cellular respiration which occurs if UQCRH is removed while maintaining super complex structure [219], suggesting it may not be critical for cellular respiration but may in fact be a respiration regulator which is mtROS sensitive, again implicating ROS as a tuning mechanism for the increased respiration which occurs during T cell activation. Indeed it has been shown that under periods of oxidative stress such as in T cell oxidation, CIII and more specifically UQCRH are particularly susceptible to oxidation [220].

Additionally, the metabolic protein Dihydrolipoyl dehydrogenase (DLD) is known to be uniquely reduced from mtROS which emanates from CIII [62], was observed in my study as significantly reduced following PMA stimulation at Cys477 (-7%). DLD has a function in its monomeric form, that is the oxidation of NADH to NAD+ in the mitochondria [221]. DLD may therefore act as a CIII dependent regulator of the $NADH/NAD^+$ ratio following T cell stimulation and increased electron leakage.

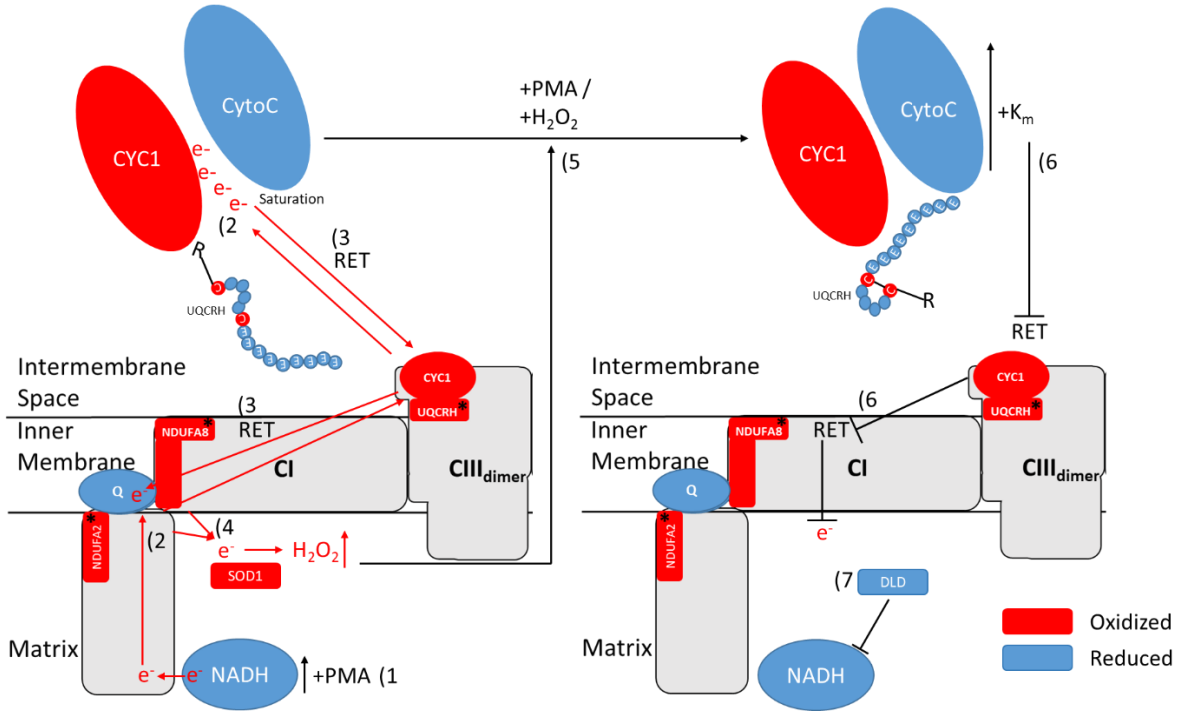

Figure 38: Model of how the respirasome fine-tunes mtROS through electron transfer efficiency via CI and CIII

1). Stimulation with PMA triggers an initial metabolic switch which generates excessive NADH which feeds into CI in the respirasome. 2). Increased electron transfer saturates the soluble electron transport enzymes such as Q and CtyoC. 3). RET causes electrons to funnel back to CI. 4). Electrons leak out of CI (NDUFA2/8) which are quickly converted to H_2O_2 through dismutation by SOD1. 5). Increased H_2O_2 mediates a structural disulfide in UQCRH at positions Cys53 and Cys67 which improves the electron transfer kinetics between CYC1 and CytoC. 6). Subsequently, RET is reduced and H_2O_2 with it leading to a fine tuning of mtROS based on the proportion of oxidized UQCRH. 7). Additionally, DLD functions to oxidize NADH to NAD^+ reducing the e^- entering CI

Outside of the respirasome, the MICOS complex subunit Mic19 (MIC19) which is a component of the mitochondrial contact site and cristae organizing system (MICOS) is involved in the formation of mitochondrial cristae and has been implicated in tuning mitochondrial electron transfer through bringing respirasome complexes into closer contact [222] allowing for more efficient electron transfer and proton pumping. I have identified a conserved cysteine oxidation of +8% located on C183 which is a part of the 2 CHCH helix structural motifs and has been seen in the literature to be oxidized to mediate the cristae formation [223]. Suggesting, that during stimulation the change in mitochondrial morphology[139] may be mediated in part by mtROS.

When looking at both the respirasome subunits NDUFA8 and MIC19 it is known that both proteins are imported into the mitochondria through the Mitochondrial Intermembrane space Assembly machinery (MIA) importer [152,223,224]. As such, it is pertinent to assume that this mtROS signal may also mediate improved mitochondrial protein import following stimulation with PMA.

Taken together, this data implicates the combination of the MICOS complex, CI and CIII in finetuning electron leakage. MIC19 mediates an improved respirasome electron transfer through cristae remodeling. While electron leakage is increased *via* CI RET which is fine tuned through structural reorganization of CIII which modulates the amount of electrons leaked via CI.

5.2.2 Oxidation of PRDX5 and SOD1 in the mitochondria propagates a known antioxidant phenotype

As mentioned above, the respirasome fine-tunes electron leakage through CI and CIII cooperation. However, oxidative stress is inevitable [225]. As such, mitochondria require a number of antioxidant molecules to prevent oxidative stress and damage. Peroxiredoxin 5 (PRDX5) is a member of the PRDX class of proteins, it is uniquely targeted to the mitochondria when transcribed in its elongated form which includes a mitochondrial targeting sequence [226]. PRDX5, in cooperation with Superoxide dismutase [Cu-Zn] (SOD1) , copper chaperone for superoxide dismutase (CCS), BAG family molecular chaperone regulator 2 (BAG2) and DLD, has been implicated in an antioxidant signaling cascade propagated by mtROS signal [227]. Strikingly, I have observed statistically significant modifications in all of these proteins, except SOD1, which was however found irreversibly oxidized and reversibly oxidized (+5%) following stimulation with PMA (Supplementary Table. 15 & Supplementary Table. 3 respectively). Subsequently, PRDX5 has been previously implicated in the antioxidant response of mitochondria [228], in which an increase in mtROS triggers oxidation in both PRDX5 and SOD1 which propagates and antioxidant signaling cascade through the action of DLD.

When observing the shift in oxidation of PRDX5, it was found to have undergone an increase in oxidation of 10% at Cys204, which is its redox sensitive disulfide bond utilized for its antioxidant activity [226]. Therefore, it is pertinent to assume an increase in oxidation of the redox active disulfide correlates with an increase in the oxidative environment in the mitochondria and antioxidant activity of PRDX5.

Additionally, while I did not identify a significant reversible oxidation in SOD1, significant oxidations at its chaperone CCS (+4%) were identified at Cys244. CCS is known to incorporate copper and zinc into the Apo enzyme leading to activation of SOD1 [229]. Oxidations at the copper coordinating cysteine residues Cys244 and Cys246 were observed in CCS, which suggests that T cell stimulation leads to an increase in copper chelation by CCS and a subsequent activation of SOD1 [230]. Interestingly, as mentioned previously I also observed irreversible sulfonic and sulfinic acid oxidations on Cys58 in SOD1 which is its copper chelating cysteine residue (Supplementary Table. 15). Taken together, this suggests that ROS levels do potentially exceed physiological conditions leading to an increase in SOD1 regeneration as well as the an assumed signaling cascade which activates NF-κB (Figure. 39) [227,231].

DLD, which was shown to be regulated in my study previously (Chapter. 5.2.1) forms a homodimer, which prevents its activity. Under mtROS producing conditions generated by PMA, the DLD homodimer dissociates and DLD is activated to mediate the proteolytic processing of IκBε [221], which is a negative regulator of NF-κB and leads to NF-κB upregulation and subsequent antioxidant action [232]. I hypothesize that the reduction observed in DLD of Cys477 leads to the dissociation of the homodimer and the activation of DLD's proteolytic activity, this is structurally feasible due to Cys477 being at the homodimer interface [233].

In this vein, BAG2 can stabilize PTEN-induced kinase 1 (PINK1) which is involved in mitochondrial anti-oxidative stress response in the mitochondrial matrix [234], and which is known to stabilize the DLD homodimer preventing the DLD activity. I theorize that the oxidation of BAG2 at Cys162 (6%) disrupts this stabilization causing a fraction of PINK1 to dissociate from the DLD homodimer and upregulate activity leading to NF-κB upregulation, which also may mediate an mitochondrial immune response.

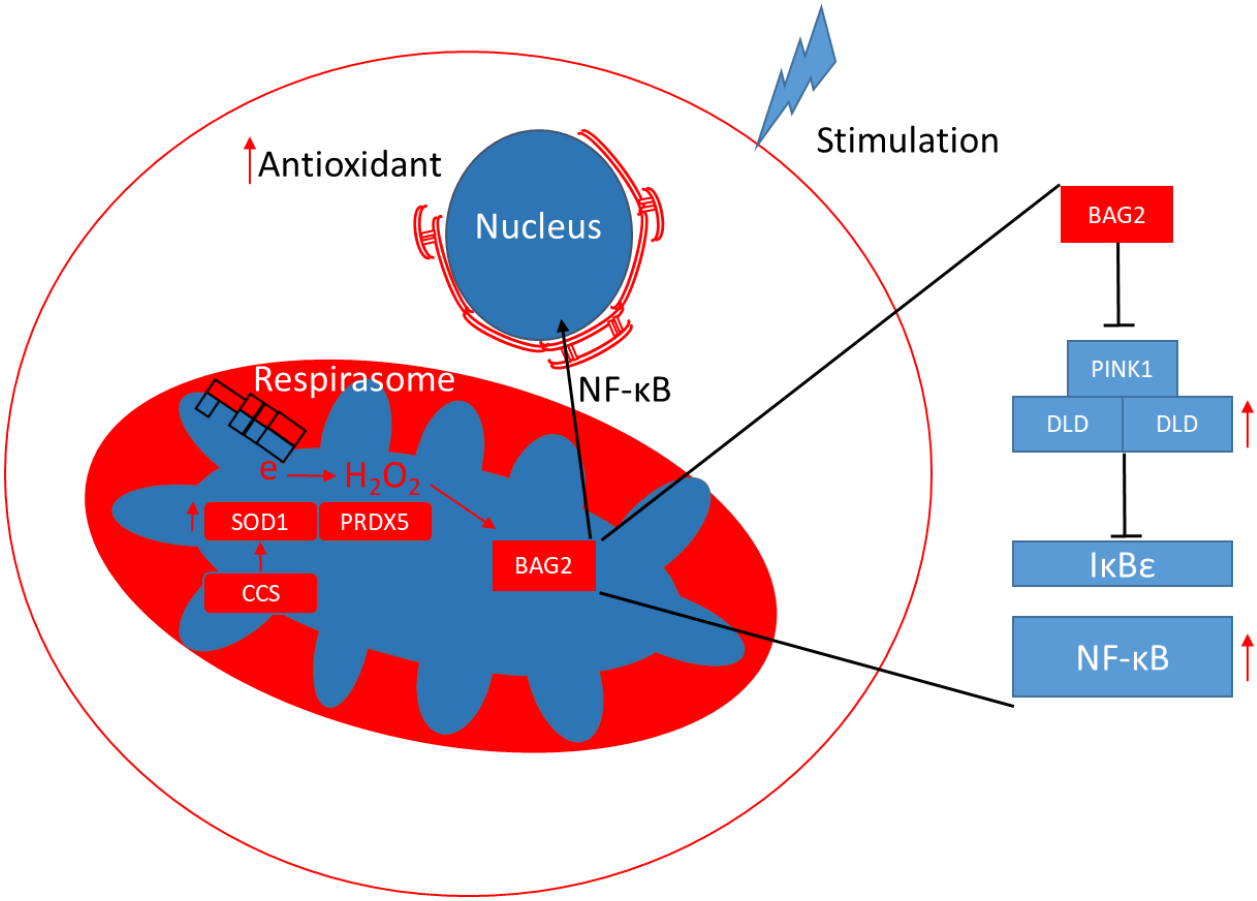

Figure 39: mtROS-triggered antioxidant signaling model following PMA stimulation.

Following stimulation, electron leakage from the respirasome increases, these electrons are converted to H_2O_2 (mtROS) by SOD1 and reduced to H_2O by PRDX5. An excess of mtROS oxidizes and inactivates BAG2 which triggers degradation of PINK1 and subsequent activation of the proteolytic action of DLD which degrades IκBε. Loss of the inhibitory IκBε triggers NF-κB localization to the nucleus and activation of antioxidant systems.

In addition to the potential mechanism outlined above, a number of additional antioxidant systems were found significantly oxidized in the mitochondria. Including, Thiosulfate Sulfurtransferase like Domain Containing 1 (TSTD1) which regenerates thioredoxin (TXN) in the mitochondria [235]. I observed a significant stimulation induced oxidation (+3%) of TSTD1 at Cys79 which is the redox stimulated thiolate of the enzyme utilized in the transfer of the persulfide moiety to TXN. This oxidation suggests that TXN undergoes regeneration following T cell stimulation [236]. Concurrently, it was observed that the redox stimulated cysteine of TXN was largely

unoxidised (Supplementary Table. 3) after 1h of PMA stimulation, suggesting it has been regenerated after 1 hour.

5.2.3 Oxidation of GIMAP1 and ERO1A suggest ER stress responses following $CD4^+$ T cell activation

It is known that the endoplasmic reticulum (ER) is particularly oxidizing [237], due to the unique Glutathione (GSH) redox state in the ER, in that instead of an abundance of reduced GSH (G-SH) there is instead an abundance of oxidized GSH (GSSG) [238]. The excess of GSSG facilitates the formation of disulfide bonds in the ER which is necessary for protein folding.

GTPase, IMAP family member 1 (GIMAP1) is an ER & Golgi associated protein [239,240] found particularly oxidized (+10%) at Cys76 which has been implicated in mitochondrial function and T cell survival before [160,241] and is present in the GTPase domain. Data of this thesis suggest that the oxidation may mediate a redox switch, activating the GTPase activity during ER stress following T cell activation. GTPases are known to be ROS sensors in literature [242–244]. Therefore, literature suggest that GIMAP1 is oxidized to mediate a protein misfolding response [245]. In a following chapter (5.3.1), I have identified additional GTPase related proteins that also show ROS sensitivity.

ERO1-like protein alpha (ERO1A) is another protein in the ER that was found increasingly oxidized by +8% following PMA incubation at Cys131. ERO1A mediates the production of disulfide bonds in newly synthesized proteins and therefore mediates protein oxidation [246]. Cys131 forms a regulatory disulfide [247] to reduce the activity of ERO1A in the presence of oxidative stress [248], this suggests that following PMA stimulation ERO1A undergoes inhibition to prevent the production of oxidized proteins.

Alongside PRDX5 in the mitochondria (Figure. 4.2.2), the redox stimulated PRDX6 which resides in the cytoplasm was also found to be significantly oxidized in its redox stimulated sulfenic acid moiety at Cys47 [156]. A shift of +8% was quantified in peroxiredoxin 6 (PRDX6), the oxidation of PRDX6 was lower than PRDX5 which suggests that the levels of mtROS in the mitochondria are higher than that of the cytoplasm, which concurs with our microscopy data that the mtROS emanates from the mitochondria into the cytoplasm (Figure. 12). However, the oxidation of PRDX6 also suggests that the cytoplasm undergoes an increase in mtROS following PMA stimulation.

Taken together, it is clear that on T cell activation the mtROS generates an increase in oxidation within the mitochondrial compartment. This oxidative signal may generate a number of signaling cascades with the purpose of oxidative stress response in the mitochondria but also in other organelles in the periphery *via* the diffusion of H_2O_2. This strengthens the theory that $CD4^+$ T cells are professional mtROS producing cells that can fine-tune the abundance of ROS to mediate physiological signaling on a global level.

5.2.4 NF-κB signaling is upregulated upon extreme oxidative stress in $CD4^+$ T cells

My data suggests that NF-κB signaling is utilized on multiple levels of oxidative stress. Data generated from stimulating $CD4^+$ T cells with PMA in the presence of 100μM

H_2O_2 additionally identified a targeted upregulation of NF-κB signaling events (Chapter 4.2.4). Exogenous H_2O_2 elucidated a moderate but targeted group of proteins aimed towards the singular goal which seemed to be the upregulation of antioxidant effector functions (Table 3). I hypothesize that the lower number of candidates in this data was due to the fact that under these high oxidative conditions most proteins undergo non-reducible oxidation which would prevent them being labelled by our redox proteomics methodology and invisible to our analysis. While these antioxidant proteins identified in my data set (Table. 7) are mostly present in the nucleus and may have an additional protective mechanism to prevent there ROS damage such as through Protein/nucleic acid deglycase DJ-1 (PARK7 –HSP33 in bacteria) [84].

Serine/threonine-protein kinase A-Raf (ARAF) is a protein known to activate the ras-raf-mek-erk pathway signaling which has major antioxidant effects [249] and upregulates NF-κB activity. It is known that ARAF dimerizes [250] for its function**.** A conserved oxidation at C597 (+15%) which is on the outside of the protein was identified. Therefore, I hypothesize that in the case of high oxidative stress this protein may form a structural disulfide to mediate a stress response through NF-κB. Additionally, serine/threonine-protein kinase D2 (PRKD2) has been implicated as a regulator of oxidative stress and was found to be oxidized at C217 (+27%). Following an increase in oxidative conditions a number of tyrosine residues of PRKD2 become phosphorylated and auto phosphorylated, this yields a cell survival and proliferative effect through NF-κB activity [251]. I postulate that the oxidation at C217 is a structural disulfide which would allow the tyrosine residues to come into close contact for auto phosphorylation reactions [252]. Phosphatidylinositol 3,4,5-trisphosphate 5-phosphatase 1 (INPP5D/SHIP-1) has major impact in oxidative stress response through mediating NF-κB signaling processes [253]. I observed an oxidation at C1088 (+10%), this residue is part of the anchoring site of SHIP-1 with the cell membrane. It is tempting to speculate that under oxidative stress this cysteine mediates an enhanced binding and differential signaling in SHIP-1 allowing for antioxidant signaling [254].

In addition to NF-κB signaling, there were a number of other antioxidant responses triggered by 100μM H_2O_2. The PITH domain-containing protein 1 (PITHD1) was found oxidized at C14 (+21%), this may be an inactivating oxidation as it is known that a knockdown of PITHD1 leads to knockdown of Runt-related transcription factor 1 (RUNX1) [255,256] which upregulates Forkhead box protein (FOXO1) [257]. FOXO1 is a transcription factor associated with oxidative stress response and cell survival, indeed upregulating FOXO1 leads to upregulation of most antioxidant redoxins and catalase proteins [258].

CUGBP Elav-like family member 2 (CELF2) was conversely found to be reduced at C174 (-17%) suggesting that CELF2 is being reduced by an antioxidant system, which suggests an unknown protective mechanism that I hypothesized at the start of this chapter. This antioxidant system leads to protection of CELF2 activity which has been found to mediate an anti-oxidative stress response by regulating Dual specificity mitogen-activated protein kinase kinase 7 (MKK7) alternative splicing [259]. Finally, the protein Hepatoma-derived growth factor-related protein 2 (HDGFL2) was found to exhibit an oxidation at C631 of +20% in a major signaling sequence stretch very close

to a number of conserved phosphorylation sites. Therefore, I assume that this oxidation might be a site of regulation of HDGFL2 activity with the goal of enhanced activation. HDGFL2 is known to enhance cyclin D1 protein levels which is a cell survival protein that has been shown to upregulate cell survival [260], suggesting additional antioxidant systems upregulated in cell stress apart from NF-κB.

5.2.5 Summary

It is apparent that following stimulation, $CD4^+$ T cells undergo a metabolic shift with the purpose of producing biosynthetic intermediates to support immune responses including cell growth and clonal expansion. Additionally, NADH production is strikingly increased through mobilization of glutamine and subsequent α-KG production (Chapter. 1.2.1).

NADH feeds into CI of the respirasome generating an abundance of electrons which saturate the UQCRH-CYC1/CytoC electron transfer interface leading to RET and leakage of electrons out of CI through NDUFA2 (Figure. 38). As a consequence, electron leakage increases dramatically. These electrons are converted to mtROS by SOD1 which is activated by CCS. Subsequent mtROS levels increase and are controlled somewhat by PRDX6. However the increase in mtROS mediates the structural reorganization of the respirasome subunit UQCRH which improves the affinity and electron transfer rate of the CYC1/CytoC interface (Figure. 38). This reduces electron leakage vie RET and subsequently fine-tunes the mtROS signal to utilize it for signaling without oxidative damage. To prevent oxidative stress, however, a number of antioxidant systems are upregulated, primarily mediated through NF-κB upregulation through DLD activity which is known to be activated by ROS emanating from CIII of the respirasome. Indeed, NF-κB signaling is suggested by this work to act as the major mediator of antioxidant action in $CD4^+$ T cells under physiological conditions and stress conditions.

Indeed, it was observed that if the oxidative signal overwhelms the catalytic capacity of antioxidant proteins such as PRDX5/6 then $CD4^+$ T cells may selectively protect NF-κB signaling components such as ARAF, PRKD2 and SHIP-1 to potentially mediate an induction of increased antioxidant signaling. It is therefore hypothesized that $CD4^+$ T cells are capable of mediating oxidative stress responses over a large dynamic range.

5.3 mtROS signaling network targets actin cytoskeleton dynamics to control cell motility and immune function

5.3.1 Actin cytoskeleton dynamics are a major component of the mtROS signaling network

The thiol switching strategy and redox proteomics (Chapter. 4.2.3) enriched actin cytoskeleton processes, in particular, actin branching and lammeliopodia formation, in the group of oxidized candidates upon T cell activation (Figure. 22). Actin branching has been implicated in the formation of the immunological synapse (IS) [261], and involves the Arp2/3 complex. APR2/3 is also known to localize to the IS and induce centrosome re-organization allowing localization of additional signaling components [262]. Furthermore, as the actin cytoskeleton is ubiquitous within the cytoplasm, it is logical to assume it might be modulated by the increase in mtROS demonstrated by

oxidation of PRDX6 which shows the cytoplasm becomes more oxidative following T cell activation. Herein, I describe IS formation as an mtROS mediated signaling network in T cell activation. However, this thesis examines non-polarized, non-migrating T cells as part of PBMC fractions which were activated by PMA. In the following, I will discuss how mtROS potentially modulate actin dynamics in order to prime T cells for conjugations and IS mediated responses.

With this in mind, the ARP2/3 subunit Actin-related protein 2/3 complex subunit 1B (ARPC1B) was determined to contain oxidized (+2%) cysteine residues at positions Cys342 and Cys346. Although these cysteine residues have not been implicated in the activity of complexation of the protein it is known that the ARP2/3 complex utilizes intermolecular disulfide bonds for its activity [263–265]. ARP2/3 has been found to mediate localization of components to the IS and interacts with the wave regulatory complex (WRC) which is known to instigate lammeliopodia formation [266] at the IS [267] (Figure. 40). However, the mechanistic data of the immunomodulatory function of the WRC is lacking.

In line with this, a major activator of the WRC, Cytoplasmic FMR1-interacting protein 1 (CYFIP1) was found oxidized at positions Cys1087 and Cys1088 (+7%). CYFIP1 interacts with Ras-related C3 botulinum toxin substrate 1 (RAC1), which is an activator of the WRC [268] and transduces signalling to ARP2/3. RAC1 has been shown to utilize disulfide formation for its activity at its redox active Cys18 [269]. While I did not observe RAC1 under physiological mtROS conditions, RAC1 was found reduced at Cys178 (-6.67%) when cells were incubated with exogenous H_2O_2 to mediate oxidative stress conditions (Chapter. 4.2.4). Suggesting RAC1 is protected during oxidative stress conditions and is therefore critical for cytoskeleton dynamics in oxidative stress. It is tempting to speculate therefore, that CYFIP1 may modulate RAC1 activity and therefore the WRC and ARP2/3 activity though formation of activating disulfide bonds to induce motility. Additionally, the ARP2/3 binding protein, Protein diaphanous homolog 1 (DIAPH1/mDia1) was determined to be oxidized following T cell activation and has been found to modulate lammeliopodia formation [270,271]. mDIA accomplishes this through modulation of ARP2/3 activity and provides a point of actin nucleation for APR2/3 to mediate actin branching.

mDIA contains a DAD regulatory domain which inhibits its action and therefore actin branching by ARP2/3. I observed oxidation of Cys1227 (+7%), which is a flanking residue of the DAD regulatory domain of the protein as well as the last cysteine in the protein. I hypothesize that a disulfide bond between Cys1227 and for example Cys1027 in the protein may prevent exposure of this DAD site preventing the auto-inhibitory function of mDIA [270] and inducing its activity. Again suggesting a mechanism of redox modulation of actin branching through ARP2/3.

Continuing with ARP2/3 binding proteins, Filamin A (FLNA) is a protein known to be necessary for actin branching in tandem with ARP2/3 [272]. FLNA is of particular interest as it seems to exist in multiple redox states being both found to be oxidized at Cys444 and Cys2160 (+5% and 15% respectively) while being reduced at position Cys2479 (-2%), potentially suggesting a reversible oxidation mechanism. Conversely, FLNA may provide direct evidence to suggest that these cytoskeleton dynamic proteins mentioned above can exhibit multiple oxidation states, which also suggests

they inhabit 2 differential redox microenvironments. It is well accepted that the cytoplasm has differential ROS microenvironments [195,273,274], which mediate redox biochemistry that requires localized high levels of ROS while the total ROS level in the cell is not stressful. This makes the use of the redox ratio equation $((CysOx^{A}/CysOx^{I})/(CysFree^{A}/CysFree^{I}))$ preferential to using the % change equation (Figure. 15C top equation). These local ROS high environments may only impact a small fraction of the total cellular content of a single protein, which may not generate a large total shift in cysteine oxidation for a specific protein. However, the ratio equation will detect a functional regulation. Additionally, the reduction of FLNA cannot be explained by actin cytoskeleton proteins at the plasma membrane being oxidized as was the case with surface markers (Chapter 6.1). As such, this suggests that the actin cytoskeleton is not merely oxidized due to localization near the plasma membrane.

GTPases were mentioned previously as a putative redox sensor (Chapter. 4.2.3). The Rho-related GTP-binding protein RhoF (RHOF/RIF) which binds mDIA to form protrusions from the lammeliopodia [275] was found to be oxidized at Cys131 (+6%). Additionally, the protein Brain-specific angiogenesis inhibitor 1-associated protein 2 (BAIAP2) can form filopodia [276] and is modulated by the regulatory protein 14-3-3 protein gamma(YWHAG/14-3-3γ) which was found oxidized at Cys112 (3%). 14-3-3γ was found to interact with ARPC1B [277], additionally, YWHAG is also known to be a regulator of BAIAP2 filopodia [278] which suggests that YWHAG co-localizes with BAIAP2 and therefore RHOF and mDia1. As such, all components mentioned so far exhibit the same spatial location and could therefore be mediated by the same mtROS environment

As well as regulatory components I also identified a number of potential binding partners of ARP2/3 and the WRC, which can also form scaffolds for protein localization [279], potentially at the IS. The protein Thyroid receptor-interacting protein 11(TRIP11/GMAP-210) is known to interact with ARP2/3 at the IS [280], interestingly it also is known to control vesicle trafficking, for example in transporting LAT proteins to the IS [281] potentially suggesting that the WRC mediates an anchoring of IS components through structural disulfide bonds.

Myosin-IIa (MYH9) has been found to bind the wave complex [282] and controls lammeliopodia formation [283]. However, the mechanism of this interaction is unknown. I suggest that disulfide bond formation is a principle mechanism to mediate this interaction through Cys91 and Cys896, which were both found to be oxidized in T cell activation.

Tubulin beta-4B chain (TUBB4B) represents a crosstalk between the actin cytoskeleton and microtubule network [284]. TUBB4B was found to be oxidized (+4%) at Cys239 which was found to be necessary for the polymerization of alpha and beta tubulin [285], it is hypothesized that higher oxidation suggests more polymerization which is in line with polymerization which occurs during T cell activation [286]. In cooperation with this microtubule polymerization, I have also identified Kinesin-like protein KIF2A (KIF2A) which is a motor protein that travels along microtubules to allow vesicle transport to the IS [287] The increased oxidation of this component (+4%) at

Cys309, which is in the same change in oxidation as TUBB4B, may indicate a localization to the cell cortex [288] which I have found to be more oxidizing (Chapter. 6.1)

Collectively, the data suggests that following PMA stimulated mtROS production, H_2O_2 diffuses into the cytoplasm and oxidizes selected components of the actin cytoskeleton (Figure. 40). These oxidations may induce lammeliopodia formation as well as microtubule cytoskeleton polymerization leading to an mtROS mediated lammeliopodia formation. Cytoskeleton oxidations may constitute a novel mechanism for priming IS formation following the generation of an mtROS microenvironment. This can be tested by isolating the IS through the use of laser microdissection[289] and to purify the IS proteome to confirm the presence of oxidized WRC components at the IS to support TCR signaling events.

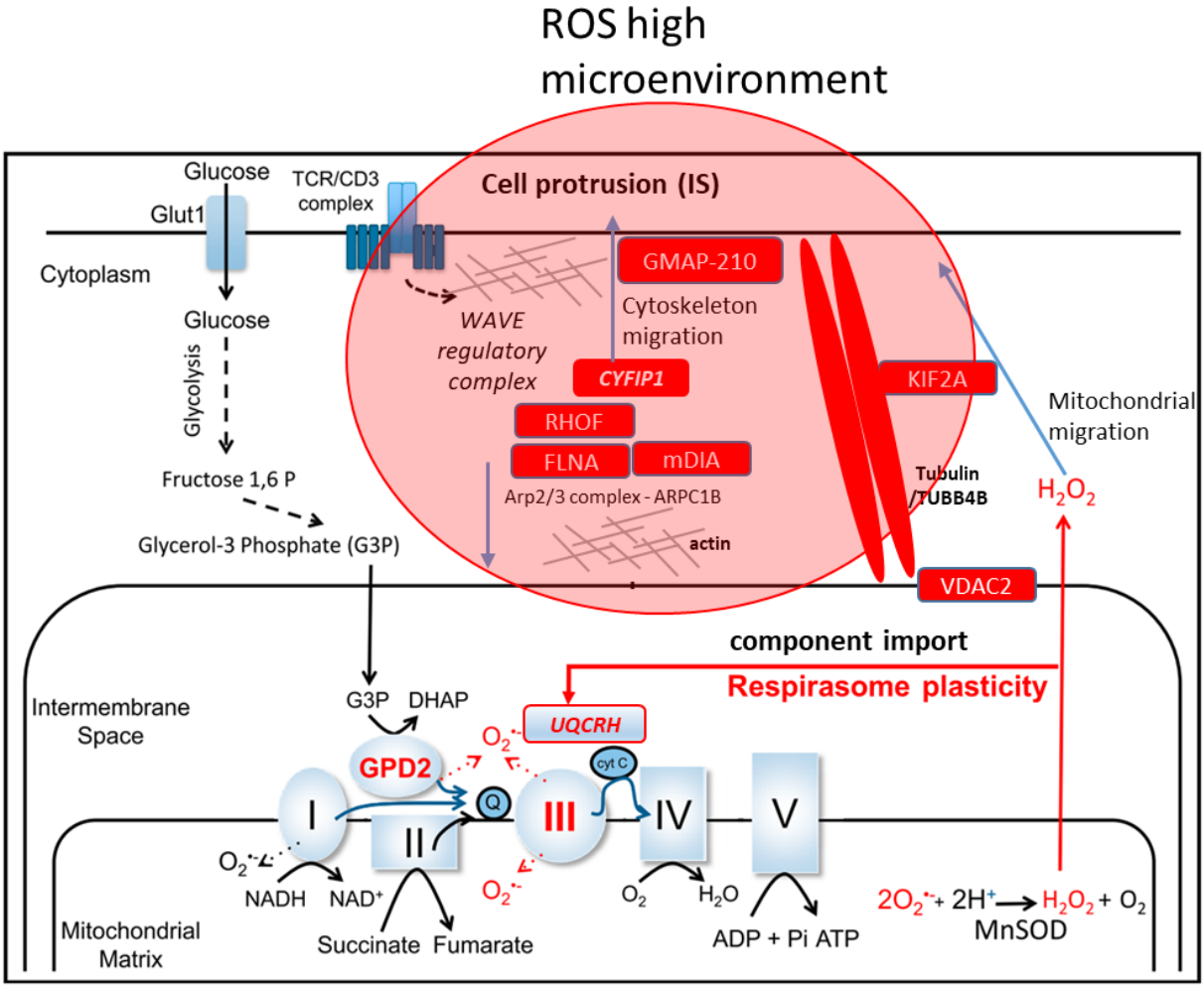

Figure 40: mtROS signaling is likely to support molecular interactions between oxidation sensitive cytoskeleton components regulating IS formation. As well as potential mitochondrial migration through disulfide formation of VDAC2 and TUBB4B.

mtROS from PMA stimulation induces a mtROS high microenvironment, this mediates interprotein disulfide bond formation of several cytoskeleton dynamic proteins including ARPC1B, CYFIP,1, RHOF, mDIA, FLNA and GMAP-210 which potentially primes these proteins for migration and formation of the IS. Additionally, mitochondrial migration is also potentially mediated through cytoskeleton dynamics via disulfide bond formation of VDAC, TUBB4B and KIF2A which constitute a putative mtROS sensitive migration of mitochondria along microtubules.

Having observed that cytoskeleton dynamics constitute a major target of the mtROS signal, I asked the question whether or not organelle migration such as the mitochondria can also be mediated in this manner. The actin cytoskeleton enmeshes the mitochondrial outer membrane where it is known to modulate mitochondrial fission and fusion, known as actin cycling [287,290] as well as migration[291]. I have also implicated mtROS already in mitochondrial morphology through the MICOS complex (Chapter. 5.2.1).

Additionally, it has been proven that mitochondria travel to the periphery of the cells via microtubules [292,293]. However the impact of mtROS on this mechanism has not been elucidated. My data suggests that TUBB4B and KIF2A may form disulfide bonds with the outer membrane of the mitochondria, which has been shown in literature for TUBB4B and the Voltage-dependent anion-selective channel protein 2 (VDAC2) [294]. VDAC2 was found oxidized in my study but not significantly (Supplementary Table. 3). It is therefore tempting to speculate that mtROS may mediate mitochondrial migration to the IS by anchoring mitochondria through VDAC2 to TUBB4B and KIF2A and then stimulating polymerization of tubulin to the IS.

5.3.2 Actin cytoskeleton stiffening in T cells to prevent migration to H_2O_2 rich environments?

The above chapter suggests that physiological mtROS induces cell mobility to induce IS formation in stimulated $CD4^+$ T cells. However, at stress response levels, it seems that ROS acts to downregulate actin/cell mobility. It is known that while H_2O_2 is required for innate immune cell recruitment to wounds [295], it has been shown that H_2O_2 leads to inhibition of adaptive immune cell motility, it was suggested this is to prevent accumulation of adaptive immune cells which are not required initially at the site of injury [132].

With this in mind, the most statistically significant change in oxidation in my data (Chapter. 4.2.4. Figure. 27) was the High mobility group protein B1 (HMGB1) which was found reduced (-5%) at Cys23 which is known to be reduced by glutathione under oxidative stress [296]. HMGB1 is a redox active protein localized to the plasma membrane in the presence of exogenous H_2O_2 stress [167]and acts a signal for inflammatory conditions [167,297]. Suggesting that the $CD4^+$ T cells were indeed under oxidative stress. As such I hypothesize that under these conditions $CD4^+$ T cells undergo actin stiffening to prevent traveling to inflammatory conditions which has been suggested in literature [132]. I aimed to supplement knowledge regarding the mechanism behind this actin stiffening phenotype.

To accomplish actin stiffening, Coronin-1C (CORO1C) is a protein known to mediate its function through a number of specific binding regions in its tertiary structure. CORO1C is also a known inhibitor of the ARP2/3 complex [298] through formation of transient disulfide bonds. I mentioned earlier that ARP2/3 complex is known to mediate actin/cell motility and forms transient disulfide bonds to mediate function of other proteins (Chapter 5.3.1). I hypothesize that in the presence of exogenous H_2O_2 CORO1C may act to prevent actin dynamics and cell motility by forming a disulfide bond with ARP2/3 through the Cys420 in CORO1C (+9%) following stimulation with H_2O_2. APRC1B mentioned above (Chapter. 5.3.1) was found oxidized in my data with

an oxidation of (21%) but it was not significant (Supplementary Table. 8) This decrease in motility has been seen in literature with the mitochondrial migration being reduced with exogenous H_2O_2 [287]. Additionally, Plectin (PLEC) is known to form disulfides with actin and induce stiffness in oxidative stress [168]. I observed an oxidation of +11% at Cys4994 which is on the protein surface and may mediate interprotein disulfide formation to induce stiffness.

With this in mind, Ran GTPase-activating protein 1 (RANGAP1) is involved in linking the nuclear envelope to the actin cytoskeleton and is known to mediate transfer of proteins between the nucleus and the cytoplasm [299]. Potentially, oxidation at C274 (+8%) leads to increased disulfide formation to the nucleus by the actin cytoskeleton and reduces transport leading to protection of nuclear localized proteins. Reduced nuclear transport via actin polymerization has been suggested in literature[300], but no mechanisms are known.

Conversely, Plastin-1 (LCP1) was found to be reduced at residue C618 (-18%). LCP1 is known to mediate actin cytoskeleton dynamics and was found in literature to be redox sensitive. That is to say oxidation of Cys101 was found to inhibit actin mobility [301] and reduced actin/cell motility. On the contrary, reduction of LCP1 would lead to improved actin mobility [302] suggesting that T cells act to improve actin mobility in an antioxidant mechanism. This was also seen with RAC1 which, as mentioned previously, was also found reduced (-6.67%) with exogenous H_2O_2.

5.3.3 Summary

Taken together, this data suggests that under physiological mtROS producing conditions, a number of ARP2/3 and WRC binding proteins are oxidized to potentially mediate disulfide bond formation and migration of actin binding proteins to the IS. Primarily, ARPC1B, CYFIP1, mDIA and FLNA. Additionally of note, is the potential mechanism of mtROS mediated migration of the mitochondria through the known interprotein disulfide bond formation between TUBB4B and VDAC2[294] and mtROS mediated tubulin polymerization.

Conversely, under high oxidative stress conditions my data suggests there is a stiffening of cytoskeleton dynamics as implied by high degrees of oxidation in known actin stiffening proteins such as CORO1C and PLEC. This data further contributes to knowledge of molecular mechanisms behind the well-known T cell dysfunction when in high ROS microenvironments such as the tumor microenvironment [303]. Consequently, extreme oxidative stress seem to induce the cell to protect its most important proteins for avoidance of oxidative stress, such as LCP1 and RAC1. This suggests that even though actin stiffening is a product of high oxidative stress the cell works to reverse this phenotype. Additionally, it is tempting to speculate that potentially actin stiffening could constitute a putative method in which a cell can induce unidirectional movement. That is to say “stiffening” the actin in one direction while maintaining a reducing environment in the direction of travel. As mentioned previously the cell is capable of inducing redox microenvironments within the cytoplasm [274,301].

It is possible however to theorize that actin stiffening may be a method to induce a lack of movement in the cell in, cooperation with anchoring cell surface receptors such

as integrins [304]. For example in T cell activation through T cell receptor (TCR) engagement, it is known that the actin cytoskeleton forms a ramifying structure on with the goal of keeping a T cell immobile[305], mtROS may mediate interprotein disulfide bonding of the actin cytoskeleton to prevent movement, while utilizing a reducing microenvironment to mediate migration of vesicles.

5.4 The potential role of Zinc finger proteins as mtROS inducible regulators of T cell activation

Cysteine residues within the zinc finger motif are susceptible to ROS due to the coordinated zinc (Zn^{2+}) ion leading to deprotonation of the conjugated cysteine residue via electrostatic interaction with the thiolate conjugate base. Furthermore, it is known that ROS can mediate exclusion of zinc and a subsequent structural reorganization of the zinc finger motif changing the function. as such, it has been referenced multiple times that zinc finger motifs can function as reversible redox switches [306,307] which can alter protein function transiently.

A well-known example of zinc finger modulation by ROS is Protein/nucleic acid deglycase DJ-1 (PARK7 –HSP33 in bacteria). Oxidation-induced reversible disulfide formation leads to elimination of the Zn^{2+} in PARK7 which causes the zinc motif to open and allows the protein to bind to oxidation sensitive proteins preventing degradation via oxidative stress [83,84]. Additionally, in the case of PKC-ɵ, one of the primary propagators of T cell activation induced cell signaling, the zinc finger motifs present in its DAG binding site have been implicated in its activation. Suggesting a similar method to PARK7 [107].

On a global level it is known that on T cell activation there is an increase in intracellular zinc [308]. The mechanism hereof is not well understood, I therefore hypothesize that the exclusion of zinc from zinc binding proteins (Figure. 41) represents a novel mechanism to explain this phenomenon. Wherein, an induced oxidative environment oxidizes the cysteine residues within the zinc finger. Subsequently, the zinc finger undergoes structural reorganization and either loses function or functions differently. Finally, reestablishment of the reducing environment by thioredoxin (TXN) and reinsertion of the zinc leads to reformation of the zinc finger motif. It is known that zinc itself can be utilized as an additional secondary messenger [309] in T cell function [157] which also could suggest this mechanism is necessary to release extracellular zinc to induce signaling.

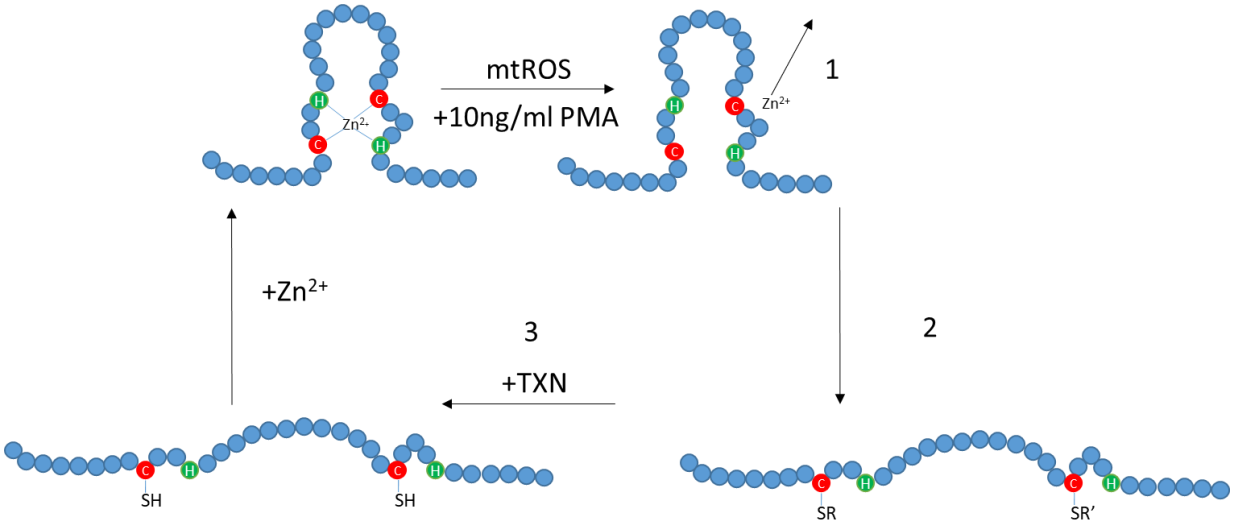

Figure 41: Model of zinc exclusion from zinc finger proteins following mtROS signal generation

1) ROS high environment induces oxidation of cysteine residues leading to zinc exclusion and structural reorganization of the zinc finger motif. 2) Zinc finger now mediates an additional function. 3) Reduction of ROS levels by TRX/GRDX and reinsertion of zinc leads to reformation of original zinc finger.

5.4.1 $CD4^+$ T cell activation and mtROS regulate zinc finger proteins

Zinc finger proteins are particularly interesting as a target of mtROS signaling as it demonstrates a putative method of mtROS mediated transcription/translation regulation. Loss of activity or differential activity can lead to a change in the protein synthesis of a cell which can implicate mtROS as a mediator of T cell effector function, as was introduced previously with Myc proto-oncogene protein Myc (Chapter. 1.4.1). Below I will discuss those zinc finger proteins that underwent a reduction greater than 5% in the redox active cysteine residue.

mRNA decay activator protein 36 (ZFP36/ Tristetraprolin) is known to downregulate $CD4^+$ T cell activity through targeted downregulation of a number of T cell activator mRNAs including Interleukin-2 (IL-2) and cluster of differentiation 4 (CD4) [310]. IL-2 is responsible for clonal expansion in $CD4^+$ T cells (Chapter. 1.2). Subsequently, reduction of ZFP36 at Cys109 (-10%) is hypothesized to mediate upregulation of $CD4^+$ T cell activation by loss of activity [311] of the ZFP36 zinc finger. Leading to upregulation of IL-2 and CD4 transcription. In a similar manner Vascular endothelial zinc finger 1 (VEZF1) is known to downregulate Interleukin-3 (IL-3), IL-3 is known to be produced by $CD4^+$ T cells and to activate mast cells and other T cells [312,313]. Therefore, loss of zinc finger binding through reduction of the zinc finger motif (CXXC) Cys176, Cys179 (-5%) zinc finger could mediate upregulation of IL-3 transcription inducing T cell activation.

Furthermore, the 60S ribosomal protein L37a (RPL37A) is known to impact the upregulation of cellular tumor antigen p53 (p53) through upregulation of the Mdm2-p53-MdmX network [314]. p53 is known to downregulate $CD4^+$ T cell activity in a TCR independent mechanism [315], a similar strategy of activation as used in this study. Incidentally, it is hypothesized that inactivation of RPL37A by reduction in its Cys39, Cys42, zinc finger motif (-5%) found in my data can upregulate $CD4^+$ T cell activity by downregulating transcription of P53.

In line with T cell activation signaling, it is known that the Cysteine-rich protein 2 (CRIP2) downregulates NF-κB activity by repressing its transcription. Therefore, loss of activity of CRIP2 by reduction of its CXXC LIM domain at Cys8 (-5%) could lead to upregulation of NF-κB signaling [316], which is known as an activating transcription factor (Chapter. 1.2). It is hypothesized that CRIP2 may also have an impact on the potential NF-κB signaling mentioned above (Chapters. 5.2.2 and Chapter 5.2.4)

5.4.2 Summary

Taken together it is evident from this data that not only are zinc fingers a highly ROS susceptible functional group. In addition, they can be mtROS modified in a manner that allows for coordinated downstream transcription/translation to impact discrete cellular effector functions, in this case $CD4^+$ T cell activation.

It was surprising to see that the zinc fingers were reduced considering that the model hypothesized (Figure. 41) relies on zinc exclusion by oxidation of the cysteine residues. However, I hypothesize that this is a temporal observation as I only looked on a 1h time point, i believe I am observing the time point in which TXN has reduced the cysteine residues. In future it would be necessary to observe the kinetic effect of this mechanism.

5.5 Shedding light on mtROS dependent immune responses

A major target of mtROS was identified as NF-κB signaling, which among T cell activation mediates immune responses. These NF-kB pathways are well characterized; [317,318] the fact that mtROS targets NF-kB generally suggests its role in transcription factor regulation. This thesis for the first time has utilized non-canonical amino acids (NCAAs), to characterize the protein synthesis that follows PMA stimulation in $CD4^+$ T cells in the presence or absence of catalase which complements our understanding of how mtROS establishes and supports T cell immune responses.

5.5.1 Identifying protein translation in PMA-activated T cells complements information on metabolic switch pathways, NF-κB signaling and cytoskeleton dynamics

My study for the first time looks on PMA signaling at an early stage of T cell activation (1h), which is known as an mtROS critical phase[51,61]. Previous work has characterized protein synthesis following T cell stimulation [171]. However, calcium signaling was integrated, which introduces many convoluting pathways. Furthermore, the time points utilized were past the optimal time point for monitoring mtROS. Nevertheless, it was found that there was significant overlap with my data and previously published data from Dieterich and colleagues (Table. 9 and Figure. 42).

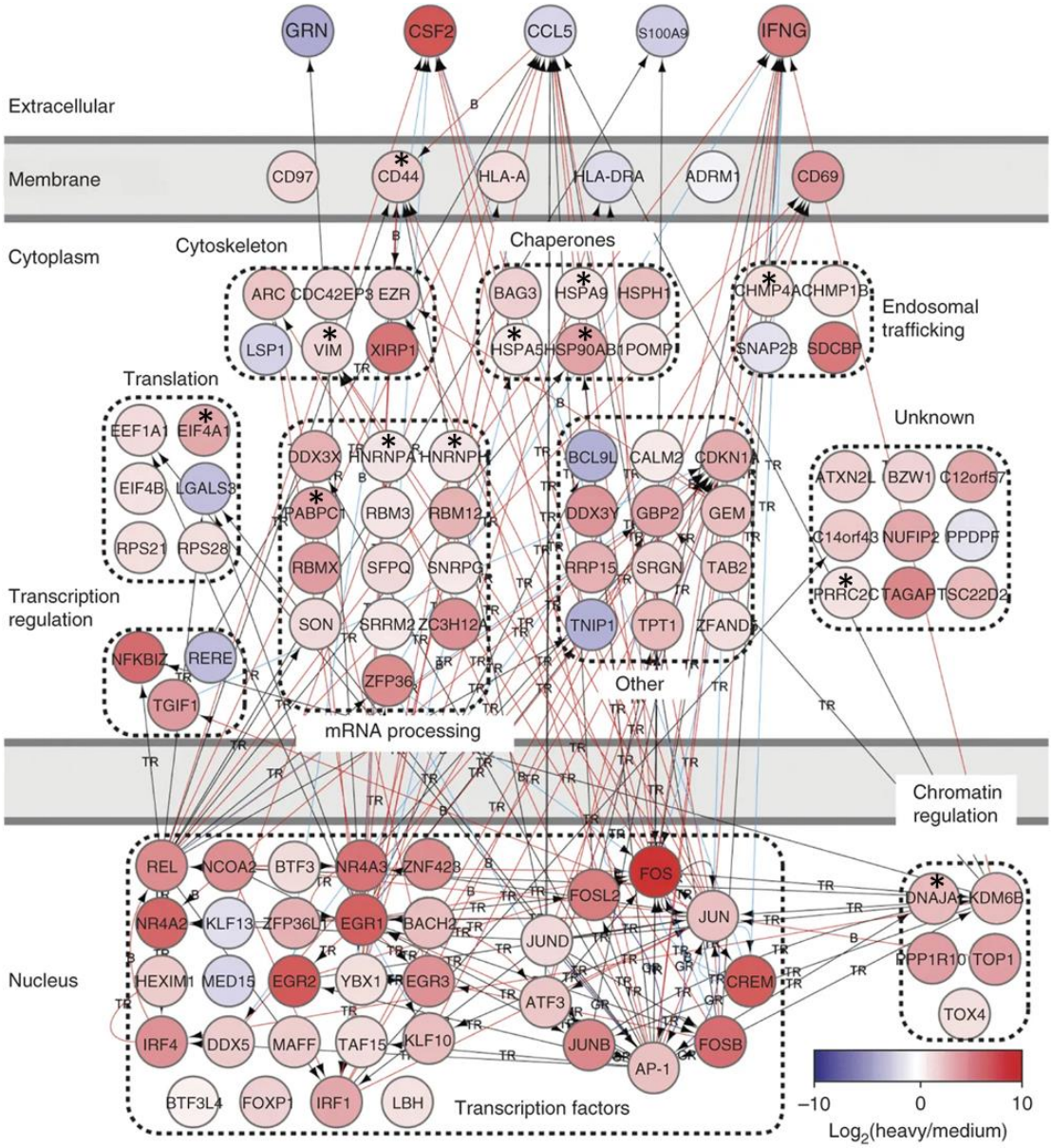

Figure 42: Crossover in most significant protein transcriptional upregulation between my data and [171]. Asterisks indicate crossover between my data and literature

As 50% of my data overlapped with previous data I assumed that the experimental data I generated can complement previous literature. Specifically in the case of Translation, mRNA processing, and chaperone proteins which were found to be particularly similar (Figure. 42).

Furthermore, I have complemented information by identifying novel candidates transcribed following PMA stimulation. Indeed, metabolic reprogramming proteins were found upregulated, such as Pyruvate Kinase (PKM) which can upregulate glutaminolytic pathways (+1.87 fold change) [30], as well as Insulin Receptor Substrate 2 (IRS2) which was found transcribed (+3.1 fold change) has been implicated in the metabolic modulation of other immune cells [319]. This is in line with literature that demonstrates that during the initial period of T cell activation (<24h) there is an initial metabolic reprogramming phase (Chapter. 1.2.1).

Additionally, my data suggests that following 1 hour PMA stimulation (Chapter. 4.3.1) $CD4^+$ T cells selectively upregulate DNA binding proteins. These proteins include; Eukaryotic initiation factor 4A-III (EIF4A3) and Elongation factor 1-delta (EEF1D) which are known to mediate activation of NF-κB signaling in higher ROS conditions (+2.78 and +5.48 fold changes respectively) [320]. Moreover, Heterogeneous nuclear ribonucleoprotein U (HNRNPU) was transcribed (+1.29 fold change) and upregulates TNFα activity [321] which acts to also upregulate NF-κB [322].

Downstream of NF-κB upregulation, Eukaryotic initiation factor 4A-I (EIF4A1) and Eukaryotic initiation factor 4A-III (EIF4A3) transcription (+1.84 and +2.78 fold change respectively) is known to be induced by NF-κB to mediate cell growth in cancer in a similar manner as T cells [323]. While transcription (+1.47 fold change) of Heterogeneous nuclear ribonucleoprotein A1 (HNRNPA1) down regulates NFATc1 [324], an effect that is prevalent in a subsequent chapter (Chapter. 5.6.5). There is overlap with established literature (Table. 10 [171]) and I have expanded the understanding by implicating all but EIF4A1 (seen in overlap - Table. 10) as newly identified PMA mediated transcription factors.

Interestingly, in my data set I identified the strong transcription (+6.14 fold change) of Family with sequence similarity 49 member B (FAM49B) which was found to play a role at both the Major histocompatibility complex (MHC) and cytoskeleton dynamics [173] by inhibiting RAC1 activity [325]. Cytoskeleton dynamics and RAC1 have been implicated previously as redox sensitive (Chapter. 5.3.1 and 5.3.2). Redox proteomics hinted at the upregulation immunological synapse (IS) dynamics at the early time point of 1h. Interestingly, FAM49B transcription suggests that after 16h (Figure. 28 Step 3) the T cell upregulates activity of actin stiffening to prevent disruption of IS formation[305]. Additionally, this may also be an impact of oxidative stress response which was hinted at previously (Chapter. 5.3.3). This data complements the current understanding of PMA induced T cell activation as it was not shown by Dieterich and colleagues.

Additionally in regards to cytoskeleton dynamics, both Heat shock protein HSP 90-alpha and beta (HSP90AA1, HSP90AB1) were found similarly transcribed with PMA stimulation (+2.63 and +2.72 fold changes respectively) and are known to induce T cell activity and survival [175,176] via MHC interactions and cytoskeleton dynamics [177]. In particular, through the action of Antigen presenting cells (APCs) [326], this may be indicative of the role of the PBMC fraction in activating T cells as these proteins could potentially be upregulated from being transferred via APCs. Additionally, these proteins are known to bind actin which is branched by the ARP2/3 complex [327,328]. These proteins were confirmed to be transcribed by Dieterich and colleagues.

In summary, this data set extends our understanding that PMA alone is capable of inducing well accepted T cell activation transcription processes, in comparison to PMA and ionomycin activation [171]. Additionally, I have complemented the state of understanding and theorize that PMA stimulated mtROS production upregulates NF-κB signaling. Additionally, it is apparent that PMA stimulation upregulates cytoskeleton dynamic regulatory processes through the heat shock protein gene family. It is apparent that the immune response mediated by PMA shows similarity with previously

implicated mtROS signaling components (Chapter. 5.2.3, 5.2.4, 5.3) further indicating the impact of mtROS signaling on downstream T cell transcription.

5.5.2 A model of how Catalase signaling leads to reduced respiration and endocytosis Catalase was able to quench mtROS production in PBMC-localized T cells (Chapter. 4.1.5) As it has been shown in literature that catalase can be secreted by cells [329], this mechanism may constitute a physiological action in tissue resident T cells which are more effected by the extracellular environment [330] than peripheral T cells.

To examine this mechanism, I looked on the impact of catalase in the absence of confounding PMA signaling. Under this condition I observed uniquely downregulated protein transcription. That is to say, besides keratin (Figure. 32) which is due to the higher keratin amount in the inactive conditions (Chapter. 4.3 Figure. 28B right). I observed specifically, the downregulation of transcription of processes involved in cellular respiratory pathways. Namely, inhibited transcription (-1.17 fold change) of 2-oxoglutarate dehydrogenase (OGDH) which would downregulate decarboxylation of α-KG in the TCA cycle [331], while reduced transcription (-1.53 fold change) of Triosephosphate isomerase 1 (TPI1) would reduce the activity of the pentose-phosphate pathways [332] and downregulation (-1.28 fold change) of Transitional endoplasmic reticulum ATPase (VCP) which would lead to a decrease in oxidative phosphorylation [333]. Therefore, my data suggests that catalase potentially downregulates mtROS production by reducing the translation of components from the TCA cycle, PPP as well as oxidative phosphorylation which are known to induce NADH and mtROS as NADH upregulates OXPHOS, which is the generator of mtROS (Chapter. 1.3.1).

Additionally, of the two proteins which were found to have their transcription upregulated by catalase. The most interesting candidate transcribed (+1.57 fold change) was Ras-related protein Rab-7a (RAB7A) which is known to mediate endocytosis of catalase [142]. Additionally, RAB7A is known to downregulate activity of Solute carrier family 2, facilitated glucose transporter member 1 (GLUT1) [334], which is responsible for the influx of glucose following T cell activation (Chapter. 1.4.1). Therefore, reducing import of glucose may induce the downregulation of the glucose dependent pathways mentioned above, which has been observed in literature [335].

In summary, I conclude that catalase mediates the downregulation of three independent respiratory pathways which are all mediated by glucose concentration (1, 2 and 3 in Figure. 43). As such, I hypothesize that catalase incubation is sensed by $CD4^+$ T cells which upregulates RAB7A to mediate catalase uptake (data not shown). Following which, I hypothesize that catalase either blocks activity of GLUT1 via inhibitory binding or upregulates RAB7A which is a known inhibitor of GLUT1. The end result is the downregulation of cell respiration which mediates a reduction in mtROS.

Potential evidence of this glucose depletion is that catalase lead to higher ROS in unstimulated T cells (Figure. 13), it is known that glucose depletion leads to ROS production via a nutrient stress response [336]. I address how to test this theory in the outlook (Chapter. 6.4).

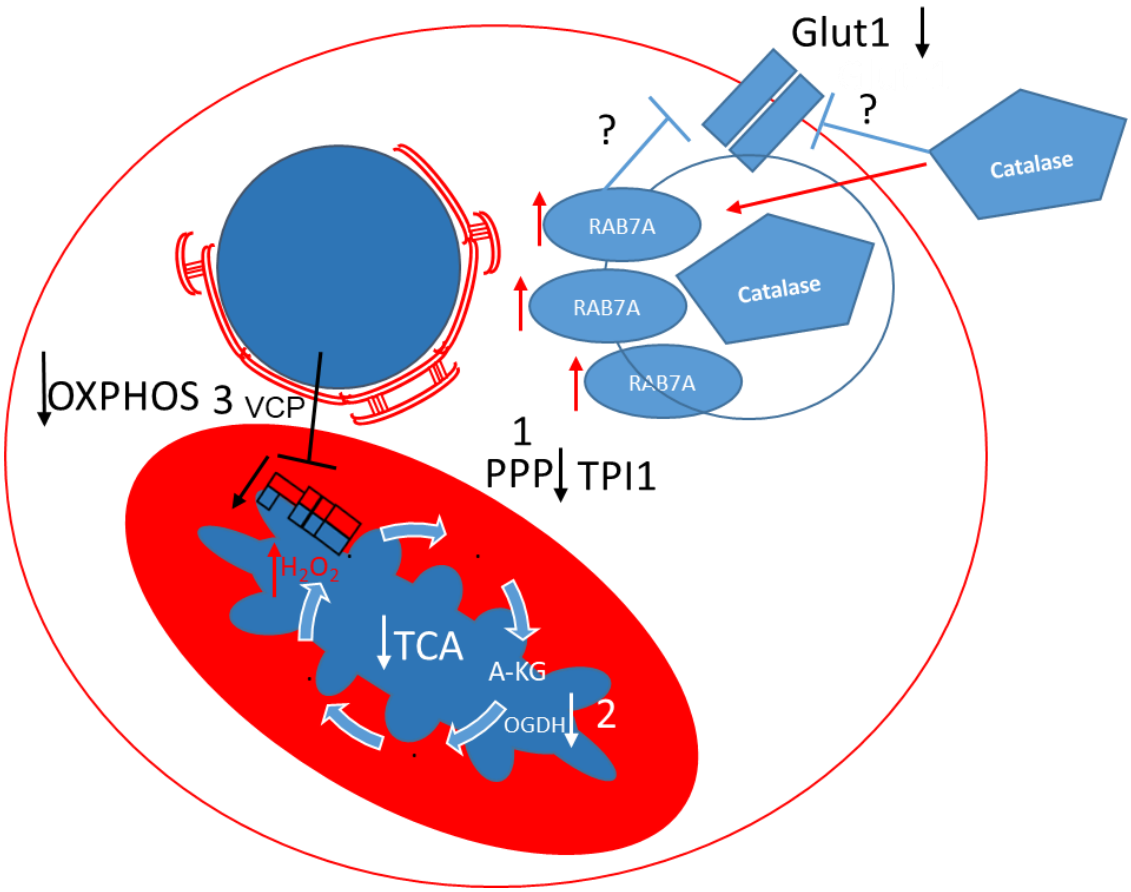

Figure 43: Model of the Impact of catalase incubation on T cell mtROS potentially mediated by inhibition of glucose dependent pathways

Incubation with catalase works to downregulate the glucose importer GLUT1 either direct inhibition through binding of glucose or the downregulation from the catalase mediated transcription of TAB7A. This yields a downregulation in the transcription of glucose dependent respiratory mechanisms including; 1) the pentose-phosphate pathways via Triosephosphate isomerase (TPI), 2) oxidation of pyruvate via the Tricarboxylic acid cycle through 2-oxoglutarate dehydrogenase (OGDH) and 3) oxidative phosphorylation by downregulation of Transitional endoplasmic reticulum ATPase (VCP). Restricting transcription of these components works to downregulate NADH generation which inhibits OXPHOS via 1 and 2 as well as the direct inhibition of OXPHOS via 3.

5.5.3 Catalase modulates cytoskeleton dynamics following PMA stimulation of T cells

Having explored the impact of catalase on unstimulated cells, I asked the question what would be its cooperative impact of T cell stimulation with PMA. I recognized that major upregulated components in the catalase dependent T cell activation were involved in actin mobility. As was seen in the H_2O_2 redox study (Chapter. 4.2.4 and Chapter. 5.3.2) it was recognized that actin stiffness was indicative of oxidative stress [132] as such I was not surprised to observe actin motility accompanying the lack of oxidative signal, as it has also been suggested in literature [287]. Below I define the cytoskeleton dynamic phenotype observed in PMA stimulation in the absence of mtROS signal, due to the action of catalase in the PBMC fraction.

Beginning with, Actin (ACTB), this protein composes the majority of the actin cytoskeleton and transcriptional upregulation (+2.36 fold change) of ACTB may be to mediate enhanced cytoskeleton dynamics, which would be expected when removing the mtROS signal which I have previously implicated in modulating cytoskeleton dynamics (Chapter. 5.3). In this line, the protein Ezrin (EZR) is known to link the actin

cytoskeleton to the plasma membrane and mediate changes in cell morphology [337]. It is tempting to hypothesize that transcription of EZR (+4.73 fold change) is acting to improve actin cytoskeleton dynamics, cell mobility and evasion of H_2O_2 as has been seen in other cell types when exposed to oxidative stress [338].

Cofilin (CFL1) is a well-known redox regulated component of the actin cytoskeleton[165]. In the presence of an oxidative environment CFL1 is inactivated by oxidation at Cys139, Cys39 and Cys80, which leads to actin stiffness [166]. While under reducing conditions CFL1 activity in increased. Therefore, increasing the amount of CFL1 (+2.14 fold change) under this reducing milieu introduced by catalase would induce actin cytoskeleton dynamics and actin mobility. Additionally, in regards to the crosstalk between ROS and cytoskeleton dynamics Plastin-2 (LCP1) was found transcriptionally induced (+3.22 fold change). Additionally, LCP1 was observed to be reduced and therefore protected under oxidative stress conditions (Chapter. 5.3.2) which highlighted both its redox sensitivity as well as its known importance in cytoskeleton dynamics/ actin mobility under oxidative stress [302], in a similar manner to CFL1, suggesting catalase upregulates a number of redox active cytoskeleton regulators.

Finally, Tubulin alpha-1C chain (TUBA1C) was found transcribed (+2.89) under catalase mediated T cell activation which suggests that the entire cytoskeleton is induced and not just actin.

5.5.4 Which protein translations in activated T cells depend from mtROS?

Catalase incubation in the presence of PMA provided a reducing condition in which mtROS signal was quenched which has allowed the characterization of catalase sensitive proteins (Chapter. 5.6.2 and Chapter. 5.6.3). By looking on the proteins which are differentially transcribed in the PMA induced immune response in comparison to PMA induction in the presence of catalase allows one to speculate on the proteins that are more transcribed exclusively in the absence of catalase which would be proteins with mtROS dependent transcription.

It was found that mtROS dependent transcription enriched for proteins involved in antioxidant signaling through NF-κB. Additionally, T cell activation mechanisms which are known to me mediated by mtROS, such as NFATc1 were also transcribed.

In regards to the antioxidant signaling, the top regulated candidates induced by mtROS dependent stimulation, were (RPL13A, PABPC1 and SRPRB, Table. 15) proteins which directly interact within the protein network to facilitate antioxidative stress responses. 60S ribosomal protein L13a (RPL13A) was found transcribed in my study (+2.00 fold change). Additionally, RPL13A is known to be upregulated in other studies on $CD4^+$ T cell activation [339]. Specifically, it was seen that this upregulation was ERK signaling dependent which is downstream of the PMA activation pathway I utilized. RPL13A is a component of the IFN-γ-activated inhibitor of translation (GAIT) complex which is known to reduce mitochondrial respiration under ROS conditions [340]. Additionally, RPL13A is known to be modulated by RPL37A [341] which was identified in the redox proteome to be a mtROS sensitive zinc finger (Chapter. 5.4.1). This interaction implicates zinc finger modifications as a possible mtROS dependent transcription regulatory mechanism.

In parallel, Polyadenylate-binding protein 1 (PABPC1) demonstrated strong transcriptional upregulation (+6.06) in my data and is known to be upregulated in T cell activation [342] following oxidative stress [343,344], additionally in cooperation with RPL13A [345] suggesting this protein works in tandem with RPL13A to upregulate T cell activation transcription under oxidative stress conditions, as both of these proteins are transcription factors. Furthermore, PABPC1 is known to be modulated by ZFP36 [346]. ZFP36 is a zinc finger protein that I also identified in the redox previous study (Chapter. 5.4.1) further confirming a potential mtROS signaling transcription regulatory network.

Of the other top induced candidates specific to mtROS mediated T cell activation Insulin receptor substrate 2 (IRS2) which I found transcribed (+3.11) has been found to mediate the metabolic shift response following T cell activation [178]. Additionally, IRS2 is known to upregulate AKT/mTOR signaling which has been found to increase primary cell survival through the upregulation of NF-κB signaling [347] which I have already determined is a major oxidative stress response pathway in activated $CD4^+$ T cells (Chapters. 5.2.2, 5.2.4, 5.4.1).

In regards to previous results implicating the endoplasmic reticulum (ER) in a source of oxidative stress following PMA stimulation (Chapter. 5.2.3). Endoplasmic reticulum chaperone BiP (HSPA5/BiP) is a protein I found transcribed (+1.66 fold change) which is localized to the ER and has been shown to be induced under T cell activation [348]. It is upregulated in response to protein folding stress in the ER this overlaps with the ER stress chapter (Chapter. 5.2.3) as BiP downregulates ERO1A [349] which was found to potentially mediate oxidative stress in the ER following PMA activation. Additionally, Signal recognition particle receptor subunit beta (SRPRB) was found induced (+2.37 fold change). SRPRB is an ER localized protein. It was found that this protein is upregulated during oxidation of phospholipids[350], and may mediate an antioxidant response in the ER, as It is known that the ER is a central site of phospholipid biogenesis [351].

5.5.5 mtROS-mediated alteration of T cell activation pathways

Besides antioxidant signaling, it was apparent that the mtROS specific protein translation also induced T cell activation transcription/translation machinery. Most interestingly, is the upregulation of Interferon regulatory factor 2-binding protein 2 (IRF2BP2) (+2.54 fold change), which is a known inhibitor of NFATc1 transactivation in T cell activation [183] and acts to downregulate NFAT1c in the nucleus. My data suggests that the mtROS dependent PMA activation model may downregulate NFATc1. It was shown in literature that if mtROS levels exceed physiological levels then NFATc1 is in fact downregulated [352], suggesting IRF2BP2 potentially mediates this downregulation. Therefore I hypothesize that this protein may modulate colony stimulation in T cell activation. Additionally, when comparing my data with Dieterich and colleagues [171] IRF2BP2 was found to be downregulated when PMA is costimulated with ionomycin while PMA alone upregulates IRF2BP2 transcription. Suggesting that cooperative signaling of calcium and ROS is needed for a full T cell activation, which has been established in literature [353].

In regards to NFATc1 regulation, DnaJ homolog subfamily A member 1 (DNAJA1) is a zinc finger protein known to be transcribed under periods of oxidative stress [354] and was found in my data upregulated on the level of transcription (+4.25 fold change). In addition to a direct binding of NFATc1 [185], DNAJA1 additionally, in high ROS conditions found in cancer cells, downregulates c-Jun activity, which subsequently downregulated NFATc1 transcriptional activity [355]. This concurs with IRF2BP2's action suggesting NFATc1 is inhibited at the protein activity and transcriptional level by IRF2BP2 and DNAJA1 respectively. Potentially this effect could be tested by measuring NFATc1 activity under PMA activation conditions.

In parallel, one of the most commonly recurring pathways throughout my thesis was NF-κB which has been heavily implicated as mediated by multiple aspects of mtROS signaling (Chapters. 5.2.2, 5.2.4, 5.4.1, 5.6.4), therefore it was not surprising that one of the significant transcription factors upregulated in the mtROS dependent immune response was Nuclear factor NF-kappa-B p100 subunit (NFKB2) (+3.72 fold change). This protein was found to be upregulated in oxidative stress in mice [356], additionally this protein has been known to modulate ROS production in T cells [357,358].

5.5.6 Summary

When characterizing the PMA induced protein translation it was apparent that $CD4^+$ T cells upregulate DNA modulating pathways which are known to impact NF-κB signaling, such as EIF4A3, EEF1D and HNRNPU. With this in mind it was hypothesized that T cells utilize mtROS as a method to signal through known antioxidant pathways to mediate an activation phenotype. This is feasible due to the diverse number of signaling pathways of NF-κB. In this line, heat shock proteins, such as HSP90AA1, HSP90AB1, HSPA9 and HSPD1 which are usually associated with stress conditions [359] were found to mediate cytoskeleton dynamics regulatory processes.

Conversely, when looking on catalase mediated signaling it was found that independent of PMA, catalase downregulates $CD4^+$ T cell respiration through potential downregulation of glucose uptake and glucose dependent respiratory pathways such as the PPP through TPI1, the TCA cycle through OGDH and oxidative phosphorylation via downregulation of VCP. Additionally, it was found that catalase most likely is taken up by $CD4^+$ T cells through endocytic mechanisms which upregulate RAB7A, which may mediate downregulation of GLUT1.

These effects were not however apparent when catalase was coincubated with PMA activation. Instead, it was found that catalase worked to upregulate actin mobility through ACTB, EZR, CFL1 and LCP1, in comparison to actin stiffening which is a phenotype of oxidative stress (Chapter. 5.3.2).

Looking on the regulated proteins which are dependent on generation of the mtROS signal it was found that RPL13A and PABPC1 mediate antioxidant effects and might be inhibited by the zinc finger proteins RPL37A and ZFP36, respectively. This data again suggests mtROS dependent transcription/translation is mediated by zinc finger modifications as seen in previous chapters (Chapter. 5.4.1). Finally, it is assumed that while PMA stimulation upregulates NF-κB signaling, it may in fact induce inhibitory

regulation of NFATc1 through IRF2BP2 which only in cooperation with calcium signaling allows for IL-2 transcription and transcriptional activity.

This data serves to draw a number of links between mtROS signaling which occurs in the first hour of PMA induced stimulation and the downstream protein translation confirming the impact of the mtROS signaling network on downstream T cell activation and function.

6.0 Outlook

In conclusion, this thesis has served to characterize the mtROS signaling network in primary $CD4^+$ T cells. Redox proteomics constitutes a facile analytical method to analyze (i) the regulatory impact of mtROS on cysteine residue specific oxidation. (ii) The quantification of the differential protein synthesis that is induced by mtROS signals.

It is apparent that PMA (acting via PKC-Θ) induces a robust mtROS signal from the respirasome in primary human T cells, without calcium signaling (Chapter. 4.1.2). mtROS can be regulated at multiple levels including the generation through structural reorganization of the electron transport chain (ETC) as well as inducible mitochondrial antioxidant systems which serve as ROS sensors (Chapters. 5.2.1 and 5.2.2).

Following the diffusion of mtROS from the mitochondria, cytoskeleton associated proteins are most likely mtROS modified to prime T cells for cell protrusion and molecular transport, which under physiological conditions constitute an immunological synapse (Chapter 5.3.1). Additionally, NF-κB signaling was potentially indicated to be upregulated in a dual function as (i) an antioxidant response (Chapter. 5.2.2) as well as (ii) a T cell activation transcription factor (Chapter. 5.4.1), it was found that to potenitally allow this increased activity, NF-κB proteins were additionally transcribed under mtROS conditions (Chapter. 5.6.5).

Exogenous mtROS allowed for the identification of mechanism $CD4^+$ T cells utilize once ROS exceeds the physiological range needed for signaling. It was found that NF-κB again mediates a strong antioxidant response (Chapter. 5.2.4), more so than in the physiological condition, elucidating the dynamic range of NF-κB signaling. Another link between the physiological and oxidative stress conditions was the shift from actin mobility to actin stiffening (Chapter. 5.3.2), suggesting that under oxidative stress cells become less mobile, which is known in T cell dysfunction in cancerous tumors.

It was found that catalase signaling in PMA stimulated conditions induces actin mobility suggesting a dual axis of cytoskeleton dynamics depending on the redox state which was exemplified by the 3 proteins Filamin A (FLNA) (Chapter. 5.3.1) as well as Plastin-2 (LCP1) and Cofilin (CFL1) (Chapters. 5.3.2 and 5.6.3).

This study determined a number of novel mechanisms that can be expanded upon to further divulge the impact of mtROS signaling on T cell activation.

6.1 Protein localization to the cell membrane can be quantified by redox proteomics

An interesting and unexpected mechanism that could be observed in the thiol switching technique (Chapter. 4.2.2) correlated with proteins that have a known trans-localization to the cell membrane following T cell activation. Indeed, it was obvious that the cell surface marker CD69, which signifies T cell activation and NF-κB and AP-1 signaling [360,361], demonstrated a shift in the cysteine oxidation. The extracellular residues of CD69, namely Cys186 and Cys194, shifted from 20% oxidized to 70% oxidized, which was the largest shift observed in the data set (Figure. 19B). This suggested that redox proteomics can be used as a method of detecting proteins which localize to the cell surface in T cell activation. Indeed, in our data set I also identified

a large number of other CD molecules with average increase in cysteine residue oxidations ranging from +9% to +5% (Table. 16).

From the candidate list I observed, CD97 which is an early activation marker [362], similar to CD69. Additionally CD97 is a ligand for CD55 surface expression [363] which may explain the similar degrees of oxidation as CD97 and CD55 have a costimulatory model. CD53 is a surface marker similarly to CD69, however with slower kinetics [364] which could explain why it has a lower degree of oxidation as it is exposed later after activation and therefore the majority of the protein pool might still be intercellular. Also the lesser oxidized candidates CD2, CD5 and CD6 are recruited to the IS and therefore may only sparsely decorate the cell surface [365,366]. In this case however, I assume the reduced oxidation is that PMA does not induce IS formation and therefore the surface migration of these proteins are attenuated.

This degree of oxidation may also serve as a method of quantifying the kinetics of surface marker presentation, with higher increases in oxidation correlating with the speed of presentation of CD molecules and other transmembrane proteins.

Table 16: Cell surface marker oxidation following activation

Sequence	Gene Name	% Change in Oxidation	Extracellular
NTEVSSMECEK	CD69	47.20	X
NLYWICNKPYK	CD69	46.11	X
FSDCWNTEGSYDCVCSPGYEPVSGAK	CD97	10.26	X
WSTAVEFCK	CD55	9.23	X
IPGEKDSVICLK	CD55	8.85	X
ATVMFECDK	CD46	8.70	X
EDAGAVCSEHQSWR	CD6	8.56	X
NIQFSCK	CD38	8.48	X
QELLCAFWK	CD97	8.19	X
KVEGCYAK	CD53	8.08	X
FKCTAGNK	CD2	7.95	X
VLALLCSGFQPK	CD5	7.46	X
TFHETLDCCGSSTLTALTTSVLK	CD81	7.32	X
GLFCPHQK	CD5	7.23	X
IEDMDDNCYLK	CD48	7.11	
LTGGADRCEGQVEVHFR	CD6	6.82	X
LGTQTVPCNK	CD38	6.73	X
IEKIEDMDDNCYLK	CD48	6.59	
CTAGNKVSK	CD2	6.48	X
VTCAENR	CD6	6.36	X
SSLRWEEVCR	CD5	6.13	X
LSQCHELWER	CD5	5.67	X
VLCQSLGCGTAVERPK	CD6	5.66	X
EQQCGSVNSYR	CD5	5.55	X
CYTCQVSNSVSSK	CD48	5.32	
TEAADLCK	CD44	5.04	X

Additionally, it was observed that the majority of proteins exhibiting a greater than 20% increase in oxidation following PMA induction (Supplementary Table. 3) were also known to translocate to the plasma membrane (GSK3B [367], RTRAF[368], GNL1 [369] and PARP10[370]) or the cell cortex (CYTIP [371]). With this in mind, it was hypothesized that this thiol switching technique could be used to quantify the proportion of these proteins which are localized to the cell membrane or cortex, as described above for CD proteins. A reason for the oxidation is that, extracellular proteins are in contact with approximately 200µM of molecular oxygen in cell culture media [372] and lack a reducing environment. Additionally, the cell cortex is close to this oxidizing environment [98]. However, it seems like the donor variation is particularly striking here as none of these proteins were found significantly oxidized. However, due to PMA stimulation being independent of TCR engagement, no IS formation was present. IS formation has been implicated in providing a reducing environment via APC thiol secretion [373]. As such this method may prove novel in identifying cell surface markers involved in the IS as these surface markers will not undergo the large shift in oxidation that seems to be indicative of non-IS localized cell surface markers. Therefore, future experiments comparing cell-contact dependent and cell-contact independent Redox proteomics could elucidate candidates that are specifically translocated to the IS (Figure. 44).

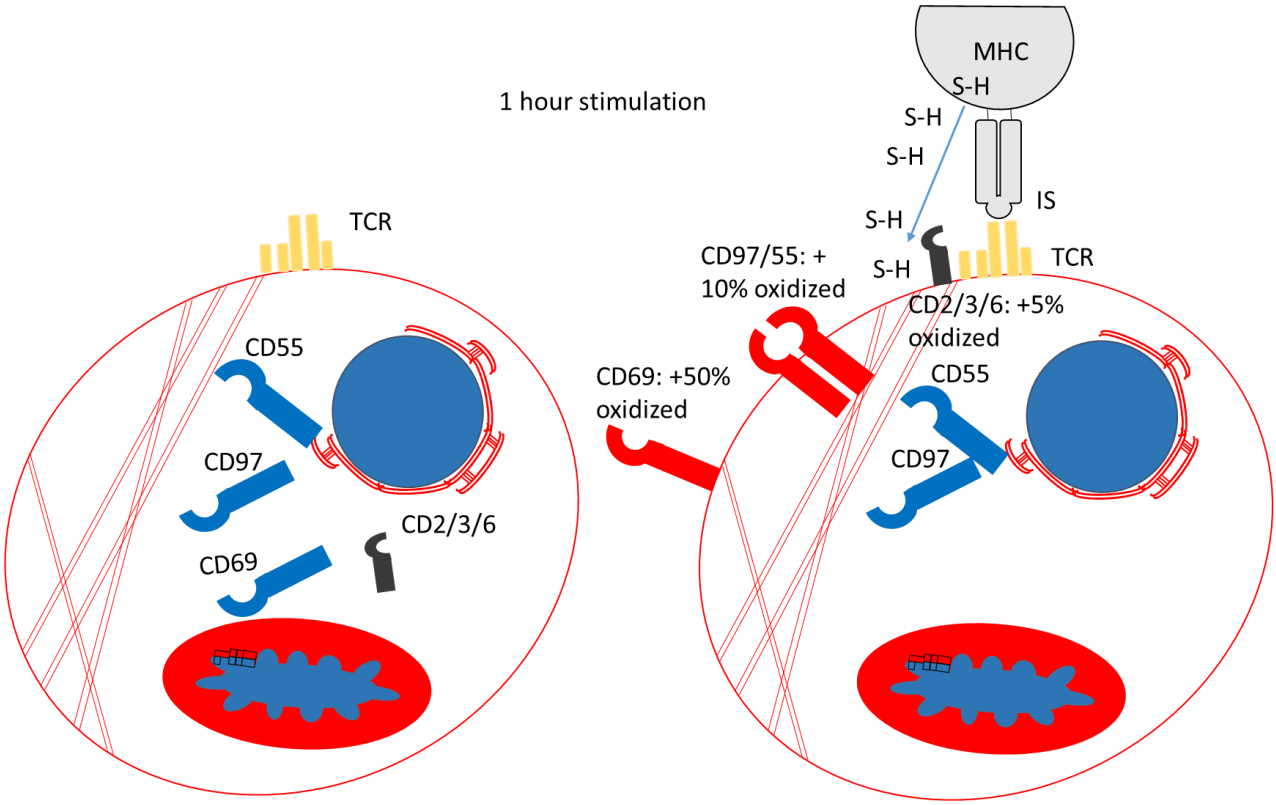

Figure 44: Model of cell surface marker expression oxidation following TCR engagement vs IS localized cell surface marker

Cell surface markers at the cell surface undergo a large shift in oxidation, indicative of the ratio of intercellular vs cell surface localized protein amount. IS localized cell surface markers will remain largely reduced due to reducing conditions of the IS.

6.2 Determination of the regulatory and functional role of mtROS-modified T cell proteins

Redox proteomics has identified a number of differentially oxidized components indicating their role in an mtROS-signaling network (Chapter. 4.2). Each of those components might act as an mtROS sensor in order to control functional related cellular processes, which however could not be further examined in the framework of this thesis. Basically, the identified components can be classified in candidates that help to regulate and balance respiration and mtROS production, as well as candidates which potentially mediate mtROS-induced downstream immune responses. Thus, perspective studies shall focus on respirasome dynamics and the newly identified class of zinc finger proteins:

6.2.1 Study candidates and new regulatory mechanisms of respirasome dynamics

Redox proteomics has identified several candidates which are known key components of the mitochondrial metabolism. These include, UQCRH, NDUFA2, MIC19 and DLD. These proteins all contain differentially oxidized cysteine residues which may constitute novel mechanism to elucidate the mtROS dependency of the respirasome and indeed the mitochondria as a whole. Subsequently, Future work is to generate site specific knockouts of candidate cysteine residues utilizing CRISPR/Cas9 technology to determine the physiological relevance of these disulfide bonds to the activity and structure of the respirasome as well as mitochondrial morphology.

It this line, we might ironically make use of the Jurkat cell line. Although my data has shown the inappropriateness of Jurkat cells to measure the induction of mtROS (Figure. 4.1), this cell type, however, proves an acceptable model system to study the perturbation of mtROS. As such this allows us to clarify the biological relevance of the respirasome associated proteins mentioned above in regard to electron transfer efficiency and mtROS generation.

Additionally, as it was observed in my data that mtROS alone seems to induce a downregulation of NFATc1 activity and transcription (Chapter. 5.6.5) it would be interesting to confirm this as it would suggest a cooperation of calcium signaling and mtROS signaling beyond generating different PTMs. As such it is planned to mutate the serines 191 and 194 on NFATc1 [19] which mediates constitutive nuclear localization of NFATc1, and observe whether in the presence of mtROS NFATc1 localizes to the nucleus and upregulates IL-2 activity. More specifically, the absence or presence of calcium signaling mediated by ionomycin could shed a more detailed light onto the molecules / proteins involved in mtROS signaling in T cells.

6.2.2 Validation of the zinc binding proteins as a new class of mtROS dependent transcription/translation regulators

Whereas the importance of zinc in immunity is well accepted, the molecular mechanisms are still incompletely understood. More recent data suggest the regulation of zinc binding since zinc influx was demonstrated at immunological synapses of activated T cells [308].

Zinc fingers have been shown in other studies as well as in this thesis to mediate mtROS dependent transcription/translation (Chapter. 5.4.1 and Chapter. 5.6.4). However, this needs to be further confirmed via orthogonal methodology. Preliminarily,

we have utilized an immobilized metal affinity chromatography (IMAC) protocol to selectively enrich zinc binding proteins under oxidative conditions.

Wherein the zinc ion has been expelled from the zinc finger motif and is available to bind the resin. It has been shown from this preliminary data (not shown) that components such as IARS2 show the hypothesized mechanism (Figure. 41) that zinc is excluded following oxidative stress and is reinserted following a reductive milieu. Additionally, the use of exogenous Thioredoxin (TXN) could allow for the confirmation of the known regenerative mechanism of oxidized zinc fingers such as in Protein/nucleic acid deglycase DJ-1 (PARK7 – HPS33 in bacteria) [84]. In that, incubation with TXN removes this metal affinity binding as the zinc ion has been reinserted into the zinc finger.

Again, CRISPR/Cas9 knock out mutants could indicate the global importance of zinc finger proteins for the T cell phenotype, whereas cysteine-specific mutations would clarify then their regulatory role in response to mtROS.

6.3 mtROS microenvironments constitute a potential compartmentalization of signaling

Additionally, an open question from this work in respect to the zinc fingers are the spatial aspects. As PMA does not induce formation of an immunological synapse, it is tempting to speculate that under physiological activation conditions the migration of mitochondria in the cells to the IS will induce the generation of an oxidative IS as mtROS emanates from the mitochondria. Consequently, it is hypothesized that this will induce a specific mtROS-high microenvironment which may elucidate more specific TCR dependent zinc fingers as well as oxidation susceptible proteins [143,373].

To accomplish this analysis, it is planned to utilize a bi-cellular model system in that immortalized B-cells can induce the formation of an IS with primary T cells, by which the hypothesized mtROS high IS microenvironment will be induced. The latter can be confirmed utilizing ROS sensitive fluorescent probes as well as high resolution microscopy. Subsequently, utilizing laser dissection microscopy it is planned to enrich this microenvironment and characterize the redox compartment therein.

Additionally, it is planned to utilize cysteine site specific knockouts of wave regulatory complex (WRC) components as well as ARP2/3 components identified as mtROS sensitive from this thesis to elucidate whether or not in the bi-cellular model system the mitochondria and other TCR signaling components migrate to the IS in an mtROSdependent manner. Furthermore, those mutants would allow to determine whether mtROS constitutes the mechanistic link between actin dynamic dependent processes in T cell activation.

6.4 Catalase signaling network determination

This thesis established catalase-dependent assays that based on the selectivity of this enzyme, for the first time, allowed to discover mtROS-dependent T cell proteins. The further characterization and validation of catalase-dependent processes is therefore of utmost importance. Leading hypothesis was that catalase is simply endocytosed and then able to quench mtROS signaling in T cells. However, experiments using

either PBMCs or sorted $CD4^+$ T cells indicated a differential quenching which suggested that peripheral cell populations in the PBMC fraction could significantly support the reduction of mtROS in T cells indicating mtROS regulatory pathways which are currently undefined. To clarify this we plan on utilizing flow cytometry to systematically evaluate the impact of both PMA activation on the mtROS of all PBMC resident cell types as well as the impact of catalase incubation to elucidate the responding cell types which may impact $CD4^+$ T cell activation.

While data generated in this thesis has hinted at the dual antioxidant signaling mechanism of catalase in $CD4^+$ T cells within the PBMC fraction. It is not completely characterized how this signaling is propagated. Therefore, it is planned to utilize additional PTM analysis such as phosphorylation which will allow the further elucidation of the impact that catalase has on T cells to mediate the quenching of mtROS. This is particularly interesting as it is known that catalase can be secreted to the extracellular space [329]. Which may therefore suggest this interaction is a physiological signaling network between cells in PBMCs. Additionally it is planned to utilize intracellular Fluorescence-activated cell sorting (FACS) staining as well as generating orthogonal Western blot data to determine whether catalase is being taken up via endocytosis. In regards to the impact of the endocytosis of catalase. It is planned to measure the glucose uptake in cells over time with and without catalase as this is hypothesized to be impacted by the endocytosis of catalase. As well as generating knockouts of RAB7A to look on differential GLUT-1 activity (Chapter. 5.6.2).

From these further experiments we hope to further elucidate the impact of mtROS signaling on the immune response providing further mechanistic data on the global importance of ROS as a secondary messenger in T cell function.

7.0 References

1. Schatz DG, Ji Y. Recombination centres and the orchestration of V(D)J recombination. Nat Rev Immunol. 2011;11(4):251–63.
2. Baldwin TA, Hogquist KA, Jameson SC. The Fourth Way? Harnessing Aggressive Tendencies in the Thymus. J Immunol. 2004;173(11):6515–20.
3. Crotty S, Org S. A brief history of T cell help to B cells A timeline of B cell help discoveriess HHS Public Access. Nat Rev Immunol. 2015;15(3):185–9.
4. Brown FD, Turley SJ. Fibroblastic Reticular Cells: Organization and Regulation of the T Lymphocyte Life Cycle. J Immunol. 2015;194(4):1389–94.
5. Jones N, Cronin JG, Dolton G, Panetti S, Schauenburg AJ, Galloway SAE, et al. Metabolic adaptation of human CD4+ and CD8+ T-cells to T-cell receptor-mediated stimulation. Front Immunol. 2017;8(NOV).
6. Wieczorek M, Abualrous ET, Sticht J, Álvaro-Benito M, Stolzenberg S, Noé F, et al. Major histocompatibility complex (MHC) class I and MHC class II proteins: Conformational plasticity in antigen presentation. Front Immunol. 2017;8(MAR):1–16.
7. Bretscher P. On analyzing how the Th1/Th2 phenotype of an immune response is determined: Classical observations must not be ignored. Front Immunol. 2019;10(JUN):1–7.
8. Luckheeram RV, Zhou R, Verma AD, Xia B. CD4 +T cells: Differentiation and functions. Clin Dev Immunol. 2012;2012.
9. Chambers CA, Kuhns MS, Egen JG, Allison JP. C TLA -4-M EDIATED I NHIBITION IN R EGULATION OF T C ELL R ESPONSES : Mechanisms and Manipulation in Tumor Immunotherapy . Annu Rev Immunol. 2001;19(1):565–94.
10. Aktas E, Kucuksezer UC, Bilgic S, Erten G, Deniz G. Relationship between CD107a expression and cytotoxic activity. Cell Immunol [Internet]. 2009;254(2):149–54. Available from: http://dx.doi.org/10.1016/j.cellimm.2008.08.007
11. Cao Y, Rathmell JC, Macintyre AN. Metabolic reprogramming towards aerobic glycolysis correlates with greater proliferative ability and resistance to metabolic inhibition in CD8 versus CD4 T cells. PLoS One. 2014;9(8):1–15.
12. Gerner MC, Niederstaetter L, Ziegler L, Bileck A, Slany A, Janker L, et al. Proteome analysis reveals distinct mitochondrial functions linked to interferon response patterns in activated CD4+ and CD8+ T cells. Front Pharmacol. 2019;10(July):1–13.
13. Van Den Broek T, Borghans JAM, Van Wijk F. The full spectrum of human naive T cells. Nat Rev Immunol [Internet]. 2018;18(6):363–73. Available from: http://dx.doi.org/10.1038/s41577-018-0001-y
14. De Rosa SC, Herzenberg LA, Herzenberg LA, Roederer M. 11-color, 13-

parameter flow cytometry: Identification of human naive T cells by phenotype, function, and T-cell receptor diversity. Nat Med. 2001;7(2):245–8.

15. M.R. W, W. Z, J. L, H. H, M. A, Z. M. Organization of proximal signal initiation at the TCR:CD3 complex. Immunol Rev [Internet]. 2009;232(1):7–21. Available from: http://www.embase.com/search/results?subaction=viewrecord&from=export&id=L615391902%0Ahttp://dx.doi.org/10.1007/s10461-015-1052-8%0Ahttp://wt3cf4et2l.search.serialssolutions.com?sid=EMBASE&issn=15733254&id=doi:10.1007%2Fs10461-015-1052-8&atitle=Female+Con

16. Wang H, Kadlecek TA, Au-Yeung BB, Goodfellow HES, Hsu LY, Freedman TS, et al. ZAP-70: an essential kinase in T-cell signaling. Cold Spring Harb Perspect Biol. 2010;2(5):1–18.

17. Wardenburg JB, Fu C, Jackman JK, Flotow H, Wilkinson SE, Williams DH, et al. Phosphorylation of SLP-76 by the ZAP-70 protein-tyrosine kinase is required for T-cell receptor function. J Biol Chem. 1996;271(33):19641–4.

18. Liu J. Calmodulin-dependent phosphatase, kinases, and transcriptional corepressors involved in T-cell activation Jun. Immunol Rev. 2009;228(1):184–98.

19. Beals CR, Clipstone NA, Ho SN, Crabtree GR. Nuclear localization of NF-ATc by a intramolecular interaction. Genes Dev. 1997;4:824–34.

20. Vaeth M, Maus M, Klein-Hessling S, Freinkman E, Yang J, Eckstein M, et al. Store-Operated Ca2+ Entry Controls Clonal Expansion of T Cells through Metabolic Reprogramming. Immunity [Internet]. 2017;47(4):664-679.e6. Available from: https://doi.org/10.1016/j.immuni.2017.09.003

21. Dutta D, Barr VA, Akpan I, Mittelstadt PR, Singha LI, Samelson LE, et al. Recruitment of calcineurin to the T cell receptor positively regulates T cell activation. Nat Immunol. 2019;18(2):196–204.

22. Dower NA, Stang SL, Bottorff DA, Ebinu JO, Dickie P, Ostergaard HL, et al. RasGRP is essential for mouse thymo-cyte differentiation and TCR signaling. Nat Immunol [Internet]. 2000;1(4):317–21. Available from: http://immunol.nature.xn--com-up0a

23. Hayashi K, Altman A. Protein kinase C theta (PKCθ): A key player in T cell life and death. Pharmacol Res. 2007;55(6):537–44.

24. Rathmell JC. T Cell Myc-tabolism. Immunity [Internet]. 2011;35(6):845–6. Available from: http://dx.doi.org/10.1016/j.immuni.2011.12.001

25. Wang R, Green DR. The immune diet: Meeting the metabolic demands of lymphocyte activation. F1000 Biol Rep. 2012;4(1):3–7.

26. Warburg O. On the Origin of Cancer Cells. Science (80-) [Internet]. 1956 Feb 24;123(3191):309–14. Available from: https://www.sciencemag.org/lookup/doi/10.1126/science.123.3191.309

27. Menk A V., Scharping NE, Moreci RS, Zeng X, Guy C, Salvatore S, et al. Early TCR Signaling Induces Rapid Aerobic Glycolysis Enabling Distinct Acute T Cell Effector Functions. Cell Rep [Internet]. 2018;22(6):1509–21. Available

from: https://doi.org/10.1016/j.celrep.2018.01.040

28. Salmond RJ. mTOR regulation of glycolytic metabolism in T cells. Front Cell Dev Biol. 2018;6(SEP):1–9.

29. Kruger NJ, von Schaewen A. The oxidative pentose phosphate pathway: structure and organisation. Curr Opin Plant Biol [Internet]. 2003 Jun;6(3):236–46. Available from: https://linkinghub.elsevier.com/retrieve/pii/S1369526603000396

30. Carr EL, Kelman A, Wu GS, Gopaul R, Senkevitch E, Aghvanyan A, et al. Glutamine Uptake and Metabolism Are Coordinately Regulated by ERK/MAPK during T Lymphocyte Activation. J Immunol. 2010;185(2):1037–44.

31. Klysz D, Tai X, Robert PA, Craveiro M, Cretenet G, Oburoglu L, et al. Glutamine-dependent α-ketoglutarate production regulates the balance between T helper 1 cell and regulatory T cell generation. Sci Signal. 2015;8(396).

32. Michalek RD, Gerriets VA, Nichols AG, Inoue M, Kazmin D, Chang CY, et al. Estrogen-related receptor-α is a metabolic regulator of effector T-cell activation and differentiation. Proc Natl Acad Sci U S A. 2011;108(45):18348–53.

33. Ganeshan K, Chawla A. Metabolic Regulation of Immune Responses. Annu Rev Immunol. 2014;32(1):609–34.

34. Mirebeau-Prunier D, Le Pennec S, Jacques C, Gueguen N, Poirier J, Malthiery Y, et al. Estrogen-related receptor α and PGC-1-related coactivator constitute a novel complex mediating the biogenesis of functional mitochondria. FEBS J. 2010;277(3):713–25.

35. Guo R, Gu J, Zong S, Wu M, Yang M. Structure and mechanism of mitochondrial electron transport chain. Biomed J [Internet]. 2018;41(1):9–20. Available from: https://doi.org/10.1016/j.bj.2017.12.001

36. Sazanov LA. A giant molecular proton pump: Structure and mechanism of respiratory complex I. Nat Rev Mol Cell Biol. 2015;16(6):375–88.

37. Horsefield R, Yankovskaya V, Sexton G, Whittingham W, Shiomi K, Omura S, et al. Structural and computational analysis of the quinone-binding site of complex II (succinate-ubiquinone oxidoreductase): A mechanism of electron transfer and proton conduction during ubiquinone reduction. J Biol Chem. 2006;281(11):7309–16.

38. Rieske JS. Composition, structure, and function of complex III of the respiratory chain. Biochim Biophys Acta - Rev Bioenerg [Internet]. 1976 Sep;456(2):195–247. Available from: https://linkinghub.elsevier.com/retrieve/pii/0304417376900124

39. Ma YY, Zhang XL, Wu TF, Liu YP, Wang Q, Zhang Y, et al. Analysis of the mitochondrial complex I-V enzyme activities of peripheral leukocytes in oxidative phosphorylation disorders. J Child Neurol. 2011;26(8):974–9.

40. Gu J, Wu M, Guo R, Yan K, Lei J, Gao N, et al. The architecture of the mammalian respirasome. Nat Publ Gr [Internet]. 2016;537(7622):639–43. Available from: http://dx.doi.org/10.1038/nature19359

41. Lapuente-Brun E, Moreno-Loshuertos R, Aciń-Pérez R, Latorre-Pellicer A, Colaś C, Balsa E, et al. Supercomplex assembly determines electron flux in the mitochondrial electron transport chain. Science (80-). 2013;340(6140):1567–70.

42. Maranzana E, Barbero G, Falasca AI, Lenaz G, Genova ML. Mitochondrial respiratory supercomplex association limits production of reactive oxygen species from complex i. Antioxidants Redox Signal. 2013;19(13):1469–80.

43. Moreno-Lastres D, Fontanesi F, García-Consuegra I, Martín MA, Arenas J, Barrientos A, et al. Mitochondrial complex I plays an essential role in human respirasome assembly. Cell Metab. 2012;15(3):324–35.

44. Acin-Perez R, Enriquez JA. The function of the respiratory supercomplexes: The plasticity model. Biochim Biophys Acta - Bioenerg [Internet]. 2014;1837(4):444–50. Available from: http://dx.doi.org/10.1016/j.bbabio.2013.12.009

45. Karunadharma PP, Basisty N, Chiao YA, Dai DF, Drake R, Levy N, et al. Respiratory chain protein turnover rates in mice are highly heterogeneous but strikingly conserved across tissues, ages, and treatments. FASEB J. 2015;29(8):3582–92.

46. Turrens JF. Mitochondrial formation of reactive oxygen species. JPhysiol. 2003;2(552):335–44.

47. Stein LR, Imai S. The dynamic regulation of NAD metabolism in mitochondria. Trends Endocrinol Metab [Internet]. 2012 Sep;23(9):420–8. Available from: https://linkinghub.elsevier.com/retrieve/pii/S1043276012001063

48. Wei J, Raynor J, Nguyen TLM, Chi H. Nutrient and metabolic sensing in T cell responses. Front Immunol. 2017;8(MAR):1–14.

49. Yi JS, Holbrook BC, Michalek RD, Laniewski NG, Grayson JM. Electron Transport Complex I Is Required for CD8 + T Cell Function . J Immunol. 2006;177(2):852–62.

50. Devadas S, Zaritskaya L, Rhee SG, Oberley L, Williams MS. Discrete Generation of Superoxide and Hydrogen Peroxide by T Cell Receptor Stimulation. J Exp Med [Internet]. 2002 Jan 7;195(1):59–70. Available from: https://rupress.org/jem/article/195/1/59/8261/Discrete-Generation-of-Superoxide-and-Hydrogen

51. Kamiński MM, Sauer SW, Kamiński M, Opp S, Ruppert T, Grigaravičius P, et al. T cell Activation Is Driven by an ADP-Dependent Glucokinase Linking Enhanced Glycolysis with Mitochondrial Reactive Oxygen Species Generation. Cell Rep. 2012;2(5):1300–15.

52. Lee HB, Yu MR, Song JS, Ha H. Reactive oxygen species amplify protein kinase C signaling in high glucose-induced fibronectin expression by human peritoneal mesothelial cells. Kidney Int. 2004;65(4):1170–9.

53. Terrazzano G, Rubino V, Damiano S, Sasso A, Petrozziello T, Ucci V, et al. T cell activation induces CuZn superoxide dismutase (SOD)-1 intracellular re-localization, production and secretion. Biochim Biophys Acta - Mol Cell Res

[Internet]. 2014;1843(2):265–74. Available from: http://dx.doi.org/10.1016/j.bbamcr.2013.10.020

54. Fridovich I. Superoxide Dismutase: A Comparison of Rate Constants. Arch Biochem Biophys. 1973;(158):396–400.

55. Li S, Case AJ, Yang RF, Schultz HD, Zimmerman MC. Over-expressed copper/zinc superoxide dismutase localizes to mitochondria in neurons inhibiting the angiotensin II-mediated increase in mitochondrial superoxide. Redox Biol [Internet]. 2013;2(1):8–14. Available from: http://dx.doi.org/10.1016/j.redox.2013.11.002

56. De Simoni S, Goemaere J, Knoops B. Silencing of peroxiredoxin 3 and peroxiredoxin 5 reveals the role of mitochondrial peroxiredoxins in the protection of human neuroblastoma SH-SY5Y cells toward MPP+. Neurosci Lett [Internet]. 2008 Mar;433(3):219–24. Available from: https://linkinghub.elsevier.com/retrieve/pii/S0304394008000554

57. Alfonso-Prieto M, Biarnés X, Vidossich P, Rovira C. The molecular mechanism of the catalase reaction. J Am Chem Soc. 2009;

58. Nohl H, Hegner D. EVIDENCE FOR THE EXISTENCE OF CATALASE IN THE MATRIX SPACE OF RAT-HEART MITOCHONDRIA. FEBS Lett. 1978;89(1):126–30.

59. Montalbetti CAGN, Falque V. Amide bond formation and peptide coupling. Tetrahedron. 2005;61(46):10827–52.

60. Kudin AP, Bimpong-buta NY, Vielhaber S, Elger CE, Kunz WS. Characterization of Superoxide-producing Sites in Isolated Brain Mitochondria *. 2004;279(6):4127–35.

61. Sena LA, Li S, Jairaman A, Prakriya M, Ezponda T, Hildeman DA, et al. Mitochondria Are Required for Antigen-Specific T Cell Activation through Reactive Oxygen Species Signaling. Immunity [Internet]. 2013;38(2):225–36. Available from: http://dx.doi.org/10.1016/j.immuni.2012.10.020

62. Yan LJ, Sumien N, Thangthaeng N, Forster MJ. Reversible inactivation of dihydrolipoamide dehydrogenase by mitochondrial hydrogen peroxide. Free Radic Res. 2013;47(2):123–33.

63. Marinho HS, Real C, Cyrne L, Soares H, Antunes F. Hydrogen peroxide sensing, signaling and regulation of transcription factors. Redox Biol. 2014;2(1):535–62.

64. Chen Q, Vazquez EJ, Moghaddas S, Hoppel CL, Lesnefsky EJ. Production of Reactive Oxygen Species by Mitochondria. J Biol Chem. 2003;278(38):36027–31.

65. Herlein JA, Fink BD, Henry DM, Yorek MA, Teesch LM, Sivitz WI. Mitochondrial superoxide and coenzyme Q in insulin-deficient rats : increased electron leak. Am J Physiol Regul Integr Comp Physiol. 2011;(301):1616–24.

66. Muller FL, Roberts AG, Bowman MK, Kramer DM, Chemistry B, State W, et al. Architecture of the Q o Site of the Cytochrome bc 1 Complex Probed by Superoxide. Biochemistry. 2003;(42):6493–9.

67. Kareyeva A, Vinogradov A. Molecular identification of the enzyme responsible for the mitochondrial NADH-supported ammonium-dependent hydrogen peroxide production. FEBS Lett. 2011;585(2):385–9.

68. Cemerski S, Cantagrel A, Meerwijk JPM Van, Romagnoli P. Reactive Oxygen Species Differentially Affect T Cell Receptor-signaling Pathways. J Biol Chem. 2002;277(22):19585–93.

69. Zheng X, Qian Y, Fu B, Jiao D, Jiang Y, Chen P, et al. Mitochondrial fragmentation limits NK cell-based tumor immunosurveillance. Nat Immunol [Internet]. 2019;20(December). Available from: http://dx.doi.org/10.1038/s41590-019-0511-1

70. Chang C, Qiu J, Sullivan O, Schreiber RD, Pearce EJ, Pearce EL, et al. Metabolic Competition in the Tumor Microenvironment Is a Driver of Cancer Progression Article Metabolic Competition in the Tumor Microenvironment Is a Driver of Cancer Progression. Cell [Internet]. 2015;162(6):1229–41. Available from: http://dx.doi.org/10.1016/j.cell.2015.08.016

71. Eil R, Vodnala SK, Clever D, Klebanoff CA, Sukumar M, Pan JH, et al. Ionic immune suppression within the tumour microenvironment limits T cell effector function. Nat Publ Gr [Internet]. 2016;537(7621):539–43. Available from: http://dx.doi.org/10.1038/nature19364

72. Uzzo RG, Clark PE, Rayman P, Bloom T, Rybicki L, Novick AC, et al. Alterations in NF-KB Activation in T Lymphocytes of Patients With Renal Cell Carcinoma. J Natl Cancer Instutute. 1999;91(8):718–21.

73. Petersson M, Hansson J, Masucci G, Wasserman K, Anderson P. Hydrogen peroxide secreted by tumor-derived zeta molecules and inhibits tumor-specific T cell- and natural killer cell-mediated cytotoxicity. Eur J Immunol. 1996;(26):1308–13.

74. Reth M. Hydrogen peroxide as second messenger in lymphocyte activation. Nat Immunol. 2002;3(12):1129–34.

75. Jones P, Suggett A. The catalse-hydrogen peroxide system. Kinetics of catalatic action at high substrate concentrations. Biochem J. 1968;110(4):617–20.

76. Zeida A, Babbush R, Estrin D. Molecular basis of the mechanism of thiol oxidation by hydrogen peroxide in aqueous solution: challenging the SN 2 paradigm. Chem Res Toxicol. 2013;25(3):741–6.

77. Witt AC, Lakshminarasimhan M, Remington BC, Hasim S, Pozharski E, Wilson MA. Cysteine pKa Depression by a Protonated Glutamic Acid in Human DJ-1. Biochemistry. 2009;47(28):7430–40.

78. Iqbalsyah TM, Moutevelis E, Warwicker J, Errington N, Doig AJ. The CXXC motif at the N terminus of an α-helical peptide. Protein Sci. 2006;15(8):1945–50.

79. Kortemme T, Creighton TE. Ionisation of Cysteine Residues at the Termini of Model a -Helical Peptides . Relevance to Unusual Thiol p K a Values in Proteins of the Thioredoxin Family. J Mol Biol. 1995;(253):799–812.

80. Naor MM, Jensen JH. Determinants of cysteine pKa values in creatine kinase and α1-antitrypsin. Proteins Struct Funct Genet. 2004;57(4):799–803.

81. Denu JM, Dixont JE. Protein tyrosine phosphatases: mechanisms of catalysis and regulation. Curr Opin Chem Biol [Internet]. 1998;2(5):633–41. Available from: http://biomednet.com/elecref/13675

82. Ferrer-sueta G, Manta B, Botti H, Radi R, Trujillo M, Denicola A. Factors Affecting Protein Thiol Reactivity and Specificity in Peroxide Reduction. Chem Res Toxicol. 2011;(24):434–50.

83. Ilbert, Marianne. Graf, Paul. Jakob U. Zinc Centre as Redox Switch - New Function for an Old Motif. Antioxid Redox Signal. 2006;8:835–46.

84. Jakob U, Muse W, Eser M, Bardwell JCA. Chaperone activity with a redox switch. Cell. 1999;96(3):341–52.

85. Franchina DG, Dostert C, Brenner D. Reactive Oxygen Species: Involvement in T Cell Signaling and Metabolism. Trends Immunol. 2018;39(6):489–502.

86. Zhi L, Ustyugova I V., Chen X, Zhang Q, Wu MX. Enhanced Th17 Differentiation and Aggravated Arthritis in IEX-1–Deficient Mice by Mitochondrial Reactive Oxygen Species-Mediated Signaling. J Immunol. 2012;189(4):1639–47.

87. Feske S, Vaeth M. NFAT control of immune function: New Frontiers for an Abiding Trooper. F1000Research. 2018;7(0):1–13.

88. Lo Conte M, Carroll KS. The redox biochemistry of protein sulfenylation and sulfinylation. J Biol Chem. 2013;288(37):26480–8.

89. Gupta V, Carroll KS. Sulfenic acid chemistry, detection and cellular lifetime. Biochim Biophys Acta - Gen Subj [Internet]. 2014;1840(2):847–75. Available from: http://dx.doi.org/10.1016/j.bbagen.2013.05.040

90. Pooles LB, Claiborne A. The Non-flavin Redox Center of the Streptococcal NADH Peroxidase. 1989;(May 2014).

91. Anderson LB, Hertzel AV, Das A. Agrobacterium tumefaciens VirB7 and VirB9 form a disulfide-linked protein complex. Proc Natl Acad Sci U S A. 1996;93(17):8889–94.

92. Xu C, Call ME, Wucherpfennig KW. A membrane-proximal tetracysteine motif contributes to assembly of CD3δε and CD3γε dimers with the T cell receptor. J Biol Chem. 2006;281(48):36977–84.

93. Stojanovski D, Müller JM, Milenkovic D, Guiard B, Pfanner N, Chacinska A. The MIA system for protein import into the mitochondrial intermembrane space. Biochim Biophys Acta - Mol Cell Res. 2008;1783(4):610–7.

94. Brandes N, Schmitt S, Jakob U. Thiol-based redox switches in eukaryotic proteins. Antioxidants Redox Signal. 2009;11(5):997–1014.

95. Chauvin JR, Pratt DA. Bioorganic Chemistry On the Reactions of Thiols , Sulfenic Acids , and Sulfinic Acids with Hydrogen Peroxide. Angew Chem Int Ed. 2017;2(56):6255–9.

96. Kwon J, Devadas S, Williams MS. T cell receptor-stimulated generation of hydrogen peroxide inhibits MEK-ERK activation and lck serine phosphorylation. Free Radic Biol Med. 2003;35(4):406–17.

97. Michalek RD, Nelson KJ, Holbrook BC, Yi JS, Stridiron D, Daniel LW, et al. The Requirement of Reversible Cysteine Sulfenic Acid Formation for T Cell Activation and Function. J Immunol. 2007;179(10):6456–67.

98. Gelderman KA, Hultqvist M, Holmberg J, Olofsson P, Holmdahl R. T cell surface redox levels determine T cell reactivity and arthritis susceptibility. Proc Natl Acad Sci U S A. 2006;103(34):12831–6.

99. Griffith CE, Zhang W, Wange RL. ZAP-70-dependent and -independent Activation of Erk in Jurkat T Cells. J Biol Chem. 1998;273(17):10771–6.

100. Thurm C, Poltorak MP, Reimer E, Brinkmann MM, Leichert L, Schraven B, et al. Zap70 stability and activity. Oncotarget. 2017;8(19):30805–16.

101. Veillette A, Dumont S, Fournel M. Conserved cysteine residues are critical for the enzymatic function of the lymphocyte-specific tyrosine protein kinase p56(lck). J Biol Chem. 1993;268(23):17547–53.

102. Cunnick JM, Dorsey JF, Mei L, Wu J. Reversible regulation of SHP-1 tyrosine phosphatase activity by oxidation. Biochem Mol Biol Int. 1998;45(5):887–94.

103. Angelini G, Gardella S, Ardy M, Ciriolo MR, Filomeni G, Di Trapani G, et al. Antigen-presenting dendritic cells provide the reducing extracellular microenvironment required for T lymphocyte activation. Proc Natl Acad Sci U S A. 2002;99(3):1491–6.

104. Dennis MK, Field AS, Burai R, Ramesh C, Whitney K, Bologa CG, et al. Postranscriptional control of T cell effector function by aerobic glycolysis. Cell. 2012;127(6):358–66.

105. Devadas S, Zaritskaya L, Rhee SG, Oberley L, Williams MS. Discrete generation of superoxide and hydrogen peroxide by T cell receptor stimulation: Selective regulation of mitogen-activated protein kinase activation and Fas ligand expression. J Exp Med. 2002;195(1):59–70.

106. Mak TW, Grusdat M, Duncan GS, Dostert C, Nonnenmacher Y, Cox M, et al. Glutathione Primes T Cell Metabolism for Inflammation. Immunity. 2017;46(4):675–89.

107. Zhao F, Ilbert M, Varadan R, Cremers CM, Hoyos B, Acin-Perez R, et al. Are zinc-finger domains of protein kinase C dynamic structures that unfold by lipid or redox activation? Antioxidants Redox Signal. 2011;14(5):757–66.

108. Hehner SP, Breitkreutz R, Shubinsky G, Unsoeld H, Schulze-Osthoff K, Schmitz ML, et al. Enhancement of T Cell Receptor Signaling by a Mild Oxidative Shift in the Intracellular Thiol Pool. J Immunol. 2000;165(8):4319–28.

109. Previte DM, Connor ECO, Novak EA, Martins CP, Mollen P, Piganelli JD. Reactive oxygen species are required for driving efficient and sustained aerobic glycolysis during CD4 + T cell activation. PLoS One. 2017;1–22.

110. Karpievitch Y V., Polpitiya AD, Anderson GA, Smith RD, Dabney AR. Liquid

chromatography mass spectrometry-based proteomics: Biological and technological aspects. Ann Appl Stat. 2010;4(4):1797–823.

111. Kaitlin M. Grinias, Justin M. Godinho, Edward G. Franklin, Jordan T. Stobaugh and JWJ. Development of a 45 kpsi Ultrahigh Pressure Liquid Chromatography Instrument for Gradient Separations of Peptides Using Long Microcapillary Columns and Sub-2 µm Particles. J Chromatogr A. 2016;1469:60–7.

112. Furey A, Moriarty M, Bane V, Kinsella B, Lehane M. Ion suppression; A critical review on causes, evaluation, prevention and applications. Talanta [Internet]. 2013 Oct;115:104–22. Available from: https://linkinghub.elsevier.com/retrieve/pii/S0039914013001975

113. Wang R, Zhang L, Zhang Z, Tian Y. Comparison of ESI– and APCI–LC–MS/MS methods: A case study of levonorgestrel in human plasma. J Pharm Anal [Internet]. 2016;6(6):356–62. Available from: http://dx.doi.org/10.1016/j.jpha.2016.03.006

114. Ulintz P, Yocum A, Bodenmiiller B, Aebersold R, Andrews P, Nesvizhskii A. Comparison of MS2 -only, MSA, and MS2 /MS3 Methodologies for Phosphopeptide Identification. J Proteome Res. 2009;8(2):887–99.

115. Singh S, Lämmle S, Giese H, Kämmerer S, Meyer-Roxlau S, Alfar EA, et al. The reduced activity of PP-1α under redox stress condition is a consequence of GSH-mediated transient disulfide formation. Sci Rep. 2018;8(1):1–14.

116. Fernandez-Caggiano M, Schröder E, Cho HJ, Burgoyne J, Barallobre-Barreiro J, Mayr M, et al. Oxidant-induced interprotein disulfide formation in cardiac protein DJ-1 occurs via an interaction with peroxiredoxin 2. J Biol Chem. 2016;291(19):10399–410.

117. Farah ME, Sirotkin V, Haarer B, Kakhniashvili D, Amberg DC. Diverse protective roles of the actin cytoskeleton during oxidative stress. Cytoskeleton. 2011;68(6):340–54.

118. Guan X, Zhang L, Wypych J. Direct mass spectrometric characterization of disulfide linkages. MAbs [Internet]. 2018;10(4):572–82. Available from: https://doi.org/10.1080/19420862.2018.1442998

119. Resemann A, Liu-Shin L, Tremintin G, Malhotra A, Fung A, Wang F, et al. Rapid, automated characterization of disulfide bond scrambling and IgG2 isoform determination. MAbs [Internet]. 2018;10(8):1200–13. Available from: https://doi.org/10.1080/19420862.2018.1512328

120. Li J, Zhang Y, Zhang Y, Lü S, Miao Y, Yang J, et al. GSNOR modulates hyperhomocysteinemia-induced T cell activation and atherosclerosis by switching Akt S-nitrosylation to phosphorylation. Redox Biol [Internet]. 2018;17(May):386–99. Available from: https://doi.org/10.1016/j.redox.2018.04.021

121. Qu Z, Meng F, Bomgarden RD, Viner RI, Li J, Rogers JC, et al. Proteomic quantification and site-mapping of S -nitrosylated proteins using isobaric iodoTMT reagents. J Proteome Res. 2014;13(7):3200–11.

122. Stewart II, Thomson T, Figeys D. 18O labeling: A tool for proteomics. Rapid Commun Mass Spectrom. 2001;15(24):2456–65.

123. Ong SE, Blagoev B, Kratchmarova I, Kristensen DB, Steen H, Pandey A, et al. Stable isotope labeling by amino acids in cell culture, SILAC, as a simple and accurate approach to expression proteomics. Mol Cell Proteomics. 2002;1(5):376–86.

124. Dieterich DC, Lee JJ, Link AJ, Graumann J, Tirrell DA, Schuman EM. Labeling, detection and identification of newly synthesized proteomes with bioorthogonal non-canonical amino-acid tagging. Nat Protoc. 2007;2(3):532–40.

125. Kalesh K, Denny PW. A BONCAT-iTRAQ method enables temporally resolved quantitative profiling of newly synthesised proteins in Leishmania mexicana parasites during starvation. PLoS Negl Trop Dis. 2019;13(12):e0007651.

126. Rothenberg DA, Taliaferro JM, Huber SM, Begley TJ, Dedon PC, White FM. A Proteomics Approach to Profiling the Temporal Translational Response to Stress and Growth. iScience [Internet]. 2018;9:367–81. Available from: https://doi.org/10.1016/j.isci.2018.11.004

127. McShane E, Sin C, Zauber H, Wells JN, Donnelly N, Wang X, et al. Kinetic Analysis of Protein Stability Reveals Age-Dependent Degradation. Cell [Internet]. 2016;167(3):803-815.e21. Available from: http://dx.doi.org/10.1016/j.cell.2016.09.015

128. Perkins DN, Pappin DJC, Creasy DM, Cottrell JS. Probability-based protein identification by searching sequence databases using mass spectrometry data. Electrophoresis. 1999;20(18):3551–67.

129. Hughes CS, Moggridge S, Müller T, Sorensen PH, Morin GB, Krijgsveld J. Single-pot, solid-phase-enhanced sample preparation for proteomics experiments. Nat Protoc. 2019;14(1):68–85.

130. Team Rs. RStudio: Integrated Development for R. [Internet]. RStudio. 2018. Available from: http://www.rstudio.com

131. Ponath V, Kaina B. Death of monocytes through oxidative burst of macrophages and neutrophils: Killing in trans. PLoS One. 2017;12(1):1–20.

132. Ball JA, Vlisidou I, Blunt MD, Wood W, Ward SG. Hydrogen Peroxide Triggers a Dual Signaling Axis To Selectively Suppress Activated Human T Lymphocyte Migration. J Immunol. 2017;198(9):3679–89.

133. Calabriso N, Gnoni A, Stanca E, Cavallo A, Damiano F, Siculella L, et al. Hydroxytyrosol ameliorates endothelial function under inflammatory conditions by preventing mitochondrial dysfunction. Oxid Med Cell Longev. 2018;2018.

134. Watts JD, Affolter M, Krebs DL, Wange RL, Samelson LE, Aebersold R. Identification by electrospray ionization mass spectrometry of the sites of tyrosine phosphorylation induced in activated Jurkat T cells on the protein tyrosine kinase ZAP-70. J Biol Chem. 1994;269(47):29520–9.

135. Maqsood MI, Matin MM, Bahrami AR, Ghasroldasht MM. Immortality of cell lines: Challenges and advantages of establishment. Cell Biol Int.

2013;37(10):1038–45.

136. Liou G-Y, Storz P. Reactive oxygen species in cancer. Free. 2010;44(5).

137. Cibrián D, Sánchez-Madrid F. CD69: from activation marker to metabolic gatekeeper. Eur J Immunol. 2017;47(6):946–53.

138. Darzynkiewicz Z. Critical Aspects in Analysis of Cellular DNA Content. Curr Protoc Cytom. 2010;7(2):1–9.

139. Buck MDD, O'Sullivan D, Klein Geltink RII, Curtis JDD, Chang CH, Sanin DEE, et al. Mitochondrial Dynamics Controls T Cell Fate through Metabolic Programming. Cell [Internet]. 2016;166(1):63–76. Available from: http://dx.doi.org/10.1016/j.cell.2016.05.035

140. Belikov A V., Schraven B, Simeoni L. T cells and reactive oxygen species. J Biomed Sci [Internet]. 2015;22(1):1–11. Available from: http://dx.doi.org/10.1186/s12929-015-0194-3

141. SUNDQVIST T, LIU SM. Hydrogen peroxide stimulates endocytosis in cultured bovine aortic endothelial cells. Acta Physiol Scand [Internet]. 1993 Oct;149(2):127–31. Available from: http://doi.wiley.com/10.1111/j.1748-1716.1993.tb09604.x

142. Shin MH, Rhie GE, Kim YK, Park CH, Cho KH, Kim KH, et al. H2O2 accumulation by catalase reduction changes MAP kinase signaling in aged human skin in vivo. J Invest Dermatol [Internet]. 2005;125(2):221–9. Available from: http://dx.doi.org/10.1111/j.0022-202X.2005.23823.x

143. Chen X, Song M, Zhang B, Zhang Y. Reactive Oxygen Species Regulate T Cell Immune Response in the Tumor Microenvironment. Oxid Med Cell Longev. 2016;2016:11–6.

144. Miki H, Funato Y. Regulation of intracellular signalling through cysteine oxidation by reactive oxygen species. J Biochem. 2012;151(3):255–61.

145. López-Mirabal HR, Winther JR. Redox characteristics of the eukaryotic cytosol. Biochim Biophys Acta - Mol Cell Res. 2008;1783(4):629–40.

146. Araki K, Kusano H, Sasaki N, Tanaka R, Hatta T, Fukui K, et al. Redox sensitivities of global cellular cysteine residues under reductive and oxidative stress. J Proteome Res. 2016;15(8):2548–59.

147. Vajrychova M, Salovska B, Pimkova K, Fabrik I, Tambor V, Kondelova A, et al. Quantification of cellular protein and redox imbalance using SILAC-iodoTMT methodology. Redox Biol [Internet]. 2019;24(January):101227. Available from: https://doi.org/10.1016/j.redox.2019.101227

148. Calvo SE, Clauser KR, Mootha VK. MitoCarta2.0: An updated inventory of mammalian mitochondrial proteins. Nucleic Acids Res. 2016;44(D1):D1251–7.

149. Zhao Y, Xu JX. The operation of the alternative electron-leak pathways mediated by cytochrome c in mitochondria. Biochem Biophys Res Commun. 2004;317(4):980–7.

150. Zhao Y, Wang ZB, Xu JX. Effect of cytochrome c on the generation and

elimination of O2.- and H2O2 in mitochondria. J Biol Chem. 2003;278(4):2356–60.

151. Sánchez-Caballero L, Guerrero-Castillo S, Nijtmans L. Unraveling the complexity of mitochondrial complex i assembly: A dynamic process. Biochim Biophys Acta - Bioenerg [Internet]. 2016;1857(7):980–90. Available from: http://dx.doi.org/10.1016/j.bbabio.2016.03.031

152. Szklarczyk R, Wanschers BFJ, Nabuurs SB, Nouws J, Nijtmans LG, Huynen MA. NDUFB7 and NDUFA8 are located at the intermembrane surface of complex i. FEBS Lett [Internet]. 2011;585(5):737–43. Available from: http://dx.doi.org/10.1016/j.febslet.2011.01.046

153. Tucker EJ, Wanschers BFJ, Szklarczyk R, Mountford HS, Wijeyeratne XW, van den Brand MAM, et al. Mutations in the UQCC1-Interacting Protein, UQCC2, Cause Human Complex III Deficiency Associated with Perturbed Cytochrome b Protein Expression. PLoS Genet. 2013;9(12).

154. Xie K, Bunse C, Marcus K, Leichert LI. Quantifying changes in the bacterial thiol redox proteome during host-pathogen interaction. Redox Biol [Internet]. 2019;21(December 2018):101087. Available from: https://doi.org/10.1016/j.redox.2018.101087

155. Rhee SG. Overview on Peroxiredoxin. Mol Cells. 2016;39(1):1–5.

156. Fisher A. Peroxiredoxin 6 in the repair of peroxidized cell membranes and cell signaling. Arch Biochem Biophys. 2016;617:68–83.

157. Topf U, Suppanz I, Samluk L, Wrobel L, Böser A, Sakowska P, et al. Quantitative proteomics identifies redox switches for global translation modulation by mitochondrially produced reactive oxygen species. Nat Commun [Internet]. 2018;9(1). Available from: http://dx.doi.org/10.1038/s41467-017-02694-8

158. Hu J, Dong L, Outten CE. The redox environment in the mitochondrial intermembrane space is maintained separately from the cytosol and matrix. J Biol Chem. 2008;283(43):29126–34.

159. Marchi S, Patergnani S, Pinton P. The endoplasmic reticulum-mitochondria connection: One touch, multiple functions. Biochim Biophys Acta - Bioenerg [Internet]. 2014;1837(4):461–9. Available from: http://dx.doi.org/10.1016/j.bbabio.2013.10.015

160. Saunders A, Webb LMC, Janas ML, Hutchings A, Pascall J, Carter C, et al. Putative GTPase GIMAP1 is critical for the development of mature B and T lymphocytes. Blood. 2010;115(16):3249–57.

161. Belton RJ, Chen L, Mesquita FS, Nowak RA. Basigin-2 is a cell surface receptor for soluble basigin ligand. J Biol Chem. 2008;283(26):17805–14.

162. H. Brown M. CD6 as a Cell Surface Receptor and As a Target for Regulating Immune Responses. Curr Drug Targets [Internet]. 2016 Mar 24;17(6):619–29. Available from: http://www.eurekaselect.com/openurl/content.php?genre=article&issn=1389-4501&volume=17&issue=6&spage=619

163. Sharma M, Merkulova Y, Raithatha S, Parkinson LG, Shen Y, Cooper D, et al. Extracellular granzyme K mediates endothelial activation through the cleavage of protease-activated receptor-1. FEBS J. 2016;283(9):1734–47.

164. Manji SSM, Parker NJ, Williams RT, Van Stekelenburg L, Pearson RB, Dziadek M, et al. STIM1: A novel phosphoprotein located at the cell surface. Biochim Biophys Acta - Protein Struct Mol Enzymol. 2000;1481(1):147–55.

165. Klemke M, Wabnitz GH, Funke F, Funk B, Kirchgessner H, Samstag Y. Oxidation of Cofilin Mediates T Cell Hyporesponsiveness under Oxidative Stress Conditions. Immunity. 2008;29(3):404–13.

166. Samstag Y, John I, Wabnitz GH. Cofilin: A redox sensitive mediator of actin dynamics during T-cell activation and migration. Immunol Rev. 2013;256(1):30–47.

167. Yu Y, Tang D, Kang R. Oxidative stress-mediated HMGB1 biology. Front Physiol. 2015;6(MAR).

168. Janda L, Damborský J, Rezniczek GA, Wiche G. Plectin repeats and modules: Strategic cysteines and their presumed impact on cytolinker functions. BioEssays. 2001;23(11):1064–9.

169. Shukla AA, Hinckley P. Host cell protein clearance during protein a chromatography: Development of an improved column wash Step. Biotechnol Prog. 2008;24(5):1115–21.

170. Van Den Broek T, Borghans JAM, Van Wijk F. The full spectrum of human naive T cells. Nat Rev Immunol. 2018;18(6):363–73.

171. Howden AJM, Geoghegan V, Katsch K, Efstathiou G, Bhushan B, Boutureira O, et al. QuaNCAT: Quantitating proteome dynamics in primary cells. Nat Methods. 2013;10(4):343–6.

172. Mi H, Muruganujan A, Ebert D, Huang X, Thomas PD. PANTHER version 14: More genomes, a new PANTHER GO-slim and improvements in enrichment analysis tools. Nucleic Acids Res. 2019;47(D1):D419–26.

173. Shang W, Jiang Y, Boettcher M, Ding K, Mollenauer M, Liu Z, et al. Genome-wide CRISPR screen identifies FAM49B as a key regulator of actin dynamics and T cell activation. Proc Natl Acad Sci U S A. 2018;115(17):E4051–60.

174. Chattaragada MS, Riganti C, Sassoe M, Principe M, Santamorena MM, Roux C, et al. FAM49B, a novel regulator of mitochondrial function and integrity that suppresses tumor metastasis. Oncogene [Internet]. 2018;37(6):697–709. Available from: http://dx.doi.org/10.1038/onc.2017.358

175. Haase M, Fitze G. HSP90AB1: helping the good and the bad. Gene. 2016;575(2):171–86.

176. Li W, Jiang Z, Li T, Wei X, Zheng Y, Wu D, et al. Genome-wide analyses identify KLF4 as an important negative regulator in T-cell acute lymphoblastic leukemia through directly inhibiting T-cell associated genes. Mol Cancer. 2015;14(1):1–13.

177. Zuehlke A, Beebe K, Neckers L, Prince T. Regulation and function of the

human HSP90AA1 gene. Gene. 2015;570(1):8–16.

178. Wang G, Wang J-J, Guan R, Sun Y, Shi F, Gao J, et al. Targeting Strategies for Glucose Metabolic Pathways and T Cells in Colorectal Cancer. Curr Cancer Drug Targets [Internet]. 2019 Aug 2;19(7):534–50. Available from: http://www.eurekaselect.com/166264/article

179. Bettonville M, D'Aria S, Weatherly K, Porporato PE, Zhang J, Bousbata S, et al. Long-term antigen exposure irreversibly modifies metabolic requirements for T cell function. Elife [Internet]. 2018 Jun 18;7. Available from: https://elifesciences.org/articles/30938

180. Huang L, Yu Z, Zhang Z, Ma W, Song S, Huang G. Interaction with Pyruvate Kinase M2 Destabilizes Tristetraprolin by Proteasome Degradation and Regulates Cell Proliferation in Breast Cancer. Sci Rep. 2016;6(February):1–11.

181. Sécca C, Faget D V., Hanschke SC, Carneiro MS, Bonamino MH, de-Araujo-Souza PS, et al. IRF2BP2 transcriptional repressor restrains naive CD4 T cell activation and clonal expansion induced by TCR triggering. J Leukoc Biol. 2016;100(5):1081–91.

182. Szklarczyk D, Gable AL, Lyon D, Junge A, Wyder S, Huerta-Cepas J, et al. STRING v11: Protein-protein association networks with increased coverage, supporting functional discovery in genome-wide experimental datasets. Nucleic Acids Res. 2019;47(D1):D607–13.

183. Carneiro FRG, Ramalho-Oliveira R, Mognol GP, Viola JPB. Interferon Regulatory Factor 2 Binding Protein 2 Is a New NFAT1 Partner and Represses Its Transcriptional Activity. Mol Cell Biol. 2011;31(14):2889–901.

184. Chuvpilo S, Avots A, Berberich-Siebelt F, Glöckner J, Fischer C, Kerstan A, et al. Multiple NF-ATc isoforms with individual transcriptional properties are synthesized in T lymphocytes. J Immunol. 1999;162(12):7294–301.

185. Gabriel CH, Gross F, Karl M, Stephanowitz H, Hennig AF, Weber M, et al. Identification of novel nuclear factor of activated T cell (NFAT)-associated proteins in T cells. J Biol Chem. 2016;291(46):24172–87.

186. Flescher E, Ledbetter JA, Schieven GL, Vela-Roch N, Fossum D, Dang H, et al. Longitudinal exposure of human T lymphocytes to weak oxidative stress suppresses transmembrane and nuclear signal transduction. J Immunol. 1994;153(11):4880–9.

187. Chen ACH, Arany PR, Huang YY, Tomkinson EM, Sharma SK, Kharkwal GB, et al. Low-Level laser therapy activates NF-kB via generation of reactive oxygen species in mouse embryonic fibroblasts. PLoS One. 2011;6(7):1–8.

188. Belikov A V., Schraven B, Simeoni L. TCR-triggered extracellular superoxide production is not required for T-cell activation. Cell Commun Signal. 2014;12(1):1–10.

189. Cong L, Ran A, Cox D, Lin S, Barretto R, Habib N, et al. Multiplex Genome Engineering Using CRISPR/Cas Systems. Science (80-). 2013;339:819–24.

190. Aharoni-Simon M, Shumiatcher R, Yeung A, Shih AZL, Dolinsky VW, Doucette

CA, et al. Bcl-2 regulates reactive oxygen species signaling and a redox-sensitive mitochondrial proton leak in mouse pancreatic β-cells. Endocrinology. 2016;157(6):2270–81.

191. Gill T, Levine AD. Mitochondria-derived hydrogen peroxide selectively enhances T cell receptor-initiated signal transduction. J Biol Chem. 2013;288(36):26246–55.

192. Gülow K, Kamiński M, Darvas K, Süss D, Li-Weber M, Krammer PH. HIV-1 Trans-Activator of Transcription Substitutes for Oxidative Signaling in Activation-Induced T Cell Death. J Immunol. 2005;174(9):5249–60.

193. Lee K, Esselman WJ. Inhibition of PTPs by H2O2 regulates the activation of distinct MAPK pathways. Free Radic Biol Med. 2002;33(8):1121–32.

194. Kamiński MM, Sauer SW, Klemke C-D, Süss D, Okun JG, Krammer PH, et al. Mitochondrial Reactive Oxygen Species Control T Cell Activation by Regulating IL-2 and IL-4 Expression: Mechanism of Ciprofloxacin-Mediated Immunosuppression. J Immunol. 2010;184(9):4827–41.

195. Frossi B, De Carli M, Piemonte M, Pucillo C. Oxidative microenvironment exerts an opposite regulatory effect on cytokine production by Th1 and Th2 cells. Mol Immunol. 2008;45(1):58–64.

196. Agbas A, Moskovitz J. The Role of Methionine Oxidation/Reduction in the Regulation of Immune Response. Curr Signal transduct Ther. 2009;4(1):46–50.

197. Kenyon GL, DeMarini DM, Fuchs E, Galas DJ, Kirsch JF, Leyh TS, et al. Defining the mandate of proteomics in the post-genomics era: workshop report. Mol Cell Proteomics. 2002;1(10):763–80.

198. Thermo Fisher. DTNB Thermo Fisher order catalog [Internet]. Available from: https://www.thermofisher.com/order/catalog/product/22582#/22582

199. Thermo Fisher. iodoTMT Thermo Fisher order catalog [Internet]. Available from: https://www.thermofisher.com/order/catalog/product/90101#/90101

200. Britto PJ, Knipling L, McPhie P, Wolff J. Thiol-disulphide interchange in tubulin: Kinetics and the effect on polymerization. Biochem J. 2005;389(2):549–58.

201. James AM, Hoogewijs K, Logan A, Hall AR, Ding S, Fearnley IM, et al. Non-enzymatic N-acetylation of Lysine Residues by AcetylCoA Often Occurs via a Proximal S-acetylated Thiol Intermediate Sensitive to Glyoxalase II. Cell Rep [Internet]. 2017;18(9):2105–12. Available from: http://dx.doi.org/10.1016/j.celrep.2017.02.018

202. Zheng L, Zanivan S, Gottlieb E. Proteome-wide analysis of cysteine oxidation reveals metabolic sensitivity to redox stress. Nat Commun [Internet]. 2018; Available from: http://dx.doi.org/10.1038/s41467-018-04003-3

203. McDonagh B, Sakellariou GK, Smith NT, Brownridge P, Jackson MJ. Differential cysteine labeling and global label-free proteomics reveals an altered metabolic state in skeletal muscle aging. J Proteome Res. 2014;13(11):5008–21.

204. Leichert LI, Gehrke F, Gudiseva H V., Blackwell T, Ilbert M, Walker AK, et al. Quantifying changes in the thiol redox proteome upon oxidative stress in vivo. Proc Natl Acad Sci U S A. 2008;105(24):8197–202.

205. Wu M, Gu J, Guo R, Huang Y, Yang M. Structure of Mammalian Respiratory Supercomplex I1III2IV1. Cell. 2016;167(6):1598-1609.e10.

206. Fischer M, Horn S, Belkacemi A, Kojer K, Petrungaro C, Habich M, et al. Protein import and oxidative folding in the mitochondrial intermembrane space of intact mammalian cells. Mol Biol Cell. 2013;24(14):2160–70.

207. Guarás A, Perales-Clemente E, Calvo E, Acín-Pérez R, Loureiro-Lopez M, Pujol C, et al. The CoQH2/CoQ Ratio Serves as a Sensor of Respiratory Chain Efficiency. Cell Rep. 2016;15(1):197–209.

208. Kamiński MM, Röth D, Krammer PH, Gülow K. Mitochondria as oxidative signaling organelles in T-cell activation: Physiological role and pathological implications. Arch Immunol Ther Exp (Warsz). 2013;61(5):367–84.

209. Lanciano P, Hassani B, Selamoglu N, Ghelli A, Rugolo M, Daldal F. Molecular Mechanisms of Superoxide Production by Complex III: A Bacterial versus Human Mitochondrial Comparative Case Study. Biochim Biophys Acta. 2011;1827(0):1332–9.

210. Kamiński MM, Röth D, Sass S, Sauer SW, Krammer PH, Gülow K. Manganese superoxide dismutase: A regulator of T cell activation-induced oxidative signaling and cell death. Biochim Biophys Acta - Mol Cell Res. 2012;1823(5):1041–52.

211. Darrouzet E, Valkova-Valchanova M, Moser CC, Dutton PL, Daldal F. Uncovering the [2Fe2S] domain movement in cytochrome bc1 and its implications for energy conversion. Proc Natl Acad Sci U S A. 2000;97(9):4567–72.

212. Nakai M, Endo T, Hase T, Tanaka Y, Trumpower BL, Ishiwatari H, et al. Acidic regions of cytochrome c1 are essential for ubiquinol-cytochrome c reductase activity in yeast cells lacking the acidic QCR6 protein. J Biochem. 1993;114(6):919–25.

213. Kuramitsu S, Wakabayashi S, Miyazuki T, Mukai K, Matsubara H. Identity of the Heme-Not-Containing Protein in Bovine Heart Cytochrome a Preparation with the Protein Mediating ci-c Complex Formation — A Protein with High. J Biochem. 1982;91(56113004):2077–85.

214. Kuramitsu S, Wakabayashi S, Miyazuki T, Mukai K, Matsubara H. Dissociation of Bovine Cytochrome cl Subcomplex and the Status of Cysteine Residues in the Subunits. J Biochem. 1985;98(5):1417–25.

215. Stonehuerner J, O'Brien P, Geren L, Millett F, Steidl J, Yu L, et al. Identification of the binding site on cytochrome c1 for cytochrome c. J Biol Chem. 1985;260(9):5392–8.

216. Tropeano C V., Aleo SJ, Zanna C, Roberti M, Scandiffio L, Loguercio Polosa P, et al. Fine-tuning of the respiratory complexes stability and supercomplexes assembly in cells defective of complex III. Biochim Biophys Acta - Bioenerg

[Internet]. 2020;1861(2):148133. Available from: https://doi.org/10.1016/j.bbabio.2019.148133

217. Protasoni M, Pérez-Pérez R, Lobo-Jarne T, Harbour ME, Ding S, Peñas A, et al. Respiratory supercomplexes act as a platform for complex III -mediated maturation of human mitochondrial complexes I and IV . EMBO J. 2020;1–19.

218. Sun C, Benlekbir S, Venkatakrishnan P, Wang Y, Hong S, Hosler J, et al. Structure of the alternative complex III in a supercomplex with cytochrome oxidase. Nature [Internet]. 2018;557:123–6. Available from: http://dx.doi.org/10.1038/s41586-018-0061-y

219. Cruciat CM, Brunner S, Baumann F, Neupert W, Stuart RA. The cytochrome bc1 and cytochrome c oxidase complexes associate to form a single supracomplex in yeast mitochondria. J Biol Chem. 2000;275(24):18093–8.

220. Owens KM, Kulawiec M, Desouki MM, Vanniarajan A, Singh KK. Impaired OXPHOS complex III in breast cancer. PLoS One. 2011;6(8).

221. Babady NE, Pang YP, Elpeleg O, Isaya G. Cryptic proteolytic activity of dihydrolipoamide dehydrogenase. Proc Natl Acad Sci U S A. 2007;104(15):6158–63.

222. Darshi M, Trinh KN, Murphy AN, Taylor SS. Targeting and import mechanism of coiled-coil helix coiled-coil helix domain-containing protein 3 (ChChd3) into the mitochondrial intermembrane space. J Biol Chem. 2012;287(47):39480–91.

223. Sakowska P, Jans DC, Mohanraj K, Riedel D, Jakobs S, Chacinska A. The Oxidation Status of Mic19 Regulates MICOS Assembly. Mol Cell Biol. 2015;35(24):4222–37.

224. Modjtahedi N, Tokatlidis K, Dessen P, Kroemer G. Mitochondrial Proteins Containing Coiled-Coil-Helix-Coiled-Coil-Helix (CHCH) Domains in Health and Disease. Trends Biochem Sci [Internet]. 2016;41(3):245–60. Available from: http://dx.doi.org/10.1016/j.tibs.2015.12.004

225. Larbi A, Kempf J, Pawelec G. Oxidative stress modulation and T cell activation. Exp Gerontol. 2007;42(9):852–8.

226. Kropotov A, Usmanova N, Serikov V, Zhivotovsky B, Tomilin N. Mitochondrial targeting of human peroxiredoxin V protein and regulation of PRDX5 gene expression by nuclear transcription factors controlling biogenesis of mitochondria. FEBS J. 2007;274(22):5804–14.

227. Malty RH, Aoki H, Kumar A, Phanse S, Amin S, Zhang Q, et al. A Map of Human Mitochondrial Protein Interactions Linked to Neurodegeneration Reveals New Mechanisms of Redox Homeostasis and NF-κB Signaling. Cell Syst [Internet]. 2017;5(6):564-577.e12. Available from: https://doi.org/10.1016/j.cels.2017.10.010

228. De Simoni S, Linard D, Hermans E, Knoops B, Goemaere J. Mitochondrial peroxiredoxin-5 as potential modulator of mitochondria-ER crosstalk in MPP+-induced cell death. J Neurochem. 2013;125(3):473–85.

229. Wong PC, Waggoner D, Subramaniam JR, Tessarollo L, Bartnikas TB, Culotta

VC, et al. Copper chaperone for superoxide dismutase is essential to activate mammalian Cu/Zn superoxide dismutase. Proc Natl Acad Sci U S A. 2000;97(6):2886–91.

230. Brown NM, Torres AS, Doan PE, O'Halloran T V. Oxygen and the copper chaperone CCS regulate posttranslational activation of Cu,Zn superoxide dismutase. Proc Natl Acad Sci U S A. 2004;101(15):5518–23.

231. Lingappan K. NF-κB in Oxidative Stress. Curr Opin Toxicol. 2018;7:81–6.

232. Morgan MJ, Liu ZG. Crosstalk of reactive oxygen species and NF-κB signaling. Cell Res [Internet]. 2011;21(1):103–15. Available from: http://dx.doi.org/10.1038/cr.2010.178

233. Yang X, Song J, Yan LJ. Chronic inhibition of mitochondrial dihydrolipoamide dehydrogenase (DLDH) as an approach to managing diabetic oxidative stress. Antioxidants. 2019;8(2).

234. Qu D, Hage A, Don-Carolis K, Huang E, Joselin A, Safarpour F, et al. BAG2 gene-mediated regulation of PINK1 protein is critical for mitochondrial translocation of PARKIN and neuronal survival. J Biol Chem. 2015;290(51):30441–52.

235. Libiad M, Motl N, Akey DL, Sakamoto N, Fearon ER, Smith JL, et al. Thiosulfate sulfurtransferase-like domain–containing 1 protein interacts with thioredoxin. J Biol Chem [Internet]. 2018 Feb 23;293(8):2675–86. Available from: http://www.jbc.org/lookup/doi/10.1074/jbc.RA117.000826

236. Libiad M, Motl N, Akey DL, Sakamoto N, Fearon ER, Smith JL, et al. Thiosulfate sulfurtransferase-like domain-containing 1 protein interacts with thioredoxin. J Biol Chem. 2018;293(8):2675–86.

237. Margittai É, Enyedi B, Csala M, Geiszt M, Bánhegyi G. Composition of the redox environment of the endoplasmic reticulum and sources of hydrogen peroxide. Free Radic Biol Med [Internet]. 2015 Jun;83:331–40. Available from: https://linkinghub.elsevier.com/retrieve/pii/S0891584915000398

238. Hwang C, Sinskey AJ, Lodish HF. Oxidized redox state of glutathione in the endoplasmic reticulum. Science (80-). 1992;257(5076):1496–502.

239. Stamm O, Krücken J, Schmitt-Wrede HP, Benten WPM, Wunderlich F. Human ortholog to mouse gene imap38 encoding an ER-localizable G-protein belongs to a gene family clustered on chromosome 7q32-36. Gene. 2002;282(1–2):159–67.

240. Wong VWY, Saunders AE, Hutchings A, Pascall JC, Carter C, Bright NA, et al. The autoimmunity-related GIMAP5 GTPase is a lysosome-associated protein. Self/Nonself - Immune Recognit Signal. 2010;1(3):259–68.

241. Datta P, Webb LMC, Avdo I, Pascall J, Butcher GW. Survival of mature T cells in the periphery is intrinsically dependent on GIMAP1 in mice. Eur J Immunol. 2017;47(1):84–93.

242. Messina S, De Simone G, Ascenzi P. Cysteine-based regulation of redox-sensitive Ras small GTPases. Redox Biol [Internet]. 2019;26(July):101282. Available from: https://doi.org/10.1016/j.redox.2019.101282

243. Aghajanian A, Wittchen ES, Campbell SL, Burridge K. Direct Activation of RhoA by Reactive Oxygen Species Requires a Redox-Sensitive Motif. PLoS One. 2009;4(11).

244. Bar-Sagi D, Hall A. Ras and Rho GTPases: A family reunion. Cell. 2000;103(2):227–38.

245. Kemp K, Poe C. Stressed: The unfolded protein response in T cell development, activation, and function. Int J Mol Sci. 2019;20(7).

246. Blais JD, Chin KT, Zito E, Zhang Y, Heldman N, Harding HP, et al. A small molecule inhibitor of Endoplasmic Reticulum Oxidation 1 (ERO1) with selectively reversible thiol reactivity. J Biol Chem. 2010;285(27):20993–1003.

247. Inaba K, Masui S, Iida H, Vavassori S, Sitia R, Suzuki M. Crystal structures of human Ero1α reveal the mechanisms of regulated and targeted oxidation of PDI. EMBO J [Internet]. 2010;29(19):3330–43. Available from: http://dx.doi.org/10.1038/emboj.2010.222

248. Appenzeller-Herzog C, Riemer J, Christensen B, Sørensen ES, Ellgaard L. A novel disulphide switch mechanism in Ero1α balances ER oxidation in human cells. EMBO J. 2008;27(22):2977–87.

249. Rezatabar S, Karimian A, Rameshknia V, Parsian H, Majidinia M, Kopi TA, et al. RAS/MAPK signaling functions in oxidative stress, DNA damage response and cancer progression. J Cell Physiol. 2019;234(9):14951–65.

250. Freeman AK, Ritt DA, Morrison DK. The importance of Raf dimerization in cell signaling. Small GTPases. 2013;4(3).

251. Cobbaut M, Derua R, Döppler H, Lou HJ, Vandoninck S, Storz P, et al. Differential regulation of PKD isoforms in oxidative stress conditions through phosphorylation of a conserved Tyr in the P+1 loop. Sci Rep. 2017;7(1):1–17.

252. Navarro MN, Sinclair L V., Feijoo-Carnero C, Clarke R, Matthews SA, Cantrell DA. Protein kinase D2 has a restricted but critical role in T-cell antigen receptor signalling in mature T-cells. Biochem J. 2012;442(3):649–59.

253. Gloire G, Charlier E, Rahmouni S, Volanti C, Chariot A, Erneux C, et al. Restoration of SHIP-1 activity in human leukemic cells modifies NF-κB activation pathway and cellular survival upon oxidative stress. Oncogene. 2006;25(40):5485–94.

254. Cady CT, Rice JS, Ott VL, Cambier JC. Regulation of hematopoietic cell function by inhibitory immunoglobulin G receptors and their inositol lipid phosphatase effectors. Immunol Rev. 2008;224(1):44–57.

255. Lu B, Sun X, Chen Y, Jin Q, Liang Q, Liu S, et al. Novel function of PITH domain-containing 1 as an activator of internal ribosomal entry site to enhance RUNX1 expression and promote megakaryocyte differentiation. Cell Mol Life Sci. 2015;72(4):821–32.

256. Li W, Thakor N, Xu EY, Huang Y, Chen C, Yu R, et al. An internal ribosomal entry site mediates redox-sensitive translation of Nrf2. Nucleic Acids Res. 2009;38(3):778–88.

257. Wang L, Brugge JS, Janes KA. Intersection of FOXO- and RUNX1-mediated gene expression programs in single breast epithelial cells during morphogenesis and tumor progression. Proc Natl Acad Sci U S A. 2011;108(40).

258. Akasaki Y, Alvarez-Garcia O, Saito M, Caramés B, Iwamoto Y, Lotz MK. FoxO transcription factors support oxidative stress resistance in human chondrocytes. Arthritis Rheumatol. 2014;66(12):3349–58.

259. Martinez N, Agosto L, Qiu J, Mallory M, Gazzara M, Barash Y, et al. Widespread JNK-dependent alternative splicing induces a positive feedback loop through CELF2-mediated regulation of MKK7 during T-cell activation. Genes Dev. 2015;29:2054–66.

260. Laphanuwat P, Likasitwatanakul P, Sittithumcharee G, Thaphaengphan A, Chomanee N, Suppramote O, et al. Cyclin D1 depletion interferes with oxidative balance and promotes cancer cell senescence. J Cell Sci. 2018;131(12):jcs214726.

261. Jankowska K, Burkhardt J. Analyzing Actin Dynamics at the Immunological Synapse. Methods Mol Biol [Internet]. 2017;1584:7–29. Available from: http://link.springer.com/10.1007/978-1-4939-6881-7

262. Gomez TS, Kumar K, Medeiros RB, Shimizu Y, Leibson PJ, Billadeau DDD. Formins Regulate the Actin-Related Protein 2/3 Complex-Independent Polarization of the Centrosome to the Immunological Synapse. Immunity. 2007;26(2):177–90.

263. Ti SC, Jurgenson CT, Nolen BJ, Pollard TD. Structural and biochemical characterization of two binding sites for nucleation-promoting factor WASp-VCA on arp2/3 complex. Proc Natl Acad Sci U S A. 2011;108(33):463–71.

264. Rodnick-Smith M, Luan Q, Liu SL, Nolen BJ. Role and structural mechanism of WASP-triggered conformational changes in branched actin filament nucleation by Arp2/3 complex. Proc Natl Acad Sci U S A. 2016;113(27):E3834–43.

265. Lassing I, Schmitzberger F, Björnstedt M, Holmgren A, Nordlund P, Schutt CE, et al. Molecular and Structural Basis for Redox Regulation of β-Actin. J Mol Biol. 2007;370(2):331–48.

266. Billadeau D, Burkhardt J. Regulation of Cytoskeletal Dynamics at the Immune Synapse: New Stars Join the Actin Troupe. Traffic. 2006;7(11):1451–60.

267. Zipfel PA, Bunnell SC, Witherow DS, Gu JJ, Chislock EM, Ring C, et al. Role for the Abi/Wave protein complex in T cell receptor-mediated proliferation and cytoskeletal remodeling. Curr Biol. 2006;16(1):35–46.

268. Kobayashi K, Kuroda S, Fukata M, Nakamura T, Nagase T, Nomura N, et al. p140Sra-1 (specifically Rac1-associated protein) is a novel specific target for Rac1 small GTPase. J Biol Chem. 1998;273(1):291–5.

269. Hobbs GA, Mitchell LE, Arrington ME, Harsha P, Decristo MJ, Loeser RF, et al. Redox regulation of Rac1 by thiol oxidation. Free Radic Biol Med. 2015;79:237–50.

270. Isogai T, van der Kammen R, Leyton-Puig D, Kedziora KM, Jalink K, Innocenti

M. Initiation of lamellipodia and ruffles involves cooperation between mDia1 and the Arp2/3 complex. J Cell Sci. 2015;128(20):3796–810.

271. Litschko C, Brühmann S, Csiszár A, Stephan T, Dimchev V, Damiano-Guercio J, et al. Functional integrity of the contractile actin cortex is safeguarded by multiple Diaphanous-related formins. Proc Natl Acad Sci U S A. 2019;116(9):3594–603.

272. Flanagan LA, Chou J, Falet H, Neujahr R, Hartwig JH, Stossel TP. Filamin A, the Arp2/3 complex, and the morphology and function of cortical actin filaments in human melanoma cells. J Cell Biol. 2001;155(4):511–7.

273. Kaludercic N, Deshwal S, Di Lisa F. Reactive oxygen species and redox compartmentalization. Front Physiol. 2014;5 JUL(August):1–15.

274. Tsutsumi R, Harizanova J, Stockert R, Schröder K, Bastiaens PIH, Neel BG. Assay to visualize specific protein oxidation reveals spatio-temporal regulation of SHP2. Nat Commun [Internet]. 2017;8(1):1–14. Available from: http://dx.doi.org/10.1038/s41467-017-00503-w

275. Goh WI, Sudhaharan T, Lim KB, Sem KP, Lau CL, Ahmed S. Rif-mDia1 interaction is involved in filopodium formation independent of Cdc42 and rac effectors. J Biol Chem. 2011;286(15):13681–94.

276. Goh WI, Lim KB, Sudhaharan T, Sem KP, Bu W, Chou AM, et al. mDia1 and WAVE2 proteins interact directly with IRSp53 in filopodia and are involved in filopodium formation. J Biol Chem. 2012;287(7):4702–14.

277. Häupl B, Ihling CH, Sinz A. Protein Interaction Network of Human Protein Kinase D2 Revealed by Chemical Cross-Linking/Mass Spectrometry. J Proteome Res. 2016;15(10):3686–99.

278. Kast DJ, Dominguez R. Mechanism of IRSp53 inhibition by 14-3-3. Nat Commun [Internet]. 2019;10(1). Available from: http://dx.doi.org/10.1038/s41467-019-08317-8

279. Westphal RS, Soderling SH, Alto NM, Langeberg LK, Scott JD. Scar/WAVE-1, a Wiskott±Aldrich syndrome protein, assembles an actin-associated multi-kinase scaffold Ryan. EMBO J. 2000;19(17):4589–600.

280. Galgano D, Onnis A, Pappalardo E, Galvagni F, Acuto O, Baldari CT. The T cell IFT20 interactome reveals new players in immune synapse assembly. J Cell Sci. 2017;130(6):1110–21.

281. Zucchetti AE, Bataille L, Carpier JM, Dogniaux S, San Roman-Jouve M, Maurin M, et al. Tethering of vesicles to the Golgi by GMAP210 controls LAT delivery to the immune synapse. Nat Commun [Internet]. 2019;10(1). Available from: http://dx.doi.org/10.1038/s41467-019-10891-w

282. Moraes L, Zanchin NIT, Cerutti JM. ABI3, a component of the WAVE2 complex, is potentially regulated by PI3K/AKT pathway. Oncotarget. 2017;8(40):67769–81.

283. Betapudi V. Myosin II motor proteins with different functions determine the fate of lamellipodia extension during cell spreading. PLoS One. 2010;5(1).

284. Martín-Coíreces NB, Alarcón B, Sańchez-Madrid F. Tubulin and actin interplay at thet cell and antigen-presenting cell interface. Front Immunol. 2011;2(JUL):1–6.

285. Bai R li, Lin CM, Nguyen NY, Liu TY, Hamel E. Identification of the Cysteine Residue of β-Tubulin Alkylated by the Antimitotic Agent 2,4-Dichlorobenzyl Thiocyanate, Facilitated by Separation of the Protein Subunits of Tubulin by Hydrophobic Column Chromatography. Biochemistry. 1989;28(13):5606–12.

286. Hui KL, Upadhyaya A. Dynamic microtubules regulate cellular contractility during T-cell activation. Proc Natl Acad Sci U S A. 2017;114(21):E4175–83.

287. Debattisti V, Gerencser AA, Saotome M, Das S, Hajnóczky G. ROS Control Mitochondrial Motility through p38 and the Motor Adaptor Miro/Trak. Cell Rep. 2017;21(6):1667–80.

288. Zhu C, Zhao J, Bibikova M, Leverson J, Wetzel E, Fan J, et al. Functional Analysis of Human Microtubule-based Motor Proteins, the Kinesins and Dyneins, in Mitosis/Cytokinesis Using RNA Interference. Mol Biol Cell. 2005;16:5356–72.

289. Bevilacqua C, Ducos B. Laser microdissection: A powerful tool for genomics at cell level. Mol Aspects Med [Internet]. 2018 Feb;59:5–27. Available from: https://linkinghub.elsevier.com/retrieve/pii/S0098299717301292

290. Moore AS, Wong YC, Simpson CL, Holzbaur ELF. Dynamic actin cycling through mitochondrial subpopulations locally regulates the fission-fusion balance within mitochondrial networks. Nat Commun. 2016;7(May 2015).

291. Suelmann R, Fischer R. Mitochondrial movement and morphology depend on an intact actin cytoskeleton inAspergillus nidulans. Cell Motil Cytoskeleton [Internet]. 2000 Jan;45(1):42–50. Available from: http://doi.wiley.com/10.1002/%28SICI%291097-0169%28200001%2945%3A1%3C42%3A%3AAID-CM4%3E3.0.CO%3B2-C

292. Sun QY, Wu GM, Lai L, Park KW, Cabot R, Cheong HT, et al. Translocation of active mitochondria during pig oocyte maturation, fertilization and early embryo development in vitro. Reproduction. 2001;122(1):155–63.

293. Boldogh IR, Pon LA. Mitochondria on the move. Trends Cell Biol. 2007;17(10):502–10.

294. Maldonado EN. VDAC-tubulin, an anti-Warburg pro-oxidant switch. Front Oncol. 2017;7(JAN):1–11.

295. Wittmann C, Chockley P, Singh SK, Pase L, Lieschke GJ, Grabher C. Hydrogen peroxide in inflammation: Messenger, guide, and assassin. Adv Hematol. 2012;2012.

296. Hoppe G, Talcott KE, Bhattacharya SK, Crabb JW, Sears JE. Molecular basis for the redox control of nuclear transport of the structural chromatin protein Hmgb1. Exp Cell Res. 2006;312(18):3526–38.

297. Zhao P, Ye T, Yan X, Hu X, Liu P, Wang X. HMGB1 release by H 2 O 2 - induced hepatocytes is regulated through calcium overload and 58-F interference. Cell Death Discov. 2017;3(November 2016).

298. Tilley FC, Williamson RC, Race PR, Rendall TC, Bass MD. Integration of the Rac1- and actin-binding properties of Coronin-1C. Small GTPases. 2015;6(1):36–42.

299. Datta S, Snow CJ, Paschal BM. A pathway linking oxidative stress and the Ran GTPase system in progeria. Mol Biol Cell. 2014;25(8):1202–15.

300. Giampetruzzi A, Danielson EW, Gumina V, Jeon M, Boopathy S, Brown RH, et al. Modulation of actin polymerization affects nucleocytoplasmic transport in multiple forms of amyotrophic lateral sclerosis. Nat Commun [Internet]. 2019;10(1). Available from: http://dx.doi.org/10.1038/s41467-019-11837-y

301. Balta E, Hardt R, Liang J, Kirchgessner H, Orlik C, Jahraus B, et al. Spatial oxidation of L-plastin downmodulates actin-based functions of tumor cells. Nat Commun [Internet]. 2019;10(1). Available from: http://dx.doi.org/10.1038/s41467-019-11909-z

302. Morley SC. The actin-bundling protein L-plastin supports T-cell motility and activation. Immunol Rev. 2014;256(1):48–62.

303. Weinberg F, Ramnath N, Nagrath D. Reactive oxygen species in the tumor microenvironment: An overview. Cancers (Basel). 2019;11(8).

304. Hogg N, Laschinger M, Giles K, McDowall A. T-cell integrins: More than just sticking points. J Cell Sci. 2003;116(23):4695–705.

305. Fritzsche M, Fernandes RA, Chang VT, Colin-York H, Clausen MP, Felce JH, et al. Cytoskeletal actin dynamics shape a ramifying actin network underpinning immunological synapse formation. Sci Adv. 2017;3(6).

306. Kröncke KD, Klotz LO. Zinc fingers as biologic redox switches? Antioxidants Redox Signal. 2009;11(5):1015–27.

307. Webster KA, Prentice H, Bishopric NH. Oxidation of zinc finger transcription factors: Physiological consequences. Antioxidants Redox Signal. 2001;3(4):535–48.

308. Yu M, Lee WW, Tomar D, Pryshchep S, Czesnikiewicz-Guzik M, Lamar DL, et al. Regulation of T cell receptor signaling by activation-induced zinc influx. J Exp Med. 2011;208(4):775–85.

309. Hojyo S, Fukada T. Roles of Zinc Signaling in the Immune System. J Immunol Res. 2016;2016.

310. Ogilvie RL, Abelson M, Hau HH, Vlasova I, Blackshear PJ, Bohjanen PR. Tristetraprolin Down-Regulates IL-2 Gene Expression through AU-Rich Element-Mediated mRNA Decay . J Immunol. 2005;174(2):953–61.

311. Moore M, Blachere N, Fak J, Park C, Sawicka K, Salina P, et al. ZFP36 RNA-binding proteins restrain T cell activation and anti-viral immunity. Biochem Biophys Res Commun. 2004;320(3):920–6.

312. Aglietta M, Pasquino P, Sanavio F, Stacchini A, Severino A, Fubini L, et al. Granulocyte-Macrophage colony stimulating factor and interleukin 3: Target cells and kinetics of response in vivo. Stem Cells. 1993;11(2 S):83–7.

313. Kumar A, Rani L, Mhaske ST, Pote ST, Behera S, Mishra GC, et al. IL-3 Receptor Expression on Activated Human Th Cells Is Regulated by IL-4, and IL-3 Synergizes with IL-4 to Enhance Th2 Cell Differentiation. J Immunol. 2020;204(4):819–31.

314. Daftuar L, Zhu Y, Jacq X, Prives C. Ribosomal Proteins RPL37, RPS15 and RPS20 Regulate the Mdm2-p53-MdmX Network. PLoS One. 2013;8(7).

315. Watanabe M, Moon KD, Vacchio MS, Hathcock KS, Hodes RJ. Downmodulation of tumor suppressor p53 by T cell receptor signaling is critical for antigen-specific CD4+ T cell responses. Immunity [Internet]. 2014;40(5):681–91. Available from: http://dx.doi.org/10.1016/j.immuni.2014.04.006

316. Cheung AKL, Ko JMY, Lung HL, Chan KW, Stanbridge EJ, Zabarovsky E, et al. Cysteine-rich intestinal protein 2 (CRIP2) acts as a repressor of NF-κB-mediated proangiogenic cytokine transcription to suppress tumorigenesis and angiogenesis. Proc Natl Acad Sci U S A. 2011;108(20):8390–5.

317. Oeckinghaus A, Ghosh S. The NF-kappaB family of transcription factors and its regulation. Cold Spring Harb Perspect Biol. 2009;1(4):1–14.

318. Liu T, Zhang L, Joo D, Sun SC. NF-κB signaling in inflammation. Signal Transduct Target Ther. 2017;2(April).

319. Jones R, Pearce E. MenTORing Immunity: mTOR Signaling in the Development and Function of Tissue-Resident Immune Cells. Immunity. 2017;46(5):730–42.

320. Ferrario A, Cro L, Zucal N, Lionetti M, Bertoni F, Nobili L, et al. Clinical-Biological Characterization of Variant B Chronic Lymphocytic Leukemia, Characterized by a Mantle Cell Lymphoma-Like Immunophenotype, t(11;14)(q13;q32) Negative. Blood [Internet]. 2009 Nov 20;114(22):1259–1259. Available from: https://ashpublications.org/blood/article/114/22/1259/110189/ClinicalBiological-Characterization-of-Variant-B

321. Yugami M, Kabe Y, Yamaguchi Y, Wada T, Handa H. hnRNP-U enhances the expression of specific genes by stabilizing mRNA. FEBS Lett. 2007;581(1):1–7.

322. Hayden M, Ghosh S. Regulation of NF-κB by TNF Family Cytokines. Semin Immunol. 2014;26(3):253–66.

323. Fiume G, Rossi A, de Laurentiis A, Falcone C, Pisano A, Vecchio E, et al. Eukaryotic Initiation Factor 4H Is under Transcriptional Control of p65/NF-κB. PLoS One. 2013;8(6):1–9.

324. Zhang L, Chen Q, An W, Yang F, Maguire EM, Chen D, et al. Novel pathological role of hnRNPA1 (heterogeneous nuclear ribonucleoprotein A1) in vascular smooth muscle cell function and neointima hyperplasia. Arterioscler Thromb Vasc Biol. 2017;37(11):2182–94.

325. Yuki KE, Marei H, Fiskin E, Eva MM, Gopal AA, Schwartzentruber JA, et al. CYRI/FAM49B negatively regulates RAC1-driven cytoskeletal remodelling and

protects against bacterial infection. Nat Microbiol [Internet]. 2019;4(9):1516–31. Available from: http://dx.doi.org/10.1038/s41564-019-0484-8

326. Li R, Quan J, Zhang W, Fu W, Du J, Jiang H, et al. Human heat shock protein-specific cytotoxic T lymphocytes display potent antitumour immunity in multiple myeloma. Br J Haematol. 2014;166(5):690–701.

327. Park SJ, Suetsugu S, Sagara H, Takenawa T. HSP90 cross-links branched actin filaments induced by N-WASP and the Arp2/3 complex. Genes to Cells [Internet]. 2007 May;12(5):611–22. Available from: http://doi.wiley.com/10.1111/j.1365-2443.2007.01081.x

328. Koyasu S, Nishida E, Kadowaki T, Matsuzaki F, Iida K, Harada F, et al. Two mammalian heat shock proteins, HSP90 and HSP100, are actin-binding proteins. Proc Natl Acad Sci U S A. 1986;83(21):8054–8.

329. Böhm B, Heinzelmann S, Motz M, Bauer G. Extracellular localization of catalase is associated with the transformed state of malignant cells. Biol Chem. 2015;396(12):1339–56.

330. Liu Y, Ma C, Zhang N. Tissue-specific control of tissue-resident memory T cells. Crit Rev Immunol. 2018;38(2):79–103.

331. Allen EL, Ulanet DB, Pirman D, Mahoney CE, Coco J, Si Y, et al. Differential Aspartate Usage Identifies a Subset of Cancer Cells Particularly Dependent on OGDH. Cell Rep [Internet]. 2016;17(3):876–90. Available from: http://dx.doi.org/10.1016/j.celrep.2016.09.052

332. Zhang W, Luo X, Zhang F, Zhu Y, Yang B, Hou M, et al. SjTat-TPI facilitates adaptive T-cell responses and reduces hepatic pathology during Schistosoma japonicum infection in BALB/c mice. Parasites and Vectors [Internet]. 2015;8(1):1–9. Available from: http://dx.doi.org/10.1186/s13071-015-1275-6

333. Bartolome F, Wu H-C, Burchell VS, Preza E, Wray S, Mahoney CJ, et al. Pathogenic VCP Mutations Induce Mitochondrial Uncoupling and Reduced ATP Levels. Neuron [Internet]. 2013 Apr;78(1):57–64. Available from: https://linkinghub.elsevier.com/retrieve/pii/S0896627313001864

334. Edinger AL, Cinalli RM, Thompson CB. Rab7 prevents growth factor-independent survival by inhibiting cell-autonomous nutrient transporter expression. Dev Cell. 2003;5(4):571–82.

335. Liu Y, Cao Y, Zhang W, Bergmeier S, Qian Y, Akbar H, et al. A small-molecule inhibitor of glucose transporter 1 downregulates glycolysis, induces cell-cycle arrest, and inhibits cancer cell growth in vitro and in vivo. Mol Cancer Ther. 2012;11(8):1672–82.

336. Marambio P, Toro B, Sanhueza C, Troncoso R, Parra V, Verdejo H, et al. Glucose deprivation causes oxidative stress and stimulates aggresome formation and autophagy in cultured cardiac myocytes. Biochim Biophys Acta - Mol Basis Dis [Internet]. 2010;1802(6):509–18. Available from: http://dx.doi.org/10.1016/j.bbadis.2010.02.002

337. Gautreau A, Poullet P, Louvard D, Arpin M. Ezrin, a plasma membrane-microfilament linker, signals cell survival through the phosphatidylinositol 3-

kinase/Akt pathway. Proc Natl Acad Sci U S A. 1999;96(13):7300–5.

338. Elliott BE, Meens JA, SenGupta SK, Louvard D, Arpin M. The membrane cytoskeletal crosslinker ezrin is required for metastasis of breast carcinoma cells. Breast Cancer Res. 2005;7(3):365–73.

339. Asmal M, Colgan J, Naef F, Yu B, Lee Y, Magnasco M, et al. Production of ribosome components in effector CD4+ T cells is accelerated by TCR stimulation and coordinated by ERK-MAPK. Immunity. 2003;19(4):535–48.

340. Johnson GP, Stavenschi E, Eichholz KF, Corrigan MA. Condensin II protein dysfunction impacts mitochondrial respiration and stress response. J Cell Sci. 2019;(October).

341. Kenney SP, Meng XJ. Identification and fine mapping of nuclear and nucleolar localization signals within the human ribosomal protein S17. PLoS One. 2015;10(4).

342. Getnet D, Maris CH, Hipkiss EL, Grosso JF, Harris TJ, Yen H-R, et al. Tumor Recognition and Self-Recognition Induce Distinct Transcriptional Profiles in Antigen-Specific CD4 T Cells. J Immunol. 2009;182(8):4675–85.

343. Xie D, Zhou Y, Luo X. Amorphous silica nanoparticles induce tumorigenesis via regulating ATP5H/ SOD1-related oxidative stress, oxidative phosphorylation and EIF4G2/PABPC1-associated translational initiation. PeerJ. 2019;2019(3):1–18.

344. Katzenellenbogen RA, Vliet-Gregg P, Xu M, Galloway DA. Cytoplasmic Poly(A) Binding Proteins Regulate Telomerase Activity and Cell Growth in Human Papillomavirus Type 16 E6-Expressing Keratinocytes. J Virol. 2010;84(24):12934–44.

345. Suman S, Mishra A, Kulshrestha A. A systems approach for the elucidation of crucial genes and network constituents of cervical intraepithelial neoplasia 1 (CIN1). Mol Biosyst [Internet]. 2017;13(3):549–55. Available from: http://dx.doi.org/10.1039/c6mb00615a

346. Zhang X, Chen X, Liu Q, Zhang S, Hu W. Translation repression via modulation of the cytoplasmic poly(A)-binding protein in the inflammatory response. Elife. 2017;6:1–23.

347. Hung CM, Garcia-Haro L, Sparks CA, Guertin DA. mTOR-dependent cell survival mechanisms. Cold Spring Harb Perspect Biol. 2012;4(12):1–17.

348. Takano S, Ando T, Hiramatsu N, Kanayama A, Maekawa S, Ohnuma Y, et al. T cell receptor-mediated signaling induces GRP78 expression in T cells: The implications in maintaining T cell viability. Biochem Biophys Res Commun. 2008;371(4):762–6.

349. Eletto D, Chevet E, Argon Y, Appenzeller-Herzog C. Redox controls UPR to control redox. J Cell Sci. 2014;127(17):3649–58.

350. Hitzel J, Lee E, Zhang Y, Bibli SI, Li X, Zukunft S, et al. Oxidized phospholipids regulate amino acid metabolism through MTHFD2 to facilitate nucleotide release in endothelial cells. Nat Commun. 2018;9(1).

351. Fagone P, Jackowski S. Membrane phospholipid synthesis and endoplasmic reticulum function. J Lipid Res. 2009;50(SUPPL.):311–6.

352. Zhang X, Gibhardt CS, Will T, Stanisz H, Körbel C, Mitkovski M, et al. Redox signals at the ER –mitochondria interface control melanoma progression . EMBO J. 2019;38(15):1–22.

353. Hempel N, Trebak M. Crosstalk between calcium and reactive oxygen species signaling in cancer. Cell Calcium [Internet]. 2017 May;63:70–96. Available from: https://linkinghub.elsevier.com/retrieve/pii/S0143416016302202

354. Li G, Zhao H, Zhang X, Zhang Y, Zhao H, Yang X, et al. Environmental stress responses of DnaJA1, DnaJB12 and DnaJC8 in Apis cerana cerana. Front Genet. 2018;9(OCT):1–13.

355. Behrens A, Sabapathy K, Graef I, Cleary M, Crabtree GR, Wagner EF. Jun N-terminal kinase 2 modulates thymocyte apoptosis and T cell activation through c-Jun and nuclear factor of activated T cell (NF-AT). Proc Natl Acad Sci U S A. 2001;98(4):1769–74.

356. Helenius M, Hänninen M, Lehtinen SK, Salminen A. Aging-induced up-regulation of nuclear binding activities of oxidative stress responsive NF-kB transcription factor in mouse cardiac muscle. J Mol Cell Cardiol. 1996;28(3):487–98.

357. Yu J, Zhou X, Nakaya M, Jin W, Cheng X, Sun S-C. T Cell–Intrinsic Function of the Noncanonical NF-κB Pathway in the Regulation of GM-CSF Expression and Experimental Autoimmune Encephalomyelitis Pathogenesis. J Immunol. 2014;193(1):422–30.

358. Choi BY, Kim JH, Kho AR, Kim IY, Lee SH, Lee BE, et al. Inhibition of NADPH oxidase activation reduces EAE-induced white matter damage in mice. J Neuroinflammation [Internet]. 2015;12(1):1–15. Available from: ???

359. Tiwari S, Thakur R, Shankar J. Role of Heat-Shock Proteins in Cellular Function and in the Biology of Fungi. Biotechnol Res Int. 2015;2015:1–11.

360. Castellanos MDC, Muñoz C, Montoya MC, Lara-Pezzi E, López-Cabrera M, De Landázuri MO. Expression of the Leukocyte Early Activation Antigen CD69 Is Regulated by the Transcription Factor AP-1. J Immunol. 1997;159(11):5463–73.

361. Lopez-Cabrera M, Munoz E, Blazquez M V., Ursa MA, Santis AG, Sanchez-Madrid F. Transcriptional regulation of the gene encoding the human C-type lectin leukocyte receptor AIM/CD69 and functional characterization of its tumor necrosis factor-α-responsive elements. J Biol Chem. 1995;270(37):21545–51.

362. Spendlove I, Sutavani R. The Role of CD97 in Regulating Adaptive T-Cell Responses. In 2010. p. 138–48. Available from: http://link.springer.com/10.1007/978-1-4419-7913-1_12

363. Capasso M, Durrant LG, Stacey M, Gordon S, Ramage J, Spendlove I. Costimulation via CD55 on Human CD4 + T Cells Mediated by CD97 . J Immunol. 2006;177(2):1070–7.

364. Puls KL, Hogquist KA, Reilly N, Wright MD. CD53, a thymocyte selection

marker whose induction requires a lower affinity TCR-MHC interaction than CD69, but is up-regulated with slower kinetics. Int Immunol. 2002;14(3):249–58.

365. Singleton K, Parvaze N, Dama KR, Chen KS, Jennings P, Purtic B, et al. A Large T Cell Invagination with CD2 Enrichment Resets Receptor Engagement in the Immunological Synapse. J Immunol. 2006;177(7):4402–13.

366. Gimferrer I, Farnós M, Calvo M, Mittelbrunn M, Enrich C, Sánchez-Madrid F, et al. The accessory molecules CD5 and CD6 associate on the membrane of lymphoid T cells. J Biol Chem. 2003;278(10):8564–71.

367. Beurel E, Grieco SF, Jopea RS. GSK3: regulation, actions, and diseases. Vol. 0, Pharmacol Ther. 2015. 114–131 p.

368. Rodriguez-Frandsen A, De Lucas S, Pérez-González A, Pérez-Cidoncha M, Roldan-Gomendio A, Pazo A, et al. HCLE/C14orf166, a cellular protein required for viral replication, is incorporated into influenza virus particles. Sci Rep [Internet]. 2016;6(July 2015):1–11. Available from: http://dx.doi.org/10.1038/srep20744

369. McFarlane HE, Watanabe Y, Yang W, Huang Y, Ohlrogge J, Samuels AL. Golgi- and trans-golgi network-mediated vesicle trafficking is required for wax secretion from epidermal cells. Plant Physiol. 2014;164(3):1250–60.

370. Vyas S, Chesarone-Cataldo M, Todorova T, Huang YH, Chang P. A systematic analysis of the PARP protein family identifies new functions critical for cell physiology. Nat Commun. 2013;4.

371. Boehm T, Hofer S, Winklehner P, Kellersch B, Geiger C, Trockenbacher A, et al. Attenuation of cell adhesion in lymphocytes is regulated by CYTIP, a protein which mediates signal complex sequestration. EMBO J. 2003;22(5):1014–24.

372. Reynafarje B, Costa LE, Lehninger AL. O2 solubility in aqueous media determined by a kinetic method. Anal Biochem. 1985;145(2):406–18.

373. Yan Z, Banerjee R. Redox remodeling as an immunoregulatory strategy. Biochemistry. 2010;49(6):1059–66.

8.0 Supplementary

8.1 Supplementary Figures

Gating Strategy

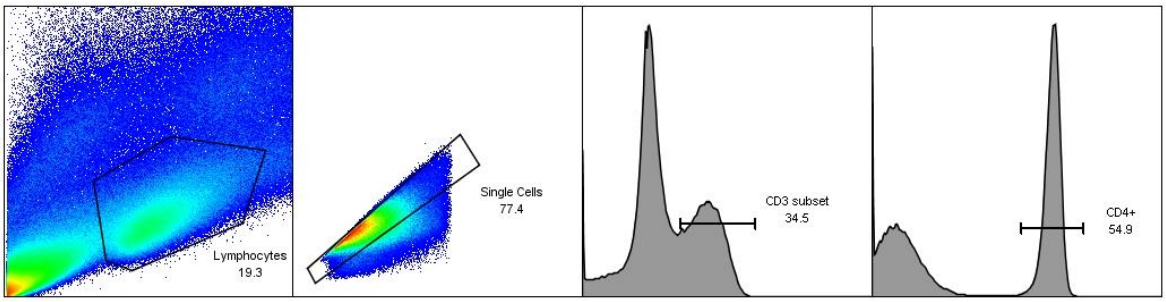

Supplementary Figure 1: Gating strategy to isolate CD3+CD4+ T cells from primary human PBMCs.

Cells were first gated on size by utilizing the forward and side scatter scales to gate on the lymphocyte population, linear single cell populations were then isolated by gating cells which follow a linear increase in size and density. Following size gating, cells were isolated based on positive expression of the CD3 cell surface receptor and then the CD4 cell surface receptor.

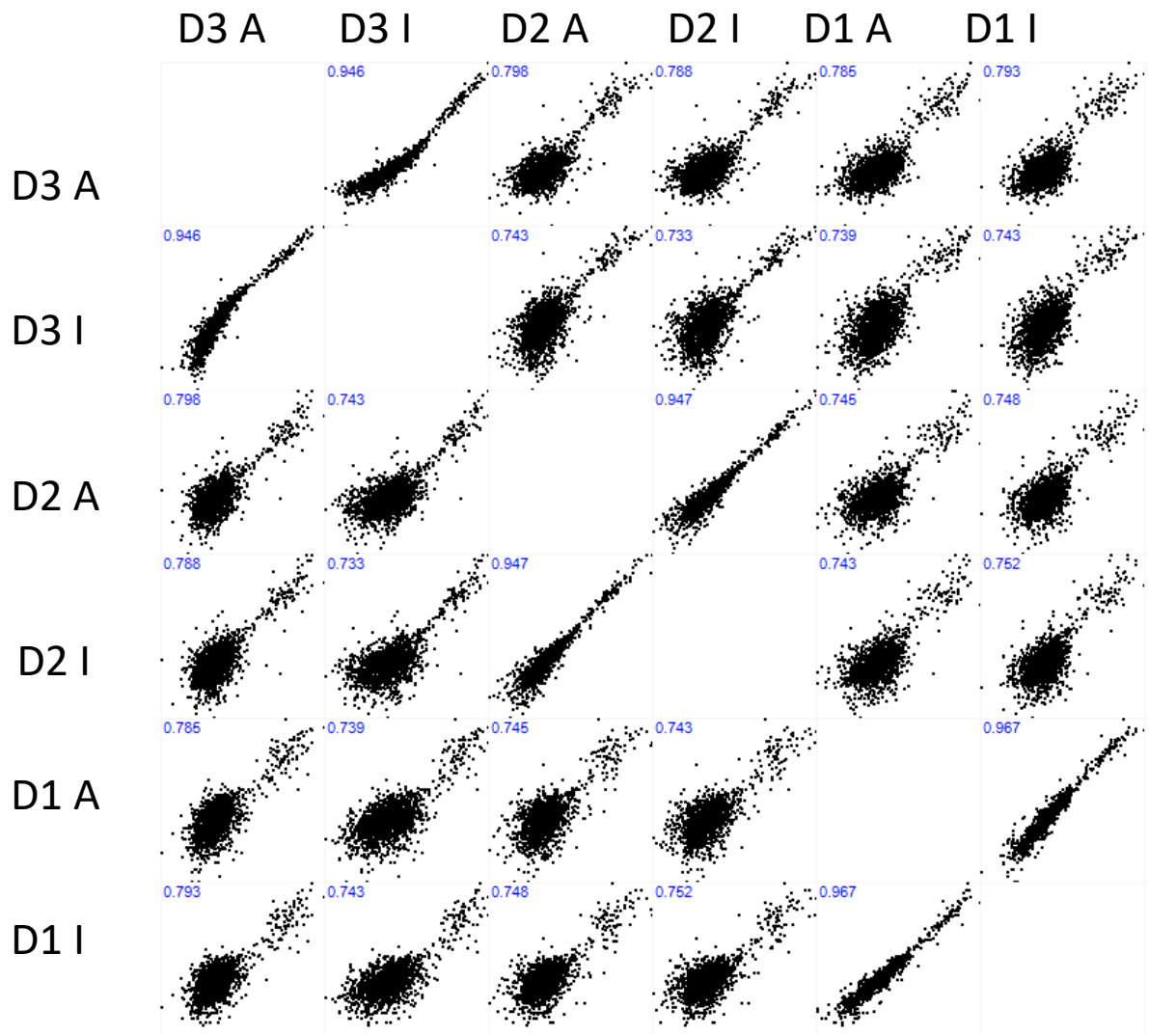

Supplementary Figure 2: Spearman rank correlation coefficients between all donor samples used in redox proteomic analysis

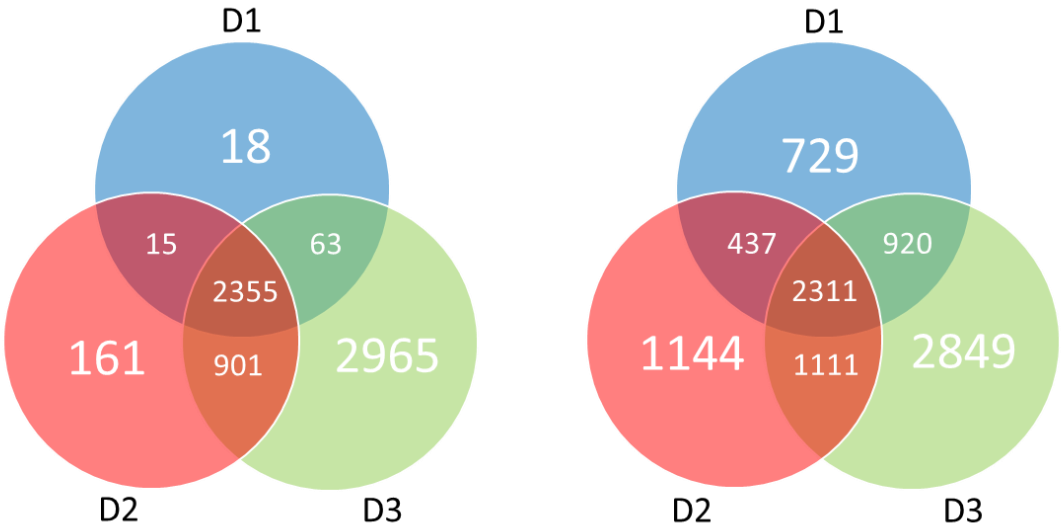

Supplementary Figure 3: Variation in protein identification (left) vs only cysteine containing peptide identification (right) for all biological donors used in redox proteomics experiments.

8.2 Supplementary Tables

Supplementary Tables. 1-15 are included as in the attached USB memory stick accompanying this thesis.

8.3 R scripts

Script 1

```
#R script for generating redox protemic (fold change) volcano plot adapted
from Wenjie
setwd("C:/Users/dme16/Desktop/19-9-9_Figures for paper/Redox proteomics/nON
NORM")
library(dplyr)
library(tidyr)
library(readxl)
D1 <- read_excel("D1.xlsx", col_types = c("text",
                                          "text", "skip", "skip", "skip",
"skip",
                                          "numeric", "numeric"))

D2 <- read_excel("D2.xlsx", col_types = c("text",
                                          "text", "skip", "skip", "skip",
"skip",
                                          "numeric", "numeric"))

D3 <- read_excel("D3.xlsx", col_types = c("text",
                                          "text", "skip", "skip", "skip",
"skip",
                                          "numeric", "numeric"))


##Merge datasets based on Accesssion
All.D <- as.data.frame(merge(merge(D1, D2, by = "Sequence",all = TRUE),D3,
by = "Sequence", all = TRUE))
##Coalesce gene names and protein names
All.D$c<- coalesce(All.D$GN.x, All.D$GN.y, All.D$GN)
##Discard repetitive columns
all.merge <- All.D[,-c(2,5,8)]
all.merge[,2:7]<- log2(all.merge[,2:7])
```

```
#Triple.data$Sum<-apply(Triple.data[4:6], 1, sum)

#Triple.data <- Triple.data[order(Triple.data$Sum),]
##Renames columns
#colnames(Triple.data)[2:6] <- c("Protein_names","Gene_names","First",
"Second", "Third")
all.merge$D1 <- all.merge$`D1 Active`-all.merge$`D1 Inactive`
all.merge$D2 <- all.merge$`D2 Active`-all.merge$`D2 Inactive`
all.merge$D3 <- all.merge$`D3 Active`-all.merge$`D3 Inactive`

#Define columns for Ratio
ratio <- c(9:11)


#Create an empty matrix for p vlue
two.sided <- matrix(nrow=nrow(all.merge), ncol=1)
#Calculate p value for each protein
for(i in 1:nrow(all.merge))
{
  #Filter out the proteins have more than 2 NA value
  if(sum(is.na(all.merge[i,ratio])) < 2 )
    #Calculate p value based on Ratio
  {
    two.sided[i,1] <- t.test(all.merge[i,ratio],mu=0,alternative
="two.sided",)$p.value
  }
}
#Calculate the fold change
Difference<- apply(all.merge[,ratio],1,mean,na.rm=TRUE)
#Add p value and fold change into matrix
Volcano.data_actual <- cbind(all.merge, P = -log10(two.sided),Diff =
Difference)

library(ggrepel)
library(ggplot2)
P.cut <- -log10(0.05)
Diff.cut <- 0.05
Actualvolplot <- ggplot(Volcano.data_actual, aes(y=P,x=Diff))+ #volcanoplot
with log2Foldchange versus pvalue
  geom_point(size=1,alpha=0.5,color="grey")+
  ylab(expression(paste("-Log" ["10"], "P")))+
  xlab(expression(paste("Log" ["2"], "(+P+C/-P+C)")))+
  scale_y_continuous(expand = c(0, 1))+
  scale_x_continuous(limits = c(-4,4))+
  #geom_vline(xintercept = 0,color="grey") +
  #geom_hline(yintercept = 0,color="grey") +
  geom_vline(xintercept = c(-Diff.cut, Diff.cut),
linetype="dashed",color="grey")+
  geom_hline(yintercept = P.cut, linetype="dashed",color="grey")+
  theme_classic(base_size = 9) +
  theme(text = element_text(size=9),axis.text = element_text(color =
"black",size = 9))+
  geom_point(data=filter(Volcano.data_actual, P>P.cut&
abs(Diff)>Diff.cut),size=1.5, color="red")+
  geom_text_repel(data=filter(Volcano.data_actual, P>P.cut &
abs(Diff)>Diff.cut), aes(label=c),size=3,color="red")
#adding text for the proteins within threshold
print(Actualvolplot)
ggsave("Redoxplot_0_5.pdf",width = 200, height = 200,units = "mm")
```

Script 2

```
#R script for generating redox protemic (% change) volcano plot by Daniel
```

```
setwd("C:/Users/dme16/Desktop/19-9-9_Figures for paper/Redox proteomics/nON
NORM/change in ox")
library(dplyr)
library(tidyr)
library(readxl)
D1 <- read_excel("D1.xlsx", col_types = c("text",
                                          "text", "skip", "skip", "skip",
"skip",
                                          "numeric", "numeric"))

D2 <- read_excel("D2.xlsx", col_types = c("text",
                                          "text", "skip", "skip", "skip",
"skip",
                                          "numeric", "numeric"))

D3 <- read_excel("D3.xlsx", col_types = c("text",
                                          "text", "skip", "skip", "skip",
"skip",
                                          "numeric", "numeric"))


##Merge datasets based on Accesssion
All.D <- as.data.frame(merge(merge(D1, D2, by = "Sequence",all = TRUE),D3,
by = "Sequence", all = TRUE))
##Coalesce gene names and protein names
All.D$c<- coalesce(All.D$GN.x, All.D$GN.y, All.D$GN)
##Discard repetitive columns
all.merge <- All.D[,-c(2,5,8)]

#Triple.data <- Triple.data[order(Triple.data$Sum),]
##Renames columns
all.merge$D1 <- all.merge$`D1 Active`-all.merge$`D1 Inactive`
all.merge$D2 <- all.merge$`D2 Active`-all.merge$`D2 Inactive`
all.merge$D3 <- all.merge$`D3 Active`-all.merge$`D3 Inactive`

#Define columns for Ratio
ratio <- c(9:11)


#Create an empty matrix for p vlue
two.sided <- matrix(nrow=nrow(all.merge), ncol=1)
#Calculate p value for each protein
for(i in 1:nrow(all.merge))
{
  #Filter out the proteins have more than 2 NA value
  if(sum(is.na(all.merge[i,ratio])) < 2 )
    #Calculate p value based on Ratio
  {
    two.sided[i,1] <- t.test(all.merge[i,ratio],mu=0,alternative
="two.sided",)$p.value
  }
}
#Calculate the fold change
Difference<- apply(all.merge[,ratio],1,mean,na.rm=TRUE)
#Add p value and fold change into matrix
Volcano.data_ox <- cbind(all.merge, P = -log10(two.sided),Diff =
Difference)

library(ggrepel)
library(ggplot2)
P.cut <- -log10(0.05)
```

```
Diff.cut <- 0.05
Actualvolplot <- ggplot(Volcano.data_ox, aes(y=P,x=Diff))+ #volcanoplot
with log2Foldchange versus pvalue
  geom_point(size=1,alpha=0.5,color="grey")+
  ylab(expression(paste("-Log" ["10"], "P")))+
  xlab(expression(paste("change in oxidation")))+
  scale_y_continuous(expand = c(0, 1))+
  scale_x_continuous(limits = c(-0.25,0.25))+
  geom_vline(xintercept = c(-Diff.cut, Diff.cut),
linetype="dashed",color="grey")+
  geom_hline(yintercept = P.cut, linetype="dashed",color="grey")+
  theme_classic(base_size = 9) +
  theme(text = element_text(size=9),axis.text = element_text(color =
"black",size = 9))+
  geom_point(data=filter(Volcano.data_ox, P>P.cut&
abs(Diff)>Diff.cut),size=1.5, color="red")+
geom_text_repel(data=filter(Volcano.data_ox, P>P.cut & abs(Diff)>Diff.cut),
aes(label=c),size=3,color="red")
#adding text for the proteins within threshold
print(Actualvolplot)
ggsave("change in ox 5percent.pdf",width = 200, height = 200,units = "mm")

candidates_ox<-filter(Volcano.data_ox, P>P.cut& abs(Diff)>Diff.cut)
write.csv(candidates_ox, "C:/Users/dme16/Desktop/19-9-9_Figures for
paper/Redox proteomics/nON NORM/change in ox/candidates_changeinox.csv")
```

Script 3

```
#R script for generating protein turnover volcano plot by Daniel
setwd("C:/Users/dme16/Desktop/20-1-13_protein turnover paper")
library(readxl)
X2_valid_values <- read_excel("C:/Users/dme16/Desktop/20-1-13_protein
turnover paper/2 valid values.xlsx",
                              col_types = c("text", "text", "text",
                                            "numeric", "numeric",
"numeric",
                                            "numeric", "numeric",
"numeric",
                                            "numeric", "numeric",
"numeric",
                                            "numeric", "numeric",
"numeric"))
#deleted all values which have NA
#Valid_values_nona <- X2_valid_values[is.na(X2_valid_values)] <- 0
X2_valid_values[is.na(X2_valid_values)] <- 0
#Define columns for Ratio - Group 1 is +PMA+Cata, group 2 is +PMA-Cata,
Group 3 is -PMA+Cata, Group 4 is -PMA-Cata
n.col <- c(4:15)
group_1_2vv <- c(4,5,6)
group_2_2vv <- c(7,8,9)
group_3_2vv <- c(10,11,12)
group_4_2vv <- c(13,14,15)
Triple.ratio_2vv <- cbind(X2_valid_values[,1:3],X2_valid_values[,n.col])
#Create an empty matrix for p vlue
two.sided_2vv <- matrix(nrow=nrow(Triple.ratio_2vv), ncol=5)
#Calculate p value for each protein
for(i in 1:nrow(Triple.ratio_2vv))
{
```

```
  #Calculate p value based on Ratio P1 G1/2, P2, 1/3,P3, 1/4, P4 2/4, P5
3/4
  two.sided_2vv[i,1] <-
t.test(Triple.ratio_2vv[i,group_1_2vv],Triple.ratio_2vv[i,group_2_2vv],var.
equal = TRUE)$p.value
  two.sided_2vv[i,2] <-
t.test(Triple.ratio_2vv[i,group_1_2vv],Triple.ratio_2vv[i,group_3_2vv],var.
equal = TRUE)$p.value
  two.sided_2vv[i,3] <-
t.test(Triple.ratio_2vv[i,group_1_2vv],Triple.ratio_2vv[i,group_4_2vv],var.
equal = TRUE)$p.value
  two.sided_2vv[i,4] <-
t.test(Triple.ratio_2vv[i,group_2_2vv],Triple.ratio_2vv[i,group_4_2vv],var.
equal = TRUE)$p.value
  two.sided_2vv[i,5] <-
t.test(Triple.ratio_2vv[i,group_3_2vv],Triple.ratio_2vv[i,group_4_2vv],var.
equal = TRUE)$p.value


}

#Calculate the fold change
Diff_1_2vv<-log2(
apply(Triple.ratio_2vv[,group_1_2vv],1,median,na.rm=TRUE)/apply(Triple.rati
o_2vv[,group_2_2vv],1,median,na.rm=TRUE))
Diff_2_2vv<-
log2(apply(Triple.ratio_2vv[,group_1_2vv],1,median,na.rm=TRUE)/apply(Triple
.ratio_2vv[,group_3_2vv],1,median,na.rm=TRUE))
Diff_3_2vv<-
log2(apply(Triple.ratio_2vv[,group_1_2vv],1,median,na.rm=TRUE)/apply(Triple
.ratio_2vv[,group_4_2vv],1,median,na.rm=TRUE))
Diff_4_2vv<-
log2(apply(Triple.ratio_2vv[,group_2_2vv],1,median,na.rm=TRUE)/apply(Triple
.ratio_2vv[,group_4_2vv],1,median,na.rm=TRUE))
Diff_5_2vv<-
log2(apply(Triple.ratio_2vv[,group_3_2vv],1,median,na.rm=TRUE)/apply(Triple
.ratio_2vv[,group_4_2vv],1,median,na.rm=TRUE))
#Add p value and fold change into matrix (converted fold change to log2)
Volcano.data_2vv <- cbind(Triple.ratio_2vv, P = -
log10(two.sided_2vv),Diff_1_2vv,Diff_2_2vv,Diff_3_2vv,Diff_4_2vv,Diff_5_2vv
)


head(Volcano.data_2vv)


library("ggplot2") #Best plots
library("dplyr")
library("ggrepel") #Avoid overlapping labels
##create a file from copylist
read.excel <- function(header=TRUE,...) {
  read.table("clipboard",sep="\t",header=header,...)
}



P.cut <- -log10(0.05)
Diff.cut <- 1
VolPlot_2vv <- ggplot(Volcano.data_2vv, aes(y=P.4,x=Diff_4_2vv))+
#volcanoplot with log2Foldchange versus pvalue
  geom_point(size=1,alpha=0.5,color="grey")+
```

```
  ylab(expression(paste("-Log" ["10"], "P")))+
  xlab(expression(paste("Log" ["2"], "(+P+C/-P+C)")))+
  scale_y_continuous(expand = c(0, 0))+
  scale_x_continuous(limits = c(-4,10))+
  geom_vline(xintercept = c(-Diff.cut, Diff.cut),
linetype="dashed",color="grey")+
  geom_hline(yintercept = P.cut, linetype="dashed",color="grey")+
  theme_classic(base_size = 9) +
  theme(text = element_text(size=9),axis.text = element_text(color =
"black",size = 9))+
  geom_point(data=filter(Volcano.data_2vv, P.4>P.cut&
abs(Diff_4_2vv)>Diff.cut),size=1.5, color="red")
  geom_text_repel(data=filter(Volcano.data_2vv, P.4>P.cut&
abs(Diff_4_2vv)>Diff.cut), aes(label=Gene_Names),size=3,color="red")

print(VolPlot_2vv)

ROShigh<-filter(Volcano.data_2vv, P.4>P.cut& abs(Diff_4_2vv)>Diff.cut)

ggsave("C:/Users/dme16/Desktop/19-9-9_Figures for paper/Redox
proteomics.pdf",VolPlot,
       width = 200, height = 200,
       #width = 39.5, height = 37,
       units = "mm")
```

Acknowledgments

I would firstly give my thanks to Prof. Lothar Jänsch who has supervised my progress throughout the past 3 years and offered numerous enlightening discussions, which have triggered some very novel ideas and theories. Additionally, I thank Dr. Marco van Ham, who has went above and beyond when it comes to assisting in writing as well as in offering challenging questions which have improved the quality of my work.

I would also like to thank Dr. Josef Wissing and Dr. Manfred Nimtz, who have both been a great source of interesting discussion in the practical applications and theoretical ideas which underscore the use of LC-MS.

In regards to technical support, while I prefer to apply my ham-fisted technique to the lab bench I am indebted to Andrea Abrahamik, Kirsten Minkhart, Anja Meier and Reiner Munder. All of whom have been a great source of information and practical experience.

In terms of external collaborators I thank Lars Leichert and Daniella Dieterich who both helped me enormously with their specialised knowledge in redox proteomics and metabolic labelling techniques respectively. As well as Prof. Stefan Dübel for agreeing to evaluate my defence.

In regards to PROCOMPAS, I thank Prof. Ralf Mendel for providing me the opportunity to study in the PROCOMPAS graduate school, agreeing to evaluate my thesis and for agreeing to chair my defence. As well as Dagmar Zwerschke for her fantastic administrative help.

Outside of science I would like to thank my mother who won't stop messaging me on WhatsApp checking if I'm alive. As well as my close friend 2ays and Blu_Igel for their support throughout my post graduate academic career or throughout my time in Germany respectively. As well as Ryscan.

Finally, I would be remiss to not thank Matheus, as he has been a welcome source of support in the final phase of my PhD.

Curriculum Vitae

Daniel Meston

Muenzstrasse 1 B, Braunschweig 38100, Germany
E-Mail: djm94@hotmail.co.uk
Date of Birth: 23-02-1994, Place of Birth: South Shields, Tyne and Wear, UK Nationality: British

Personal Statement

PhD graduate looking to further my career in analytical chemistry. I have extensive experience in all conventional modes of chromatography especially in the determination of chemically diverse organic compounds via LC-MS and quantifying trace levels of compounds *via* targeted methods.

Education and Qualifications

October 2016- March 2020 TU- Braunschweig (PROCOMPAS graduate school)

Thesis title: Respirasome dynamics and turnover in activated T lymphocytes

October 2015- September 2016 University of Sunderland

MSc. Drug Discovery and Development (Distinction)

Dissertation title: Mixed mode chromatography in the simultaneous determination of baclofen from its related substances.

September 2012- May 2015 University of Sunderland

B.Sc. (Hons) BioPharmaceutical Sciences (First Class Honours)

Dissertation title: Exploitation of chiral UHPLC using chiral mobile phase additives: achiral/chiral related substances assay for brompheniramine and chlorpheniramine.

Publications

Meston, D and Lough, J. Exploitation of Chiral uHPLC using Chiral Mobile Phase Additives: Achiral/Chiral Assay and Related Substances for Brompheniramine and Chlorpheniramine. *Separations* in submission

Meston, D and Lough, J. Enantiomer Resolution via Chiral Mobile Phase Additives: A Much Exaggerated Demise? *Chromatographia* In submission

Meston, D. Soo, E. Perrera, W. Lough, J. Robustness and Accuracy of Orthogonal Phase Combinations in Pharmaceutical Related Substances Assays. in preparation

Meston, D. Bi, W. Van Ham, M. Jaench, L. Elucidating Mitochondrial ROS Derived Oxidations in CD4+ T cell Activation. in preparation

Awards

The FUJIFILM Biotechnologies Prize: for Best Final Year Performance, 2014-2015

Relevant Skills

From my PhD I have extensive experience working with LC-MS instruments (TIMS-ToF/IT/QQQ/Orbitrap) for both untargeted studies as well as targeted SIM/(d)MRM measurements of small molecules for example nM analysis of TCA metabolites. Additionally, I have extensive experience in designing analytical workflows utilising different modes of LC-MS. I have designed novel methods for designing mixed mode columns for exploiting orthogonal selectivity of chemically diverse compounds in a single chromatographic run. As well as utilising off-line orthogonal separation methods for large scale global proteomics studies, which I have used to characterise post translational modifications in protein signalling like the quantification of oxidation of cysteine residues to disulphide bridges as well as phosphorylation of serine.

In addition to applied research, I have also studied fundamental developments in mass spectrometry and stationary phase development, for example utilising (SIM/MRM) in collaboration with academic partners to develop novel identification algorithms to allow more comprehensive proteome coverage in bottom up approaches. As well as the identification of novel stationary phase reactivities through unconventional LC-MS setups with industrial partners.

Relevant Work Experience

June 2018 – Present: Chromatography Society Committee Member
Position: ChromCom Journal Editor

As editor of the ChromCom journal my responsibilities include, writing and editing articles, negotiating with sponsors, organising meetings; 2019 Emerging Separations Technologies meeting with the Royal Society of Chemistry and ISC 2022.

Personal Attributes

Motivated individual with a formidable drive to undertake research in the field of separation science. Independent but communicable and able to discuss novel ideas and challenges pragmatically.

Additional Information

Information Technology: Chemstation/Openlab, Chromeleon, Xcalibur acquisition software, Proteome Discoverer, Peaks, MaxQuant/Persues software, R coding.

Positions of Responsibility: Organiser of multiple scientific events, currently ISC2022 in Liverpool and student speaker of PROCOMPAS/HZI graduate schools with experience working in both large and small groups as well as individually.

Activities & Interests: Avid road racer, competing in England and Germany.

References (Referees)

Dr. W J Lough, Reader in Pharmaceutical Analysis, Room 123, Dale Building, Sciences Complex, University of Sunderland, City Campus, Sunderland, Tyne & Wear, SRI 3SD. Tel. no. 0191 5152570. E-mail: john.lough@sunderland.ac.uk

Prof. Lothar Jänsch, Professor of Proteomics research, Helmholtz Centre for Infection Research, Inhoffenstrasse 7, 38124 Braunschweig, Germany, Tel. no. +49 531 6181-3030. E-mail: Lothar.Jaensch@helmholtz-hzi.de